12-14-2018 2:00 PM

Photo-Isomerizable Complementary Hydrogen Bond Arrays

Jeffrey S. Pleizier
The University of Western Ontario

Supervisor
Wisner, James A.
The University of Western Ontario

Graduate Program in Chemistry
A thesis submitted in partial fulfillment of the requirements for the degree in Doctor of Philosophy

Abstract

The use of light as an external stimulus provides a non-invasive technique to induce large changes in physical and chemical properties of a substrate. The incorporation of a photochromic subunit into supramolecular polymeric systems therefore adds a potential "smart" quality for polymer manipulation. The azo moiety (-N=N-) is one of the most popular photochromic units as the *trans* to *cis* isomerization results in a large degree of spatial rearrangement. This present thesis exploits the azo group by its incorporation into complementary hydrogen bonded complexes. Hydrogen bonding acceptor groups attached to the periphery of the central azo photoswitch provided strong complexation with donor arrays in the *trans* state. Isomerization to the *cis* isomer disrupted complex stability by rearrangement from the optimal binding geometry. Furthermore, one of the azo nitrogen atoms also participated in hydrogen bonding which is a new use for these types of photoswitches.

The arrays used as photoswitchable hydrogen bonding acceptors in this work were synthesized through high yielding synthetic methods with inexpensive, commercially available starting materials. The donor arrays chosen for this work were 2-aminoindoles which are small, planar compounds. They were chosen as they have a multitude of positions where substitutions can take place which can result in a large library of compounds. Complex stability of these arrays were analyzed in solution using ^{1}H NMR titration methods and these results were validated in the solid state by X-ray diffraction analysis. It was determined that substitution patterns on the donor arrays, the

number of acceptor sites, and solvent interactions all have a large overall effect on the resulting complex stability. Association constants ranged from 90 to 1.7 x 10^5 M^{-1}.

Additionally, the spatial arrangement of the acceptor atoms resulted in a decrease of complex stability. The *trans* to *cis* isomerization provided a less optimal binding geometry towards the donor arrays. This was determined through a newly developed ^1H NMR extrapolation method which allowed for the determination of lower association constants for the *cis* isomeric complexes. The reversibility of the system was also tested and showed stability and reproducibility.

Keywords

Supramolecular, Hydrogen Bonding, Complementary, Substituent Effects, Photochromism, Azo, Trans, Cis, NMR Titrations, Extrapolations

---

Co-Authorship Statement

Dr. Janic Linares Mendez assisted in ^{1}H NMR spectra collection for the extrapolation experiments. All crystal structures were solved and refined by Dr. Paul Boyle, Dr. Bhanu Mudraboyina, or Aneta Boreki. Mass spectra were collected by Doug Hairsine. Figure 1.20 was used with permission by Springer Nature; License Number 4446540504167. All other work in this thesis was done by the author himself.

Acknowledgments

I honestly never thought I would actually finish this thesis. It has been several grueling years of ups, downs, highs, and lows. I could write another thesis on people to thank for me finally getting here, but I will trim it down.

Goes without saying, but the most thanks belongs to Dr. James Wisner. I started in his lab as an undergraduate and he just couldn't get rid me. He is a great mentor, a great chemist, a great leader, and now a great friend. His patience with me in particular has been enormous (chemistry and life). Cannot thank him enough for letting me be a part of his research group, and of course the Hong Ping lunch trips.

Everyone that I have had the pleasure to work within the Wisner lab has been amazing. Past or present, thank you all for support and knowledge. In particular, Dr. Janic Linares Mendez has been my sister from a Mexican mister my whole time here. We helped each other, in the lab and out, bounced ideas off each other and truly made each other better people. Not seeing her beside me 5 days a week for several hours will be a true hardship. Much love Janic.

Western University has bought me into contact with some amazing individuals. Dr. Paul Boyle from X-ray, Doug Hairsine from Mass Spec, Mat Willians from NMR, the ladies from ChemBioStores (and Don), my Tim Hortons ladies: Kula, Kathy, Rhonda and Brenda, I could continue. You all have helped me in life or my studies one way or another and I am truly grateful.

I truly did not think I would be here today and a lot of that is because of my friends. They have shown me nothing but support and love and even when we argue, it is

always out of respect. Steph, Mike, Jason, Chris, Cami, Kelly, Iman, Jennifer...you individuals in particular are the greatest friends a silly chemist like myself could have. This thesis would not exist without you pushing me, and I may even not be on this earth today if I didn't have you people in my life. Love you all.

Lastly, this thesis is dedicated to my late mother Grace Pleizier. She was removed from my life in March 16th, 2017 from a long fight with cancer. If there is one thing she taught me, it's perseverance. She surpassed her life expectancy two times because knew she couldn't leave yet. I know she is proud of everything I have achieved and is excited to watch my defense from above. I promised her on her hospital bed that I would get my Ph.D. and be the best dang organic chemist out there. This is my first step to that promise. Will always love and miss you mom.

Table of Contents

List of Tables

Chapter 1

Chapter 2

Chapter 3

List of Figures

Chapter 1

Chapter 2

List of Schemes

Chapter 1

List of Abbreviations and Symbols

2D	two dimensional
A	hydrogen bond acceptor
α	hydrogen bond donor properties
Ac_2O	acetic anhydride
Å	angstrom
Ar	aryl
β	hydrogen bond acceptor properties
BArF	tetrakis(3,5-bis(trifluoromethyl)phenyl)borate
Boc	tert-butoxycarbonyl
BPh_4	tetraphenylborate
^tBuOH	tert-butanol
BzCl	benzoyl chloride
CO_2Et	ethyl ester
COMe	acetyl
d	doublet
dd	doublet of doublets
D	hydrogen bond donor
DABCO	1,4-diazabicyclo[2.2.2]octane
DAP	diaminopyridinium
DCC	*N*,*N*'-dicyclohexylcarbodiimide
DCM	dichloromethane
δ	chemical shift
Δ	heat
ΔG	free energy
$\Delta\Delta G$	free energy difference
DMAP	4-dimethylaminopyridine

DMF	*N*,*N*'-dimethylformamide
DMSO	dimethylsulfoxide
DMSO-d_6	deuterated dimethylsulfoxide
DNA	deoxyribonucleic acid
DOP	degree of polymerization
DPPA	diphenylphosphoryl azide
E	entgegen or *trans*
Et	ethyl
Et_2O	diethyl ether
EtOAc	ethyl acetate
HRMS(EI)	Electron Impact Ionization High Resolution Mass Spectrometry
eq.	equivalent
g	grams
G	guest
hν	wavelength
Hz	hertz
H	host
mCPBA	meta-chloroperbenzoic acid
MHz	megahertz
MeOH	methanol
IR	infrared
IUPAC	International Union of Pure and Applied Chemistry
ITC	isothermal titration calorimetry
K	Kelvin
K_a	association constant
kcal	kilocalories
kJ	kiloJoules
$K_{t\cdot t}$	*trans-trans* complexation constant

K_{taut}	tautomerization constant
λ	wavelength
LCE	liquid crystal elastomer
LFER	linear free energy relationship
log	logarithm
M	minus-handed helicity
m	multiplet
Me	methyl
m.p.	melting point
M^{-1}	per molar
min	minutes
mL	milliliters
μL	microliters
μM	micromolar
mmol	millimole
mol^{-1}	per mole
NBS	*N*-bromosuccinimide
NCS	*N*-chlorosuccinimide
NEt_3	triethylamine
NIS	*N*-iodosuccinimide
NMF	*N*-methylformamide
NMR	Nuclear Magnetic Resonance
NOESY	Nuclear Overhauser Effect Spectroscopy
ºC	degrees Celsius
OMe	methoxide
P	plus-handed helicity
PAP	2,2'-azopyridine
$Pd(OAc)_2$	palladium (II) diacetate

$PhI(OAc)_2$	(diacetoxyiodo)benzene
π	pi orbital
Pg	protecting group
pH	minus logarithm of proton concentration
ppm	parts per million
n-PrOH	1-propanol
PSS	photostationary State
Py	pyridine
q	quartet
R	correlation coefficient
R_f	retention factor
RT	room temperature
s	singlet
Σ	sum
s-*cis*	"sigma" *cis* isomer
s-*tran*	"sigma" *trans* isomer
σ	Hammett substituent constant
σ_m	substituent constant at meta-position
σ_p	substituent constant at para-position
t	triplet
T	temperature
TBDMS	tert-butyldimethylsilyl
TFA	trifluoracetic acid
TFAA	trifluoroacetic anhydride
THF	tetrahydrofuran
TLC	thin layer chromatography
T_m	melting temperature
TMS	tetramethylsilane

toluene-d_8	deuterated toluene
TsCl	tosyl chloride
TsOH	tosyl acid
UHP	urea hydrogen peroxide adduct
UPLC	ultra performance liquid chromatography
UV	ultraviolet
VDW	van der Waals
Vis	visible light
v.s.	versus
Z	zusammen or *cis*

Chapter 1

1 Introduction

1.1 Supramolecular Polymers

E. W. Meijer is one of the highest regarded synthetic supramolecular chemists of the last 30 years. He and his fellow authors have given a precise definition of supramolecular polymers in 2001:

" *Supramolecular polymers are defined as polymeric arrays of monomeric units that are brought together by reversible and highly directional secondary interactions, resulting in polymeric properties in dilute and concentrated solutions, as well as in the bulk*."[1]

In other words, as typical polymers are mainly governed by the covalent linkages between monomers, monomers or macromonomers for supramolecular networks are held together by non-covalent forces. If these interactions are arranged properly, supramolecular polymers can behave like traditional polymers but with an added aspect of reversibility. Supramolecular monomers contain end groups which can reversibly interact with one another which is why the term "*smart* materials" has also been given to these types of materials. These end groups can self-assemble and dissociate when exposed to external stimuli of three different classifications: Physical (e.g. light),[2] Chemical (e.g. pH),[3] and Biochemical (e.g. enzymatic).[4]

1.2 Types of Supramolecular Polymers

When considering supramolecular polymer synthesis, there are 5 main scaffolds these materials can resemble.[5] An XX-type monomer utilizes a self-complementary

homo-dimerization which is common in hydrogen bonded polymers.[6] A complementary heterodimer is an XY-type which binds end to tail.[7] XX/YY-type are homoditopic monomers and complementary in structure which bind in an alternating manner.[8] The XY-type and XX/YY-type are the most commonly used monomers to construct supramolecular assemblies. Two less common examples are XYYX-type[9] and aromatic donor-acceptor type.[10] Aromatic donor-acceptor types are usually too weak to involve π-stacking on their own so other interactions are also used to help drive polymerization (ex. dipole-dipole, hydrogen bonding, etc). A variety of first three types will be explored in this dissertation.

1.3 Intermolecular Interactions

Jean-Marie Lehn's description of "*chemistry beyond the molecule*" for supramolecular chemistry is possible due to intermolecular interactions.[11] These interactions are intermolecular for supramolecular polymerization but can also occur intramolecularly for some examples. Non-covalent, supramolecular, and reversible interactions can all be used as a labels for these forces. Table 1.1 lists these interactions with ranges of respective energies which can vary from 0 to as high as 300 kJ/mol.[12]

Table 2.1 Types of molecular interactions with respective strengths, examples, and directionalities.

Molecular Interaction	Strength (kJ/mol)	Example	Directionality
Ion - Ion	200 - 300	TBAF	Low
Ion - Dipole	50 - 200	Na^+ - [15]crown-5	Medium
Dipole - Dipole	5 - 50	Acetone	Medium
Hydrogen Bonding	4 - 120	Water	Medium
Cation - π	5 - 180	K^+ - Benzene	Medium
π - π	0 - 50	Benzene - Hexafluorobenzene	Medium
van der Waals	< 5	Noble gases within crystal lattices	Low
Hydrophobic/Solvophobic	Related to solvent media	Cyclodextrins	Low

These interactions are important for constructing supramolecular systems but are also important in nature and biology. Water has a high surface tension and boiling point due to hydrogen bonding and hydrocarbon boiling points are related to their van der Waals surface areas. Arguably, the most important biological macromolecule structure is DNA and was structurally elucidated by Watson and Crick.[13] Base pairs are hydrogen bonded together along with π-stacking interactions which is all covalently bound to an anionically charged phosphate backbone to assist in charge balance and hydrophilicity (Figure 1.1). Proteins can form multiple simple and complex macromolecular assemblies which are all attributed to

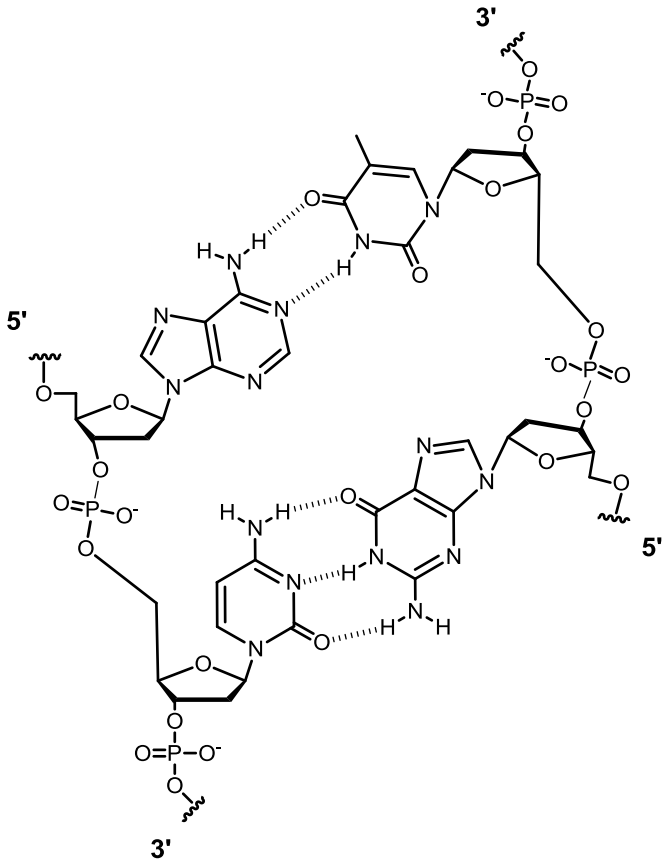

Figure 2.1 Complementary purine-pyrimidine base pairing within the DNA double helix.

interactions between amino acid side chains and amide hydrogen bonding between strands (ex. α-helices and β-pleated sheets).[14] Enzymatic processes are also highly dependent on these interactions. Emil Fischer coined the term "lock and key" for enzymes where the substrate and enzyme interact with one another to initiate a chemical transformation.[15] A good example is the enzyme chymotrypsin where cleavage at the C terminus of hydrophobic residues occurs because of a "hydrophobic pocket" next to the active site.[16] Hydrogen bonding plays a major role in many biological processes and

therefore holds a central position in the construction of supramolecular synthons because of their relative directionality and reversibility.

1.4 Hydrogen Bonding

Hydrogen bonding is an interaction classified on its own but can also be considered a dipole-dipole interaction. The IUPAC definition states that *the hydrogen bond is an attractive interaction between a hydrogen atom from a molecule or a molecular fragment **D-H** in which **D** is more electronegative than **H**, and an atom or group of atoms in the same or a different molecule (**A**), in which there is evidence of bond formation.*[17] Therefore, the electronegativity of D inductively makes the hydrogen atom electropositive in nature where then a lone pair of a different nearby electronegative atom can interact through space creating a "hydrogen bond" (Scheme 1.1)

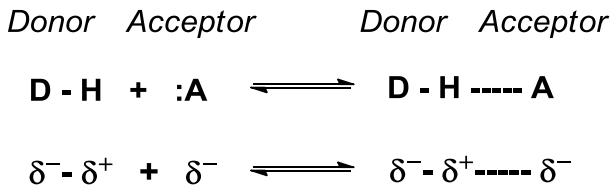

Scheme 2.1 Hydrogen bonded interaction between a donor (**D-H**) and acceptor (**A**) with a depiction of their relative dipoles.

There are two main classification methods for hydrogen bonding. The first is based on the relative strength of the binding pairs. Table 1.2 outlines these strengths, factors which affect said strength, and some typical quantitative outcomes.

Table 1.2 Strengths of Hydrogen Bonds and outcomes of those bonds.[18]

	Very Strong or Strong	**Strong to Moderate**	**Weak**
Bond Energy (kJ/mol)	60 - 170	15 - 60	< 15
Interaction Type	Strongly "Covalent"	Mainly Electrostatic	Electrostatic/Dispersed
Directionality	High	Moderate	Weak
D (D-H···A) (Å)	2.2 - 2.5	2.5 - 3.0	> 3.0
Θ (D-H···A) (°)	175 - 180	130 -180	90 - 180
Effect on Crystal Packing	Strong	Distinctive	Variable
Typical ^{1}H Chemical Shifts (ppm)	14 - 22	< 14	-
Example	$[N\cdots H\cdots N]^-$	O-H···O=C	O-H···π

This table is a broad classification but there are typical factors displayed which are evident in all hydrogen bonded complexes. The bond energies are higher when the hydrogen bonding distance are short (< 2.5 Å) and the angle taken up by the three binding atoms are as close to 180^o as structurally possible.[18,19a,b] This angle is dependent on the surface potentials of the functional groups involved where the energy maxima are at their highest (Figure 1.2).

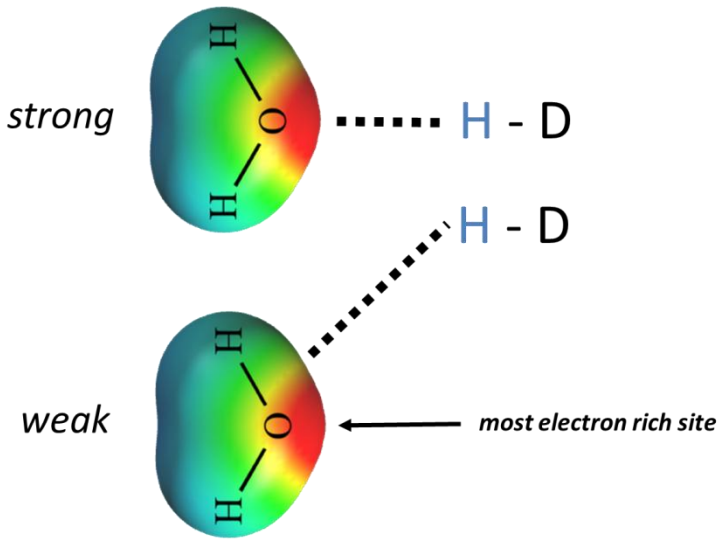

Figure 1.2 Hydrogen bonding displayed with two water molecules. The strong hydrogen bond (above) has the optimal 180° angle as the electrostatic surface potentials are maximized in dipole pairs. Red surfaces represents electron rich areas and blue surfaces and H atoms electron poor areas.

There are four main properties of intermolecular interactions to take into consideration when evaluating binding strengths due to hydrogen bonding: repulsion, induction, dispersion and electrostatics. The first three properties do not contribute a lot to hydrogen bond complexation so Hunter developed a set of parameters based on electrostatic surface potentials.[20] Expanding on the work of Abraham,[21a,b] in 2004 Hunter defined two variables α and β.

$$\alpha = E_{max}/52 \text{ kJ/mol} = 4.1(\alpha_2^H + 0.33) \qquad \beta = E_{max}/52 \text{ kJ/mol} = 10.3(\beta_2^H + 0.06)$$

α defines hydrogen bonding donor strength and β hydrogen bonding acceptor strength. α_2^H and β_2^H are variables developed by Abraham which relate the log K of interacting functional groups which are free energy related. E_{max} and E_{min} are the maxima and minima of electrostatic surface potentials determined from AM1 calculations. Hunter

created scatter plots of Abraham's variables against *E* values and the slopes of the linear regressions assisted in forming the 52 kJ/mol normalization constant. These two equations provide methods for calculating α and β. If α_2^{H} and β_2^{H} have previously been determined, they can be directly used in the equations. Conversely, if α_2^{H} and β_2^{H} are not known, α and β can be estimated by calculating the electrostatic surface potentials. These new parameters have effectively been used to estimate binding strengths between two molecules in a variety of solvents.[22]

The other method of classification is based on the binding arrangements. Figure 1.3 outlines the most common spatial arrangements observed in the literature. The most favorable being the linear array with an optimal 180^{o} angle. This mode is seen in contiguous linear complementary arrays which results in large association constants. The bent binding pair is not a strong interaction between two different arrays but is a common intramolecular interaction (see section 1.5.4). The remaining arrangements are all a combination of linear and bent binding pairs which create bi- and trifurcated structures which can vary from weak to strong depending on the nature of the participating donors and acceptors.[18,23a,b]

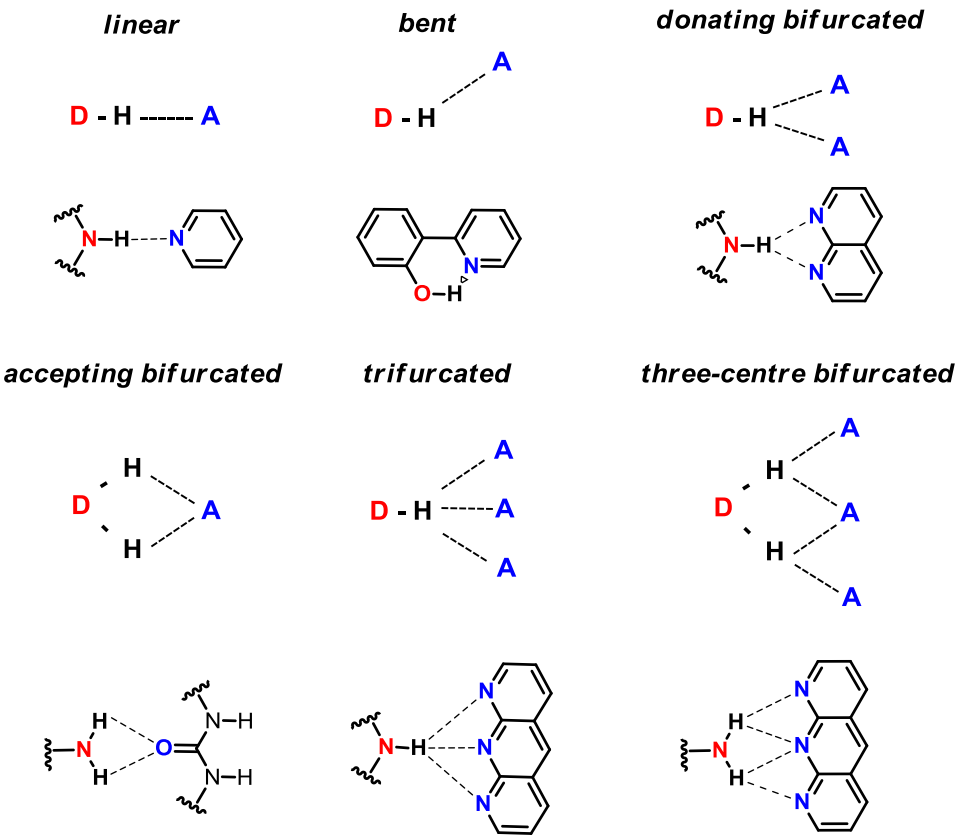

Figure 1.3 Common spatial arrangements of hydrogen bonding interactions with possible structural examples below each classification.

1.5 Factors which effect Hydrogen Bonding Complexes

Hydrogen bonds are extremely useful when creating complexes for potential supramolecular polymers. The directionality and reversibility of these interactions are powerful but there are factors that must be taken into consideration to maximize those qualities. The number of binding pairs, the sequence of those pairs, and how strongly the individual donor and acceptor atoms are polarized are primary features which, when optimized can create very strong hydrogen bonded complexes. Other factors such as

preorganization, tautomerization, and solvent competition can also influence the stabilities of hydrogen bonded complexation.

1.5.1 Number of Binding Pairs

There are two categories of hydrogen bonded complexes: complementary and self-complementary. Complementary complexes contain two different arrays where binding strengths are reported as association constants, K_a. Self-complementary complexes contain a single array where the stabilities are reported as dimerization constants, K_d, as the array spontaneously forms a dimeric complex.

The number of binding pairs in complementary complexes has been shown to be directly correlated to the strength of the complex. Leigh and co-workers have demonstrated this with the popular dihydropyridine donor array.[24] The acceptor **1-2a** contains two contiguous acceptor nitrogens shown in Figure 1.4. The association constant was measured to be 6.0×10^4 M^{-1} with dihydropyridine array **1-1**. The association constant of the same donor array with acceptor **1-2b** was observed to be 2 orders of magnitude greater (7.0×10^6 M^{-1}) as **1-2b** contains an additional pyridine acceptor which adds a linear binding pair.

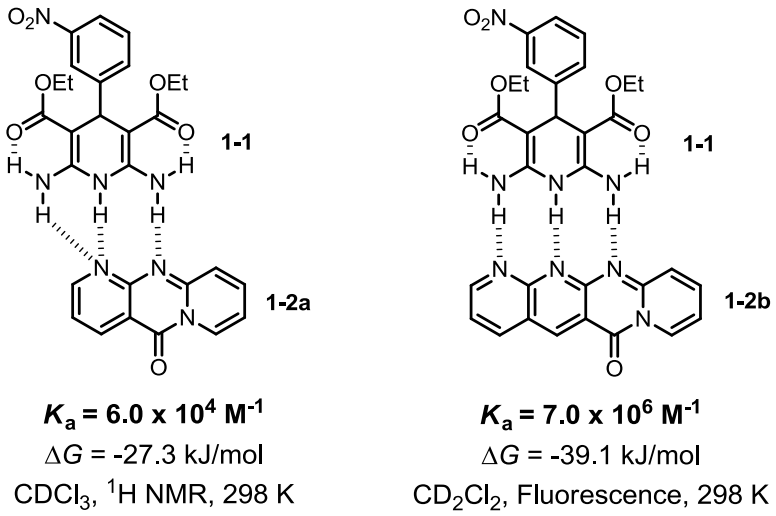

Figure 1.4 Hydrogen bonding complexes examined by Leigh and co-workers demonstrating the importance of multiple binding pairs.

1.5.2 Sequence Dependence of Binding Pairs

Hydrogen bond arrays work cooperatively when they form complexes. Since each donor and acceptor have their own dipole, when the same dipoles are in close proximity to one another, repulsions begin to occur. Conversely, if different dipoles are in close proximity, attractive interactions form. The phenomena are referred to as secondary interactions and have a large effect on complex stability. Figure 1.5 depicts these interactions using 3 triply hydrogen bonded complexes as examples. From left to right, the number of attractive secondary interactions increase as each individual array begins to contain contiguous donors or acceptors. In doing so, the association/dimerization constants also increase.

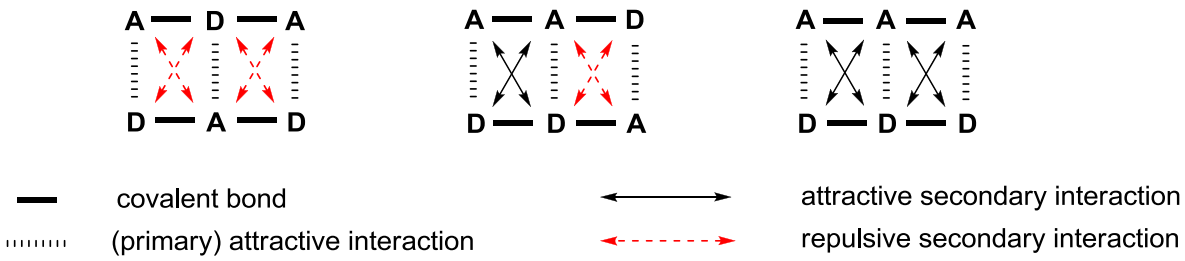

Figure 1.5 Secondary interactions in triply hydrogen bonded complexes.

Sartorious and Scheinder proposed that each primary hydrogen bond contributes 7.9 kJ/mol in free energy of complexation and secondary interactions contribute 2.9 kJ/mol in free energy.[25a,b] If these values are taken into consideration, the complexation stabilities shown in Figure 1.6 follow this trend. Complex **1-3·1-4** has the lower binding constant because half of the secondary interactions are repulsive in nature.[26] The complex with entirely attractive secondary interactions (**1-1·1-2b**) has the higher complexation constant.

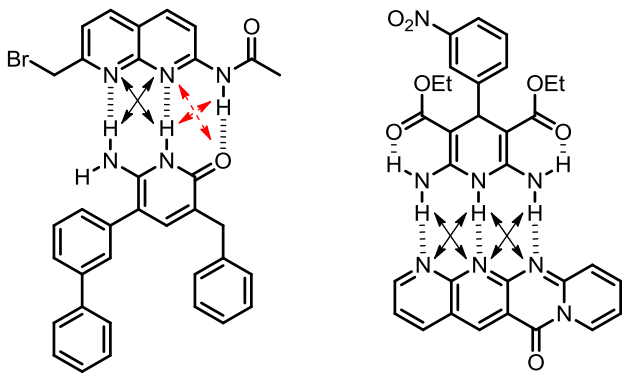

1-3·1-4

K_a = 1.7 x 10^4 M^{-1}

ΔG = -24.1 kJ/mol

1-1·1-2b

K_a = 7.0 x 10^6 M^{-1}

ΔG = -39.1 kJ/mol

Figure 1.6 Two hydrogen bonded complexes depicting their respective secondary interactions and the resulting complex strengths. Red and black arrows represent repulsive and attractive secondary interactions, respectively.

1.5.3 Polarization

Hydrogen bonded arrays can be functionalized with electron withdrawing or donating substituents to improve the resulting complex stability. Withdrawing groups attached to donor arrays increase the electropositive charge on the hydrogen atom. Conversely, electron donating groups incorporated into acceptor arrays increase the partial negative charge on the heteroatom containing the lone pair for binding. Using computational methods, Reynisson and McDonald examined this effect with a single hydrogen bond. Bond strengths of a variety of *para*-substitutued phenols were calculated with a formaldehyde acceptor and as the electron withdrawing capabilities of the phenol substituent increased, the association constant always increased.[27] Plotting the change in binding strength against the Hammett substituents constants (σ values) resulted in a positive, linear correlation (Figure 1.7). Boyd and co-workers also determined binding strengths relative to substituent variations. Again using computational methods,

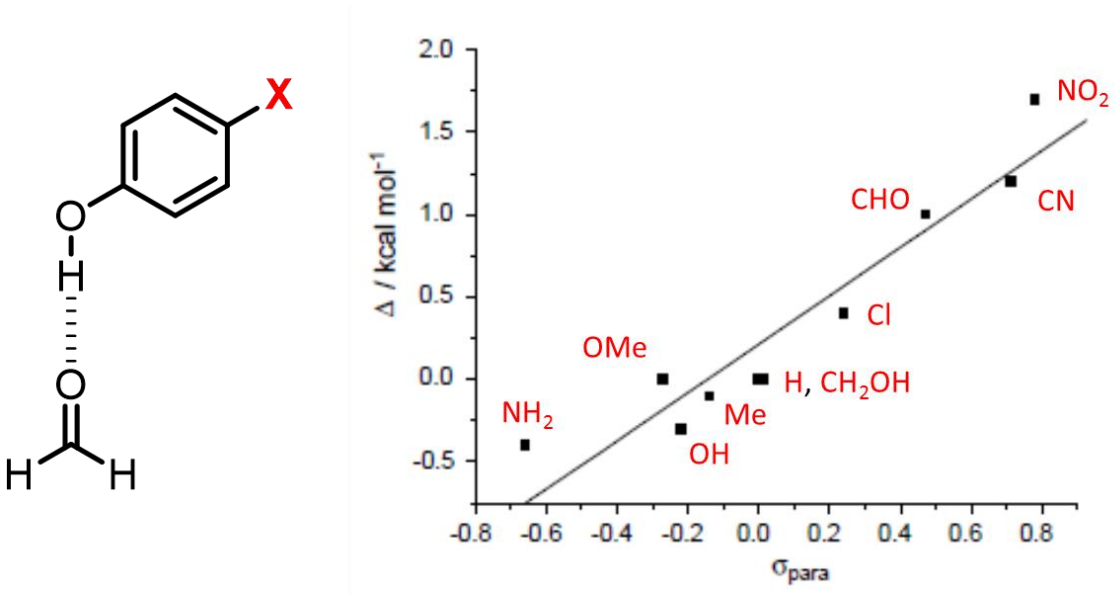

Figure 1.7 Plot of Hammett constants (σ_{para}) corresponding to substituent X on phenol derivatives with the change in binding strength with a formaldehyde acceptor studied by Reynisson and McDonald. Depiction of the singly hydrogen bonded complex is shown on the left.

a triply bonded contiguous array was examined in the gas phase and the same increase of binding strength was observed with stronger withdrawing groups (Figure 1.8).[28]

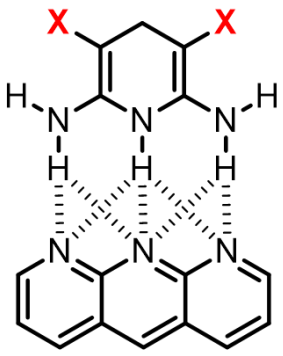

X	Binding Energy (kJ/mol)
NH_2	31.8
OH	32.2
H	32.6
F	35.6
Cl	41.0
CN	66.9
CHO	73.6
NO_2	83.7

Figure 1.8 The gas phase AAA-DDD arrays studied by Boyd and co-workers. Depiction of the complex studied shown on the left with substituents and binding energies compiled to the right.

Our group studied complementary double helical arrays with a variety of substitution patterns.[29] Bis-indolyl-thiazine dioxide hydrogen bond donor arrays were synthesized with a variety of *para*-substituted electron withdrawing groups on the indole relative to the NH. These were titrated with bis-pyridyl lutidine (Z = H) and the association constants ranged from 3.0 x 10^3 to 1.1 x 10^5 M^{-1} (Figure 1.9). Even higher still were the association constants when an amino group was installed in the acceptor array (Z = NH_2) with the highest value reaching 4.8 x 10^5 M^{-1} in $CDCl_3$. In all three examples just discussed, the greatest increase in complexation strength arose from withdrawing groups with added resonance as opposed to only inductive effects.

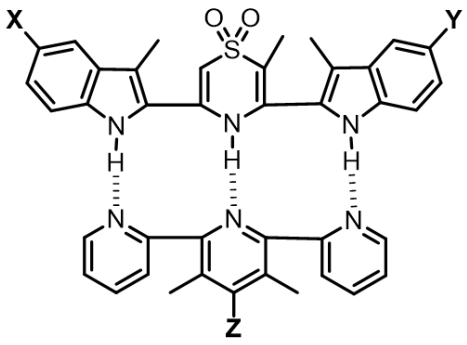

Substituents		K_a Values (M^{-1})	
X	Y	Z = H	Z = NH_2
H	H	3100	11800
Br	H	7000	NA
H	CO_2Et	11000	66000
Br	CO_2Et	26000	NA
H	CN	29000	NA
CN	Br	49000	NA
CO_2Et	CO_2Et	54000	230000
CN	CO_2Et	110000	480000

Figure 1.9 Double helical AAA-DDD complexes studied by Wisner and co-workers. Depiction of the complex shown on the left and the substituents studied with respective association constants are compiled on the right.

The addition of charges is also an efficient method to highly polarize donor or acceptor arrays. For example, diaminopyridinium and guanadinium analogues have resulted in some of the highest association constants measured to date (Figure 1.10).

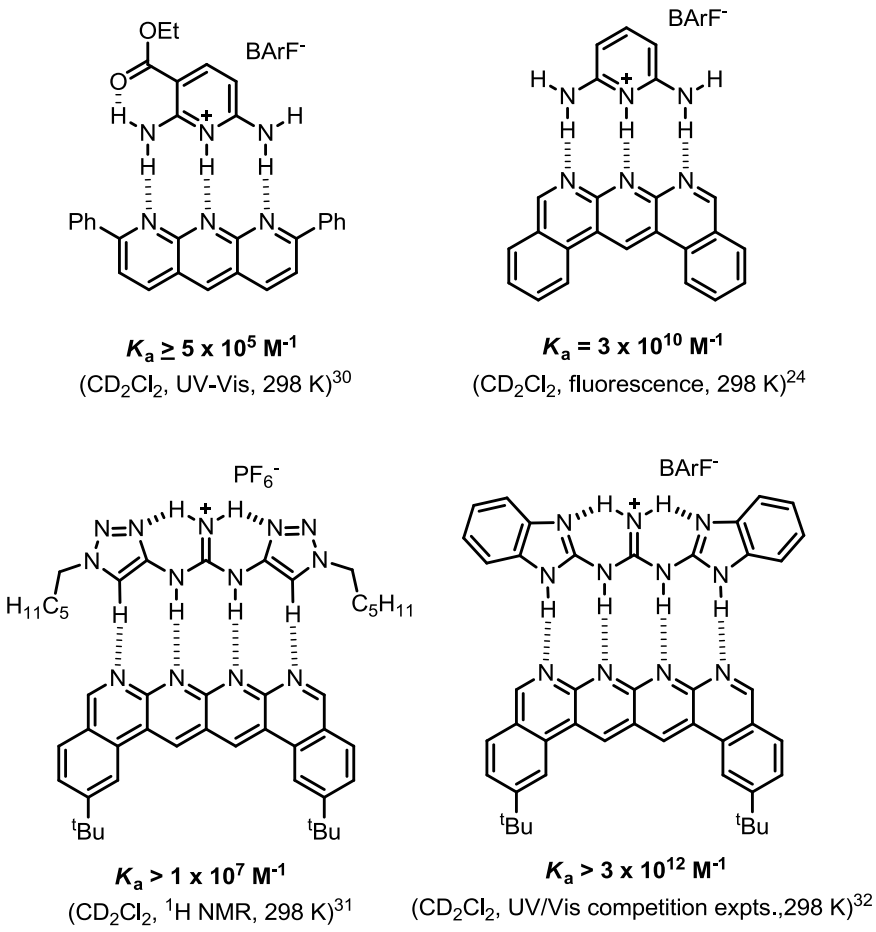

Figure 1.10 Four complementary complexes with extremely high association constants as a result of positively charged donor arrays.

1.5.4 Preorganization

The principle of preorganization was described by Cram and states that the two arrays should be optimally aligned in a low solvation environment for maximum complex stability.[33] The orientation of the interacting groups should therefore be at their optimal binding geometry with little to no position deviation for complex formation. Rotation about these groups around sigma bonds can cause disruptions in the binding arrangements and require additional energy to obtain the proper complex geometry. Zimmerman calculated that each free bond rotation within a host-guest system can cost

approximately 1 kcal/mol in free energy of the complex.[34] Cram and co-workers have extensively studied this preorganization concept with cation complexation to linear and cyclic crown ethers.[35a,b] The acyclic polyether **1-5** in Scheme 1.2 is free to exist in many conformers in solution as it is not preorganized into a macrocycle.

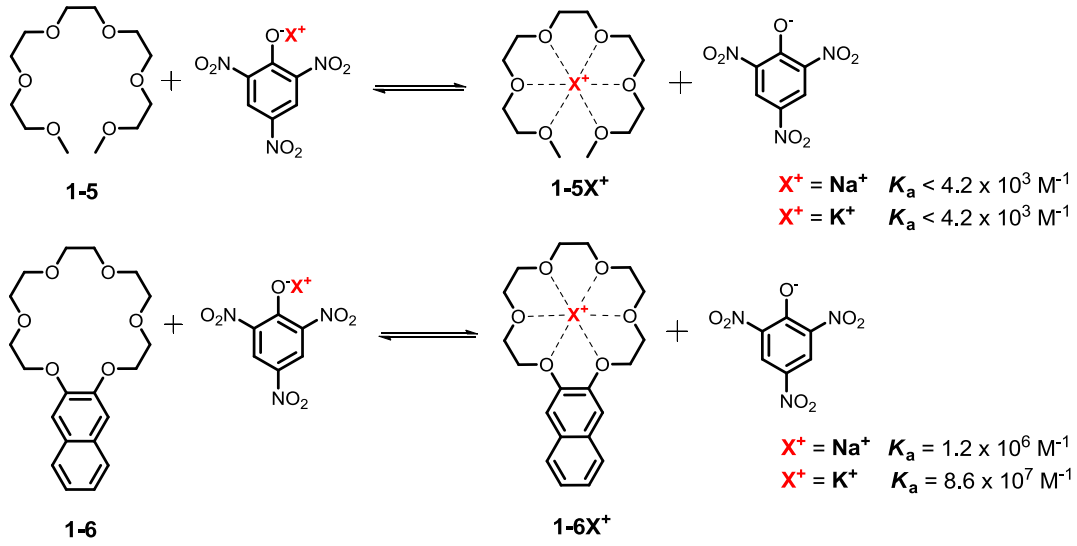

Scheme 1.2 Polyethers studied by Cram and co-workers which demonstrate a stronger affinity to cations when the ether is fused as a macrocycle.

Cram and co-workers determined the association constants with sodium and potassium cations (provided as picrate salts) were chips measured to be a maximum of 4.2 x 10^3 M^{-1}. Polyether **1-6** provided much higher association constants for the same cations, an effect attributed to the ether's fusion to the naphthalene ring. This tethering technique has since been applied to complementary linear arrays[36] and double helical arrays.[37]

Intramolecular hydrogen bonding is also a useful technique for preorganizing binding pairs. In particular, 6-membered intramolecular hydrogen bonding will form in preference over intermoleculer interactionn, as was outlined by Etter.[38] Meijer and co-

workers used this intramolecular hydrogen bonding to their advantage with ADAD self-complementary arrays (Figure 1-11). Array **1-7** contains two amide groups and the complex **1-7·1-7** exhibiting a dimerization constant of 170 M^{-1}.[39] Array **1-8** replaces one side with a ureido group which creates a 6-membered intramolecular hydrogen bond with the nitrogen on pyrimidine, which was able to increase the dimerization constant of the resultant **1-8·1-8** complex by three orders of magnitude to 2.0 x 10^5 M^{-1}.

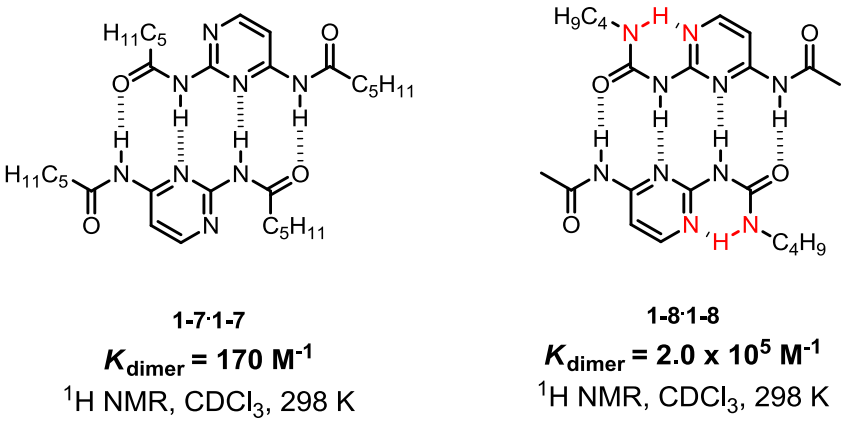

Figure 1.11 Self-complementary dimers studied by Meijer and co-workers. The complex on the right is the stronger complex due to preorganized intramolecular hydrogen bonds which are shown in red.

1.5.5 Tautomerization

Tautomerization is the rearrangement of a molecule usually by a migration of a proton or another atom with the concomitant positions of one or two bonds being altered. The DNA base pairs are known to tautomerize into different protomeric forms which can cause possible DNA mutations.[40] The construction of hydrogen bonded complexes therefore must take this concept into consideration to ensure no disruptions to complexation occur.

Meijer's 6(1*H*)-pyrimidinone (**1-9a**, Scheme 1.3) is a chief example of different protomeric isomers in solution.[41] The ADD array cannot dimerize strongly but the two tautomers can form strong self-complementary complexes. All tautomers contain a different arrangement which all include a strong 6-membered intramolecular hydrogen bond. The pyrimidinol ADAD complex (**1-9b**) was calculated to have a lower limit of 4.5 x 10^5 M^{-1} for dimerization which is the weaker of the two complexes. The other complex of 4(1*H*)-pyrimidinone (**1-9c**) resulted in a dimerization constant of greater than 10^6 M^{-1} because of the AADD arrangement.

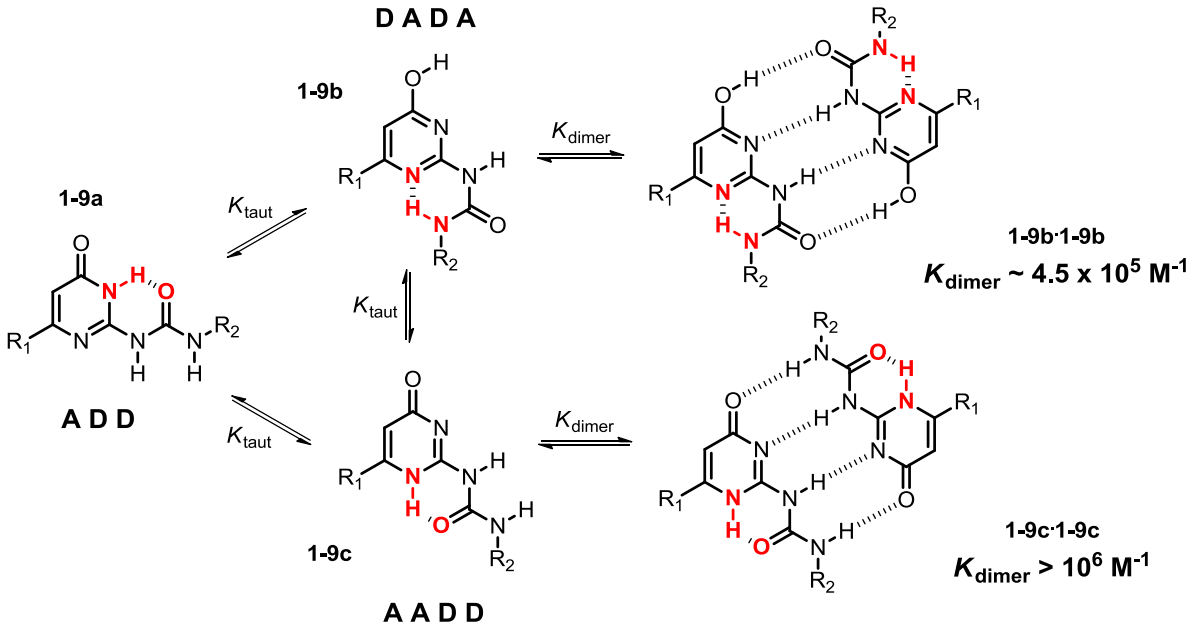

Scheme 1.3 Meijer's 6(1*H*)-pyrimidinone and its respective two tautomeric forms and their resulting complexes. Intramolecular hydrogen bonds are shown in red.

The popular dihydropyridine array is well known to exist in two tautomeric forms. The preferred DDD array exists in the 3,4-dihydro form and the 1,4-dihydro tautomer alters the binding array to a DAD configuration. In $CDCl_3$, array **1-1** exists in

approximately 33:67 for 3,4-dihydro:1,4-dihydro molecular ratios.[42] Zimmerman and Murray found that approximately 10 equivalents of array **1-10** was needed to convert all of **1-1** into the 1,4-dihydro form. The calculated association constant was approximately 10^4 M^{-1} but to account for the tautomers in solution, they estimate the actual association constant to be 10^5 M^{-1} (Scheme 1.4).

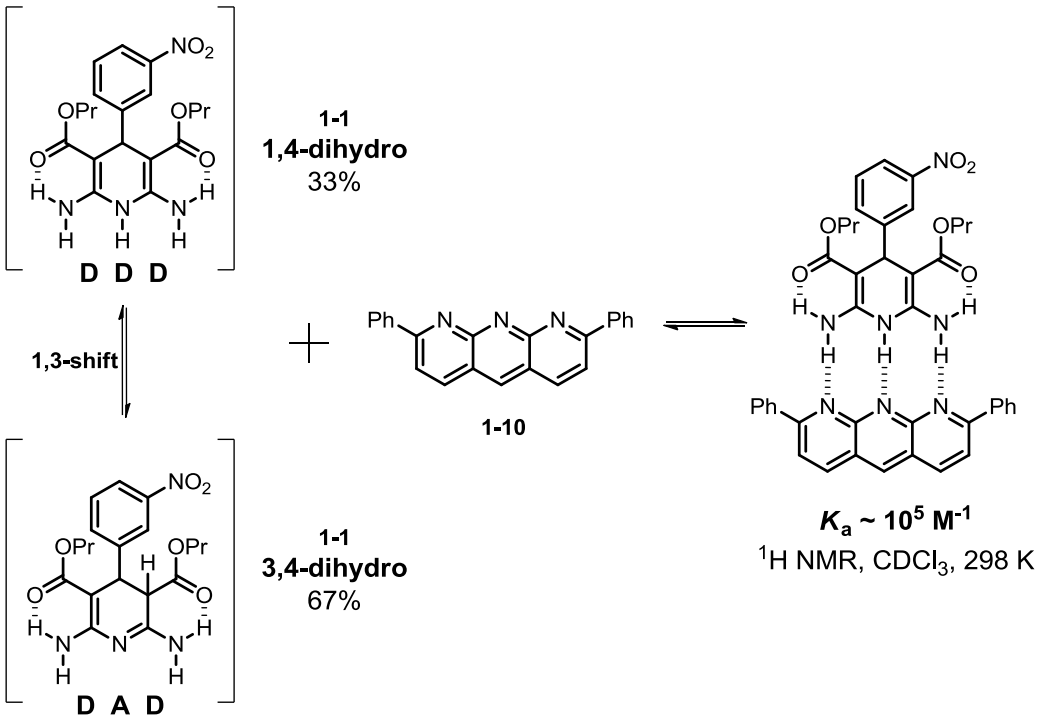

Scheme 1.4 The two tautomeric forms of dihydropyridine array and the resulting complex with a AAA array.

1.5.6 Solvation

Determination of complex strength for hydrogen bonded complexes can be performed computationally and experimentally as previously discussed. Experimental calculations can only be performed if the arrays are dissolved in solution. Supramolecular chemists have to choose carefully when selecting a solvent for complex

measurements as highly polar solvents can disrupt hydrogen bonding between arrays. Therefore, the solute-solute or solvent-solvent interactions must be greater than the solute-solvent interactions (Figure 1.12). The selection

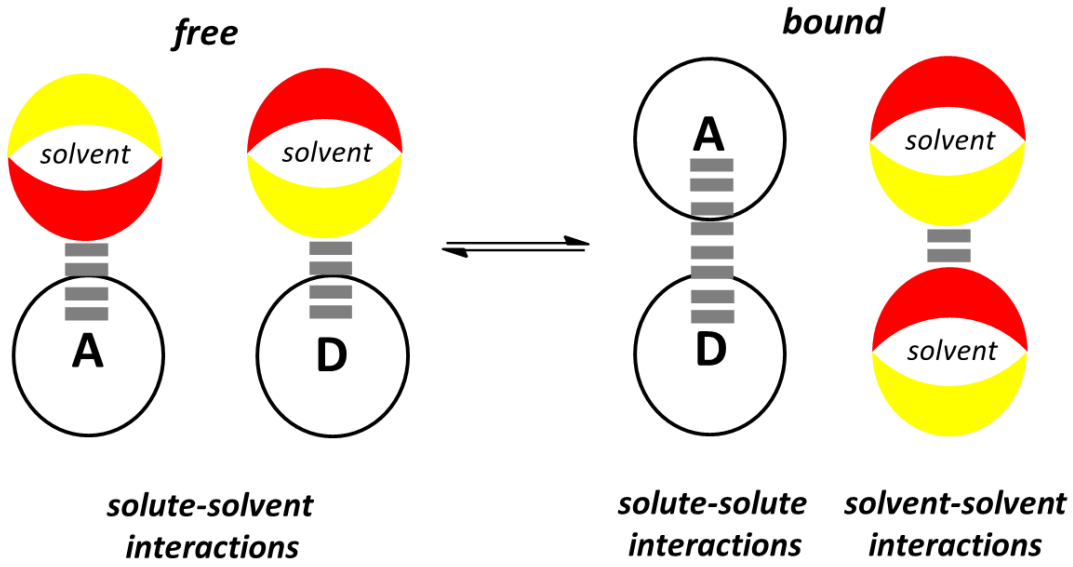

Figure 1.12 The three types of interactions involved in molecular solvation.

of an appropriate solvent can be assisted by using Hunter's hydrogen bonding scale.[20] Figure 1.13 shows 4 quadrants of the solvent and solute interactions where the new parameters shown , α_s and β_s, represent solvent parameters. The grey quadrants represent favorable functional group interactions as $\Delta\Delta G_{\text{H-Bond}}$ is negative ($\Delta\Delta G_{\text{H-Bond}} = -(\alpha-\alpha_s)(\beta-\beta_s) + 6$ kJ/mol). There are methods to overcome solubility issues without sacrificing the integrity of the solute functional groups. Long alkyl chains and fluorine atoms have been proved effective at increasing molecular solubility in organic solvents and will be explored in Chapter 3.[43a,b]

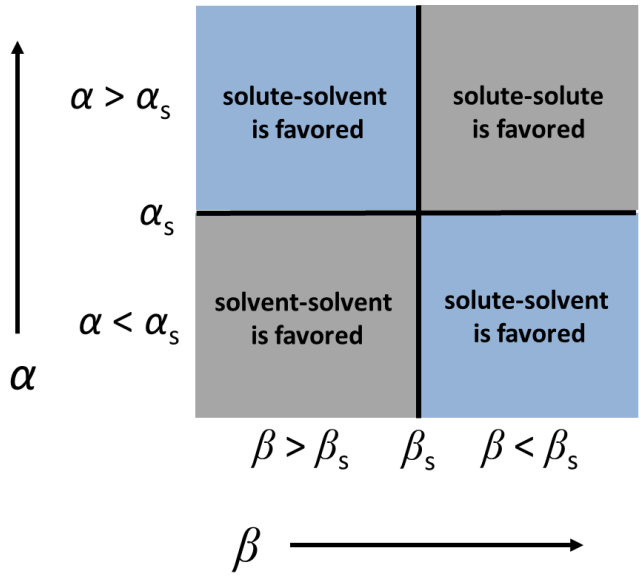

Figure 1.13 Favorable and unfavorable interactions between solvent and solute utilizing Hunter's parameters α and β.

1.6 Photochromism

The simplest definition of photochromism can be explained as a "light-induced reversible change of color". More specifically, photochromism is "a reversible transformation of a chemical species induced in one or both directions by absorption of electromagnetic radiation between two forms having different absorption spectra".[44] Species A is the thermodynamically stable photochromic entity and can be transformed into species B via irradiation (Figure 1.14). Species B can return to species A either by a photochemical process (type P) or thermally (type T). These two (meta)stable species have different absorption spectra but also have different

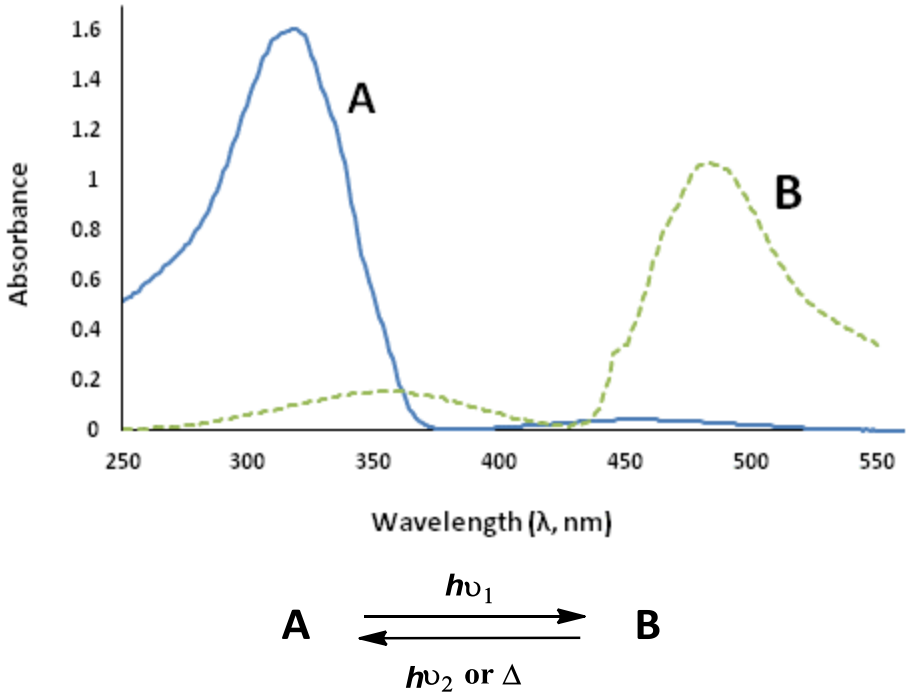

Figure 1.14 Absorbance spectra of molecule A and the absorbance spectra after of molecule B after irradiation.

chemical or physical properties, such as oxidation/reduction potentials, dipole moments, geometric structures, solubility, or refractive indices.[44-46]

Photochromism is an important part of biosynthesis pathways in the human body. For example, vitamin D production in the body requires exposure to UVB light to begin the biosynthetic procedure. 7-Dehydrocholesterol in the skin participates in an intramolecular pericyclic ring opening to previtamin D_3 when exposed to sunlight (Figure 1.15).[47] This previtamin D_3 then participates in an isomerization to vitamin D_3 which is carried to the liver and kidneys to create the active forms of vitamin D. Exposure to too much UVB light can also have negative effects on the skin, such as DNA damage

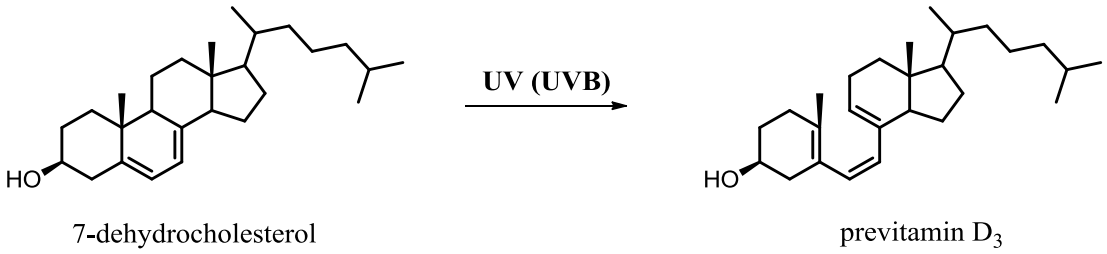

7-dehydrocholesterol previtamin D_3

Figure 1.15 Previtamin D_3**,** a precursor to vitamin D which is a result of 7-dehydrocholestrol reacting with UVB light.

between neighboring thymine or cytosine base pairs. Photocyclization occurs between these pairings creating dimers which disrupt the complementarity with the other DNA strand.[48] These dimers are usually corrected quickly in the body but if left uncorrected, DNA replication can be faulty which can lead to mutations and melanoma.

1.7 Families

Photochromic entities have become increasingly popular in the material sciences and polymer sectors of research.[49] There are certain requirements which should be fulfilled for potential photochromic applications:

1. thermal stability of both isomers

2. fatigue-resistant properties

3. high sensitivity

4. rapid responses

5. reactivity in the solid state

There are multiple families of photochromic compounds where each grouping results in an alternate photochromic process with light.[44] Schemes 1.5 to 1.8 outline some of these families where in each case $h\upsilon_2 > h\upsilon_1$.

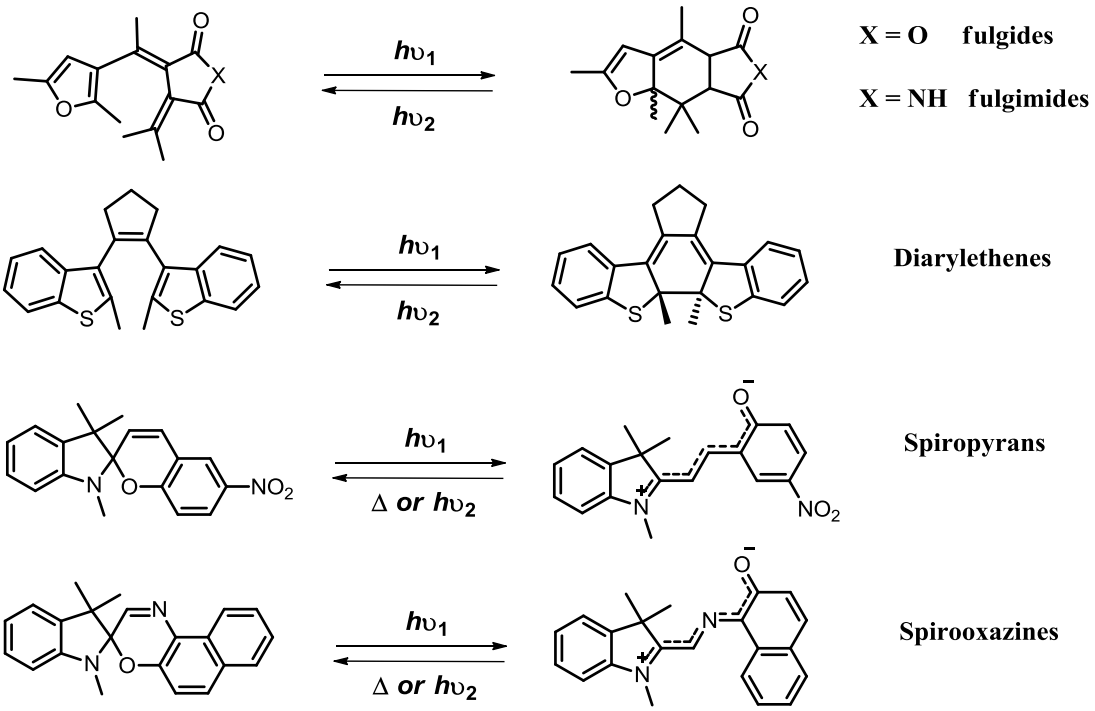

Scheme 1.5 Examples of photoswitches where isomerization occurs via intramolecular pericyclic processes.

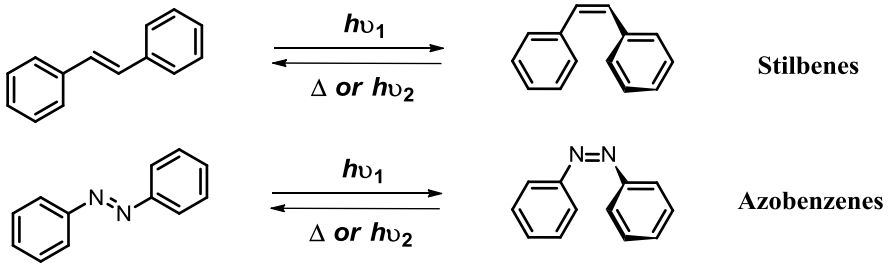

Scheme 1.6 Examples of photoswitches where isomerization occurs via *trans*/*cis* (*E*/*Z*) processes.

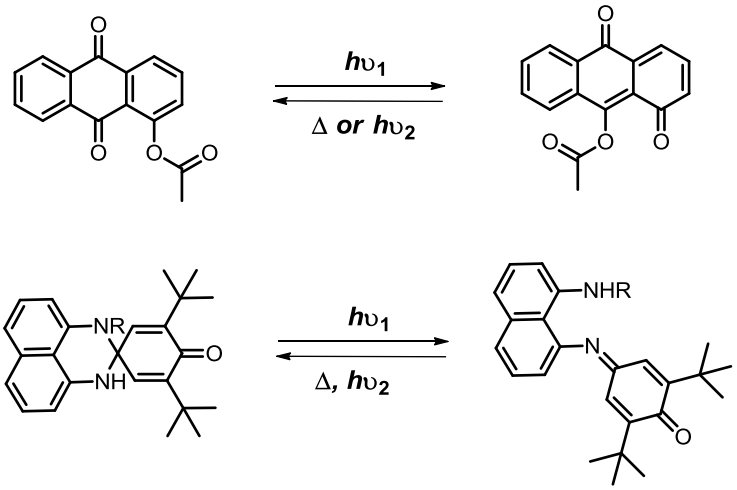

Scheme 1.7 Isomerization by intramolecular group transfer of a polycyclic quinone (above) and a perimidinespirocyclohexadienone (below).

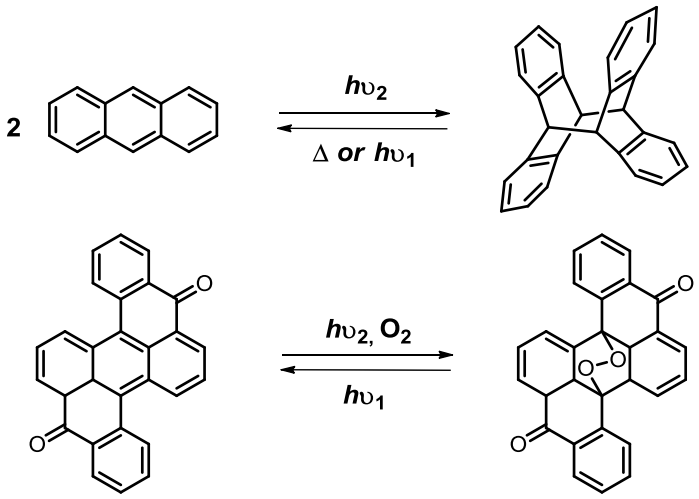

Scheme 1.8 Examples of photoswitches where isomerization occurs via intermolecular pericyclic processes.

Stilbenes are one of the more extensively studied of these photochromic compounds. The *E*/*Z* isomerization allows for a spatial rearrangement of the groups attached to the central double bond which often creates a large physical or chemical change between isomers. The photoswitchable C=C double bond has since been

incorporated onto other scaffolds creating "stilbene type" photoswitches (Scheme 1.9). The azo moiety (-N=N-) has also been extensively studied and will be discussed in detail later in this chapter.

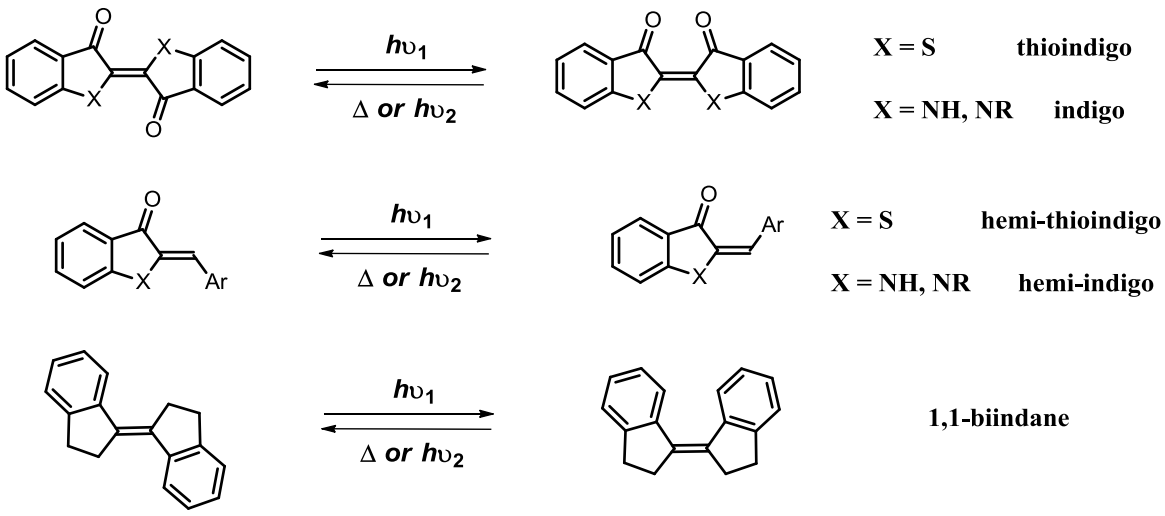

Scheme 1.9 Examples of "stilbene" type photoswitches which participate in *E*/*Z* isomerization.[50-52]

Diarylethenes are also extremely popular photoswitches as the closed isomeric form is stable and requires irradiation to re-open the molecule. These P type switches, as are fulgides and fulgamides, have been modified in countless ways to fine tune their photochromic responses. Diarylethenes have been synthesized to elicit almost every color possible[53] as well as found uses for living cell imaging[54] and anion sensing (Figure 1.16).[55]

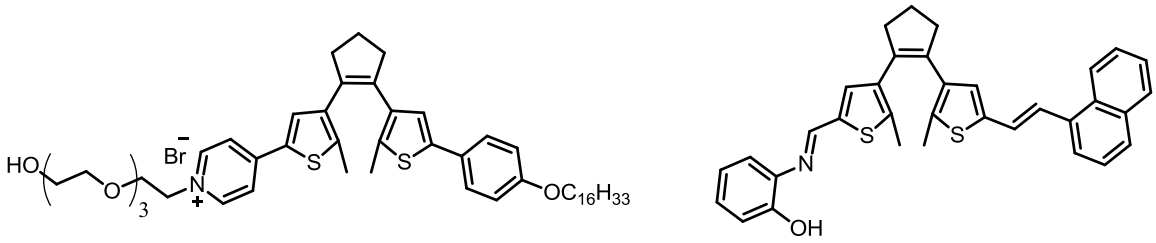

Figure 1.16 Diarylethene derivatives used in live cell imaging (left) and anion sensing (right).

1.8 Photodegradation and Fatigue Resistance

The use of light as an external stimulus is considered a non-invasive technique. In other words, no other chemical entities are entered into the system. However, photochromism usually involves an excited state form of the photoswitch or a highly reactive intermediate. These excited state entities can undergo side reactions, or photodegradation of the substrates. "*The loss of performance over time, due to chemical degradation of a material, is termed fatigue*".[44] The main culprit for chemical damage is molecular oxygen, either incorporating itself into the molecule or performing oxidation reactions.

If oxygen is not removed from the photochromic process of synthesizing *cis*-stilbene, ring closure can occur. When *cis*-stilbene is continuously irradiated, a cyclization to the dihydrophenanthrene intermediate forms (Scheme 1.10). This intermediate is unstable and can revert back to *cis*-stilbene relatively easy and quickly but oxygen will aromatize that precursor to phenanthrene which cannot be converted back to stilbene.[56]

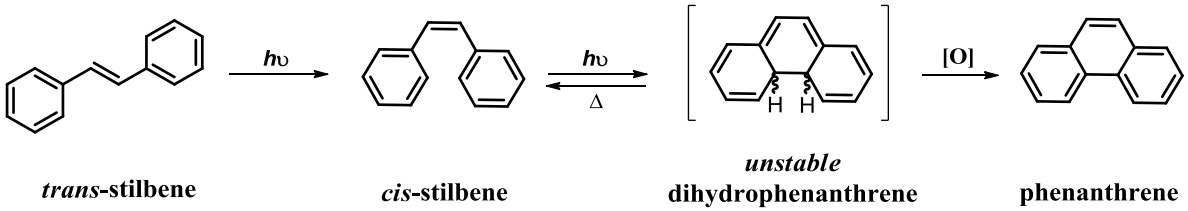

Scheme 1.10 Synthesis of phenanthrene via continuous irradiation of stilbene.

Spirooxazines and spiropyrans have been shown to be very reactive with molecular oxygen due to more than one possible open isomer form.[57] UV light can create a highly reactive diradical species which can react with molecular oxygen ($^3O_2$) which results in 1-*H*-indolyl-2-one species and tricyclic aromatic byproducts (pathway *A*, Scheme 1.10). If excited state oxygen is present ($^1O_2$), it can react with the more stable open form resulting in indolyl-2-one species and a carbonylated byproduct (pathway *B*, Scheme 1.11).[58]

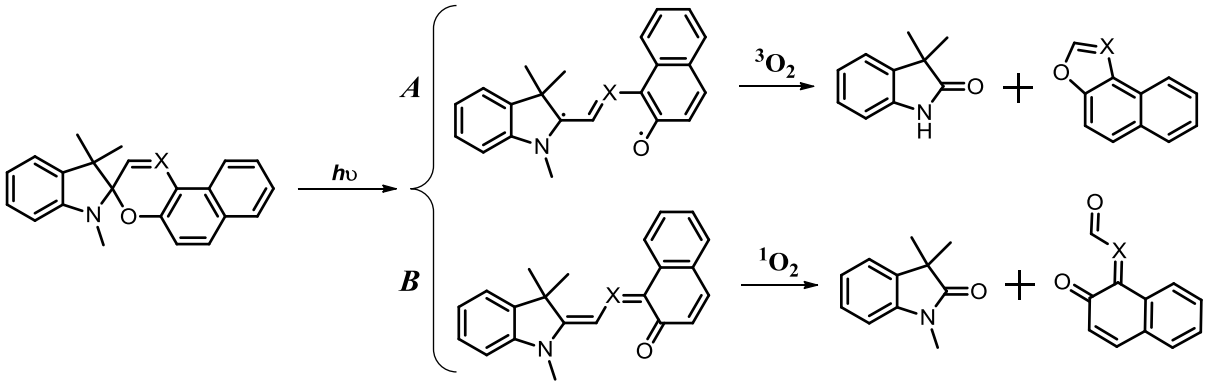

Scheme 1.11 Photodegradation of spirooxazines and spiropyrans with oxygen.

Diarylethenes have been shown to exhibit a high degree of fatigue resistance. Some examples have reached the 10^4 in cycles between open and closed states.[58] On the

other hand, some diarylethene examples are not impervious to by-product formation. If the ring-closed isomer is continuously irradiated, a 1,2-dyotropic rearrangement can occur (Scheme 1.12).[59] This annulated by-product cannot participate in the reverse reaction and is usually detected via UPLC.

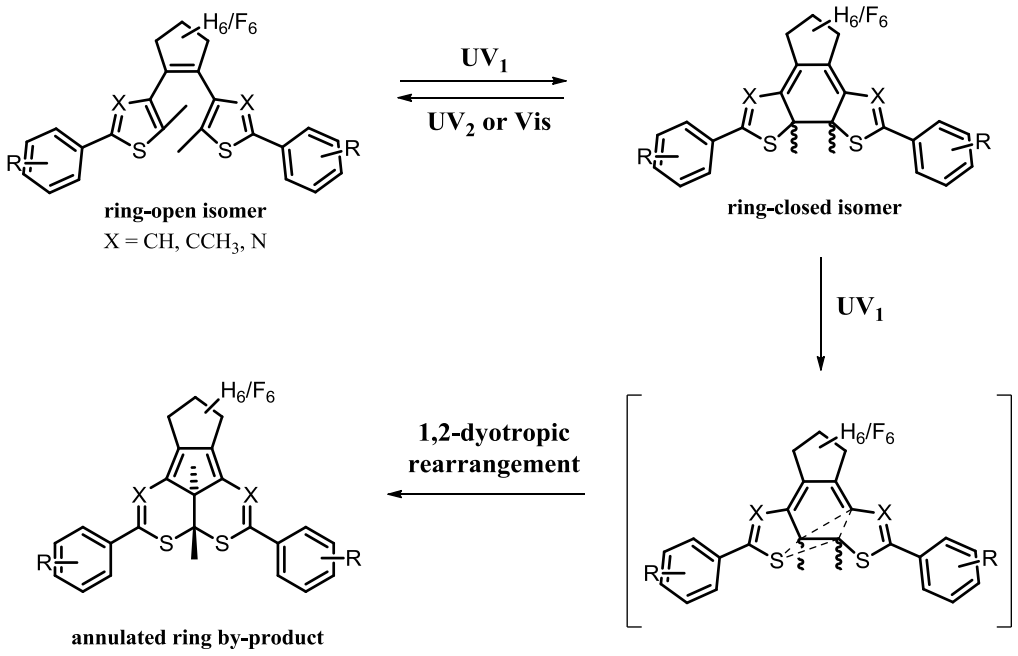

Scheme 1.12 Photodegradation of a diarylethene photoswitch via 1,2-dyotropic rearrangement.

Fatigue-resistant properties are determined by multiple cycles of isomerization. One full cycle is the transformation to one isomer and subsequent transformation to the original form. After each isomerization, the chemical signal being measured (absorbance, fluorescence, NMR signals) is monitored to detect any changes in the signal output. Figure 1.17 depicts two examples of cycling of a photochromic entity. The plot on the left demonstrates a non-fatigue resistant photoswitch as over the ten cycles, the chemical signal being measured begins to increase/decrease depending on the isomer

being examined. The right plot is a fatigue-resistant photoswitch as little to no change in signal output is observed over the ten cycles.

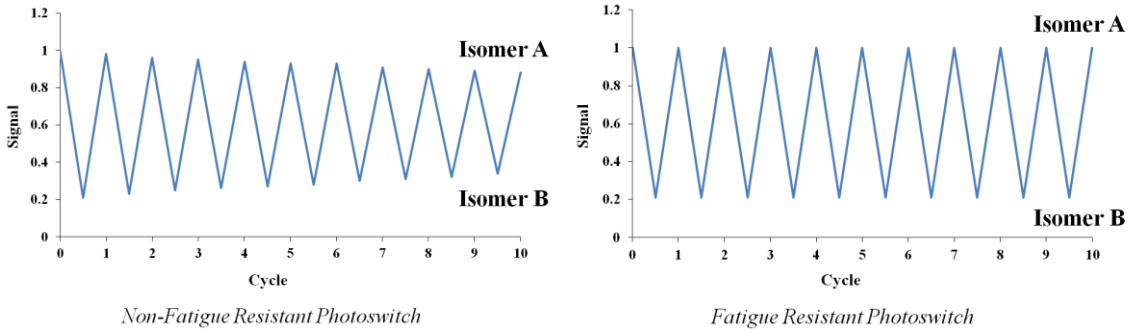

Figure 1.17 Two cycling plots of a non-fatigue resistant photoswitch (left) and a fatigue resistant photoswitch (right).

1.9 Azoaromatic Photoswitches

The *trans*/*cis*, or *E*/*Z*, isomerization of a double bond is one of the more prevalent processes involved in useful molecular switches. Azobenzenes in particular have sparked much interest in this category of photoisomerization. The *E*/*Z* isomerization about the azo moiety (-N=N-) provides a large spatial rearrangement of the aryl groups to which are attached as well as an alteration in the dipole moment (Figure 1.18).[46,60] Typically, the *Z* isomer is formed by irradiation with UV light, and the *E* isomer can be reformed with irradiation at a different wavelength (often visible light) or with heat. A common characteristic of azobenzenes is that both isomers result in two different absorption spectra. These spectra ideally should contain two largely separated λ_{max} values for *E*/*Z* irradiations. There are different classes of azobenzenes for which all typically result in different λ_{max} values.

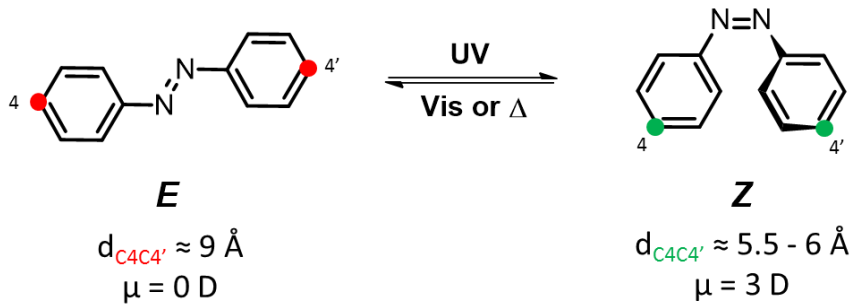

Figure 1.18 Differences between *trans*- and *cis*-azobenzene.

1.9.1 Different Classes of Azobenzenes

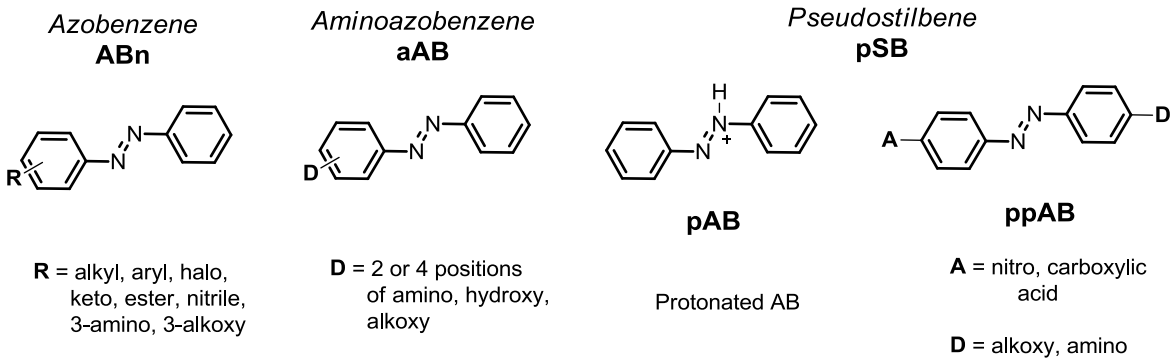

Figure 1.19 Depiction of different classes of azobenzenes.

There are three general classes of azobenzenes for which are characterized by their two main λ_{max} absorption bands.[60,61] The *trans* isomers have a strong absorption typically in the UV region corresponding to the $\pi \rightarrow \pi^*$ transition and a weaker absorption typically in the visible region which is the $n \rightarrow \pi^*$ transition. The *cis* isomers show a decrease in the $\pi \rightarrow \pi^*$ absorption and a subsequent increase in the $n \rightarrow \pi^*$ absorption. These λ_{max} bands differ for each of the classes shown in Figure 1.19:

Azobenzene type: $\pi \rightarrow \pi^*$ band is very strong in UV region and a well separated, smaller $n \rightarrow \pi^*$ band in the visible region. The functional groups listed do not alter these absorption bands as none are very electron-donating or withdrawing. Typically appear yellow.

Aminoazobenzene type: the $\pi \rightarrow \pi^*$ shifts to higher wavelengths which causes a smaller gap between that band and the $n \rightarrow \pi^*$ band. This is due to the electron-donating groups in the 2 or 4 positions. Typically appear orange.

Pseudostilbene Type: the $\pi \rightarrow \pi^*$ is shifted to even higher wavelengths to where both bands are almost degenerate in energy. This family includes protonated azobenzenes and push-pull derivatives. Since the absorption bands are now both in the visible region (red), the *cis* isomers are usually short lived.

1.9.2 Utilizing Azobenzene Isomerization

Hartley was the first to discover the *cis* isomer of azobenzene in 1937.[62] Azo-compounds are typically used as synthetic dyes due to their color but since his discovery, the isomerizations have had a greater focus. The first example of azobenzenes in biochemistry was their use in the inactivation of the enzyme chymotrypsin.[63] Kaufman and co-workers discovered that the *cis* form of *p*-phenylazodiphenylcarbamyl chloride was five times more reactive at inactivating chymotrypsin than the *trans* form.

Azobenzenes have since found their way into other biological macromolecules such as peptides[64] for modulating folding patterns, nucleic acids[65] as photoresponsive "molecular glue", and proteins[66] for regulation of ion channels.

The isomerization of the aryl groups have also been responsible for a number of photoresponsive molecular machines. Tamaoki and co-workers have created a "molecular hinge" utilizing two central azo moieties where the *trans*, *trans* isomer resembles an open hinge and the *cis*, *cis* isomer a closed hinge (Scheme 1.13).[67] Other small machines such as molecular pedals,[68] tweezers,[69] and scissors[70a,b] (Scheme 1.14) have also been characterized. The *E*/*Z* isomerization has also been applied to molecular motions such as lift,[71] nanovehicles/nanoworms,[72] and molecular shuttles.[73]

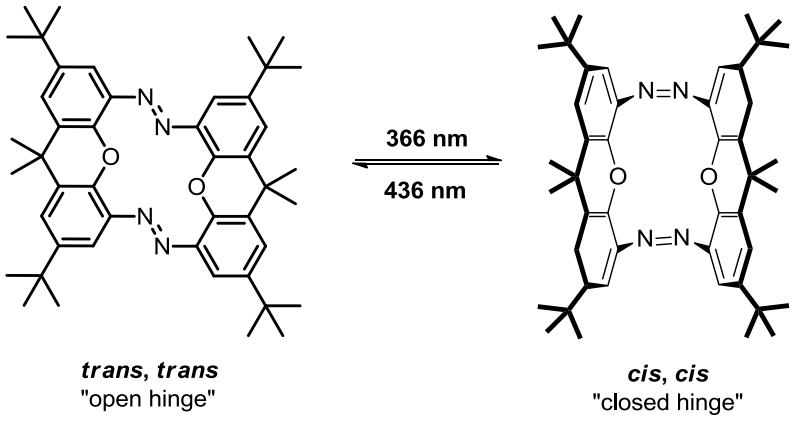

Scheme 1.13 Molecular hinge synthesized by Tamaoki and co-workers.

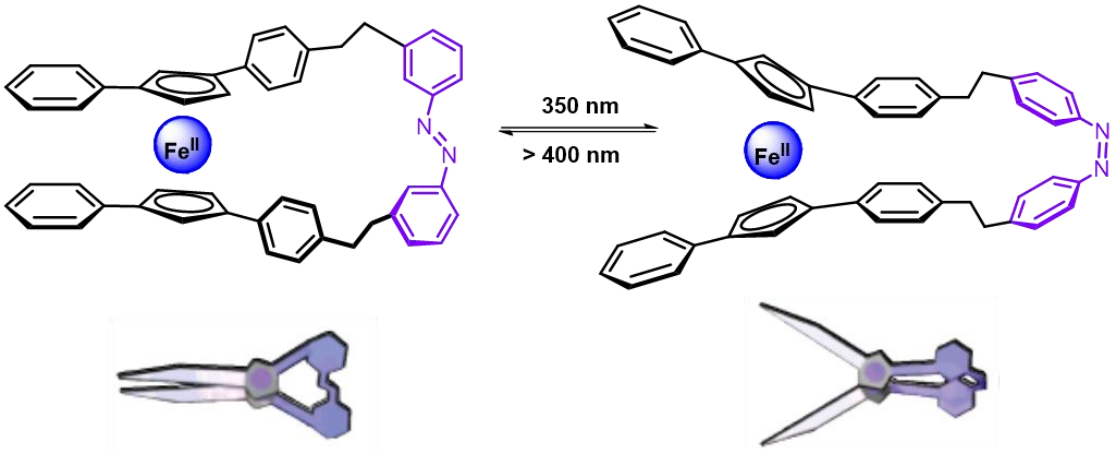

Scheme 1.14 Molecular scissors synthesized by Aida and co-workers.

A standout example of utilizing azobenzene isomerization for movement was reported by Ikeda and coworkers.[74] A liquid-crystal elastomer film (LCE) was synthesized by the polymerization of azo monomer A and cross-linking agent B in a 9:1 ratio (Figure 1.20). The initial state of the LCE is pictured in the top left corner as a flat yellow film. UV light (366 nm) was irradiated onto the LCE where the polarized plane of the light is angled by 0^{o} (the white arrows indicate the plane). The LCE starts the curl up in the plane of the light as a result of the *trans* to *cis* isomerization. Irradiation with visible light (> 540 nm) returned the LCE to the original flat state. Circling in the clockwise motion, each frame depicts a different irradiation of UV light with varying plane polarizations and the return to the flat state with visible light. The same bending upwards motion within the light plane is observed for each trial. The authors explain that this bending upwards motion is a result of volume contraction within specific domains on the surface of the film where the azobenzene units are aligned within the polarized plane of light being used. They were therefore able to turn light energy into mechanical energy utilizing the *trans* to *cis* isomerizations within the material.

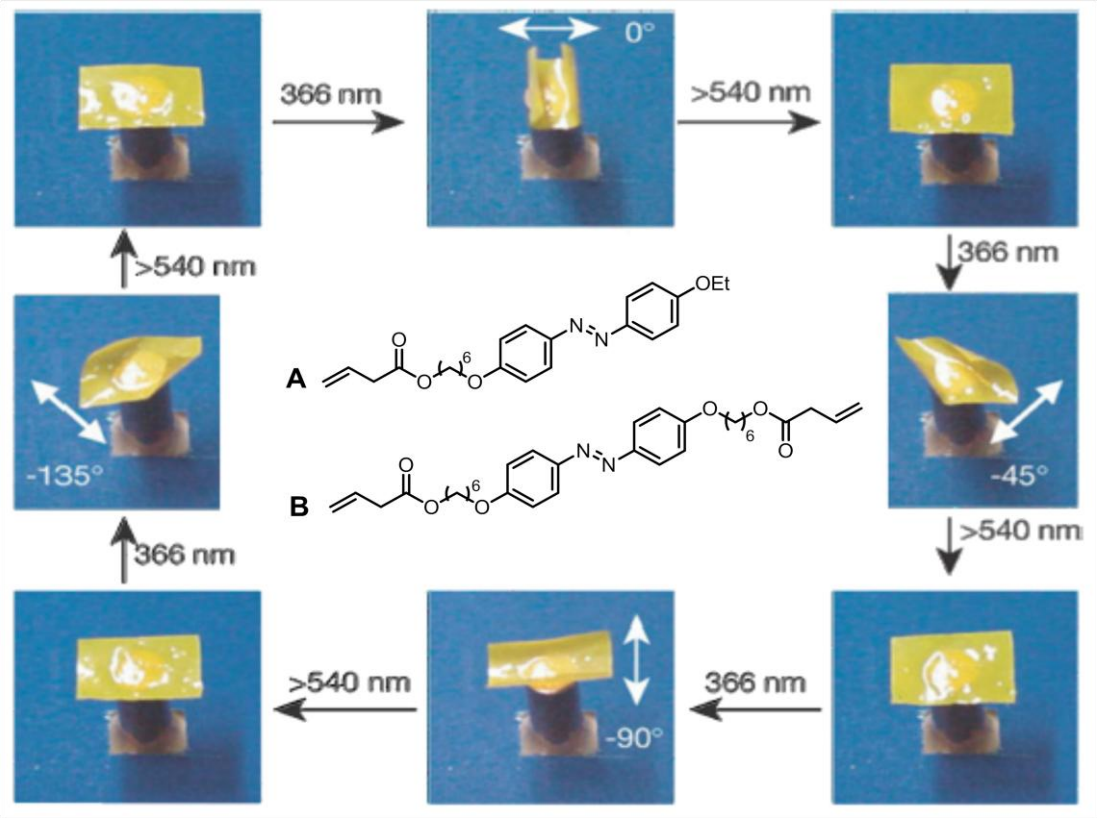

Figure 1.20 Photoresponsive liquid-crystal elastomer synthesized by Ikeda and co-workers. Figure reproduced with permission (License Number: 4446540504167).

1.10 Photocontrollable Self-Assembly

There are 3 main strategies for the effective usage of azo-aromatic compounds in photochromic self-assembly. All 3 strategies utilize the spatial rearrangements caused by the *E*/*Z* isomerization:

1. Attaching non-covalent binding sites to the periphery of the azo moiety.

2. Utilizing the planarity of the *trans* form and causing disruptions in self-assembly upon conversion to the (non-planar) *cis* form.

3. Incorporating an azobenzene moiety in close proximity to a binding site creating a steric block by induced crowding.

The *cis* isomer of azobenzene bears the aryl groups in closer to proximity to one another as opposed to the *trans* isomer. Therefore, if non-covalent binding sites are attached to these groups, a large physical change can be achieved just by their relative position to one another. Shinkai and co-workers have studied ion recognition utilizing this strategy by synthesizing 15-crown-5 moieties on both sides of an azobenzene linker.[75] The *trans* form is unable to encapsulate large cations but in the *cis* form, a 1:1 photoswitch:cation "sandwich" type complex forms (Scheme 1.15). The binding affinity for tested cations were $Rb^+ > Cs^+ > K^+ >> Na^+$. The authors note that these "phototweezers" can be useful in ion transport systems and selective cation extractions.

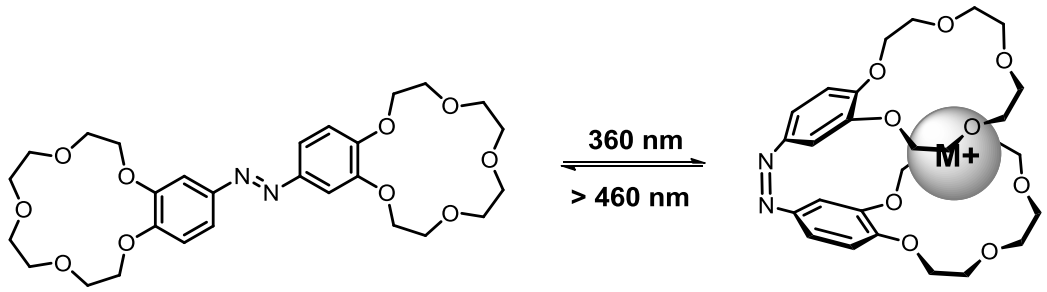

Scheme 1.15 Metal coordinating molecular "phototweezers" synthesized by Shinkai and co-workers.

Hydrogen bonding complexation using this strategy was accomplished by Hunter and co-workers.[76] The *trans-trans* form of a compound containing two azo entities with peripheral carboxylate groups was determined to have an association constant of 2200 M^{-1} with guanidinium hydrochloride in DMSO. The *cis-cis* association constant (for a 33% solution) with the guanidinium cation was measured to be 2.0×10^4 M^{-1} as a results

of the positioning of the carboxylate groups now being in a "claw-like" manner increasing the number of binding sites in contact with the cation (Scheme 1.16).

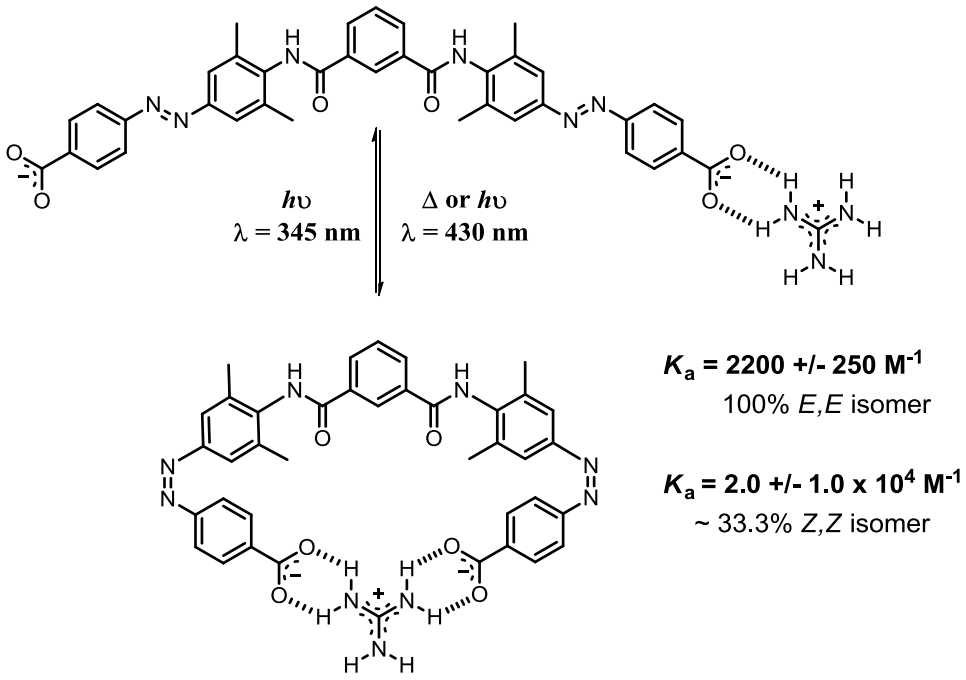

Scheme 1.16 Photoswitchable guanidinium receptor synthesized by Hunter and co-workers.

trans-Azobenzene is a planar and non-polar molecule so it is able to participate in π-stacking interactions. Komiyama and co-workers incorporated azobenzene into an oligonucleotide to examine reversible photoregulation of duplex formation.[77] The modified oligonucleotide 5'-AAAXAAAA-3' where X is the azobenzene side chain was paired with the complement strand 5'-TTTTTTTT-3'. The melting point, T_m, of the resulting duplex was determined to be 24.8 ^oC where after irradiation to *cis*-azobenzene, the T_m dropped by 8.9 ^oC to 15.9 ^oC. Irradiation back to the *trans* form returned the T_m back to the original temperature. The authors attribute these results to the planar *trans*-side chain participating in π-stacking with the adjacent bases with the *cis*-side chain

causing disruption in those interactions due to lack of planarity (Scheme 1.17). This was the first example at the time of successful photoregulation of duplex-forming oligonucleotides.

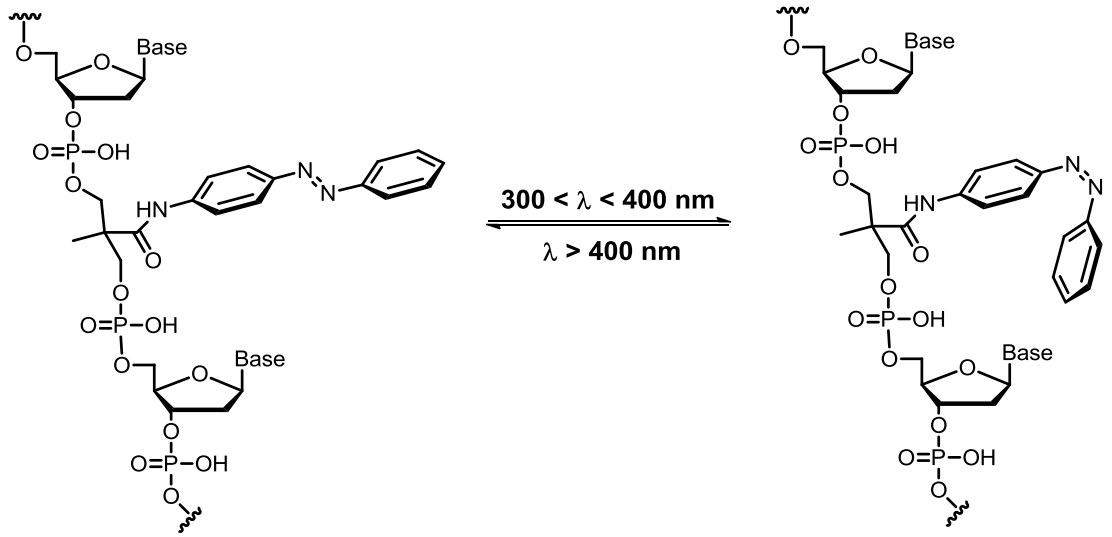

Scheme 1.17 Photoswitchable oligonucleotide synthesized by Komiyama and co-workers.

Aromatic stacking has also been successful in stabilizing host-guest hydrogen bonded complexes. Rotello and co-workers demonstrated this with ADA-DAD complementary arrays.[78] The DAD array comprises a diaminotriazine which has been synthesized in close proximity to an azobenzene group (***trans*-1-11**, Scheme 1.18). This array was then paired with the ADA naphthalenediimide derivative (**1-12**) and the association constant was calculated to be 9750 M^{-1}. Repeating the process with the *cis* form of the DAD array (***cis*-1-11**) resulted in a lower association constant of 575 M^{-1}. The 16-fold decrease in association constant was attributed to the loss of favorable stacking interactions between the *trans*-azobenzene and the naphthalenediimide.

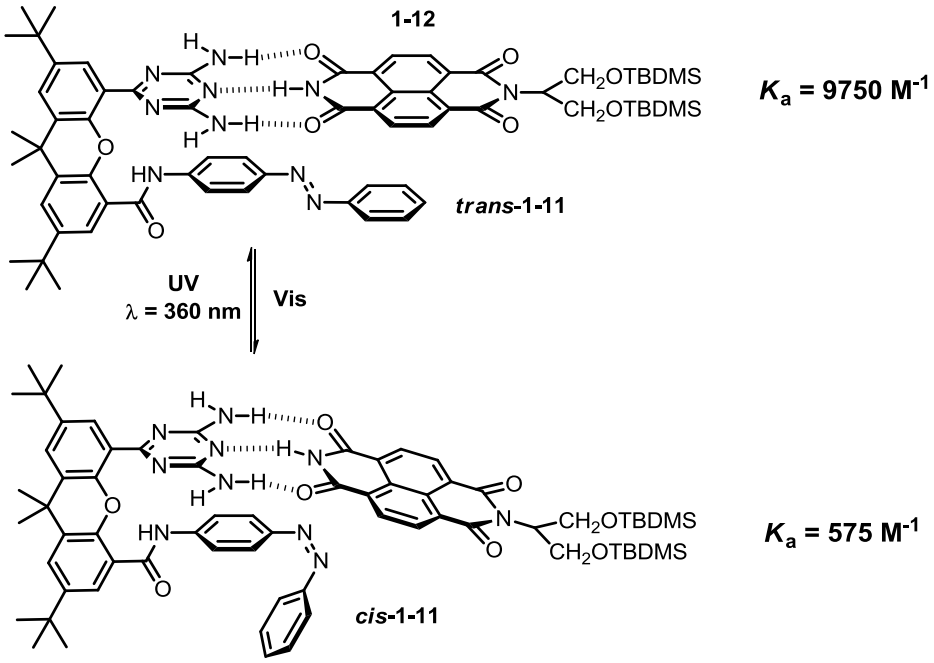

Scheme 1.18 Photoswitchable aromatic stacking host-guest complexes synthesized by Rotello and co-workers.

The movement of the aryl groups during *cis* and *trans* isomerizations allows for the unit to act as a steric block to turn responses "on" or "off". Shibasaki and co-workers used this concept to control hydrogen bonded aggregates of diamides containing an azobenzene group.[79] The amides and phenol groups act as the hydrogen bonding aggregation zone and when the azobenzene substituent is in the *trans* form this aggregation precipitates the diamides in a solution of acetonitrile (Figure 1.21). Isomerization to *cis*-azobenzene then disrupts and blocks the aggregation process and the diamides begin to dissolve. Visible light returns the system back to the original state where precipitation occurs once again. They accomplished this turning "on" and "off" of aggregation 5 times and were successful at photomodulating the precipitation process.

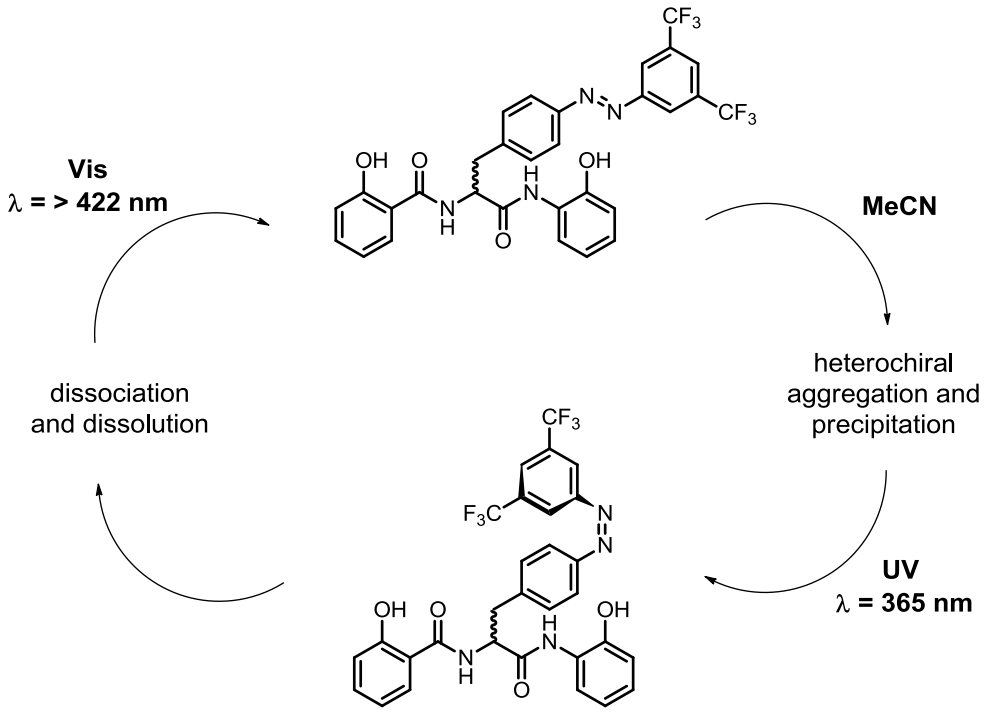

Figure 1.21 Photocontrolled precipitation and dissolution performed by Shibasaki and co-workers.

A hydrogen bonding molecular machine was synthesized by Jeong and co-workers.[80] This pseudoroxatane-based complex utilizes a *trans*-azobenzene as a steric block which prevents molecular threading of the macrocycle. Irradiation to the *cis* isomer allows the macrocycle to bind to the diamides on the thread where the association constant was calculated to be 5200 M^{-1} in $CDCl_3$ (Scheme 1.19). The original *trans* compound was formed by heating the *cis* form at 50 - 55 ^{o}C which caused de-threading of the macrocycle. This molecular machine is a prime example of how using an azobenzene as a steric block can effectively turn "on and "off" hydrogen bonding interactions.

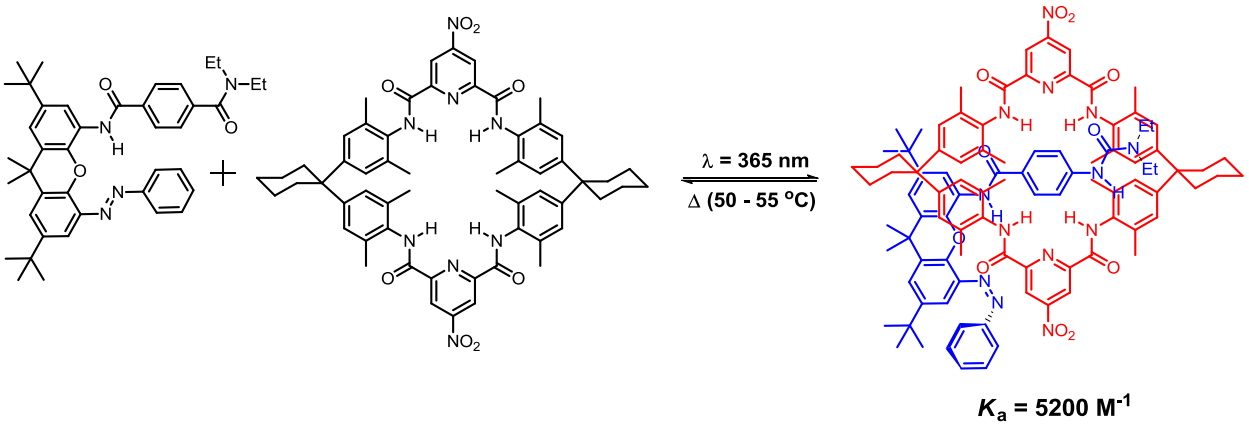

Scheme 1.19 Photocontrolled pseudorotaxane synthesized by Jeong and co-workers.

The action of steric blocking using an azobenzene group is not only applicable in self-assembled systems. Hecht and co-workers synthesized a photoswitchable catalyst which can turn "on" and "off" chemical reactions.[81] A 3,5-tert-butyl-azobenzene component was installed in close proximity to a piperidine ring which is the reactive site within this catalyst (Scheme 1.20). A nitro-aldol condensation was attempted with the *trans* isomer and little β-nitro alcohol formed in solution. The *cis* form was subjected to the same reaction conditions and the rate of product formation was greatly increased. The basic site of the piperidine ring was therefore now accessible to the incoming nitroalkane due to the repositioning of the *cis*-azobenzene component.

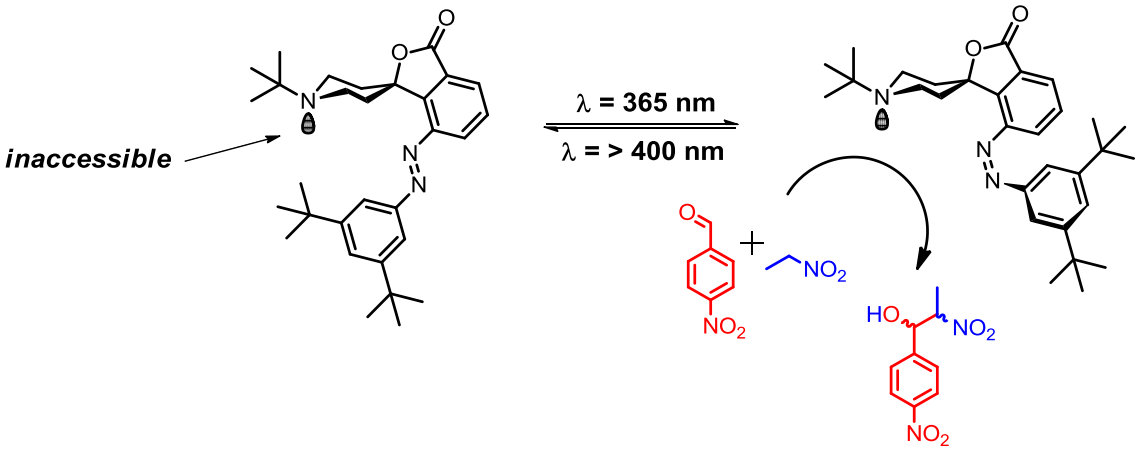

Scheme 1.20 Photoswitchable catalyst for Henry reactions synthesized by Hecht and co-workers.

1.11 Photoswitchable Hydrogen Bonded Supramolecular Polymers

The incorporation of a photoswitch into polymeric materials is a method to add a "smart" quality to create supramolecular systems. Azobenzenes with carboxylic acid groups have been observed to exhibit sol-gel properties when exposed to UV light.[82] Utilizing a pendant pyridine heterocycle with an azo moiety adds a hydrogen bonding acceptor site. Side and main chain azobenzene polymers with a pyridyl group have been mixed with different carboxylic acid derivatives to create photoactive liquid polymeric crystals. The *trans* to *cis* isomerizations were studied within these matrices which resulted in phase transitions.[83a-c] Diarylethenes are more commonly studied within this type of supramolecular polymers which is presumably due to the two isomeric forms being stable (P type). Takeshita and co-workers have synthesized a ditopic Upy monomer with a central diarylethene photoswitch (Figure 1.22).[84] This monomer was used to study effects of supramolecular polymerization in terms of particle size. The open form monomer has two free "arms" which are free to rotate and does not participate

in polymerization as the particle size was determined to be < 10 nm. The closed isomer on the other hand is locked in a rigid position and the end groups start to hydrogen bond in a zig-zag pattern where the maximum particle size was approximately 650 nm. The original particle size was restored with visible light irradiation and slight heating to assist in breaking apart hydrogen bonded aggregates. Yang and co-workers also

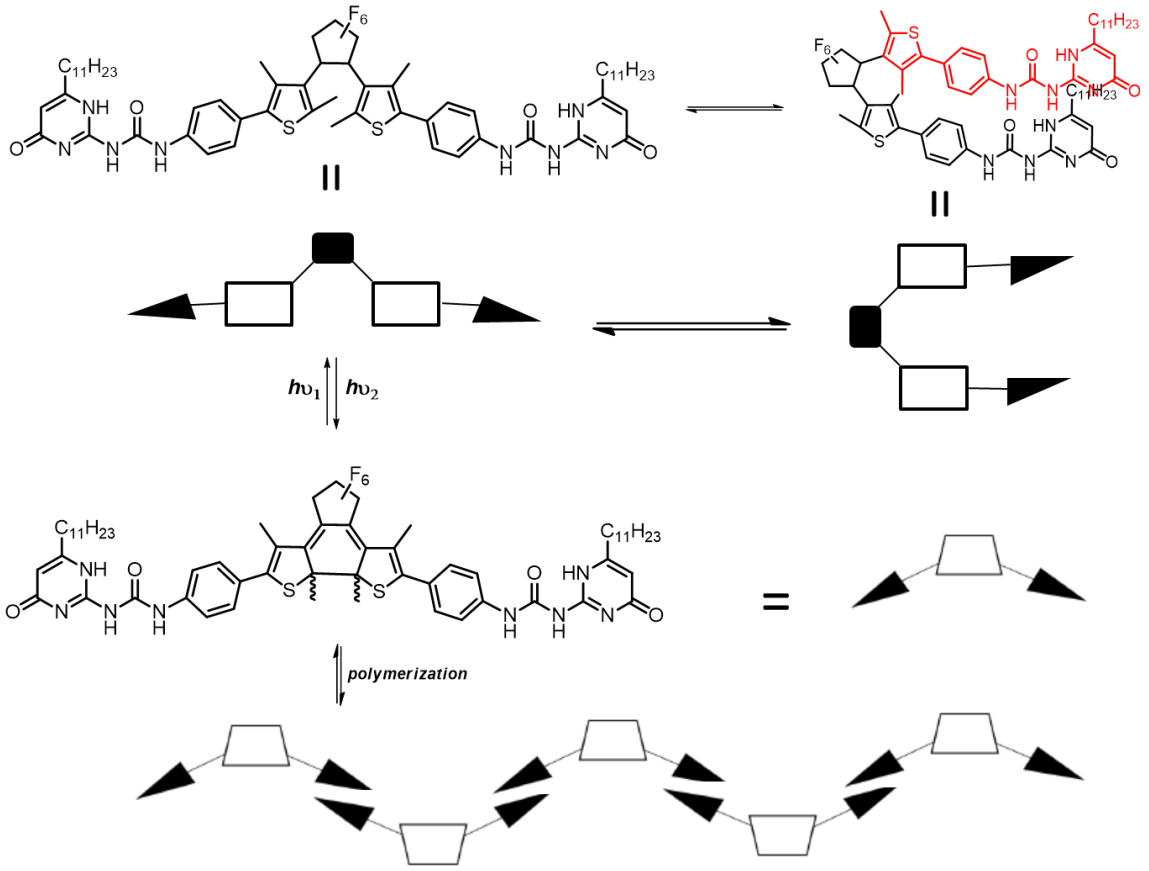

Figure 1.22 Photoswitchable hydrogen bonded supramolecular polymer containing a diarylethene moiety synthesized by Takeshita and co-workers.

utilized UPy unit but a 1,1-biindane moiety was incorporated as a photoswitch.[52] The *Z* isomer was determined to form primarily a dimer in solution (***cis*-1-13**; Scheme 1.20) whilst the *E* isomer (***trans*-1-13**; Scheme 1.21) formed a highly viscous gel.

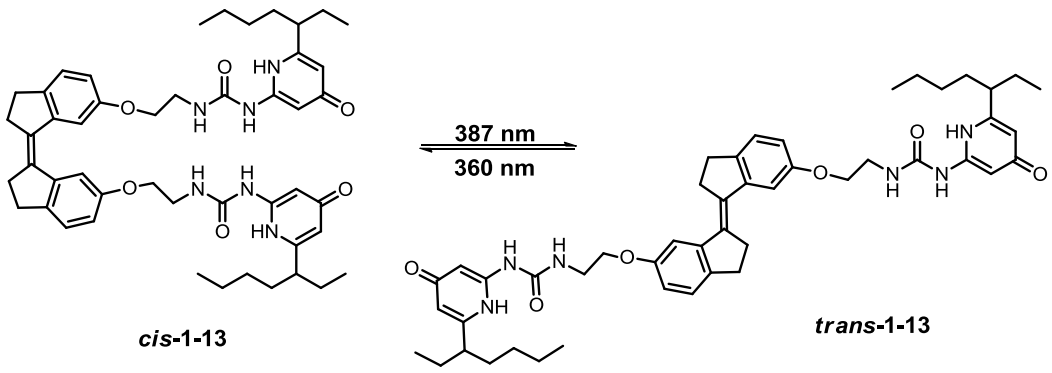

Scheme 1.21 Photoswitchable hydrogen bonded supramolecular polymer containing a 1,1-biindane moiety synthesized by Yang and co-workers.

1.12 Scope of the Thesis

The aim of this research project was to create a complementary hydrogen bonding motif which when exposed to light as an external stimulus shows a direct change in the strength of the hydrogen bonded complex. This was accomplished by using an azo functional group (-N=N-) as the photoswitchable unit where each nitrogen atom is bonded to a heterocyclic moiety which contain hydrogen bond acceptors. Along with the heterocyclic groups, we will be incorporating one of the sp^2 nitrogen atoms in the azo moiety into the hydrogen bonding array which is a new application for these types of compounds. The incorporation of this nitrogen atom into the array and subsequent *trans* to *cis* isomerization will provide a non-invasive technique to alter the spatial arrangement of the acceptor array. The result will be a weaker hydrogen bonded complex when compared to the initial state. The system will then be brought back to the original (more stable) state using a different wavelength of light, demonstrating reversibility and potential "on" and "off" hydrogen bonding modes.

Chapter 2 describes the synthesis and characterization of 2-aminoindole hydrogen bond donor arrays. A series of 3-CN and 3-CO_2Et indoles were synthesized each with varying substituents in the 5 and 6 positions on the benzenoid ring. Along with the indoles, our initial photoswitching acceptor array 2, 2' - azopyridine was prepared. The association constants (K_a) for all indoles soluble in $CDCl_3$ were determined with our acceptor array with values ranging from 10^1 to 10^3 M^{-1}. Linear free energy relationships were also constructed which showed a strong correlation between the substituents on the indole (σ values) and the resulting K_a values.

Chapter 3 describes various ways that the initial system can be altered and improved through derivatization. The 2-aminoindoles were prepared in a different manner so that the substituent in the 3 position can be modified through a variant of electrophilic reactions. Additionally, our hydrogen bonding acceptor library was increased by synthesizing two new heteroaromatic azo compounds, both with an extra acceptor group which showed as increase in the K_a values. Solubility effects were examined by changing the titration solvent from $CDCl_3$ to toluene-d_8 which also resulted in an increase in the association constants up to 10^5 M^{-1}.

Chapter 4 contains the methods and results of the photoswitchability of this complementary system. *cis* isomers of two of our acceptor arrays were isolated and characterized. Through a newly developed method of extrapolations, the binding constants of the *cis* isomers with two of our indole donors were calculated which resulted in lower K_a values when compared to the *trans* isomers. Photoswitchability experiments

were also carried out to demonstrate durability and reversibility of the binding complexes in solution.

1.13 References

1. Brunsveld, L.; Folmer, B. J. B.; Meijer, E. W.; Sijbesma, R. P. *Chem. Rev*., **2001**, *101*, 4071.

2. Folmer, B. J. B.; Cavini, E.; Sijbesma, R. P.; Meijer, E. W. *Chem. Commun*., **1998**, 1847.

3. Ma, L.; Kang, H.; Liu, R.; Huang, Y. *Langmuir*, **2010**, *26*, 18519.

4. Hu, J.; Zhang, G.; Liu, S. *Chem. Soc. Rev*., **2012**, *41*, 5933.

5. Yang, L.; Tan, X.; Wang, Z.; Zhang, X. *Chem. Rev*., **2015**, *115*, 7196.

6. Folmer, B. J. B.; Sijbesma, R. P.; Meijer, E. W. *J. Am. Chem. Soc*., **2001**, *123*, 2093.

7. Hisatome, M.; Ikeda, K; Kishibata, S.; Yamakawa, K. *Chem. Lett*., **1993**, 1357.

8. Gulik-Krzywicki, T.; Fouquey, C.; Lehn, J-M. *Proc. Natl. Acad. Sci*., **1993**, *90*, 163.

9. Liu, Y.; Yu, Y.; Gao, J.; Wang, Z.; Zhang, X. *Angew. Chem. Int. Ed*., **2010**, *49*, 6576.

10. Tian, Y-K.; Shi, Y-G.; Yang, Z-S.; Wang, F. *Angew. Chem. Int. Ed*., **2014**, *53*, 6090.

11. Lehn, J.M. *Science*, **1993**, *260*, 1762.

12. Steed, J. W., Turner, D. R. and Wallace, K. J. *Core concepts in supramolecular chemistry and nanochemistry.* Chichester : John Wiley, 2007.

13. Watson, J. D.; Crick, F. H. C. *Nature*, **1953**, *171*, 737.

14. Baker, E. N.; Hubbard, R. E. *Prog. Biophys. Molec. Biol*., **1984**, *44*, 97.

15. Fischer, E. *Ber. Dtsc. Chem. Ges*., **1984**, *27*, 2985.

16. Appel, W. *Clin, Biochem*., **1986**, *19*, 317.

17 Arunan, E.; Desiraju, G. R.; Klein, R. A.; Sadlej, J.; Scheiner, S.; Alkorta, I.; Clary, D. C.; Crabtree, R. H.; Dannenberg, J. J.; Hobza, P.; Kjaergaard, H. G.; Legon, A. C.;

Mennucci. B.; Nesbitt, D. J. *Pure Appl. Chem.*, **2011**, *83*, 1619.

18. Steiner, T. *Angew. Chem. Int. Ed*., **2002**, *41*, 48.

19. a) Desiraju, G. R. *Acc. Chem. Res*., **2002**, *35*, 565; b) Desiraju, G. R. *Angew. Chem. Int. Ed*., **2007**, *46*, 8342.

20. Hunter, C. A. *Angew. Chem. Int. Ed*., **2004**, *43*, 5310.

21. a) Abraham, M. H. *Chem. Soc. Rev*., **1993**, *22*, 73; b) Abraham, M. H.; Platts, J. A. *J. Org. Chem*., **2001**, *66*, 3484.

22. Cook, J. L.; Hunter, C. A.; Low, C. M. R.; Perez-Velasco, A.; Vinter, J. G. *Angew. Chem. Int. Ed*., **2007**, *46*, 3706.

23. a) Jeffrey, G. A.; Maluszynska, H. *Int. J. Biol. Macromol.*, **1982**, *4*, 173; b) Jeffrey, G. A., *Cryst. Rev.*, **1995**, *4*, 213.

24. Blight, B. A.; Camara-Campos, A.; Djurdjevic, S.; Kaller, M.; Leigh, D. A.; McMillan, F. M.; McNab, H.; Slawin, A. M. Z. *J. Am. Chem. Soc*., **2009**, *131*, 14116.

25. a) Jorgensen, W.L.; Pranata, J. *J. Am. Chem. Soc.* **1990**, *112*, 2008; b) Pranata, J.; Wierschke, S.G.; Jorgensen, W.L. *J. Am. Chem. Soc*., **1991**, *113*, 2810.

26. Kelly, T. R.; Zhao, C.; Bridger, G. J. *J. Am. Chem. Soc*., **1989**, *111*, 3744.

27. Reynisson, J.; McDonald, E. *J. Comput. Aid. Mol. Des*., **2004**, *18*, 421.

28. Newman, S. G.; Taylor, A.; Boyd, R. J. *Chem. Phys. Lett.*, **2008**, *450*, 210.

29. Wang, H.-B.; Mudraboyina, B. P.; Wisner, J. A. *Chem. Eur. J.*, **2012**, *18*,

1322.

30. Bell, D. A.; Anslyn, E. V. *Tetrahedron*, **1995**, *51*, 7161.

31. Leigh, D. A.; Robertson, C. C.; Slawin, A. M. Z.; Thomson, P. I. T. *J. Am. Chem. Soc*., **2013**, *135*, 9939.

32. Blight, B. A.; Hunter, C. A.; Leigh, D. A.; McNab, H.; Thompson, P. I. T. *Nat. Chem*., **2011**, *3*, 244.

33. Cram, D. J. *Angew. Chem. Int. Ed*., **1986**, *25*, 1039.

34. Zimmerman, S. C.; Mrksich, M.; Baloga, M. *J. Am. Chem. Soc*., **1989**, *111*, 8528.

35. a) Stewart, K. D.; Miesch, M.; Knobler, C. B.; Maverick, E. F.; Cram, D. J. *J. Org. Chem*., **1986**, *51*, 4327; b) Koenig, K. E.; Lein, G. M.; Stuckler, P.; Kaneda, T.; Cram, D. J. *J. Am. Chem. Soc*., **1979**, *101*, 3553.

36. Murray, T. J.; Zimmerman, S. C. *Tet. Lett*., **1995**, *36*, 7627.

37. Mudraboyina, B. P. Complementary and Self-Complementary Hydrogen Bond Double Helical Complexes. Ph.D. Dissertation, Western University, London, ON, 2012.

38. Etter, M. C. *Acc. Chem. Res*., **1990**, *23*, 120.

39. Beijer, F. H.; Kooijman, H.; Spek, A. L.; Sijbesma, R. P.; Meijer, E. W. *Angew. Chem. Int. Ed*., **1998**, *37*, 75.

40. Goodman, M. F. *Nature*, **1995**, *378*, 237.

41. Beijer, F. H.; Sijbesma, R. P.; Kooijman, H.; Spek, A. L; Meijer, E. W. *J. Am. Chem. Soc*., **1998**, *120*, 6761.

42. Murray, T. M.; Zimmerman, S. C. *J. Am. Chem. Soc*., **1992**, *114*, 4010.

43. a) Mendez, I. J. M.; Pleizier, J. S.; Wang, H-B.; Wisner, J. A. *J. Phys. Org. Chem*., **2018**, *31*, e3805; b) Mendez, I. J. M. Photo-Isomerizable Self-Complementary Hydrogen Bond Arrays. Ph.D. Dissertation, Western University, London, ON, 2016.

44. Bouas-Laurent, H.; Dürr, H. *Pure Appl. Chem*., **2001**, *73*, 639.

45. Ercole, F.; Davis, T. P.; Evans, R. A. *Polym. Chem*., **2010**, *1*, 37.

46. Russew, M-M., Hecht, S. Adv. Mater., 2010, 22, 3348.

47. Bikle, D. D. *Chem. Biol*., **2014**, *21*, 319.

48. Goodsell, D. S. *The Oncologist*, **2001**, *6*, 298.

49. Irie, M.; Fukaminato, T.; Matsuda, K.; Kobatake, S. *Chem. Rev*., **2014**, *114*, 12174.

50. Jacquemin, D.; Preat, J.; Wathelet, V.; Fontaine, M.; Perpète, E. A. *J. Am. Chem. Soc*., **2006**, *128*, 2072.

51. Zweig, J. E.; Newhouse, T. R. *J. Am. Chem. Soc*., **2017**, *139*, 10956.

52. Xu, J-F.; Chen, Y-Z.; Wu, D.; Wu, L-Z.; Tung, C-H.; Yang, Q-Z. *Angew. Chem. Int. Ed*., **2013**, *52*, 9738.

53. Pu, S.; Zheng, C.; Le, Z.; Liu, G.; Fan, C. *Tetrahedron*, **2008**, *64*, 2576.

54. Zou, Y.; Yi, T.; Xiao, S.; Li, F.; Li, C.; Gao, X.; Wu, J.; Yu, M.; Huang, C. *J. Am. Chem. Soc*., **2008**, *130*, 15750.

55. Zou, Q.; Li, X.; Zhang, J.; Zhou, J.; Sun, B.; Tian, H. *Chem. Commun*., **2012**, *48*, 2095.

56. Neo, A. G.; López, C.; Romero, V.; Antelo, B.; Delamano, J.; Pérez, A.; Fernández, D.; Almeida, J. F.; Castedo, L.; Tojo, G. *J. Org. Chem*., **2010**, *75*, 6764.

57. Yoshida, T.; Morinaka, A**.** *J. Photochem. Photobiol. A: Chem.*, **1992**, *63*, 227.

58. Crano, J. C.; Guglielmetti, R. J. *Organic photochromic and thermochromic compounds*. New York : Plenum Press, 1999.

59. Herder, M.; Schmidt, B. M.; Grubert, L.; Pätzel, M.; Schwarz, J.; Hecht, S. *J. Am. Chem. Soc*., **2015**, *137*, 2738.

60. Merino, E.; Ribagorda, M. *Beilstein J. Org. Chem*., **2012**, *8*, 1071.

61. Bandara, H. M. D.; Burdette, S. C. *Chem. Soc. Rev*., **2012**, *41*, 1809.

62. Hartley, G. S. *Nature*, **1937**, *140*, 281.

63. Kaufman, H.; Vratsanos, S. M.; Erlanger, B. F. *Science*, **1968**, *162*, 1487.

64. Avan, I. *Synthesis*, **2016**, *48*, 365.

65. Dohno, C.; Uno, S-N.; Nakatani, K. *J. Am. Chem. Soc*., **2007**, *129*, 11898.

66. Banghart, M.; Borges, K.; Isacoff, E.; Trauner, D.; Kramer, R. H. *Nat. Neurosci*., **2004**, *7*, 1381.

67. Norikane, Y.; Tamaoki, N. *Org. Lett*., **2004**, *6*, 2595. .

68. Muraoka, T.; Kinbara, K.; Aida, T. *Nature*, **2006**, *44*, 512

69. Marchi, E.; Baroncini, M.; Bergamini, G.; Van Heyst, J.; Vögtle, F.; Ceroni, P. *J. Am. Chem. Soc*., **2012**, *134*, 15277.

70. a) Muraoka, T.; Kinbara, K.; Kobayashi, Y.; Aida, T. *J. Am. Chem. Soc*., **2003**, *125*, 5612; b) Muraoka, T.; Kinbara, K.; Aida, T. *Chem. Commun*., **2007**, 1441.

71. Ferri, V.; Elbing, M.; Pace, G.; Dickey, M. D.; Zharnikov, M.; Samorì, P.; Mayor, M.; Rampi, M. A. *Angew. Chem. Int. Ed.*, **2008**, *47*, 3407.

72. Sasaki, T.; Tour, J. M. *Org. Lett*., **2008**, *10*, 897.

73. Avellini, T.; Li, H.; Coskun, A.; Barin, G.; Trabolsi, A.; Basuray, A. N.; Dey, S. K.; Credi, A.; Silvi, S.; Stoddart, J. F.; Venturi, M. *Angew. Chem Int. Ed.*, **2012**, *51*, 1611.

74. Yu, Y.; Nakano, M.; Ikeda, T. *Nature*, **2003**, *425*, 145.

75. Shinkai, S.; Nakaji, T.; Ogawa, T.; Shigematsu, K.; Manabe, O. *J. Am. Chem. Soc*., **1981**, *103*, 111.

76. Hunter, C. A.; Togrul, M.; Tomas, S. *Chem. Commun*., **2004**, 108.

77. Asanuma, H.; Ito, T.; Yoshida, T.; Liang, X.; Komiyama, M. *Angew. Chem. Int. Ed*., **1999**, *38*, 2393.

78. Goodman, A.; Breinlinger, E.; Ober, M.; Rotello, V. M. *J. Am. Chem. Soc*., **2001**, *123*, 6213.

79. Nojiri, A.; Kumagai, N.; Shibasaki, M. *Angew. Chem. Int. Ed*., **2012**, *51*, 2137.

80. Jeong, K-S., Chang, K-J., An, Y-J. *Chem. Commun*., **2003**, 1450.

81. Peters, M. V.; Stoll, R. S.; Kühn, A.; Hecht, S. *Angew. Chem. Int. Ed*., **2008**, *47*, 5968.

82. Chen, D.; Liu, H.; Kobayashi, T.; Yu, H. *J. Mater. Chem*., **2010**, *20*, 3610.

83. a) He, C.; Xu, J.; Toh, C. L.; Lu, X. *Liq. Cryst.* **2008,** *35*, 241; b) Zhao, Y.; Cui, L. *Chem. Mater.*, **2004**, *16*, 2076; c) Michinobu, T.; Eto, R.; Kumazawa, H.; Fujii, N.; Shigehara, K. *J. Macromol. Sci. A*., **2011**, *48*, 625.

84. Takeshita, M.; Hayashi, M.; Kadota, S.; Mohammed, K. H.; Yamato, T. *Chem. Commun*., **2005**, 761.

Chapter 2

2 Synthesis and Characterization of Complementary DD-AAA Hydrogen Bond Arrays

2.1 Hydrogen Bonded Supramolecular Polymers

Conventional polymeric materials are primarily controlled by the covalent bond. These bonds connect monomeric units together creating strong and versatile products which have revolutionized the industrial and material science sectors. These polymers are indeed useful but suffer one major drawback. The covalent bonds connecting monomer units together may be extremely strong, but are essentially irreversible in nature, meaning they have a definite macromolecular structure. In other words, once damage has occurred to this definite structure, such as bond breaking by external stimuli (e.g.: force, heat etc.), the polymer retains this damage and the usefulness of the material is often dramatically lowered.[1] The combination of supramolecular chemistry with the field of polymer science has attempted to overcome this problem by creating systems which lack the aforementioned definite covalent structure. Supramolecular polymers have gained momentum because, if constructed correctly, they can retain the strength and versatility of convention polymers, but possess the ability to self-assemble/self-heal after being subjected to external stimuli. This is achieved through directional secondary interactions which link end groups and/or side chains together using reversible non-covalent binding to create a virtual polymeric material in solution or bulk state. Hydrogen bonds in particular have been incorporated into monomeric units to form supramolecular polymers because of their highly directional and reversible nature. The

binding can therefore be finely tuned to the material properties desired. A single hydrogen bond is usually ineffective to generate a useful material, so multiple point hydrogen bond arrays have to be utilized, typically incorporating 3 or more interactions in tandem.

Among the choices for a suitable array to append to monomers for hydrogen bonded materials, the current leading example is 2-ureido-4[1H]-pyrimidinone, or UPy. Introduced as hydrogen bonded dimers by Meijer in 1998, these self-complementary arrays dimerize very strongly in non-polar solvents and the simplest dimers can be synthesized in one step from only two inexpensive starting materials.[2] For example, butyl isocyanate can react with 6-methylisocytosine to create the 6-methyl-2-butylureidopyrimidone analogue (Figure 2.1) which dimerizes in chloroform in the desired AADD arrangement with a dimerization constant exceeding 10^7 M^{-1}. These arrays have been shown to be effective as supramolecular subunits because they can be easily installed as telechelic groups that can participate in further hydrogen bonded

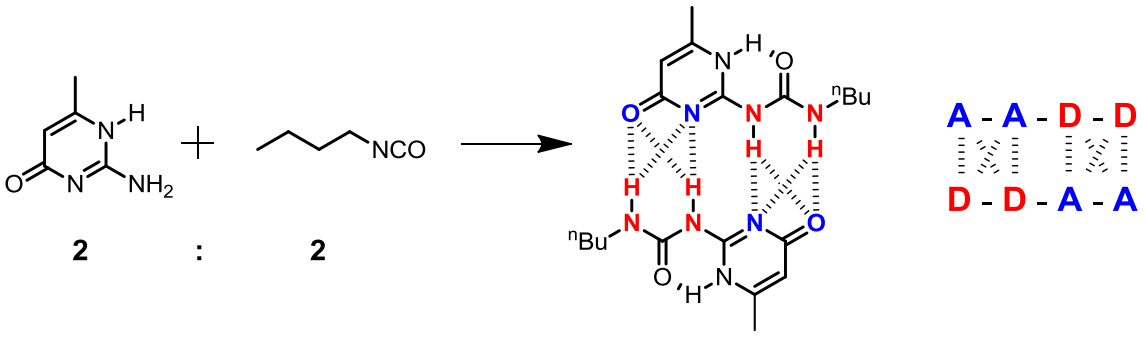

Figure 2.1 Synthesis of 6-methyl-2-butylureidopyrimidone demonstrating the popular AADD self-complementary hydrogen bonded arrangement; donors depicted in red and acceptors in blue. Dashed lines indicate attractive interactions.

polymerization. Meijer and coworkers demonstrated this by using various hydrocarbons[3] as well as polyether, polycarbonate and polyester diols and through reactions with

isocyanates, UPy moieties could be attached via carbamate linkages resulting in high molecular weight polymers (Figure 2.2).[4] These polymers form highly viscous solutions in non-polar solvents. Heating these solutions dissociate the end groups which lowers the viscosity. Removing the heat from the system returns the viscosity back to the original state demonstrating that the end groups can reanneal themselves without added additional strain to the polymers themselves making the systems truly reversible.

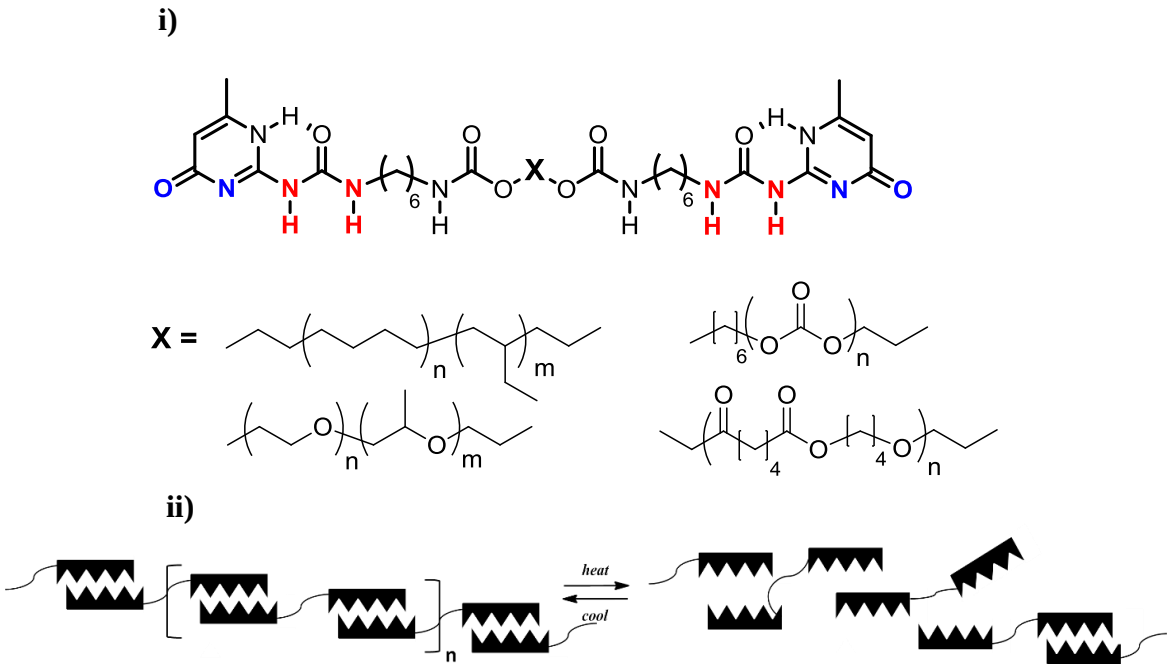

Figure 2.2 **i)** UPy terminated monomers with showing a variety of different linkers. **ii)** depiction demonstrating how these monomers bind and dissociate and reanneal upon heating and cooling.

2.2 Complementary Hydrogen Bonded Arrays

The discovery of the purine and pyrimidine base pairing in the DNA double helix[5] led to the synthesis and characterization of a large number of hydrogen bonded complexes. Many have included the aforementioned heterocycles but have also been expanded to include other simple and complex heterocyclic and fused heterocyclic

frameworks.[6] Complementary and self-complementary arrays have been created using these heterocyclic systems. Self-complementary arrays only require the synthesis of one interacting component which will dimerize spontaneously and may be difficult to control. Complementary arrays on the other hand require the synthesis of one array followed by the subsequent synthesis of its complementary array with the correct alignment and number of hydrogen bonding units for a successful complexation. The synthesis of these two arrays may not be as convenient as the self-complementary systems but if constructed properly can lead to very strong complexes, some of which have the strongest association constants known thus far.

As previously discussed, Jorgenson and Pranata demonstrated the sequence dependence of hydrogen bonding arrays.[7] These sequences of donors and acceptors in the arrays lead to either attractive or repulsive secondary interactions which can either reinforce or weaken the hydrogen bonding strength of the complex respectively. This can be illustrated by the CG base pair[8] having an estimated association constant of $10^4 – 10^5$ M^{-1} and 2-aminoadenine and alkylated cytosine[9] having an association constant of 170 M^{-1}. Both complexes have similar structures and the same number of hydrogen bonds with the same types of atom pairings (N-H···O x 2 and N-H···N x 1) but the 2-aminoadenine complex results in entirely repulsive secondary interactions, shown in red, while the CG pair contains 2 attractive and 2 repulsive secondary interactions. The repulsive effects aside, the ADA-DAD pairing is one of the more intensively studied in the literature due to the availability of starting materials preorganized in those sequences or ease of synthetic methods to produce them.[10]

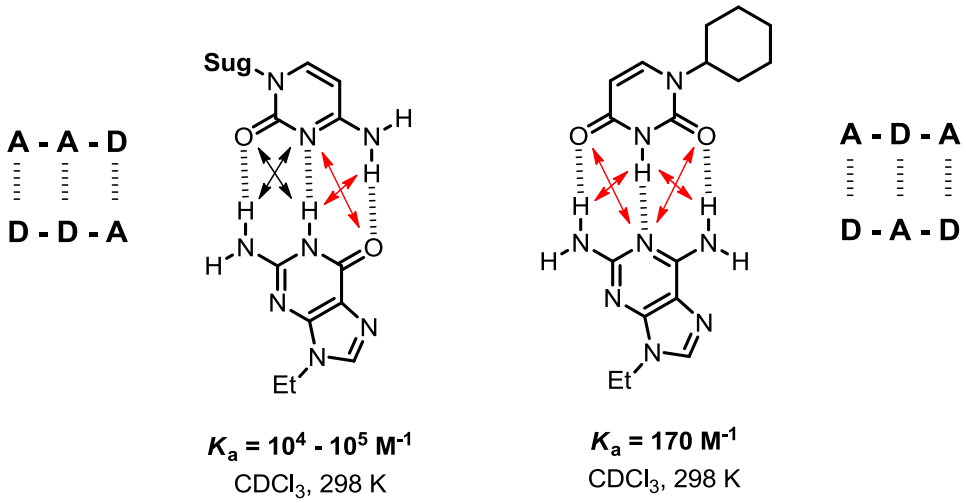

Figure 2.3 Two complementary arrays demonstrating sequence dependence when constructing complexes; black arrows indicate attractive secondary interactions and red arrows repulsive.

Lehn and coworkers have demonstrated just how useful and versatile these sequences can be if properly incorporated into supramolecular systems. Utilizing the popular 2,6-diacetamidopyridine and cyanuric acid (X = NR)/barbituric acid (X = CR_2) arrays (Figure 2.4), a double-edged 6-point hydrogen bonded complex can be created and attached onto

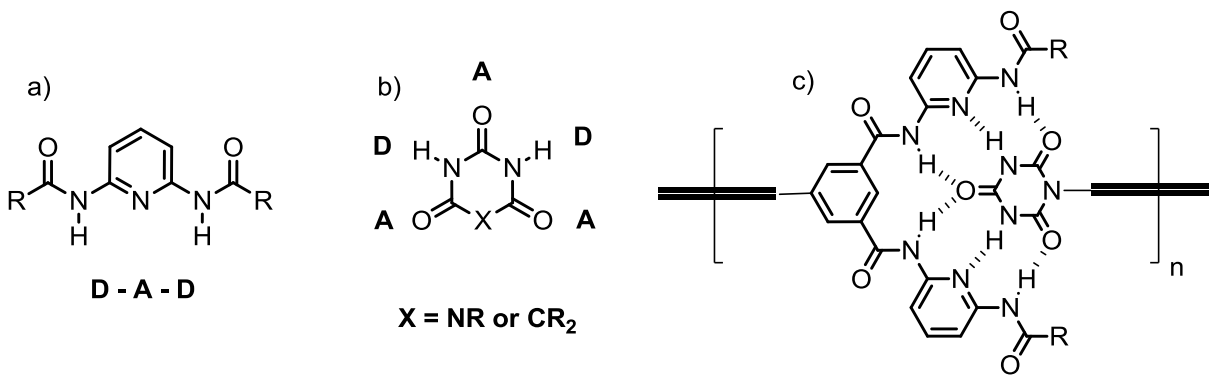

Figure 2.4 a) 2,6-Acetamidopyridine array; b) cyanuric (X = NR) and barbituric (X = CR_2) acid arrays; c) double-edged 6-point hydrogen bonded polymer created from the two arrays to which are bound to solubilizing linkers.

solubilizing linkers for supramolecular polymeric systems.[11] Homoditopic monomers can be combined for linear polymerization in solution which occurs spontaneously resulting in a high degree of polydispersity. The association strength of these moieties is so strong that in toluene at concentrations as low as 1 mM, highly viscous solutions are formed which have properties similar to that of conventional polymeric materials. This linear polymerization was qualitatively examined by ^{1}H NMR in $C_2D_2Cl_4$ where at -20 ^{o}C the amide signals appear broadened and resonate at higher chemical shifts resulting from a higher degree of entanglement and polymerization. Raising the temperature to above 50 ^{o}C, the same signals resonate at a lower chemical shift due to the rupture of the hydrogen bonds in the strands. Monotopic monomers for the manipulation of molecular weight distributions can be added to polymer networks and can be observed by ^{1}H NMR. The entangled polymers are characterized by broadened spectra which become better defined as smaller oligomers are formed. The inverse observation can be made when a homotritopic crosslinking agent is added to the linear polymer which creates a more connected network and generates broadened proton signals. Overall, concentration, solvent, stoichiometry of different types of monomers, and temperature were all external factors studied with these polymer systems. They all demonstrated reversible hydrogen bonding properties which can be tuned for specific responses, such as viscosity variations or degrees of polymerization (Figures 2.5 and 2.6).

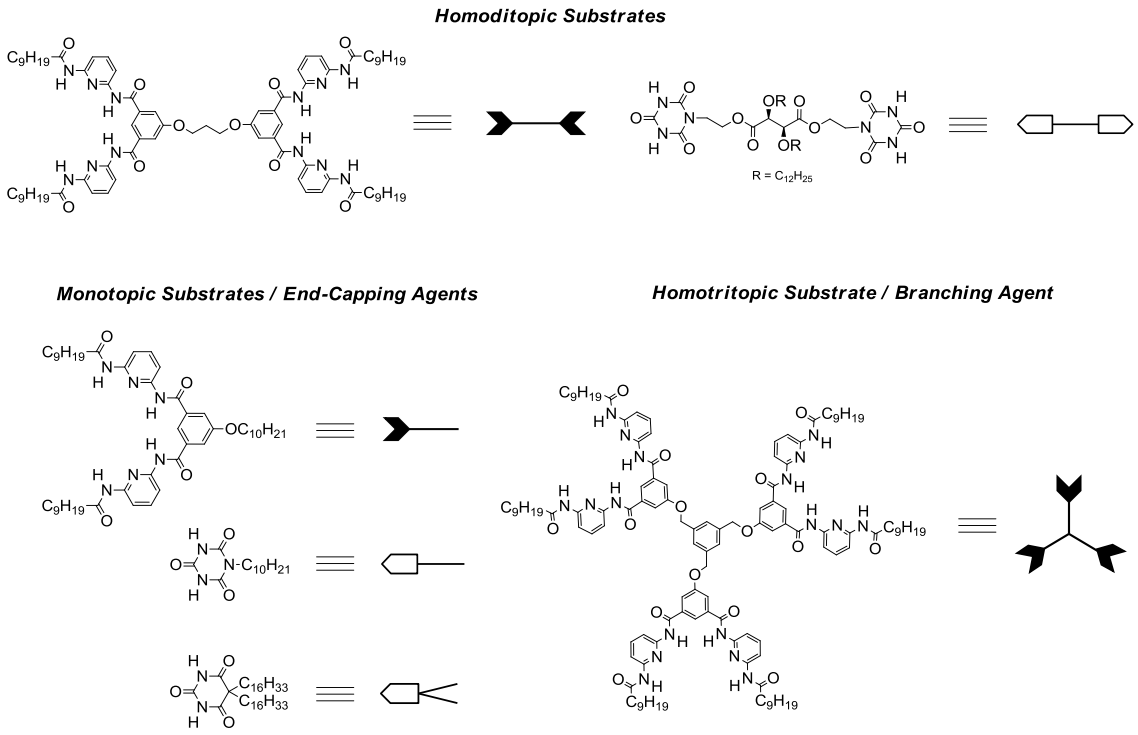

Figure 2.5 Lehn and co-workers monomers utilizing the ADA-DAD hydrogen bonding system.

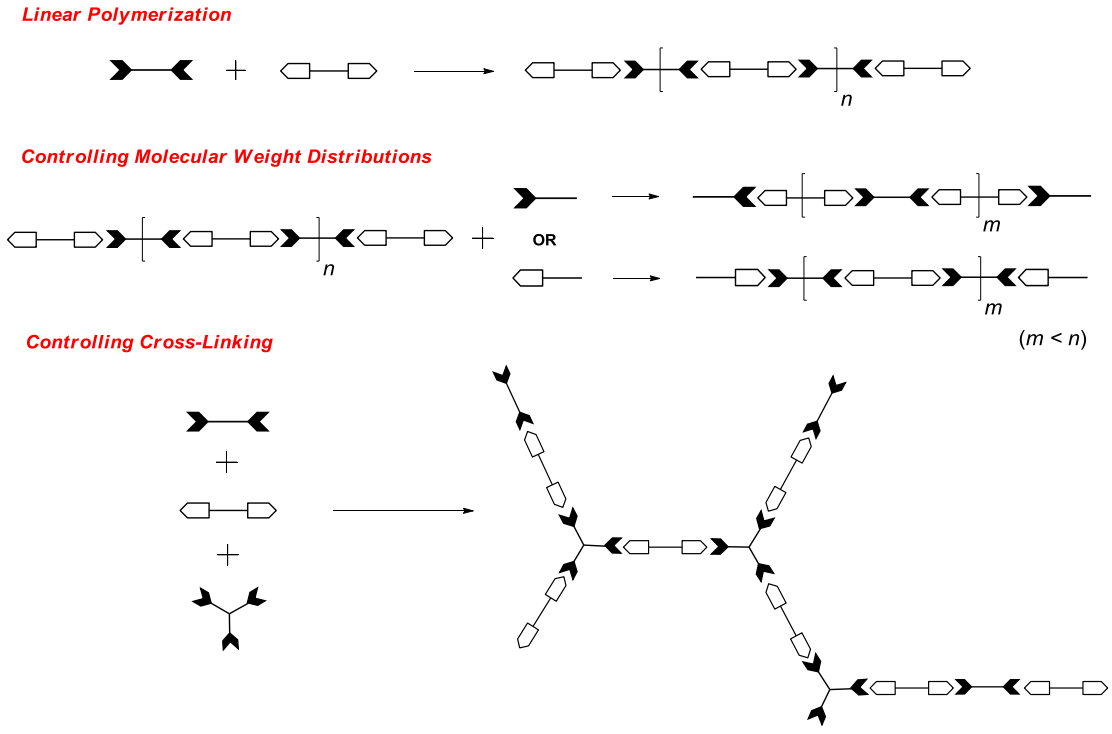

Figure 2.6 Diagram showing how Lehn and co-workers used the substrates to create and control multiple types of supramolecular polymerization.

The above examples demonstrate how complementary arrays can have all repulsive secondary attractions but if enough hydrogen bonding units are utilized, a strong polymeric material can be obtained. If all of the secondary interactions are converted from repulsive to attractive in nature, the overall stability of the resulting complexes is greatly increased and a smaller number of bonding pairs can often be utilized. Depicted below are three examples of contiguous hydrogen bonding complexes which exhibit extremely strong association constants. These are some of the strongest complexes known to date, but each suffer some sort of drawback to their design.

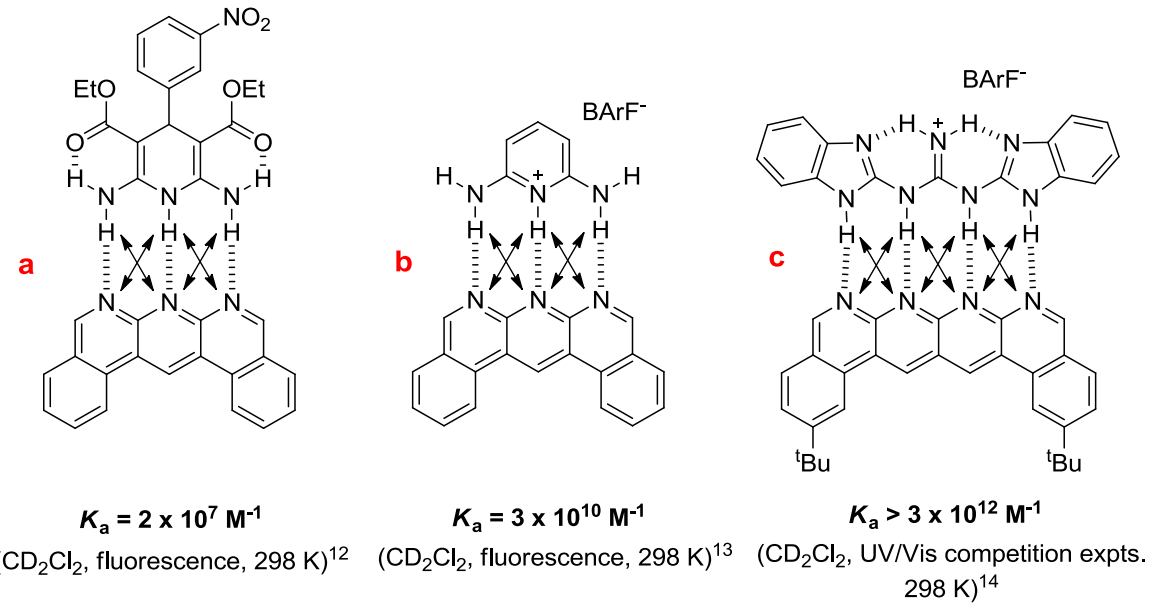

Figure 2.7 Three extremely strong complementary complexes reported by Leigh and co-workers. All attractive secondary interactions are indicated by black arrows. Experimental conditions and methods reported in brackets.

The donor component in complex **a** is depicted in the idealistic 1,4-dihydro tautomeric form but also exists as the 3,4-dihydro form.[14, 15a-c] The tautomeric shift changes the ideal DDD array into a DAD array which affects the resulting complex stability. Although

large association constants for this type of donor array are reported, inspection of the experimental fits of the plotted data draw some question as to how accurate the reported figures actually are. The diaminopyridinium cationic donor in complex **b** always exists with an associated counter anion which participates in competitive binding with the donor array which may lower the resulting binding constant. Extra complications may also arise due to proton transfer from the acidic cationic donor to the acceptor if it is a stronger base. The strongest complementary complex known to date depicted as complex **c** was too strong to be measured directly through traditional methods so tedious UV/Vis competition experiments had to be carried out to obtain an estimate of the association constant in non-polar solvents. This complex also contains a counter anion similar to that of complex **b**. The main difficulty arises when one of the benzimidazole arms rotates 180^{o} and participates in intramolecular hydrogen bonding. This non-linear conformer alters the DDDD binding site and additional energy is needed to return the system back to the optimal alignment for complexation.

Regardless of the disadvantages discussed above, these complexes still have the potential to be incorporated into hydrogen bonded polymers. Wang and his group have reported one of the very few examples of such polymers in which they synthesized a complex similar to that of complex **a** depicted (Figure 2.7) having a comparable association constant.[16] Furthermore, the donor array was synthesized in one step so that this array can then be carried forward to create the acceptor array in a further three steps. Both these arrays can then be demethylated and connected by alkyl chains to result in the desired polymeric material. This is a prime example for supramolecular systems because

the cheap, simplistic, and ease of synthesis when relating to these types of polymers is an important factor when it comes to creating potentially industrial scale materials.

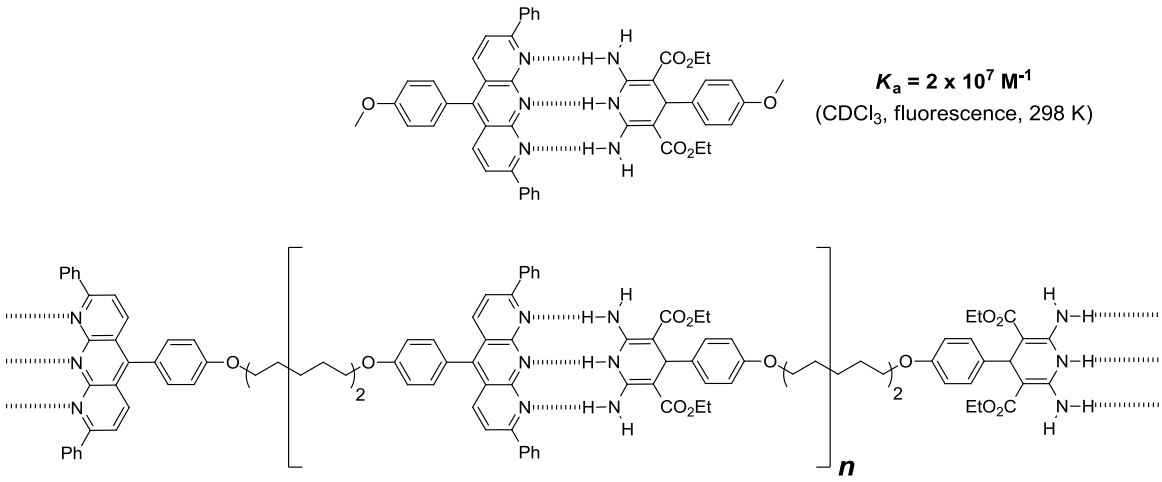

Figure 2.8 An AAA-DDD supramolecular polymer synthesized by Wang and co-workers. Experimental conditions and methods reported in brackets.

Both Lehn's and Wang's monomers exhibit hydrogen bonded polymeric properties in solution and as observed in both cases, the degree of polymerization is concentration dependant. Monomer concentration is a very important factor for these types of materials as can be seen in a logarithmic plot of association constants (K_a) versus the resulting degree of polymerization (DOP).[17] The plot illustrates that for a reversible hydrogen bonded polymer to reach a DOP of 100 in solution, the association constant must be at least 10^4 M^{-1} at 0.05 M concentration and 10^3 M^{-1} at 1.0 M. Generally, for a main chain supramolecular polymer, complex stabilities below that threshold yield solutions that consist primarily of monomers and short linear/cyclic oligomers.

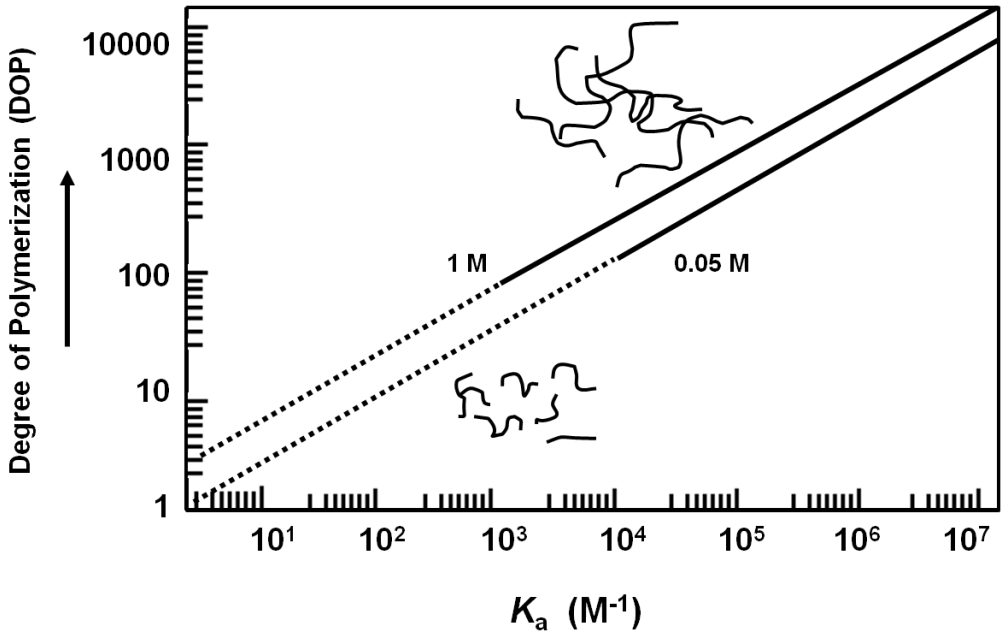

Figure 2.9 Theoretical plot demonstrating the linear relationship between association constant and the degree of polymerization for a concentration dependent supramolecular polymer.

The complementary supramolecular complexes and polymers discussed above are leading examples of how versatile and strong these hydrogen bonded materials can be. With this in mind, we set out to create our own set of new complementary complexes. Utilizing inexpensive starting materials and few synthetic steps, a library of planar DDD compounds was envisioned along with a complementary AAA acceptor. The acceptor will also contain an additional degree of functionality by incorporating a photoswitchable subunit. Photoswitching will be used to alter the hydrogen bonding modes and strengths of the complexes. The remainder of this chapter will outline our initial efforts in characterizing the efficacy and strength of these complexes. The photoswitching will be examined and discussed in later chapters.

2.3 Design of Initial Arrays

The concept for this project arose from a crystal structure obtained and published by our group in 2011.[18] Initially, the model was to create a photoswitchable AA:BB type of supramolecular polymer using bis-(diaminopyridinium) and azonaphthyridine monomers. Crystallization of diaminopyridinium tetraphenylborate with an azonaphthyridine derivative was anticipated to form a 2:1 donor:acceptor complex. However, the experiment resulted in 1:1 binding in the solid state. As depicted in Figure 2.10, one arm of the azonapthyridine flipped 180^{o} to create a strong 5-point complex with

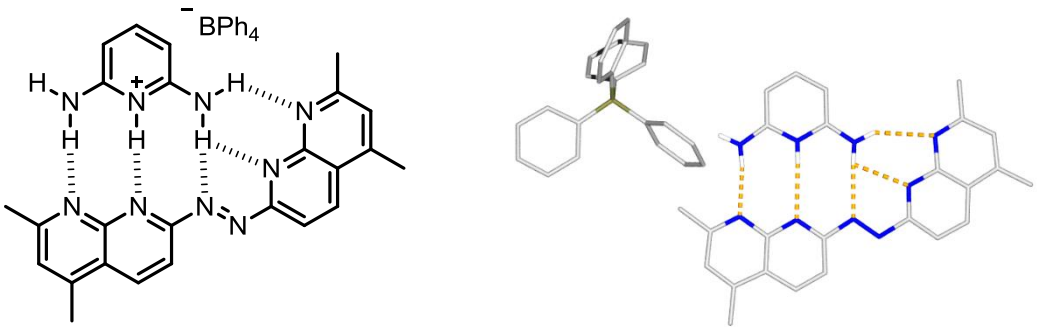

Figure 2.10 Schematic representation of 2,6-diaminopyridinium tetraphenylborate-1,2-bis(5,7-dimethyl-1,8-naphthyridin-2-yl)diazene complex (left). Stick representation of the X-Ray crystal structure obtained by Wisner and co-workers (right). C-H protons have been removed for clarity and hydrogen bonds are depicted as orange dashed lines.

the diaminopyridinium donor. The association constant and photophysics of this complex were also investigated but yielded inconclusive and unreliable results. The project was modified to create a simpler design as a starting point. The azonaphthyridine was simplified to 2,2'-azopyridine (PAP) which can be synthesized in one simple step. In addition, neutral donors which fit the organization of the acceptor sites were chosen to

eliminate any complications (e.g. solubility, counter anions) which could arise from cationic species. Initial studies began with phenylurea, as it contained the correct number and arrangement of donor groups similar to that of the previous structure. It is well known that ureas, as well as thioureas, are effective hydrogen bond donors.[19a-e] Interestingly, when the complexation between phenylurea and PAP was examined, the complex stability was extremely low in the 10 M^{-1} range. We hypothesized that this result was due to the conformational flexibility of the phenyl amide where the hydrogen bond donors may rearrange the desired binding conformation to one with little complementarity for the acceptor (Figure 2.11).

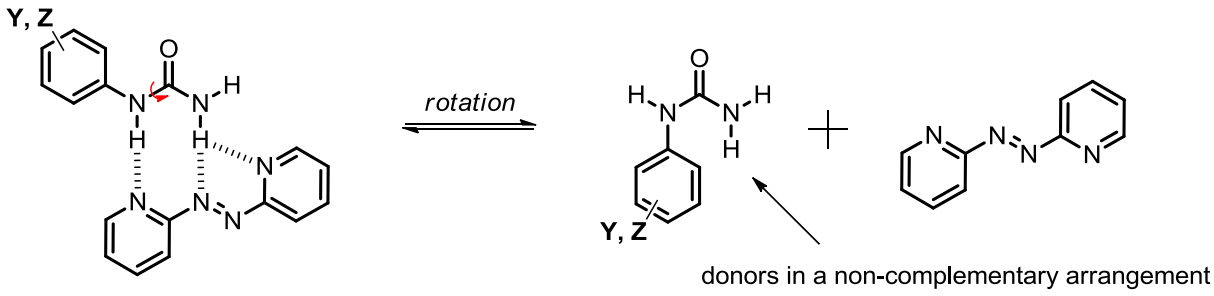

Figure 2.11 Schematic displaying how the rotation of amide bonds in ureas/thioureas would affectively block the ideal hydrogen bonding arrangement

As a solution to this sort of undesired arrangement of donor sites, we decided to focus on 2-aminoindoles. These compounds are planar and rigid in structure and contain the same general arrangement of their donor components as the diaminopyridinium and phenylurea. This indole structure essentially "ties back" the rotation of the phenyl ring and binds the same way as the azonaphthyridine complex (Figure 2.12).

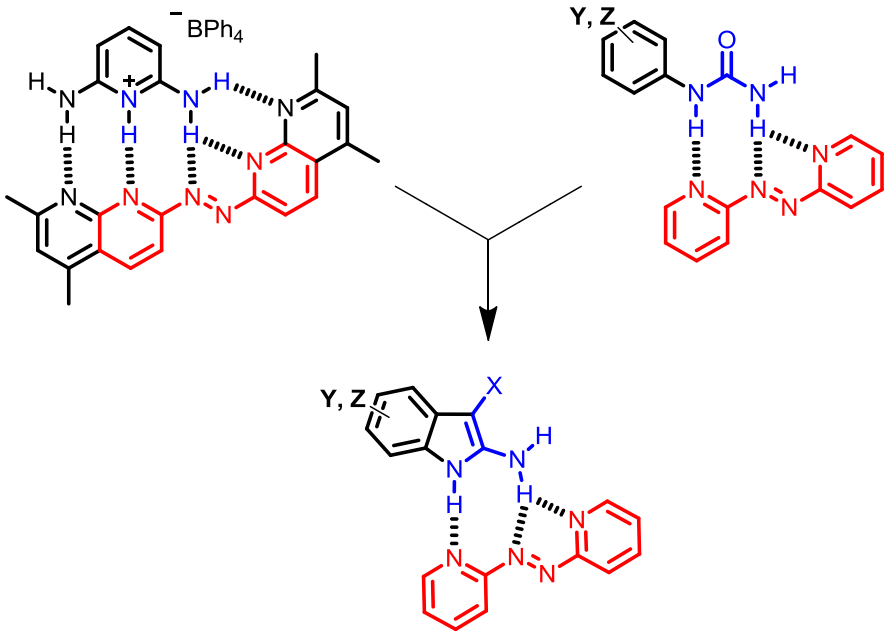

Figure 2.12 The 2-aminoindole and azopyridine complex as a combination which arose from the initial complex and urea donor system.

Another advantage of the indoles is their potential to be modified in multiple positions to affect the donor strength of both the pyrrole and amino NH groups. Dependent on synthetic schemes and starting materials, the 3, 5, and 6 positions can all contain different electron withdrawing groups where X, Y, and Z are in direct conjugation with the pyrrole NH and X and Z with the amino NH_2 (Figure 2.13). Furthermore, these positions could also act at connection points when it comes to creating supramolecular monomers. These groups do however need to be chosen carefully as when molecular polarity increases, solubility in non-polar solvents will likely decrease so

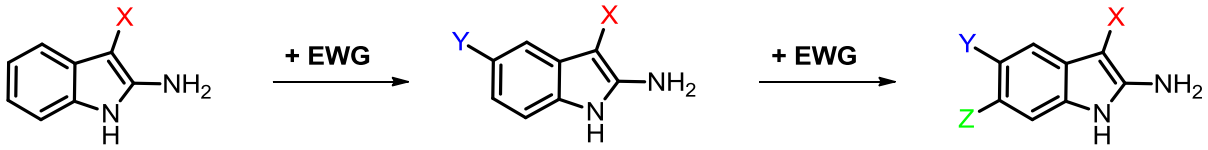

Figure 2.13 2-aminoindoles where the 3, 5, and 6 positions contain additional electron withdrawing substituents (X, Y, Z).

solubilizing substituents will need to be explored. Conversely, the indole cannot be polarized too strongly where the pyrrole NH can be deprotonated by the acceptor as that site is the most acidic. Using these parameters, a simple and cost efficient synthetic method was sought to create a library of indoles. We also explored a cheap and efficient method to synthesize PAP.

2.4 Results and Discussion

2.4.1 Synthesis of Donor Arrays: 2-Aminoindoles

The initial studies of our complementary system began with 2-aminoindole donor modules. There are a few literature methods demonstrating the synthesis of these small molecules.[20a-c] These approaches tend to have low yields and have not been used on a wide variety of substrates but there were two reactions we chose to examine more closely. Scheme 2.1 outlines how copper catalysis can be used in a one-pot, Ullman type coupling between a halo-arene containing a carbonyl directing group and an active methylene compound. A library of 2-aminoindoles can be envisioned by using different initial anilines with various electron withdrawing groups,. Method 1[21] begins with *N*-(o-iodophenyl)-formamides, catalytic CuI and K_2CO_3 in DMSO at high temperatures.

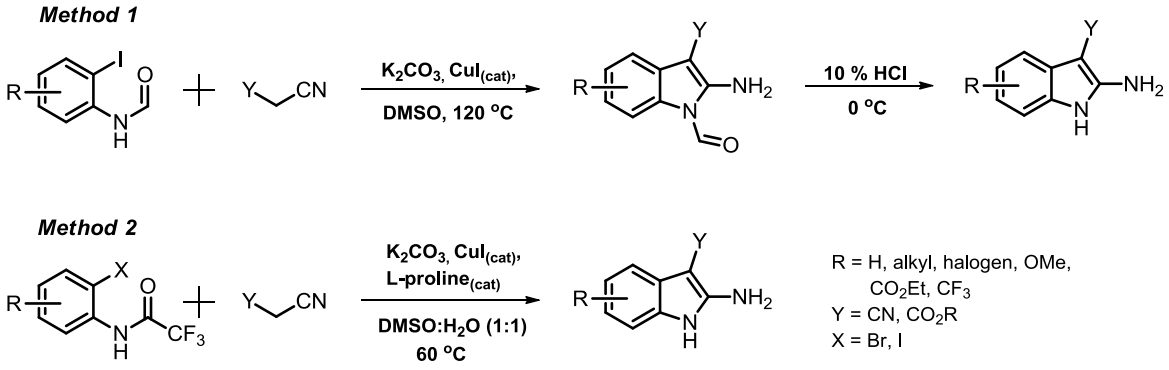

Scheme 2.1 Two indole forming reactions from the literature using Ullman Type Cu(I) coupling procedures.

These conditions combined with an inexpensive, commercially available active methylene compound (either malonitrile (Y = CN) or ethyl cyanoacetate (Y = CO_2Et)) results in a Cu complex. The active methylene moiety undergoes reductive elimination with the aryl group from the Cu complex followed by a nucleophilic attack of the amide nitrogen on the cyano group and subsequent isomerization. The formyl group is then removed by cooling and addition of dilute HCl to yield the 2-aminoindoles. Method 2[22] employs a similar approach but begins with *N*-(*o*-halophenyl)trifluoroacetamides and includes L-proline as a copper solubilizing agent. Ultimately, method 2 was chosen due to simpler access to starting materials, easier work up procedures, and less harsh reaction conditions such as lower reaction temperatures and exclusion of strong acids. Furthermore, the cyclization of the indole and subsequent removal of the carbonyl directing group can be performed simultaneously without altering the reaction environment.

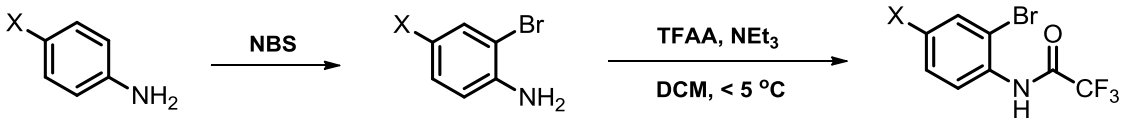

2-1a: X = CO_2Et **(79%)**
2-1b: X = CN **(75%)**
2-1c: X = NO_2 **(97%)**
2-1d: X = COMe **(92%)**
2-1e: X = CH_3 **(46%)**
2-1f: X = CF_3 **(52%)**

2-2a: X = H **(90%)**
2-2b: X = F **(83%)**
2-2c: X = Br **(81%)**
2-2d: X = CO_2Et **(92%)**
2-2e: X = COMe **(88%)**
2-2f: X = CF_3 **(81%)**
2-2g: X = CN **(95%)**
2-2h: X = NO_2 **(75%)**
2-2i: X = CH_3 **(67%)**

Scheme: 2.2 Synthesis of *o*-brominated anilines and *N*-(*o*-bromophenyl)-2,2,2-trifluoroacetamides.

Using method 2, the carbonyl directing group had to be installed onto the *ortho*-bromo-aniline derivatives. Some anilines were purchased inexpensively from commercial sources with the *o*-bromide substituent preinstalled but can also be easily synthesized using a brominating agent. NBS is a common and powerful brominating agent so reacting this reagent with a library of *para*-substituted anilines in appropriate solvents (eg: CH_3CN, $CHCl_3$), the chosen anilines were mono-brominated in moderate to excellent yields. Following bromination, the *N*-trifluoroacetamides were easily synthesized using trifluoroacetic anhydride and a slight excess of triethylamine in dry dichloromethane at low temperature. The mixture was stirred for a minimum of 4 hours but longer reaction times, ideally overnight, led to higher yields and simpler purification procedures.

When it came to performing the final step in the synthesis, the simplest *N*-(*o*-bromophenyl)-2,2,2-trifluoroacetamide (**2-2a**) was used as a test compound and ethyl cyanoacetate as the active methylene component. Performing the reaction in a 1:1 DMSO:H_2O solvent at 60 $^{\circ}$C, our results were not the indole product as expected. The major product determined from the ^{1}H NMR spectrum of the crude mixture was the

initial unacetylated bromoaniline. The trifluoroacetamide group was hydrolyzed in these conditions before the coupling of the methylene compound to the benzene ring could occur. This reaction was tested in the literature on the unacetylated bromoaniline and was found to be unsuccessful at creating the desired indoles. Given this result, the reaction was attempted again in neat dry DMSO, with the subsequent addition of a small amount of water the following day. Performing this new reaction procedure at 60 °C led to an approximate 50:50 mixture of the desired indole and deacetylated bromoaniline so the reaction was repeated at 80 °C. This method at higher temperature displayed much improved results compared to the initial reaction, primarily yielding the desired indole as the main product and only a small amount of the initial deacetylated bromoaniline starting material (Scheme 2.3).

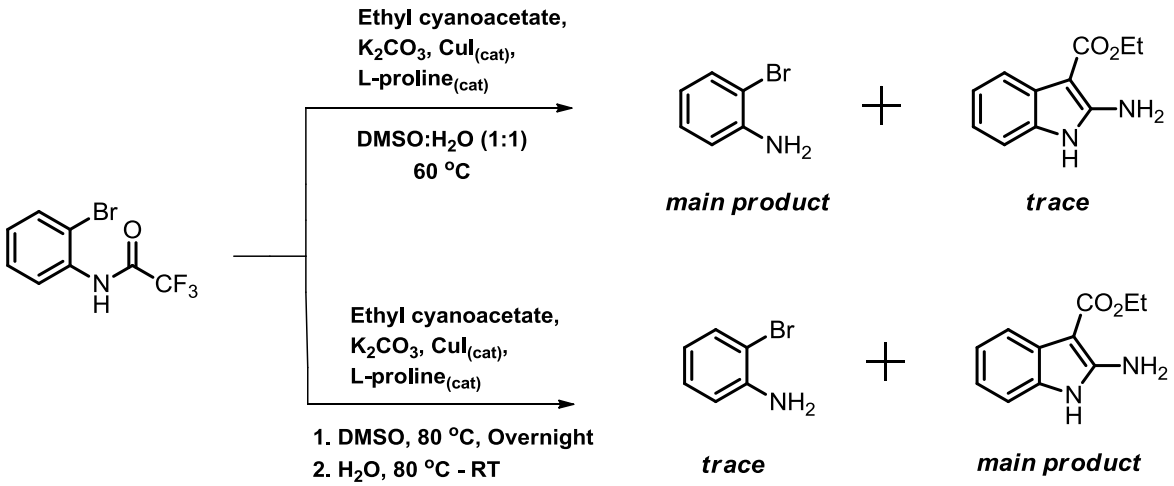

Scheme 2.3 Synthesis of 2-aminoindoles from the literature (above) and the modified procedure adapted for this project (below).

Our library of synthesized trifluoroacetamides were subjected to this last indole-forming step using the improved reaction conditions with ethyl cyanoacetate (Scheme

2.4). The yields of **2-3a-i** were low to moderate using a wide variety of aryl substitutions. Many had not been previously attempted in the literature (eg. COMe, NO_2) but all were stable in the coupling reaction.

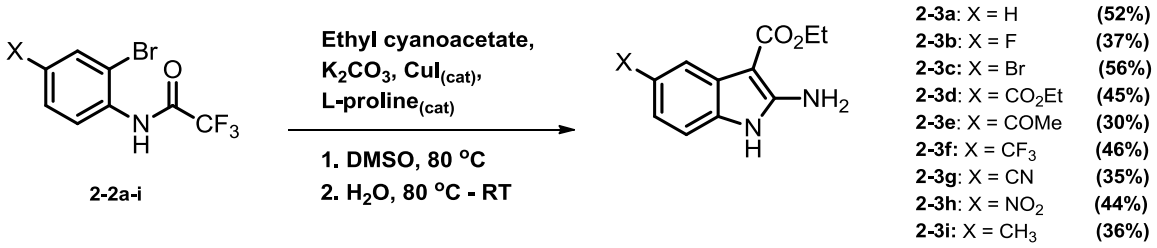

Scheme 2.4 Synthesis of 2-aminoindoles using the modified procedure.

The library so far contained all 5-substituted indoles so to further increase the variety and to create more effective hydrogen bond donors, anilines were employed with two electron withdrawing groups. These anilines were easily brominated using NBS in good yields and the trifluoroacetamide group was also installed using the same above procedure in excellent yields. The copper reaction was replicated from the above examples but lead to insignificant amounts of the desired 5,6-disubstituted indoles. We hypothesized that due to the highly electron deficient benzene ring, higher temperatures might be required for the oxidative addition step to proceed. Repeating the reaction at 100 °C and for a longer duration proved effective in raising the yields to a moderate level (Scheme 2.5).

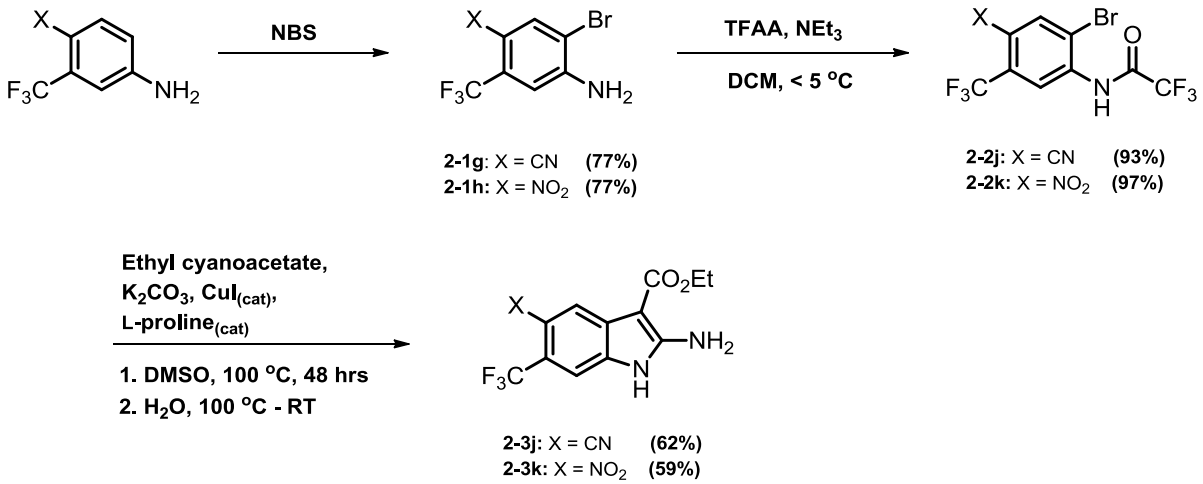

Scheme 2.5 Synthesis of 5,6-disubstitued 2-aminoindoles.

Thus far, all of the synthesized indoles incorporate an ester in the 3-position which is a moderate electron withdrawing group.[23] Ethyl cyanoacetate was therefore exchanged for malononitrile to install a cyano group in the 3-position and exert a greater electron withdrawing effect. In previous studies, it was observed that these 3-cyano derivatives are much less soluble in non-polar solvents than their ester counterparts.[24] Hence, only a select few mono-substituted and both di-substituted trifluoroacetamides were subjected to the same indole-forming cyclization in the hopes of creating stronger hydrogen bond donors (Scheme 2.6).

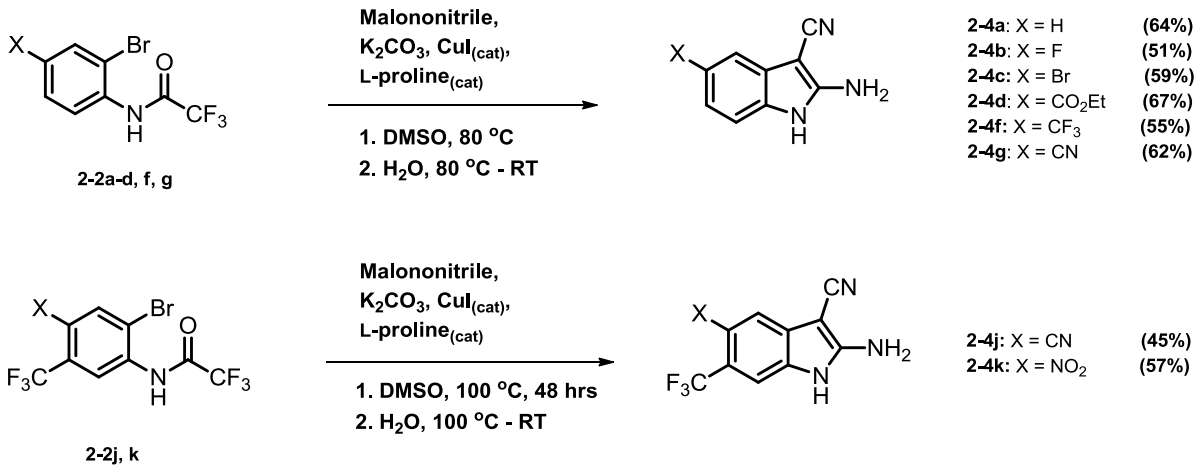

Scheme 2.6 Synthesis of 3-cyano mono-substituted and di-substituted 2-aminoindoles.

2.4.2 Synthesis of Acceptor Array: 2,2'-Azopyridine

We began with 2,2'-azopyridine (PAP) as a simple heteroaromatic azo compound complement for our donor compounds was 2,2'-azopyridine (PAP). The synthesis of symmetric azopyridine compounds is well documented in the literature using aqueous sodium hypochlorite as an oxidant with 2-, 3- or 4-aminopyridines.[25a-h] Yields are typically low for these reactions as common by-products are chlorinated derivatives which can lead to complex crude mixtures. In an attempt to raise the yield of PAP, alternative synthetic methods were attempted. Reductive coupling of 2-nitropyridine,[26] reacting 2- aceto/trifluoroaceto-pyridines with 2-nitro/2-nitrosopyridine,[27] condensation of 2-aminopyridine and 2-nitrosopyridine,[28] and copper coupling of 2-aminopyridine[29] were all examined. Unfortunately, these attempts were unsuccessful in generating improved yields of PAP. Ultimately, we returned to the NaOCl procedure because starting materials are inexpensive and no intermediates had to be synthesized (Scheme 2.7). The slow addition of cold aqueous NaOCl (bleach) into a cold, well-stirred mix of

2-aminopyridine in water formed a dark red solution with a large amount of red precipitate. Extraction of this solution with halogenated solvent and flash chromatography of the crude red oil to remove chlorinated by-products resulted in relatively pure PAP. Further purification was performed by recrystallization in boiling hexanes to yield pure red prisms in 20% yield suitable for analysis in the hydrogen bonding studies.

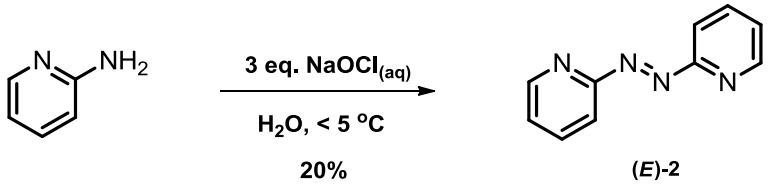

Scheme 2.7 Synthesis of 2,2'-azopyridine.

2.4.3 Solution State Studies

Complex stability needs to be determined to quantify the efficacy of these complementary arrays. Therefore, association constants (K_a values) had to be measured. There are multiple methods available for the determination of K_a values of which not all were applicable for this study. Fluorescence spectroscopy[12,13] is a useful method to determine very large association constants but cannot be employed for the present system as neither array has significant fluorescent emission. Large association constants can also be determined accurately with UV-Vis spectroscopy.[13,14] Test titrations with our two arrays indicated that the features necessary to calculate a K_a value, such as isosbestic point(s), shifts of absorbance bands, or charge transfer bands, were absent. Fluorescence and UV experiments measure the changes in photophysical properties of complexation but another characteristic which could be measured is heat evolution. Calorimetric

methods measure the enthalpic changes upon the addition of one array to the other and heat absorbed or released can be measured by an isothermal titration calorimeter (ITC) for which association constants can be determined with high accuracy.[30] However, ITC is typically only practical for K_a values greater than 1 x $10^{3\text{-}4}$ M^{-1}.

Ultimately, the method chosen to determine the binding strengths of these complexes was ^{1}H NMR spectroscopy. These methods are advantageous because our hydrogen bond donor arrays contain two different donor sites which resonate at different frequencies providing two separate signals for measuring hydrogen bonding shifts and resulting K_a values. Association constants up to 10^5 can be determined accurately with this technique where results higher than 10^5 cannot be taken as reliably.[31] Experimentally if our arrays become too strong, a different method will need to utilized (e.g. ITC).

^{1}H NMR titrations rely on the solution equilibrium between the donor, being the host H, and the acceptor, the guest G. The equilibrium is concentration dependant, and the chemical shift of the host/guest complex in solution can be analytically derived using the following equations.[32]

$$K_a = \frac{[HG]}{[H][G]} \qquad [H] + [G] \rightleftharpoons [HG] \qquad \textbf{Eq. 1}$$

Where, [HG] = concentration of the HG complex

$$[H] = \text{uncomplexed host concentration} = [H]_0 - [HG] \qquad \textbf{Eq. 2}$$

$$[G] = \text{uncomplexed guest concentration} = [G]_0 - [HG] \qquad \textbf{Eq. 3}$$

Where, $[H]_0$ and $[G]_0$= total concentration of host and guest, respectively

The chemical shifts in the equilibrium are defined as:

$$\delta_{obs} = \frac{[HG]}{[H]_0}\delta_{bound} + \frac{[H]}{[H]_0}\delta_{free} \qquad \textbf{Eq. 4}$$

Where, δ_{obs} = the host chemical shift measured at a specific concentration of guest

δ_{bound} = the chemical shift of the host protons in the complex

δ_{free} = the chemical shift of the proton(s) in the free (uncomplexed) host

Substitution of Eq. 2 and 3 into 1 followed by rearrangement into the quadratic equation, the concentration of the complex can be written as:

$$[HG] = \frac{1+K_a([H]_0+[G]_0) - \sqrt{\left(1+K_a\left([H]_0+[G]_0\right)\right)^2 - 4K_a{}^2\,[H]_0[G]_0}}{2\,K_a} \qquad \textbf{Eq. 5}$$

Since Eq. 5 defines [HG], substitution into Eq. 2 gives [H]. Knowing [HG] and [H], those substitutions into Eq. 4 gives the final solution.

$$\delta_{obs} = \frac{(\,1+K_a([H]_0+[G]_0) - \sqrt{\left(1+K_a\left([H]_0+[G]_0\right)\right)^2 - 4K_a{}^2\,[H]_0[G]_0}}{2\,K_a\,[H]_0}\delta_{bound} +$$

$$\frac{\left([H]_0 - \left(\frac{(\,1+K_a([H]_0+[G]_0) - \sqrt{\left(1+K_a\left([H]_0+[G]_0\right)\right)^2 - 4K_a{}^2\,[H]_0[G]_0}}{2\,K_a}\right)\right)}{[H]_0}\delta_{free} \qquad \textbf{Eq. 6}$$

The concentration of the host is maintained at a constant value during these titration experiments. Repeated injections of a host/guest solution are performed to slowly increase the concentration of the guest overall. The chemical shifts of the donor hydrogen atom(s) that are participating in complexation begin to resonate further downfield as electron density decreases. Once enough injections have been performed, the chemical shifts (δ_{obs}) can be plotted against the concentration of the guest using non-linear regression to solve the 1:1 binding model above. The regression solution provides the K_a for the two components being titrated for which the free energy (ΔG) can be calculated, as well as the chemical shifts of the fully complexed pair and free donor array, δ_{bound} and δ_{free} respectively. All titrations were performed in triplicate to obtain an average K_a value and calculated error was reported as twice the standard deviation to achieve a 95% confidence level.

2.4.4 Studies of Ethyl 2-Aminoindole-3-Carboxylates with (*E*)-2

The initial studies were performed with arrays containing an ester group in the 3-position (**2-3a-k**) since all of those synthesized exhibited solubility in deuterated chloroform. Alternative non-competitive solvents were tested for solubility, such as toluene, but none of **2-3a-k** displayed enough solubility for effective titrations to be carried out. Self-association between donor molecules can reduce the effectiveness of binding with the guest so a dilution of indole **2-3f** was carried out to determine if any such association is occurring. Generally, titrations were performed from 0.25 mM to a maximum of 1.0 mM indole concentrations. Beginning at that maximum concentration, a spectrum was taken in deuterated chloroform and diluted to concentrations 0.75, 0.5, and

0.25 mM with a spectrum taken at each dilution and the chemical shifts of the indole and amino protons were monitored. Figure 2.14 below shows the results of this dilution.

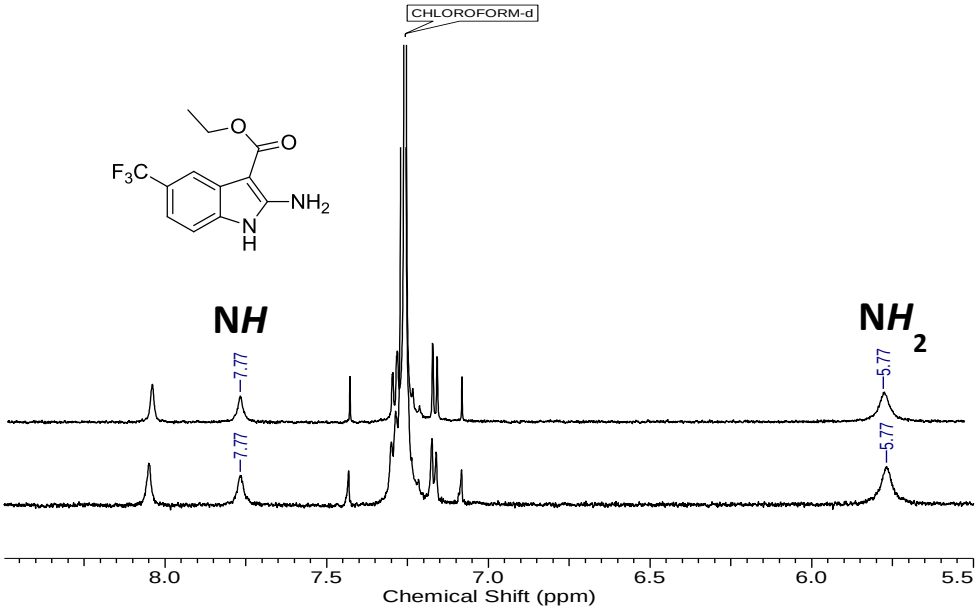

Figure 2.14 Stacked Plot of ^{1}H NMR dilution of indole **2-3f** in $CDCl_3$ at 1.0 mM and 0.25 mM (stacked top to bottom) at room temperature. ^{1}H NMR spectra at concentrations 0.75 and 0.5 mM are not shown.

The indole proton resonates at 7.77 ppm and the amino protons resonate upfield at 5.77 ppm in the 1.0 mM spectrum. Diluting the sample incrementally to 0.25 mM displays no change in both chemical shifts. It can thus be concluded that there are no significant intermolecular interactions occurring which would interfere with the binding of **(*E*)-2**. Given this result, titrations of the indoles were generally performed at the concentration of 1.0 mM to increase the signal to noise ratio unless solubility of the indole derivative was low. In those cases, the titration was performed at a lower concentration. Using Origin® data analysis software, the data was fitted to the 1:1 binding model[32] where the association constants were determined through plotting the pyrrole proton chemical shift against the concentration of **(*E*)-2**. The amino proton shifts

were also plotted and the same association constant value was calculated. The resulting data from the titrations are displayed in Table 2.1.

Table 2.1 Association constants of each indole species **2-3a-k** with **(*E*)-2** (K_a), free energies of complexation (ΔG), and calculated chemical shifts of free indole, fully complexed indole and total change in chemical shift (δ_{free}, δ_{bound} and δ_{max} respectively) in $CDCl_3$ at 298 K.

Indole	K_a (M^{-1})	ΔG (kJ mol^{-1})[a]	δ_{free} (ppm)[a] N*H* N*H*$_2$	δ_{bound} (ppm)[a] N*H* N*H*$_2$	$\Delta\delta_{max}$ (ppm) N*H* N*H*$_2$
2-3a	97 ± 8	-11.34 ± 0.21	7.63 5.67	9.66 6.38	2.03 0.71
2-3b	127 ± 9	-12.01 ± 0.17	7.59 5.70	9.94 6.44	2.35 0.74
2-3c	156 ± 8	-12.51 ± 0.13	7.64 5.72	10.30 6.62	2.66 0.90
2-3d	228 ± 22	-13.45 ± 0.34	7.79 5.74	9.64 6.25	1.85 0.51
2-3e	312 ± 26	-14.23 ± 0.21	7.81 5.76	9.67 6.41	1.86 0.65
2-3f	273 ± 15	-13.90 ± 0.14	7.80 5.77	9.67 6.35	1.87 0.58
2-3g	395 ± 27	-14.81 ± 0.17	7.87 5.83	10.33 6.70	2.46 0.87
2-3h	441 ± 118	-15.07 ± 0.68	7.94 5.87	10.67 6.72	2.73 0.85
2-3i	91 ± 16	-11.16 ± 0.44	7.55 5.63	9.47 6.33	1.92 0.70
2-3j	996 ± 77	-17.10 ± 0.19	8.08 5.98	11.30 7.18	3.22 1.20
2-3k	959 ± 64	-17.01 ± 0.17	8.09 6.00	11.34 7.20	3.25 1.20

[a] Average values calculated from Eq. 6 using the 1:1 regression software. All titrations were performed in triplicate measurements and errors are reported as twice the standard deviation to provide a 95% confidence level. K_a values reported are from the N-*H* titration results.

The association constants for the ester indoles with **(*E*)-2** range from 91 to 996 M^{-1}, or roughly 10^1 to 10^3. The lowest K_a value was measured with the 5-methyl indole (**2-3i,** Figure 2.15) which is a weak electron donating group and therefore made the complexation with **(*E*)-2** slightly weaker than the unsubstituted derivative (**2-3a**). Substituting the 5-position with increasingly stronger electron withdrawing groups develops a general trend where the complex stability increases to where the strongest derivatives with two electron withdrawing groups (**2-3j,k**) result in a K_a value almost 2 orders of magnitude greater than the unsubstituted analogue (Figure 2.16).

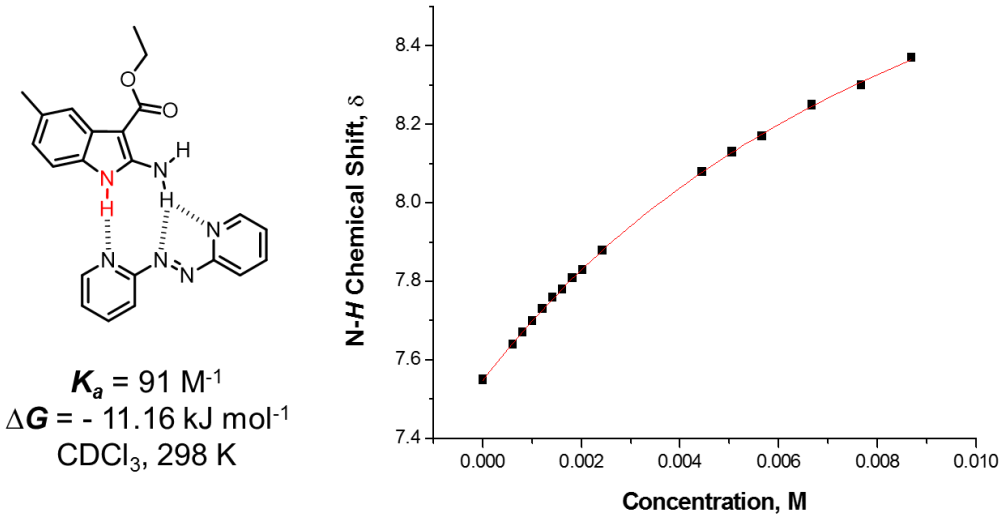

Figure 2.15 Indole N-*H* ^{1}H NMR titration data and calculated binding isotherm for complex formation between **2-3i** and **(*E*)-2**. K_a, calculated free energy of complexation and schematic of complex depicted on the left.

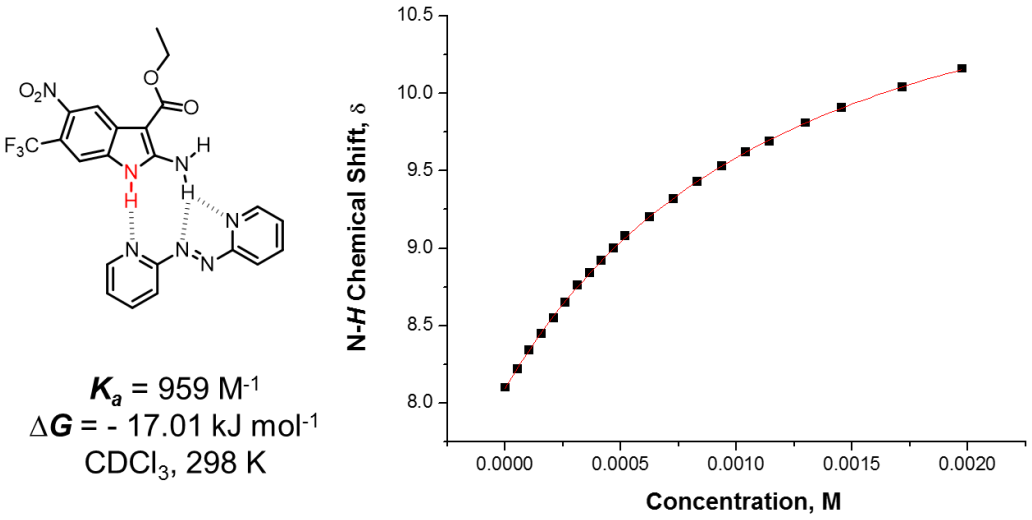

Figure 2.16 Indole N-*H* ^{1}H NMR titration data and calculated binding isotherm for complex formation between **2-3k** and **(*E*)-2**. K_a, calculated free energy of complexation and schematic of complex depicted on the left.

In all of the titrations with **2-3a-k**, the indole and the amino protons begin to shift downfield as the concentration of **(*E*)-2** increases. The weaker indole donors initially resonate at a lower chemical shift while stronger donors have higher initial values. The same trend can be seen in the fully complexed chemical shifts calculated where the strongest complexes resonate most downfield. Furthermore, stronger complexes have a larger range from the calculated δ_{free} to δ_{bound} values observed with both the pyrrole and amino groups. Figure 2.17 depicts how the amino and pyrrole resonances incrementally travel downfield during the titration process.

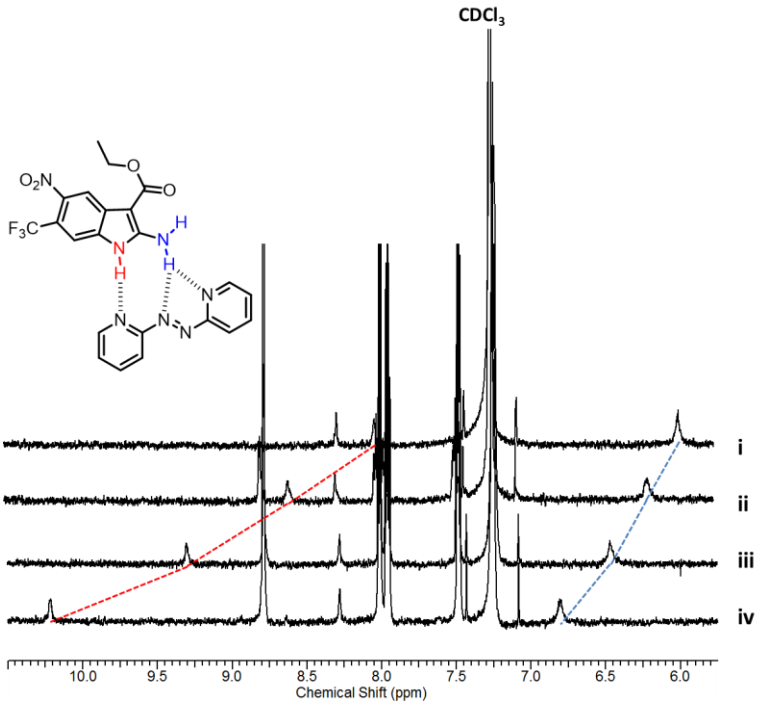

Figure 2.17 ^{1}H NMR titration stacked plot of array **2-3k·(*E*)-2** in $CDCl_3$ at 298 K; red lines corresponds to N-*H* and blue to N*H*2. i) 0 equivalents of **(*E*)-2**, ii) 1 molar equivalent of **(*E*)-2**, iii) 4 molar equivalents of **(*E*)-2**, iv) 9 molar equivalents of **(*E*)-2**.

Given the results collected in Table 2.1, we were interested in whether the association constants and the substituents were linked by a Linear Free Energy Relationship (LFER). Similar studies of substituent effects with titrations of double helical arrays have been performed.[33] Therefore, using the substituents' $\sigma_{m,p}$ values (Hammett constants)[23] relative to the pyrrole N*H* (i.e. the 5- or 5- and 6- positions), these values were plotted against the log of the K_a value. The resulting plot shows a good correlation (ρ_σ = 0.8121, R^2 = 0.9833) between these two variables and establishes a LFER. The positive ρ_σ value (0.8121) indicates that a partial negative charge is being produced on the indole donors which is being stabilized by the electron withdrawing

groups. The increasing electron withdrawing character on the benzenoid ring therefore creates stronger complexes as a result of the stabilized hydrogen bonded complex.

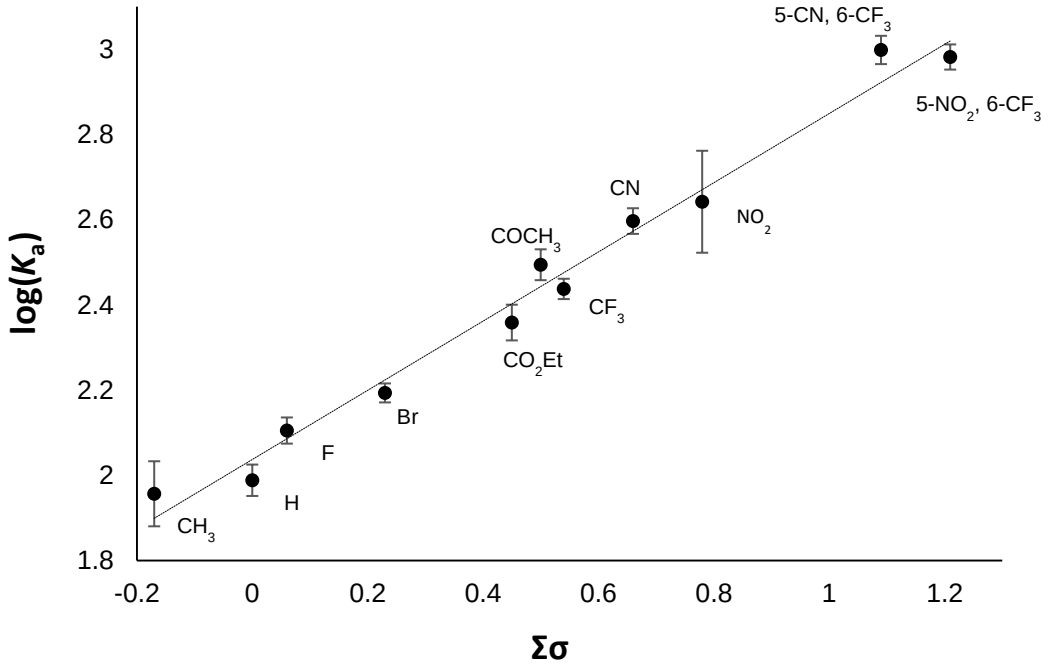

Figure 2.18 LFER of **Σσ** vs **log(K_a)** for derivatives **2-3a-k** with **(*E*)-2**. Linear fit representation by the dotted black line (ρ_σ = 0.8121, R^2 = 0.9833).

The LFER exhibited by the binding of derivatives **2-3a-k** with **(*E*)-2** shown above supports the conclusion that the binding of all complexes is occurring in the same manner. To further support this proposal of binding geometry, a ^{1}H 2D NOESY experiment was carried out with **(*E*)-2** and derivative **2-3j** in $CDCl_3$. The resulting 2D spectrum (Figure 2.19) displays the expected weak correlation between the aryl proton closest to the indole N*H* (H^c) and the *ortho* protons on the pyridine rings of **(*E*)-2** ($H^{e/e'}$). Curiously, no correlation is observed here for the amino group ($H^{b/b'}$) and $H^{e'/e}$, though the proposed complex geometry would predict one.

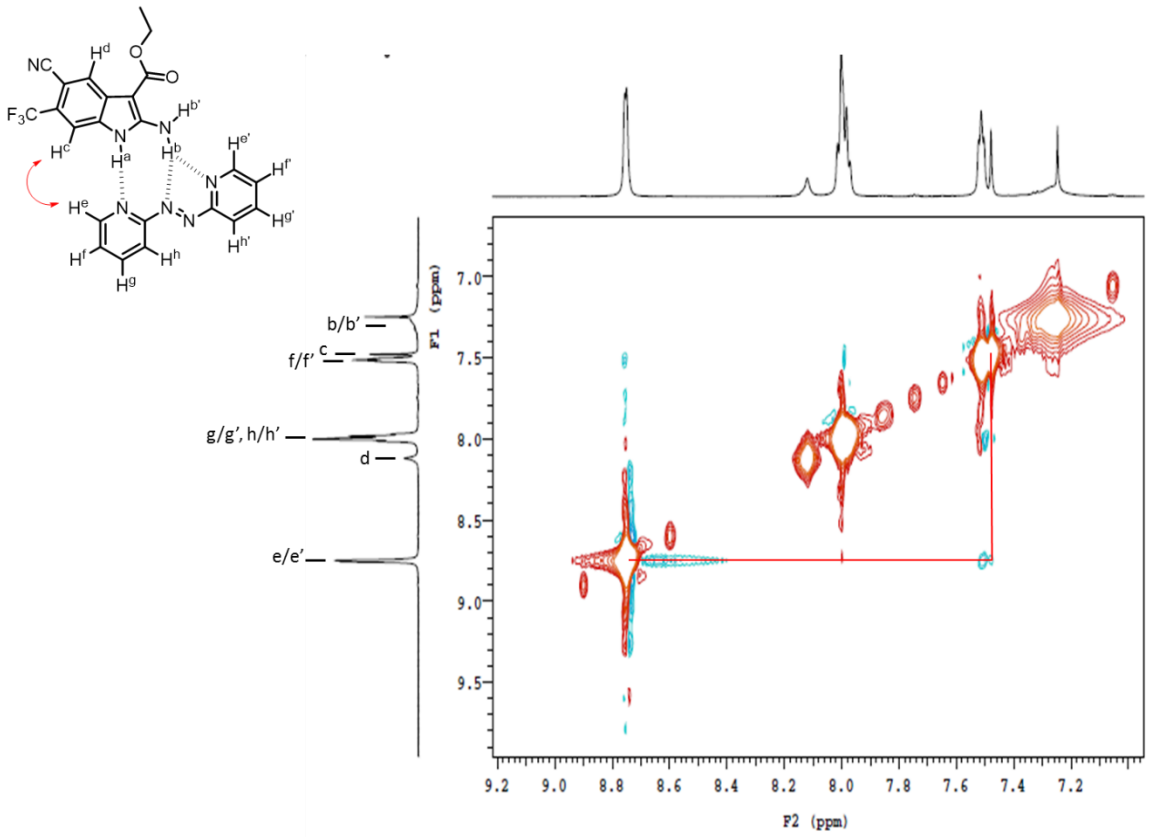

Figure 2.19 2D ^{1}H NOESY spectrum of **2-3j·(*E*)-2** in $CDCl_3$ at 298 K. Correlations of interest are indicated by red arrows in structure and red lines on spectrum.

2.4.5 Studies of 2-Aminoindole-3-carbonitriles with (*E*)-2

Given the successful complexation of derivatives **2-3a-k** with **(*E*)-2**, indoles with a cyano group at the 3 position were investigated. The first observations, as previous stated, are that the cyano derivatives are much less soluble than their ester counterparts. Only three of the synthesized derivatives were soluble in $CDCl_3$ and the titration results are listed below in Table 2.2.

Table 2.2 Association constants of each indole species **2-4a-d**, **f**, **g**, **j**, **k** with **(*E*)-2** (K_a), free energies of complexation (ΔG), and calculated chemical shifts of free indole, fully complexed indole and total change in chemical shift (δ_{free}, δ_{bound} and δ_{max} respectively) in $CDCl_3$ at 298 K . (-) indicates insolubility in $CDCl_3$.

Indole	K_a (M^{-1})	ΔG (kJ mol^{-1})[a]	δ_{free} (ppm)[a]	δ_{bound} (ppm)[a]	$\Delta\delta_{max}$ (ppm)
			N***H***	N***H***	N***H***
			NH_2	NH_2	NH_2
2-4a	237 ± 11	-13.54 ± 0.11	7.72	10.79	3.07
			4.57	5.73	1.16
2-4b	266 ± 17	-13.84 ± 0.15	7.69	11.17	3.48
			4.61	5.96	1.35
2-4c	-	-			
2-4d	-	-			
2-4f	735 ± 8	-16.35 ± 0.03	7.94	10.98	3.04
			4.72	5.87	1.15
2-4g	-	-			
2-4j	-	-			
2-4k	-	-			

[a] Average values calculated from Eq. 6 using the 1:1 regression software. All titrations were performed in triplicate measurements and errors are reported as twice the standard deviation to provide a 95% confidence level

The cyano derivatives prove to form stronger complexes than the corresponding ester derivatives (**2-3a**, **b**, **f** with **(*E*)-2**). For example, when comparing **2-3f** and **2-4f** where the 5-position is substituted with a trifluoromethyl group, the K_a has risen from 273 to 735 M^{-1} which correlates to a gain of 2.45 kJ/mol in free energy. This general increase can be seen in all three of the derivatives examined as well as a more downfield pyrrole hydrogen shift in the free donor array. The major difference is observed in the unbound amino resonance which appears further upfield than in the ester library. This is most likely a result of intramolecular hydrogen bonding with the ester carbonyl group. The cyano group does not have that ability due to its disposition in the indole relative to the amino group. Nonetheless, these compounds behaved in the same manner as the ester

library when titrated with **(*E*)-2**. The N-H chemical shifts of the pyrrole and amino groups can be plotted and the association constants calculated using the method described above.

As with derivatives **2-3a-k**, we were hoping to achieve a correlation between the association constants and the sigma values of the substituents on the benzenoid ring. However, with only 3 soluble derivatives and therefore only 3 data points, the correlation would not be very meaningful. In hopes of obtaining more data points for this analysis, two more indoles with longer alkyl chains and strong withdrawing groups were synthesized with the intention of increasing solubility in $CDCl_3$ (Scheme 2.8).

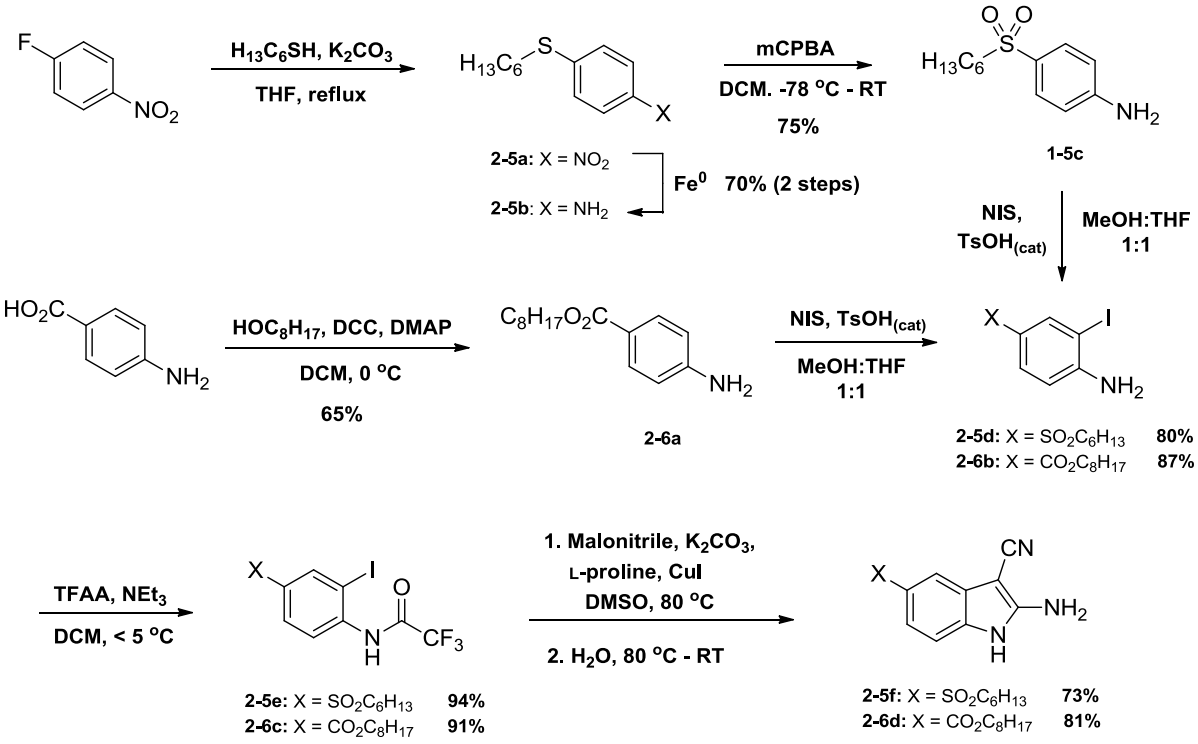

Scheme 2.8 Synthesis of 5-hexylsulphonyl-(**2-5f**) and 5-octyloxycarbonyl-(**2-6d**) 2-aminoindole-3-carbonitrile.

Derivative **2-5f** contains a hexyl sulfone group. 1-Fluoro-4-nitrobenzene, 1-hexanethiol and K_2CO_3 were refluxed in THF overnight to achieve quantitative conversion to the aryl-thioether **2-5a**. The crude nitro product was then reduced with iron metal in a mixture of acetic acid and water to produce aniline **2-5b**. Slow addition of 2 equivalents of mCPBA in DCM cooled to -78 $^{\circ}$C and subsequent warming to room temperature overnight lead to sulfone **2-5c**. The indole cyclization requires that the aniline must be *ortho*-halogenated. It was decided that a switch from *o*-bromo to *o*-iodo aniline would be beneficial at this stage. The moderate yields observed in prior *o*-bromoaniline reactions and the literature demonstrate that the iodo derivatives exhibit better yields.[21,22] Iodination with NIS at room temperature lead to a complex mixture of products of mono and di-iodinated, unreacted aniline and some azobenzene products. Lowering the temperature of the dissolved aniline in an ice bath and adding a small amount of acid catalyst followed by slow additions of NIS led to a much higher yield of mono-iodinated product. Once pure **2-5d** was isolated, the TFAA/NET_3 acetylation was performed in excellent yield without any necessary purification. The copper catalyzed cyclization was carried out as previously detailed producing good yield of indole **2-5f.** Luckily, this indole was soluble in $CDCl_3$ so the titration was carried out. A K_a value of 1270 (± 15) M^{-1} (ΔG = -17.69 ± 0.03 kJ mol^{-1}) was obtained; the highest value for a mono-substituted indole yet to be observed in this study.

The ethyl ester derivative (**2-4d**) was insoluble in $CDCl_3$, so an octyl group was installed on *para*-aminobenzoic acid using DCC coupling and carried through the same synthetic procedures described above to generate **2-6d**. Interestingly, even with the

longer octyl chain installed, the indole was completely insoluble in $CDCl_3$. Therefore, a binding constant was not able to be measured.

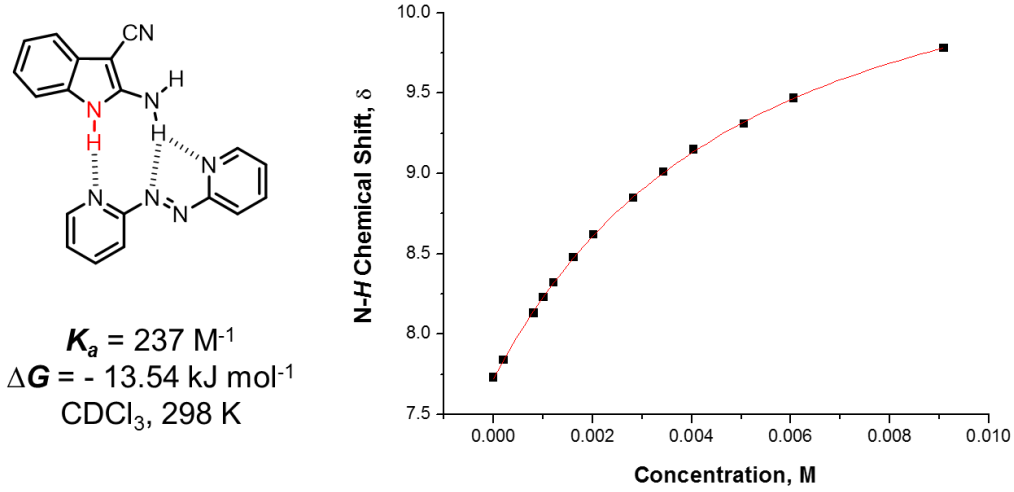

Figure 2.20 Indole N-*H* ^{1}H NMR titration data and calculated binding isotherm for complex formation between **1-4a** and **(*E*)-2**. K_a, calculated free energy of complexation and schematic of complex depicted on the left.

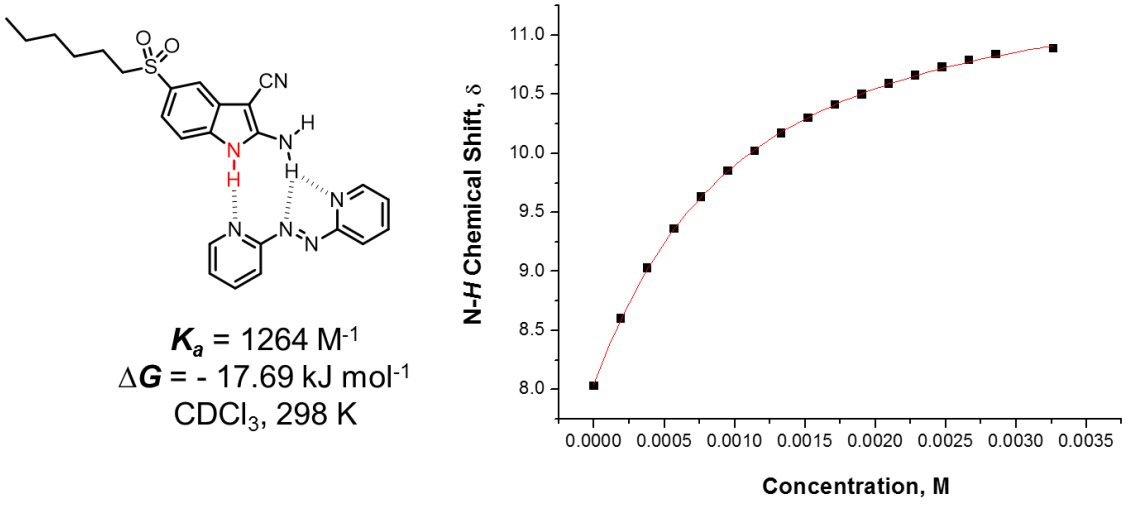

Figure 2.21 Indole N-*H* ^{1}H NMR titration data and calculated binding isotherm for complex formation between **1-5f** and **(*E*)-2**. K_a, calculated free energy of complexation and schematic of complex depicted on the left.

Now with 4 association constants in hand, a LFER similar to that of the ester derivatives can now be examined with greater accuracy. The σ_p values and the log of K_a are used as previously and a stronger correlation is observed for these derivatives (ρ_σ = 0.9401, R^2 = 0.9994). The same positive value of ρ_σ results in the same stabilization of the partial negative charge being created in the system. This value is however greater than the LFER for derivatives **2-3a-k**. This higher value (ρ_σ closer to 1)[34a,b] is attributed to the cyano group adding a greater withdrawing effect than the ester in the 3-position. Cyano groups are stronger withdrawing groups which therefore exhibit greater stabilization of the partial negative charge.

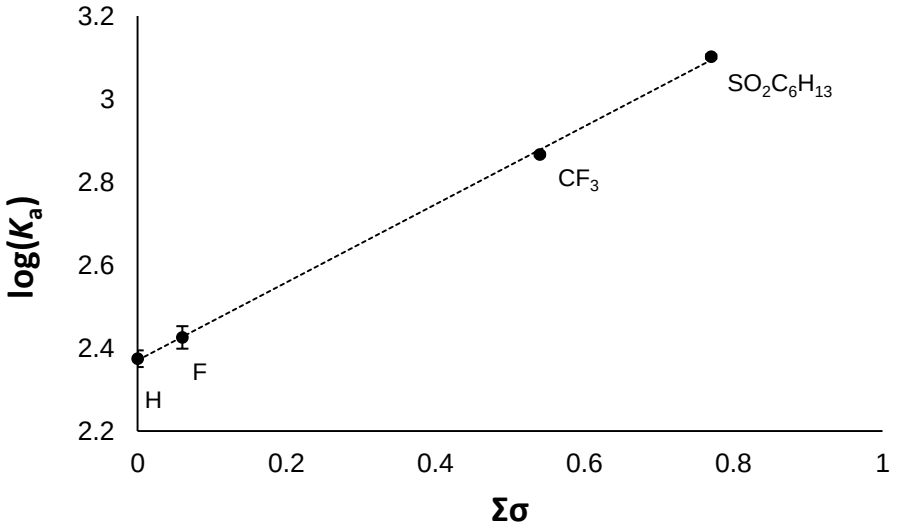

Figure 2.22 Plot of Σσ vs log(K_a) for derivatives **2-4a**, **b**, **f** and **2-5f** with **(*E*)-2**. Linear fit representation by the dotted black line (ρ_σ = 0.9401, R^2 = 0.9994).

A 2D ^{1}H NOESY spectrum was also collected to support the analogous binding of the cyano derivatives to **(*E*)-2** as observed in the ester derivatives. **2-4f** and **(*E*)-2** were

examined in $CDCl_3$ and the same H^c : $H^{f/f'}$ correlation was observed. Additionally, correlations between the indole amino protons ($H^{b/b'}$) and pyridyl *ortho*-protons $H^{f/f'}$ were present which further supports our predicted binding geometry of the complex.

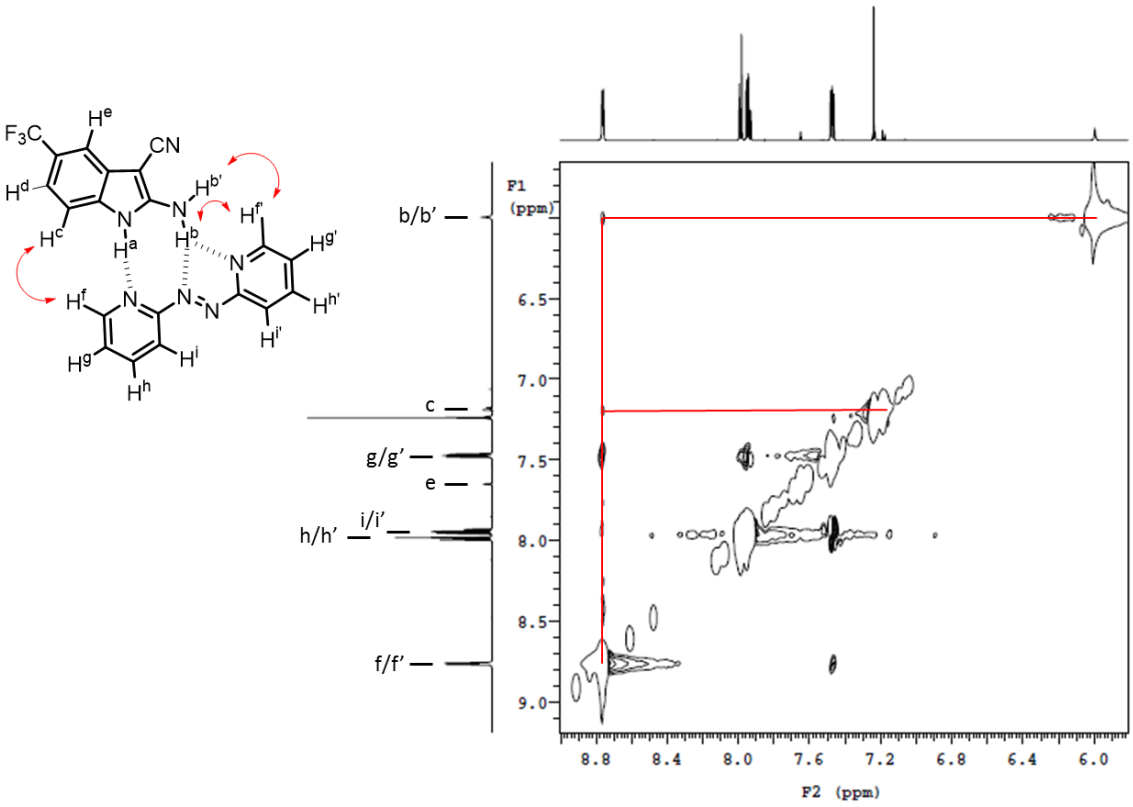

Figure 2.23 2D ^{1}H NOESY spectrum of **2-4f·(*E*)-2** in $CDCl_3$ at 298 K. Correlations of interest are depicted by red arrows in structure and red lines in spectrum.

The sulfone derivative **2-5f** was the strongest complex measured experimentally but theoretically, it is not the strongest possible indole which was synthesized. The cyano disubstituted derivatives **2-4j** and **2-4k** have two electron withdrawing groups which have a cumulative electron withdrawing character surpassing **2-5f** based on $\Sigma\sigma_{m,p}$ values. Knowing these respective $\Sigma\sigma_{m,p}$ values, their respective association constants and free energies can be estimated by using the reaction constant derived from the LFER.

Hence,

for **2-4j:** $\log(K_a) = 0.9401(1.09) + 2.3698$ **where 1.09 = $\Sigma\sigma_{m,p}$**

$$\log(K_a) = 3.39 \text{ or } K_a = 10^{3.39}\ M^{-1}$$

$$\boldsymbol{K_a = \sim 2460\ M^{-1}} \text{ and } \Delta\boldsymbol{G = -19.35\ kJ/mol}$$

Similarly, for **2-4k:** $\log(K_a) = 0.9401(1.21) + 2.3698$ **where 1.21 = $\Sigma\sigma_{m,p}$**

$$\log(K_a) = 3.51 \text{ or } K_a = 10^{3.51}\ M^{-1}$$

$$\boldsymbol{K_a = \sim 3240\ M^{-1}} \text{ and } \Delta\boldsymbol{G = -20.03\ kJ/mol}$$

The LFER plot resulted in an R^2 value of 0.9994 so, theoretically, these estimations can be considered rather precise. Unfortunately, there is no method available to verify them.

2.4.6 Solid State Analysis of Complementary Arrays

Once the indole donors and azopyridine were synthesized and titrations performed, we attempted to co-crystallize the two arrays and study any potential binding interactions in the solid state. Hopefully, the results will support the predicted binding mode in the solution state. Crystals suitable for X-ray crystallography were grown by one of two methods. Either slow evaporation of chloroform or dichloromethane containing a 1:1 mixture of each of the indole derivatives with **(*E*)-2** or slow diffusion of isopropylether or hexanes into solutions of chloroform or dichloromethane containing the same mixtures. Indoles **2-3** with the ester group in the 3-position gave generally better

results with the slow evaporation method. On the other hand, the slow diffusion method was more successful with derivatives **2-4**.

There were two common outcomes resulting from these crystallization attempts; the first being that many of these indoles prepared were either insoluble or sparingly soluble in chlorinated solvents. Upon addition of the acceptor, the mixtures became completely clear or appeared less cloudy. This indicates that the acceptor is drawing the indole donor into solution, which in turn is indicative of complexation. The second effect observed was that both methods produced a common crystal which was solely azopyridine. Therefore, azopyridine has a high propensity for self-crystallization and is competing with a co-crystallization process with the donors. In many cases, small colorless crystals also formed which were presumably crystallized indole alone. Nonetheless, solutions containing **2-3f**, **2-3g**, **2-3e**, **2-4a** and **2-4g** with **(*E*)-2** all produced dark red to violet single crystals suitable for X-ray analysis. They are easily identified by inspection as they differ from azopyridine crystals which are orange and thin in profile. The crystallographic parameters of the **2-3** complexes crystallized are listed in Table 2.3 while complexes containing **2-4** are compiled in Table 2.6.

Table 2.3 Crystallographic X-Ray Crystal Structure Data of **2-3f·(*E*)-2**, **2-3g·(*E*)-2** and **2-3e·(*E*)-2.**

Crystal Parameters	**2-3f·(*E*)-2**	**2-3g·(*E*)-2**	**2-3e·(*E*)-2**
Chemical Formula	$C_{22}H_{19}F_3N_6O_2$	$C_{22}H_{23}N_7O_2$	$C_{23}H_{22}N_6O_3$
Formula Weight	456.43	417.47	430.74
Crystal System	Monoclinic	Monoclinic	Triclinic
Space Group	$P2_1/c$	$P2_1/c$	P-1
***a* (Å)**	9.023(10)	9.514(3)	9.678(15)
***b* (Å)**	9.964(11)	26.708(8)	11.070(16)
***c* (Å)**	22.015(3)	8.529(3)	11.216(16)
***α, β, γ* (°)**	90, 99.1(3), 90	90, 113.1(2), 90	62.3(3), 81.0(4), 80.6(4)
***V* (Å)^3**	2131.8(4)	1992.84(11)	1044.9(3)
***T* (K)**	150(2)	150(2)	150(2)
Z	4	4	2
***λ* (Mo K*α*) (Å)**	0.71073	0.71073	0.71073
D_{calc} (mg/cm^3)	1.422	1.391	1.368
***μ* (mm^{-1})**	0.113	0.094	0.094
***F* (000)**	944	880	452
Total Reflections	25804	34352	15462
Unique Reflections	4371	4993	5112
Absorption	Multi-scan	Multi-scan	Multi-scan
refinement on	F^2	F^2	F^2
$R(F_0)$($I>2\sigma(I)$)	0.0668	0.0470	0.0537
$Rw(F_0^2)$($I>2\sigma(I)$)	0.1568	0.1177	0.1153
$R(F_0)$ (all data)	0.1122	0.0843	0.1208
$Rw(F_0^2)$ (all data)	0.1912	0.1404	0.1363
GOF on F^2	0.889	0.899	1.023

The solid state structure of **2-3f·(*E*)-2** contains 8 molecules per unit cell in space group $P2_1/c$. This monoclinic system contains planar arrays of the indole and azopyridine binding in the predicted manner, as discussed in the previous section. The indole N-H proton forms a primary hydrogen bond with one of the nitrogen acceptors on a pyridyl ring of **(*E*)-2** (Figure 2.24, N1-H1···N3 = 2.96 Å, N1-H1···N3 = 2.08 Å, N1-H1···N3 = 167°). One of the amino hydrogen donors forms two hydrogen bonds, one with a nitrogen acceptor of the azo moiety (N2-H2A···N4 = 3.20 Å, N2-H2A···N4 = 2.36 Å, N2-H2A···N4 = 162°) and one with the second pyridyl ring (N2-H2A···N6 = 2.97 Å, N2-H2A···N6 = 2.43 Å, N2-H2A···N6 = 121°). The other amino hydrogen forms an intramolecular hydrogen bond with the ester carbonyl (N2-H2B···O1 = 2.79 Å, N2-H2B···O1 = 2.20 Å, N2-H2B···O1 = 124°)

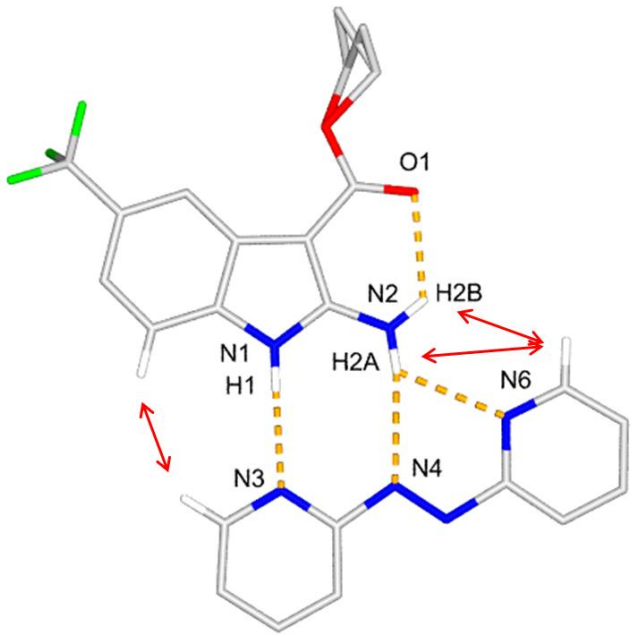

Figure 2.24 Stick representation of complex **2-3f·(*E*)-2**. Hydrogen bonds depicted as orange dashed lines. C-H bonds removed for clarity except for expected NOESY correlations, depicted by red arrows.

The observed hydrogen bonding motif is optimized by the co-planar arrangement of the sp^2-hybridized atoms in the complex. The ethyl group is disordered but excluding that and the trifluoromethyl substituent, the deviation of the remaining indole atoms of their least squares planes does not exceed ± 0.032 Å. The planarity and arrangement of the donors results in an s-*cis*, s-*trans* **(*E*)-2** conformer where the two pyridyl rings take up an angle of 4.1° between their least squares planes. The indole and azopyridine (**(*E*)-2** least squares plane ± 0.082 Å) least squares planes form a 6.2° angle. The lattice is further stabilized by sheets of π-stacked complexes.

This structure also allows us to examine the ^{1}H 2D NOESY spectral results seen in Figure 2.19. The *ortho*-pyridyl proton distance from the aryl proton is 2.70 Å which was the only observed nOe correlation. Slightly larger are the amino donor distances to the *ortho*-pyridyl proton; 3.01 Å for H2B and 3.49 Å for H2A. Theoretically, an nOe effect can be detected through space if the distance is < 5 Å.[35] The amino distances fall within that range but aren't detected, possibly due to the rotational freedom of both the amino group and the pyridyl ring.

Indoles **2-3g** and **2-3e** also formed crystals with **(*E*)-2** suitable for X-ray analysis (Figure 2.25). **2-3g·(*E*)-2** formed a monoclinic system with 8 molecules per unit cell with space group $P2_1/c$. **2-3e·(*E*)-2** formed a triclinic system with space group P-1 containing 4 molecules per unit cell. Both crystals resulted in similar hydrogen bonded complexes analogous to crystal **2-3f·(*E*)-2**. The bond lengths and bond angles of interest are compiled in Tables 2.4 and 2.5, for **2-3g·(*E*)-2** and **2-3e·(*E*)-2** respectively.

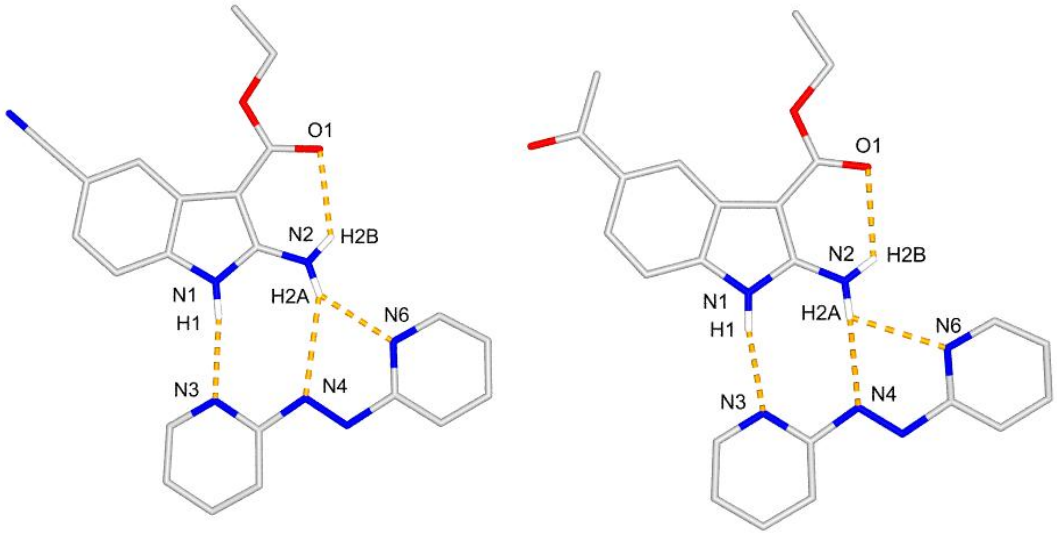

(i) **(ii)**

Figure 2.25 Stick representation of complexes **2-3g·(*E*)-2 (i)** and **2-3e·(*E*)-2 (ii)**. Hydrogen bonds depicted as orange dashed lines. C-H bonds have been removed for clarity.

Table 2.4 Bond lengths and bond angles of hydrogen bonds of interest from crystal **2-3g·(*E*)-2**.

Bond Lengths (Å)				**Bond Angles (°)**	
N1-H1···N3	2.97	N2-H2A···N6	2.92	N1-H1···N3	170
N1-H1···N3	2.10	N2-H2A···N6	2.19	N2-H2A···N4	152
N2-H2A···N4	3.39	N2-H2B···O1	2.84	N2-H2A···N6	142
N2-H2A···N4	2.61	N2-H2B···O1	2.21	N2-H2B···O1	130

Table 2.5 Bond lengths and bond angles of hydrogen bonds of interest from crystal **2-3e·(*E*)-2**.

Bond Lengths (Å)				**Bond Angles (°)**	
N1-H1···N3	2.95	N2-H2A···N6	2.97	N1-H1···N3	165
N1-H1···N3	2.09	N2-H2A···N6	2.49	N2-H2A···N4	162
N2-H2A···N4	3.11	N2-H2B···O1	2.83	N2-H2A···N6	115
N2-H2A···N4	2.26	N2-H2B···O1	2.25	N2-H2B···O1	124

As with the hydrogen bonding motif, the packing and planarity of the crystal lattice also remains similar. **(*E*)-2** in both complexes is in the s-*cis*, s-*trans* conformation with the least squares planes of the pyridyl rings taking up angles of 10.1° (**2-3g·(*E*)-2**) and 7.1° (**2-3e·(*E*)-2**). The arrays crystallized in the optimal co-planar arrangement to maximize hydrogen binding efficacy. The least squares plane of **2-3g** (± 0.073 Å; excluding substituents) and **(*E*)-2** (± 0.147 Å) take up an angle of 3.0°. On the other hand, the interplanar angle of the least squares planes of **2-3e** (± 0.047 Å; excluding substituents) and **(*E*)-2** (± 0.102 Å) is larger at 14.0°. Since all of the hydrogen bond distances and angles in all three **1-3·(*E*)-2** complexes do not deviate much from one another, the small variations in the co-planar arrangements are likely a result of crystal packing. Lastly, the same expected nOe correlations with the *ortho*-pyridyl protons were measured (not shown in Figure 2.25 for clarity) and did not deviate from the previous structure.

In all three structures discussed, there were no inter- or intramolecular interactions observed with the substituent in the 5-position on the benzenoid ring. Additionally, no intermolecular interactions with the ester in the 3-position was detected. There is however an intramolecular hydrogen bond interaction between the ester carbonyl and amino hydrogen H2B. This interaction in all complexes had similar bond lengths and angles within the theoretical O···N hydrogen bonding range (2.95 Å).[36] This phenomenon supports the observation as to why the NH_2 protons in ester derivatives (**2-3**) resonate further downfield than in the cyano indoles (**2-4**).

Table 2.6 Crystallographic X-Ray Crystal Structure Data of **2-4a·(*E*)-2** and **2-4g·(*E*)-2**.

Crystal Parameters	**2-4a·(*E*)-2**	**2-4g·(*E*)-2**
Chemical Formula	$C_{19}H_{15}N_7$	$C_{20}H_{14}N_8$
Formula Weight	341.38	366.39
Crystal System	Monoclinic	Monoclinic
Space Group	$P2_1/n$	$P2_1/n$
***a* (Å)**	10.7394(13)	18.8012(15)
***b* (Å)**	8.4014(10)	7.3208(6)
***c* (Å)**	18.832(2)	26.092(2)
***α, β, γ* (°)**	90, 98.925(3), 90	90, 99.260(3), 90
***V* (Å)^3**	1678.5(4)	3544.5(5)
***T* (K)**	150(2)	150(2)
Z	4	8
λ (Mo K*α*) (Å)	0.71073	0.71073
D_{calc} (mg/cm^3)	1.351	1.373
μ (mm^{-1})	0.087	0.089
***F* (000)**	712	1520
Total Reflections	23297	80822
Unique Reflections	2964	8775
Absorption	Multi-scan	Multi-scan
refinement on	F^2	F^2
$R(F_0)$(I>2σ (I))	0.0665	0.0484
$Rw(F_0^2)$(I>2σ (I))	0.1521	0.0986
$R(F_0)$ (all data)	0.1387	0.1040
$Rw(F_0^2)$ (all data)	0.1867	0.1199
GOF on F^2	1.020	0.994

Two crystals containing complexes of **(*E*)-2** with 3-cyano indole derivatives were successfully grown by the slow diffusion method (Figure 2.26). Both **2-4a·(*E*)-2** and **2-**

4g·(*E*)-2 crystals were red plates in monoclinic crystal systems with space group $P2_{1/n}$. The arrays formed the same hydrogen bonding arrangement with bond lengths and angles equivalent to the previously described structures. These lengths and angles are listed in Tables 2.7 and 2.8.

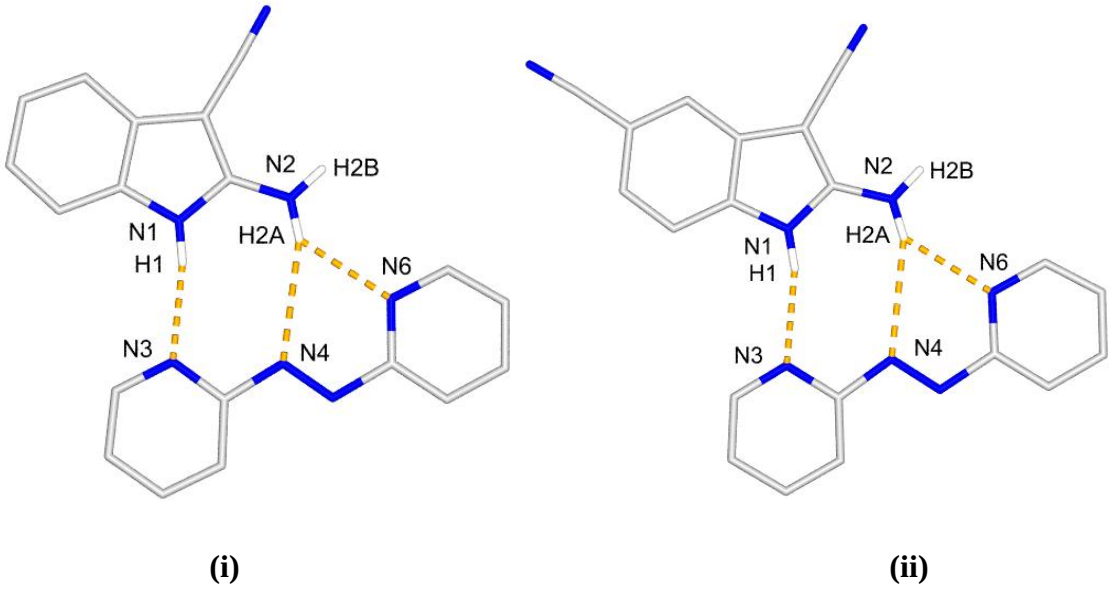

(i) **(ii)**

Figure 2.26 Stick representation of crystals **2-4a·(*E*)-2 (i)** and **2-4g·(*E*)-2 (ii)**. Hydrogen bonds depicted as orange dashed lines; C-H bonds removed for clarity.

Table 2.7 Bond lengths and bond angles of hydrogen bonds of interest from crystal **1-4a·(*E*)-2**.

Bond Lengths (Å)				Bond Angles (°)	
N1-H1···N3	2.94	N2-H2A···N4	2.62	N1-H1···N3	167
N1-H1···N3	2.08	N2-H2A···N6	2.97	N2-H2A···N4	158
N2-H2A···N4	3.45	N2-H2A···N6	2.29	N2-H2A···N6	134

Table 2.8 Bond lengths and bond angles of hydrogen bonds of interest from crystal **2-4g·(*E*)-2**.

Bond Lengths (Å)				Bond Angles (°)	
N1-H1···N3	2.89	N2-H2A···N4	2.94	N1-H1···N3	171
N1-H1···N3	2.02	N2-H2A···N6	3.02	N2-H2A···N4	137
N2-H2A···N4	3.63	N2-H2A···N6	2.36	N2-H2A···N6	132

The co-planarity of the complexed arrays also remains unchanged from the previous structures. **(*E*)-2** in crystal **2-4a·(*E*)-2** resulted in a 5.7° angle between the least squares planes of the pyridyl rings in the s-*cis*, s-*trans* conformation. The interplanar angle between the indole (least squares plane: ± 0.046 Å) and **(*E*)-2** (least squares plane: ± 0.103 Å) is 5.7°. The π-stacking distances remain unchanged in the lattice but the repeated layered sequences are perpendicular (~ 90°) to one another when in all three previous cases the layers ran parallel through the lattice.

The s-*cis*, s-*trans* **(*E*)-2** array in crystal **2-4g·(*E*)-2** has the largest angle of 13.2° between the least squares planes of the pyridyl rings when compared to all 5 complexes thus far. This in turn means **(*E*)-2**'s greatest individual deviation from the least squares plane has increased (± 0.203 Å). The indole itself still remains very planar (greatest deviation from average plane being ± 0.092 Å) and the complex itself remains coplanar with the angle between the array's least squares planes being 6.4°.

The cyano groups in the 3-positions of these indole derivatives do not participate in intramolecular interactions but in the solid state form a dimeric indole complex in the lattice. Two indoles in **2-4a·(*E*)-2** crystallized almost completely coplanar with their least squares planes angled at 1.7° (Figure 2.27, i). These hydrogen bonding interactions

can be considered relativity strong due to their short distances and near ideal angles (N2-H2B···N7'= N2'-H2B'···N7 = 3.05 Å, N2-H2B···N7'= N2'-H2B'···N7 = 2.18 Å, N2-H2B···N7'= N2'-H2B'···N7 = 174^{o}). Crystal **2-4g·(*E*)-2** also displays the same dimeric indole structure but the angle between their least squares planes is now 34.5^{o} (Figure 2.27, ii). This angle between the indoles resulted in slightly different lengths and angles between hydrogen bonded pairs (N2-H2B···N7' = 3.07 Å, N2-H2B···N7' = 2.20 Å, N2-H2B···N7' = 172^{o}, N2'-H2B'···N7 = 3.11 Å, N2'-H2B'···N7 = 2.24 Å, N2'-H2B'···N7 = 170^{o}). The dimeric structure could explain why the 3-cyano derivatives are more insoluble then the 3-ester derivatives.

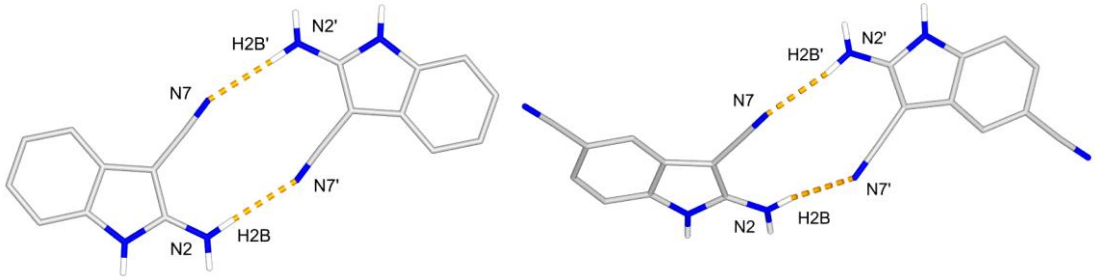

(i) **(ii)**

Figure 2.27 Stick representation of **2-4a·2-4a** dimer **(i)** and **2-4g·2-4g** dimer **(ii)**. Intermolecular hydrogen bonds depicted as dashed orange lines. C-H bonds removed for clarity.

A dilution was performed on **2-4a** (1.0 mM to 0.25 mM) and no significant proton shifts were detected. Therefore, this dimeric complex may just be a result of crystal packing to stabilize the lattice or too weak to observe at these concentrations.

As with all of the strong hydrogen bonding pairs discussed in this chapter, there are also multiple attractive secondary interactions. These interactions deviate from strong

binding pairs but contribute to the overall stability of the binding arrays in solution and the solid state. These secondary interactions for all 5 crystals discussed are listed in Table 2.9.

Table 2.9 Summary of secondary attractive hydrogen bonding lengths and angles for crystals **2-3f·(*E*)-2**, **2-3g·(*E*)-2**, **2-3e·(*E*)-2**, **2-4a·(*E*)-2**, and **2-4g·(*E*)-2**.

Bond Lengths (Å)	**1-3f·(*E*)-2**	**1-3g·(*E*)-2**	**1-3e·(*E*)-2**	**1-4a·(*E*)-2**	**1-4g·(*E*)-2**
N1-H1···N4	3.7446(33)	3.6738(21)	3.8628(24)	3.6740(33)	3.6341(19)
N1-H1···N4	3.1156(24)	2.9740(15)	3.2908(18)	2.9601(24)	2.9384(13)
N2-H2···N3	3.9681(42)	4.1806(23)	3.7801(32)	4.2013(31)	4.1076(22)
N2-H2A···N3	3.3939(30)	3.7444(25)	3.1681(23)	3.6769(22)	3.5710(15)
N2-H2B···N6	2.9005(25)	3.0454(21)	2.8104(18)	3.0603(24)	3.0572(16)
Bond Angles (^{o})					
N1-H1···N4	130.18	137.81	124.97	139.57	137.37
N2-H2A···N3	125.30	115.00	128.62	121.23	122.17
N2-H2B···N6	86.14	73.53	91.78	75.98	79.06

When comparing all five structures, they all interact through the predicted hydrogen bonding mode with similar hydrogen bonding distances and angles. This binding mode results in highly coplanar systems with angles between the arrays not exceeding 14^o. The strongest hydrogen bonds in all structures would be the indole hydrogen to the pyridyl ring (N1-H1···N3) and the amino hydrogen to the azo-nitrogen

(N2-H2A···N4) as they were found to be at the shortest distances and optimal angles for hydrogen bonding.

2.5 Summary and Conclusions

The initial studies of our complementary hydrogen bonded system compared the substitution patterns on the benzenoid ring of our 2-aminoindole arrays. Utilizing a simple synthetic method, a library of indoles with an ethyl ester or a cyano group in the 3-position was produced. An acceptor array for these donor compounds, 2, 2'-azopyridine was chosen and we measured the strengths of complexation. The ethyl ester derivatives ranged in stability from 91 to 996 M^{-1} with the 5- and 6- di-substituted derivatives being the highest. Shifting from an ester to a cyano group in the 3 position led to a decrease of solubility of many derivatives synthesized. However, indoles which were soluble, when compared to their ester counterparts had their respective free energies increase by an average factor of 1.8. The two libraries resulted in LFERs with respect to their substituent Σσ values and logs of their K_a values. The complex geometry of these arrays which we predicted was supported both by solution ^{1}H 2D NOESY experiments and multiple solid state crystal structures. The success of this initial system was examined in more depth in the following chapter by further investigating the substitution effects on the 3-position of the indole core. Also, extending the azopyridine array by adding an additional acceptor component should increase the resulting stabilities of the complexes. Furthermore, an alternative non-polar solvent will be examined assuming soluble derivatives can be synthesized.

2.6 Experimental Methodology

2.6.1 General Information

Chemicals were purchased from Sigma Aldrich, Alfa Aesar or Oakwood Products Inc. and used as received. All non-deuterated solvents were dried (if needed) using an Innovative Technology Inc. Solvent Purification System SPS-400-5. $CDCl_3$, DMSO-d_6, and Toluene-d_8 were purchased from Cambridge Isotope Laboratories or Sigma Aldrich and dried (chloroform and toluene) over 4Å molecular sieves before use. α,α,α-Trifluorotoluene (^{19}F NMR standard, $C_7H_5F_3$) was purchased from Sigma and used as received as an internal standard if mentioned in the molecular characterization data.

^{1}H ,^{13}C and ^{19}F NMR spectra were collected @ 298 K on the Varian Mercury 400 MHz or the Bruker AvIII HD 400 MHz spectrometer (operating at 400.08, 100.61 and 376.42 MHz respectively) and the Inova 600 MHz spectrometer (599.37 and 150.72 MHz respectively). ^{1}H NMR titrations were performed on a Varian Inova 600 MHz spectrometer. Spectra are reported with residual solvent peak as reference from TMS.[37] Chromatography was performed using Silicycle 40-63 μm silica gel-60 (R10030B). EI mass spectra were obtained on a Finnigan MAT 8400 mass spectrometer. X-Ray diffraction data were collected on Bruker Apex II and Nonius Kappa CCD X-Ray diffractometers using graphite monochromatic Mo-Kα radiation (γ = 0.71073 Å) and Cu-Kα radiation (γ = 1.54178 Å), respectively.

2.6.2 Titration Procedure

A stock solution of Indole was prepared in dry $CHCl_3$ to the desired concentration (from 1.0 x 10^{-3} M to 0.25 x 10^{-4} M) and 0.5 mL was transferred into an NMR tube and 4 mL in a small vial and placed under vacuum in a dessicator to remove solvents. $CDCl_3$ (0.5 mL) was added to the NMR tube and a ^1H NMR spectrum was recorded. An accurately weighed amount of guest compound, **(*E*)-2**, was added to the vial prepared along with 4 mL of $CDCl_3$ to produce a guest solution of 30 – 50 times the host concentration. As a precaution, the vial was wrapped with black tape to exclude light. Aliquots of guest solution were added successively to the NMR tube containing the host solution, the tube was shaken after each addition and the ^1H spectrum was recorded. The chemical shifts of the NH and NH_2 protons from the hydrogen bond donors in each sample were recorded and fit satisfactorily to a 1:1 binding model using Origin data analysis software.[32]

2.6.3 Synthetic Methods

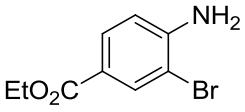

Synthesis of 2-1a: The aniline was synthesized using a literature method and purified by column chromatography using DCM as eluent. Characterization data matched that of the known product,[38] a white solid isolated in 79% yield.

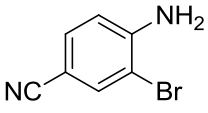

Synthesis of 2-1b: The aniline was synthesized using a literature method and purified by column chromatography using EtOAc/Hexanes

(1/3) as eluent. Characterization data matched that of the known compound,[39] a white solid was isolated in 75% yield.

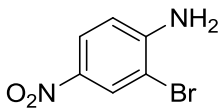

Synthesis of 2-1c: The aniline was synthesized using a literature method and no purification of the product was required. Characterization data matched that of the known compound,[40] prepared in 97% yield.

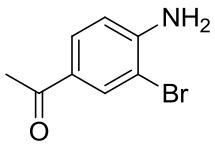

Synthesis of 2-1d: The aniline was synthesized using the same procedure as **2-1a** starting from 4-aminoacetophenone and using CH_3CN as solvent in place of $CHCl_3$. Purification by column chromatography using EtOAc/Hexanes (2/5) as eluent was carried out and characterization data matched that of the known compound,[41] a pale orange solid isolated in 92% yield.

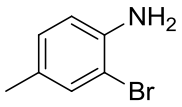

Synthesis of 2-1e: The aniline was synthesized from using a literature method[42] and purified by column chromatography using EtOAc/Hexanes (1/9) as eluent. Characterization data matched that of the known compound,[43] a red oil isolated in 46% yield.

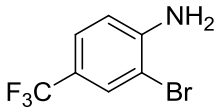

Synthesis of 2-1f: The aniline was synthesized in the same manner as **2-1a** starting with 4-(trifluoromethyl)aniline. Purification by column chromatography using EtOAc/Hexanes (1/9) as eluent was carried out and characterization data matched that of the known compound,[44] an orange solid was isolated in 52% yield.

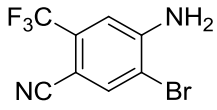

Synthesis of 2-1g: The aniline was synthesized in the same manner as **2-1a** starting with 4-amino-2-(trifluoromethyl)benzonitrile. Purification by column chromatography using EtOAc/Hexanes (2/5) as eluent was carried out and a light orange amorphous solid was isolated in 77% yield. **^{1}H NMR** (400 MHz, $CDCl_3$): δ (ppm) 7.83 (s, 1H), 7.04 (s, 1H), 4.89 (s, br, 2H). **^{13}C NMR** (100 MHz, $CDCl_3$ + 3 drops DMSO-d_6): δ (ppm) 149.0, 138.1, 132.4 (q, J = 32.2 Hz), 122.1 (q, J = 273.8 Hz), 115.6, 112.0 (q, J = 4.6 Hz), 109.0, 95.5. **^{19}F NMR** (376 MHz, $C_7H_5F_3$, $CDCl_3$): δ (ppm) -63.7. **HRMS (EI):** calc. for $C_8H_4BrF_3N_2$ $[M]^+$ 263.9510; found: 263.9506.

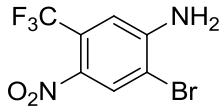

Synthesis of 2-1h: The aniline was synthesized in the same manner as **2-1a** starting with 4-nitro-3-(trifluoromethyl)benzamine. Purification by column chromatography using DCM/Hexanes (2/3) as eluent was carried out and a bright yellow amorphous solid was isolated in 77% yield. **^{1}H NMR** (400 MHz, $CDCl_3$): δ (ppm) 8.27 (s, 1H), 7.08 (s, 1H), 4.92 (s, br, 2H). **^{13}C NMR** (100 MHz, $CDCl_3$): δ (ppm) 148.8, 131.7, 125.7 (q, J = 33.7 Hz), 122.0 (q, J = 273.8 Hz), 113.0 (q, J = 6.1 Hz), 109.3. **^{19}F NMR** (376 MHz, $C_7H_5F_3$, $CDCl_3$): δ (ppm) -61.4. **HRMS (EI):** calc. for $C_7H_4BrF_3N_2O_2$ $[M]^+$ 283.9408; found: 283.9416.

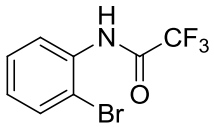

Synthesis of 2-2a: Under a N_2 atmosphere, 2-bromoaniline (1.00 g, 5.84 mmol) and NEt_3 (1.14 mL, 8.19 mmol) was added to a round bottom flask with 10 mL dry DCM and placed into an ice/water bath. With stirring, TFAA (1.00 mL, 7.02 mmol) was added slowly via syringe and the reaction was stirred

for 30 minutes on ice, the bath was removed and stirring continued for a minimum of 4 hours at room temperature and ideally overnight. The contents were diluted with an additional 20 mL DCM and washed twice with water and once with brine. The organic layer was dried with Na_2SO_4, filtered and solvent was removed under reduced pressure. The crude solid was subjected to column chromatography using EtOAc/Hexanes (1/5) as eluent and a white, crystalline solid was isolated in 90% yield. **m.p.**: 60 - 62 °C. **^{1}H NMR** (400 MHz, $CDCl_3$): δ (ppm) 8.45 (s, br, 1H), 8.32 (dd, *J* = 8.2, 1.6 Hz, 1H), 7.61 (dd, *J* = 8.2, 1.6 Hz, 1H), 7.40 (dt, *J* = 7.4, 1.6 Hz, 1H), 7.13 (dt, *J* = 7.4, 1.6 Hz, 1H). **^{13}C NMR** (100 MHz, $CDCl_3$): δ (ppm) 154.8 (q, *J* = 37.6 Hz), 133.3, 132.8, 128.9, 127.4, 122.2, 115.7 (q, *J* = 280.5 Hz), 114.3. **HRMS (EI):** calc. for $C_8H_5BrF_3NO$ $[M]^+$ 266.9507; found: 266.9496.

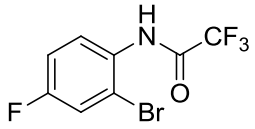

Synthesis of 2-2b: The acetamide was synthesized in the same manner as **2-2a** starting with 2-bromo-4-fluoroaniline. Purification by column chromatography using EtOAc/Hexanes (1/1) as eluent was carried out and a white, crystalline solid was isolated in 83% yield. **m.p.**: 69 - 70 °C. **^{1}H NMR** (400 MHz, $CDCl_3$): δ (ppm) 8.32 (s, br, 1H), 8.28 (dd, *J* = 9.2, 5.3 Hz, 1H), 7.37 (dd, *J* = 7.8, 2.7 Hz, 1H), 7.16 – 7.11 (m, 1H). **^{13}C NMR** (100 MHz, $CDCl_3$): δ (ppm) 159.8 (d, *J* = 281.8 Hz), 154.9 (q, *J* = 38.4 Hz), 129.7 (d, *J* = 3.1 Hz), 123.5 (d, *J* = 8.5 Hz), 120.0 (d, *J* = 26.1 Hz), 115.8 (d, *J* = 22.3 Hz), 115.7 (q, *J* = 288.7 Hz), 114.8 (d, *J* = 9.2 Hz). **HRMS (EI):** calc. for $C_8H_4BrF_4NO$ $[M]^+$ 284.9412; found: 284.9416.

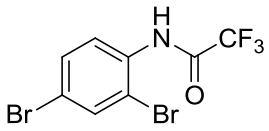

Synthesis of 2-2c: The acetamide was synthesized in the same manner as compound **2-2a** starting from 2,4-dibromoaniline. Purification by column chromatography using EtOAc/Hexanes (1/5) as eluent was carried out and a white, lightweight solid was isolated in 81% yield. **^{1}H NMR** (400 MHz, $CDCl_3$): δ (ppm) 8.40 (s, br, 1H), 8.23 (d, *J* = 9.0 Hz, 1H), 7.77 (d, *J* = 2.7 Hz, 1H), 7.52 (dd, *J* = 9.0, 2.7 Hz, 1H). **^{13}C NMR** (100 MHz, $CDCl_3$): δ (ppm) 154.8 (q, *J* = 37.6 Hz), 135.0, 132.5, 131.9, 123.1, 119.4, 115.6 (q, *J* = 288.9 Hz), 114.8. **HRMS (EI):** calc. for $C_8H_4Br_2F_3NO$ $[M]^+$ 344.8612; found: 344.8622.

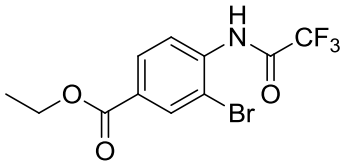

Synthesis of 2-2d: The acetamide was synthesized in the same manner as **2-2a** starting from **2-1a**. Purification by column chromatography using EtOAc/Hexanes (1/7) as eluent was carried out and a white, crystalline solid was isolated in 92% yield. **m.p.:** 69 - 71 °C. **^{1}H NMR** (400 MHz, $CDCl_3$): δ (ppm) 8.61 (s, br, 1H), 8.45 (d, *J* = 8.6 Hz, 1H), 8.29 (d, *J* = 2.0 Hz, 1H), 8.06 (dd, *J* = 8.6, 2.0 Hz, 1H), 4.39 (q, *J* = 7.0 Hz, 2H), 1.40 (t, *J* = 7.0 Hz, 3H). **^{13}C NMR** (100 MHz, $CDCl_3$): δ (ppm) 164.5, 154.8 (q, *J* = 38.4 Hz), 136.9, 133.9, 130.2, 129.2, 121.1, 115.5 (q, *J* = 288.7 Hz), 113.7, 61.7, 14.3. **HRMS (EI):** calc. for $C_{11}H_9BrF_3NO_3$ $[M]^+$ 338.9718; found: 338.9726.

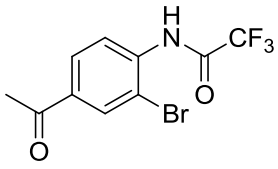

Synthesis of 2-2e: The acetamide was synthesized in the same manner as **2-2a** starting from **2-1d**. Purification by column chromatography using EtOAc/Hexanes (1/5) as eluent was carried out and an amorphous, white solid was isolated in 88% yield. **^{1}H NMR** (400

MHz, $CDCl_3$): δ (ppm) 8.63 (s, br, 1H), 8.49 (d, *J* = 8.6 Hz, 1H), 8.23 (d, *J* = 2.0 Hz, 1H), 7.96 (dd, *J* = 8.6, 2.0 Hz, 1H), 2.61 (s, 3H). **^{13}C NMR** (100 MHz, $CDCl_3$): δ (ppm) 195.4, 154.9 (q, *J* = 39.1 Hz), 137.0, 135.4, 132.6, 129.1, 121.3, 115.5 (q, *J* = 289.1 Hz), 114.3, 26.5. **HRMS (EI):** calc. for $C_{10}H_7BrF_3NO_2$ $[M]^+$ 308.9612; found: 308.9623.

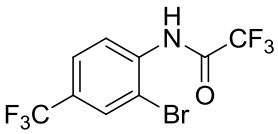

Synthesis of 2-2f: The acetamide was synthesized in the same manner as **2-2a** starting from **2-1f**. Purification by column chromatography using EtOAc/Hexanes (1/9) as eluent was carried out and a white, crystalline solid was isolated in 81% yield. **m.p.:** 58 - 60 °C. **^{1}H NMR** (400 MHz, $CDCl_3$): δ (ppm) 8.57 (s, br, 1H), 8.51 (d, *J* = 8.6 Hz, 1H), 7.89 (d, *J* = 1.6 Hz, 1H), 7.67 (dd, *J* = 8.6, 1.6 Hz, 1H). **^{13}C NMR** (100 MHz, $CDCl_3$): δ (ppm) 155.1 (q, *J* = 38.4 Hz), 136.4, 129.9 (q, *J* = 3.8 Hz), 129.3 (q, *J* = 33.8 Hz), 126.1 (q, *J* = 3.8 Hz), 122.9 (q, *J* = 272.6 Hz), 121.8, 115.5 (q, *J* = 288.7 Hz), 114.0. **HRMS (EI):** calc. for $C_9H_4BrF_6NO$ $[M]^+$ 334.9380; found: 334.9379.

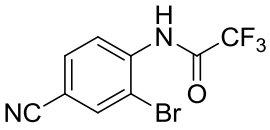

Synthesis of 2-2g: The acetamide was synthesized in the same manner as **2-2a** starting from **2-1b** and purification was not needed to continue to the next step, a white, crystalline solid was isolated in 95% yield. **m.p.:** 129 - 130 °C. **^{1}H NMR** (400 MHz, $CDCl_3$): δ (ppm) 8.60 (s, br, 1H), 8.54 (d, *J* = 8.6 Hz, 1H), 7.93 (d, *J* = 2.0 Hz, 1H), 7.71 (dd, *J* = 8.6, 2.0 Hz, 1H). **^{13}C NMR** (100 MHz, $CDCl_3$): δ (ppm) 155.0 (q, *J* = 38.4 Hz), 137.4, 136.1, 132.9, 121.8, 119.7, 116.8, 115.4 (q, *J* = 288.7 Hz), 114.0, 110.8. **HRMS (EI):** calc. for $C_9H_4BrF_3N_2O$ $[M]^+$ 291.9459; found: 291.9454.

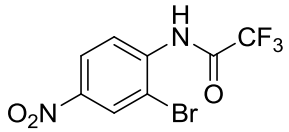

Synthesis of 2-2h: The acetamide was synthesized in the same manner as **2-2a** starting from **2-1c**. Purification by column chromatography using DCM as eluent was carried out and a lightweight, pale yellow, amoprhous solid was isolated in 75% yield. **^{1}H NMR** (400 MHz, $CDCl_3$): δ (ppm) 8.68 (s, br, 1H), 8.62 (d, *J* = 9.0 Hz, 1H), 8.54 (d, *J* = 2.7 Hz, 1H), 8.30 (dd, *J* = 9.0, 2.7 Hz, 1H). **^{13}C NMR** (100 MHz, $CDCl_3$): δ (ppm) 155.1 (q, *J* = 38.4 Hz), 144.9, 138.8, 128.2, 124.4, 121.2, 115.4 (q, *J* = 288.3 Hz), 113.7. **HRMS (EI):** calc. for $C_8H_4BrF_3N_2O_3$ $[M]^+$ 311.9357; found: 311.9341.

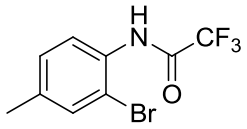

Synthesis of 2-2i: The acetamide was synthesized in the same manner as **2-2a** starting from **2-1e**. Purification by column chromatography using EtOAc/Hexanes (1/5) as eluent was carried out and a light weight, white solid was isolated in 67% yield. **^{1}H NMR** (400 MHz, $CDCl_3$): δ (ppm) 8.37 (s, br, 1H), 8.16 (d, *J* = 8.2 Hz, 1H), 7.43 (d, *J* = 2.0 Hz, 1H), 7.18 (dd, *J* = 8.2, 2.0 Hz, 1H), 2.34 (s, 3H). **^{13}C NMR** (100 MHz, $CDCl_3$): δ (ppm) 154.7 (q, *J* = 37.6 Hz), 137.8, 133.0, 130.7, 129.4, 122.0, 115.8 (q, *J* = 289.1 Hz), 114.2, 20.8. **HRMS (EI):** calc. for $C_9H_7BrF_3NO$ $[M]^+$ 280.9663; found: 280.9658.

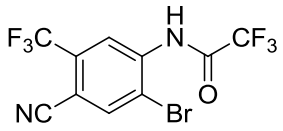

Synthesis of 2-2j: The acetamide was synthesized in the same manner as **2-2a** starting from **2-1g** and purification was not needed to continue to the next step, a pale orange, amorphous solid was isolated in 93% yield. **^{1}H NMR** (400 MHz, $CDCl_3$): δ (ppm) 8.89 (s, 1H), 8.66 (s, br, 1H), 8.10 (s, 1H).

^{13}C NMR (100 MHz, $CDCl_3$): δ (ppm) 155.3 (q, *J* = 39.1 Hz), 138.5, 137.8, 133.7 (q, *J* = 33.7 Hz), 121.7 (q, *J* = 274.5 Hz), 119.3 (q, *J* = 5.0 Hz), 117.2, 115.2 (q, *J* = 288.3 Hz), 113.7, 107.9. **HRMS (EI):** calc. for $C_{10}H_3BrF_6N_2O$ $[M]^+$ 359.9333; found: 359.9326.

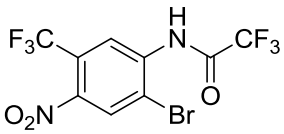

Synthesis of 2-2k: The acetamide was synthesized in the same manner as **2-2a** starting from compound **2-1h**. Purification by column chromatography using EtOAc/Hexanes (1/5) as eluent was carried out and a tan, amorphous solid was isolated in 97% yield. **^{1}H NMR** (400 MHz, $CDCl_3$): δ (ppm) 8.95 (s, 1H), 8.65 (s, br, 1H), 8.10 (s, 1H). **^{13}C NMR** (100 MHz, $CDCl_3$): δ (ppm) 155.3 (q, *J* = 39.9 Hz), 129.9, 124.9 (q, *J* = 35.3 Hz), 121.4 (q, *J* = 273.8 Hz), 120.2 (q, *J* = 6.1 Hz), 117.2, 115.2 (q, *J* = 288.3 Hz). **HRMS (EI):** calc. for $C_9H_3BrF_3N_2O_3$ $[M]^+$ 379.9231; found: 379.9234.

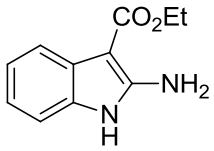

Synthesis of 2-3a: Modifying a known procedure,[22] under a dry N_2 atmosphere, a 25 mL RBF was equipped with a stirbar, **2-2a** (1.00 g, 3.75 mmol), L-proline (86.0 mg, 20 mol %), ethylcyanoacetate (510 mg, 4.51 mmol), K_2CO_3 (1.03 g, 7.47 mmol), and 5 mL dry DMSO. Contents were stirred for 10 minutes then CuI (71.0 mg, 10 mol %) was added and an air condenser was attached. The mixture was heated to 80 °C and stirred overnight for a minimum of 16 hours. After the allotted time, 3 mL DI H_2O was added and stirring was maintained for an additional hour while heating after which the flask was cooled to room temperature and vacuum filtered through a thin pad of Celite. The filter cake was washed with

methanol (3 X 3 mL) and the filtrate was poured into a separatory funnel containing 200 mL water and extracted with 4 times with EtOAc. The organic layers were combined, washed with water, brine and dried with Na_2SO_4. The solution was filtered and the solvent was removed via rotary evaporation. The crude residue was subjected to flash chromatography using petroleum ether/EtOAc (3/2) as eluent and a beige, amorphous solid was isolated in 54% yield. Characterization data matched literature values of the known compound.[21, 22]

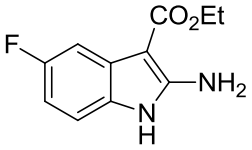

Synthesis of 2-3b: The indole was synthesized in the same manner as **2-3a** starting from **2-2b**. Purification by flash chromatography using petroleum ether/EtOAc (3/2) as eluent was carried out and a beige, amorphous solid was isolated in 37% yield. **^{1}H NMR** (600 MHz, DMSO-d_6): δ (ppm) 10.66 (s, br, 1H), 7.21 (d, J = 9.5 Hz, 1H), 7.06 (m, 1H), 6.75 (s, br, 2H), 6.66 (m, 1H), 4.22 (q, J = 6.9 Hz, 2H), 1.32 (t, J = 6.9 Hz, 3H). **^{13}C NMR** (100 MHz, DMSO-d_6): δ (ppm) 165.5, 158.1 (d, J = 231.1 Hz), 154.5, 129.1, 127.7, 110.2 (d, J = 10.0 Hz), 105.7 (d, J = 24.6 Hz), 103.6 (d, J = 26.1 Hz), 84.1, 58.2, 14.7. **HRMS (EI):** calc. for $C_{11}H_{11}FN_2O_2$ $[M]^+$ 222.0805; found: 222.0813.

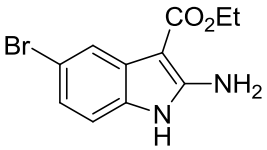

Synthesis of 2-3c: The indole was synthesized in the same manner as **2-3a** starting from **2-2c**. Purification by flash chromatography using petroleum ether/EtOAc (3/2) as eluent was carried out and a beige, amorphous solid was isolated in 56% yield. Characterization data matched literature values of the known compound.[22]

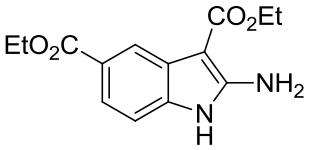

Synthesis of 2-3d: The indole was synthesized in the same manner as **2-3a** starting from **2-2d**. Purification by flash chromatography using petroleum ether/EtOAc (3/2) as eluent was carried out and a beige, amorphous solid was isolated in 45% yield. Characterization data matched literature values of the known compound.[21]

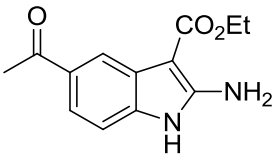

Synthesis of 2-3e: The indole was synthesized in the same manner as **2-3a** starting from **2-2e**. Purification by flash chromatography using petroleum ether/EtOAc (3/2) as eluent was carried out and a pale, red, amorphous solid was isolated in 30% yield. **^{1}H NMR** (400 MHz, DMSO-d_6): δ (ppm) 10.93 (s, br, 1H), 8.15 (s, 1H), 7.53 (d, J = 8.2 Hz, 1H), 7.15 (d, J = 8.2 Hz, 1H), 6.81 (s, br, 2H), 4.21 (q, J = 7.0 Hz, 2H), 2.45 (s, 3H), 1.30 (t, J = 7.0 Hz, 3H). **^{13}C NMR** (100 MHz, DMSO-d_6): δ (ppm) 197.3, 165.5, 154.4, 136.2, 130.1, 126.6, 120.7, 118.6, 109.4, 83.8, 58.3, 26.5, 14.7. **HRMS (EI):** calc. for $C_{13}H_{14}N_2O_3$ $[M]^+$ 246.1004; found: 246.1004.

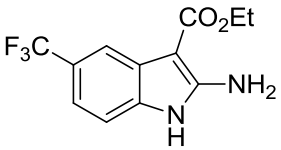

Synthesis of 2-3f: The indole was synthesized in the same manner as **2-3a** starting from **2-2f**. Purification by flash chromatography using petroleum ether/EtOAc (3/2) as eluent was carried out and a beige, amorphous solid was isolated in 46% yield. **^{1}H NMR** (400 MHz, DMSO-d_6): δ (ppm) 11.01 (s, br, 1H), 7.80 (s, 1H), 7.28 (d, J = 8.2 Hz, 1H), 7.21 (d, J = 8.2 Hz, 1H), 6.93 (s, br, 2H), 4.25 (q, J = 7.0 Hz, 2H), 1.32 (t, J = 7.0 Hz, 3H). **^{13}C**

NMR (100 MHz, DMSO-d_6): δ (ppm) 165.4, 154.5, 135.0, 126.8, 125.7 (q, J = 271.0 Hz), 121.3 (q, J = 30.87 Hz), 116.1, 114.3, 109.9, 83.7, 58.3, 14.6. **HRMS (EI):** calc. for $C_{12}H_{11}F_3N_2O_2$ $[M]^+$ 272.0773; found: 272.0772.

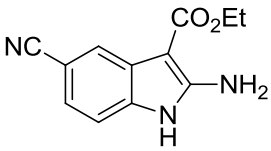

Synthesis of 2-3g: The indole was synthesized in the same manner as **2-3a** starting from **2-2g**. Purification by flash chromatography using Hexanes/EtOAc (3/2) as eluent was carried out and a beige, amorphous solid was isolated in 35% yield. **^{1}H NMR** (400 MHz, DMSO-d_6): δ (ppm) 11.15 (s, br, 1H), 7.79 (s, 1H), 7.28 – 7.27 (m, 2H), 7.02 (s, br, 2H), 4.25 (q, J = 7.0 Hz, 2H), 1.33 (t, J = 7.0 Hz, 3H). **^{13}C NMR** (100 MHz, DMSO-d_6): δ (ppm) 165.2, 154.6, 135.5, 127.1, 123.2, 121.1, 120.8, 110.6, 102.3, 83.3, 58.4, 14.7. **HRMS (EI):** calc. for $C_{12}H_{11}N_3O_2$ $[M]^+$ 229.0851; found: 229.0850.

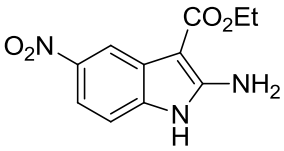

Synthesis of 2-3h: The indole was synthesized in the same manner as **2-3a** starting from **2-2h**. Purification by flash chromatography using petroleum ether/EtOAc (2/3) as eluent was carried out and a bright yellow, amorphous solid was isolated in 44% yield. **^{1}H NMR** (400 MHz, DMSO-d_6): δ (ppm) 11.30 (s, br, 1H), 8.37 (d, J = 2.3 Hz, 1H), 7.84 (dd, J = 8.6, 2.3 Hz, 1H), 7.28 (d, J = 8.6 Hz, 1H) 7.10 (s, br, 2H), 4.30 (q, J = 7.0 Hz, 2H), 1.34 (t, J = 7.0 Hz, 3H). **^{13}C NMR** (100 MHz, DMSO-d_6): δ (ppm) 165.0, 155.2, 141.8, 137.9, 126.9, 115.7, 112.9, 109.7, 84.0, 58.5, 14.7. **HRMS (EI):** calc. for $C_{11}H_{11}N_3O_4$ $[M]^+$ 249.0750; found: 249.0747.

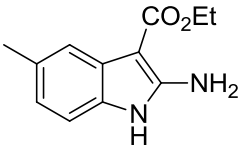

Synthesis of 2-3i: The indole was synthesized in the same manner as **2-3a** starting from **2-2i**. Purification by flash chromatography using petroleum ether/EtOAc (3/2) as eluent was carried out and a beige, amorphous solid was isolated in 36% yield. Characterization data matched literature values of the known compound.[22]

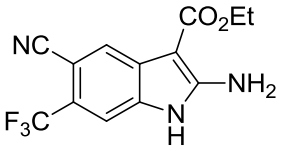

Synthesis of 2-3j: The indole was synthesized in the same manner as **2-3a** starting from **2-2j** and heated for 100 °C for three days before workup. Purification by flash chromatography using EtOAc/Hexanes (3/2) as eluent was carried out and a beige, amorphous solid was isolated in 62% yield. **^{1}H NMR** (400 MHz, DMSO-d_6): δ (ppm) 11.35 (s, br, 1H), 7.98 (s, 1H), 7.66 (s, 1H), 7.29 (s, br, 2H), 4.29 (q, J = 7.0 Hz, 2H), 1.34 (t, J = 8.0 Hz, 3H). **^{13}C NMR** (100 MHz, DMSO-d_6): δ (ppm) 164.8, 155.5, 134.0, 129.5, 123.9 (q, J = 271.8 Hz), 123.2, 121.0 (q, J = 31.6 Hz), 117.5, 108.5 (q, J = 5.3 Hz) 99.6 (q, J = 2.3 Hz), 84.2, 58.8, 14.6. **^{19}F NMR** (376 MHz, DMSO-d_6): δ (ppm) -58.8. **HRMS (EI):** calc. for $C_{13}H_{10}F_3N_3O_2$ $[M]^+$ 297.0725; found: 297.0720.

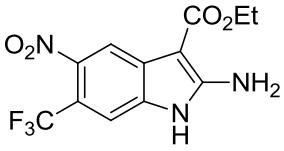

Synthesis of 2-3k: The indole was synthesized in the same manner as **2-3j** starting from **2-2k**. Purification by flash chromatography using EtOAc/Hexanes (3/2) as eluent was carried out and a bright orange, amorphous solid was isolated in 59% yield. **^{1}H NMR** (400 MHz, DMSO-d_6): δ (ppm) 11.35 (s, br, 1H), 8.12 (s, 1H), 7.65 (s, 1H), 7.33 (s, br, 2H), 4.29 (q, J = 7.0 Hz, 2H), 1.33 (t, J = 7.0 Hz, 3H). **^{13}C NMR** (100 MHz, DMSO-d_6):

δ (ppm) 164.7, 156.0, 141.8, 133.8, 129.3, 123.5 (q, *J* = 271.0 Hz), 114.3, 112.6 (q, *J* = 33.13 Hz), 108.6 (q, *J* = 6.02 Hz), 85.1, 58.8, 14.5. **HRMS (EI):** calc. for $C_{12}H_{10}F_3N_3O_4$ $[M]^+$ 317.0623; found: 317.0628.

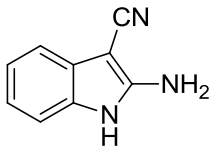

Synthesis of 2-4a: The indole was synthesized in the same manner as **2-3a** with malonitrile in place of ethyl cyanoacetate. Purification by flash chromatography with EtOAc/Hexanes (1/1) as eluent was carried out and a beige, amorphous solid was isolated in 64% yield. Characterization data matched literature values of the known compound.[21, 22]

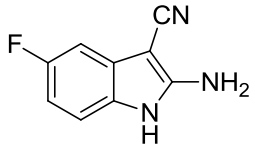

Synthesis of 2-4b: The indole was synthesized in the same manner as **2-4a** starting from **2-2b**. Purification by flash chromatography using EtOAc/Hexanes (3/2) as eluent was carried out and a green, crystalline solid was isolated in 51% yield. **m.p.:** 220 - 221 °C. **^{1}H NMR** (600 MHz, DMSO-d_6): δ (ppm) 10.72 (s, br, 1H), 7.09 – 7.07 (m, 1H), 6.87 (m, 1H), 6.85 (s, br, 2H), 6.71 – 6.67 (m, 1H). **^{13}C NMR** (150 MHz, DMSO-d_6): δ (ppm) 158.1 (d, *J* = 233.8 Hz), 154.9, 129.4 (d, *J* = 11.5 Hz), 128.6, 117.3, 110.9 (d, *J* = 9.2 Hz), 106.4 (d, *J* = 24.2 Hz), 101.1 (d, *J* = 26.5 Hz), 62.4. **^{19}F NMR** (376 MHz, $C_7H_5F_3$, DMSO-d_6): δ (ppm) – 125.7. **HRMS (EI):** calc. for $C_9H_6FN_3$ $[M]^+$ 175.0546; found: 175.0552

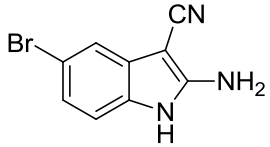

Synthesis of 2-4c: The indole was synthesized in the same manner as **2-4a** starting with **2-2c**. Purification by flash chromatography with EtOAc/Hexanes (3/2) as eluent was carried out and a beige,

amorphous solid was isolated in 59% yield. Characterization data matched literature values of the known compound.[22]

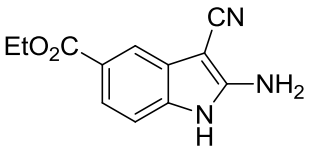

Synthesis of 2-4d: The indole was synthesized in the same manner as **2-4a** starting from **2-2d**. Purification by flash chromatography using EtOAc/Hexanes (3/2) as eluent was carried out and a white, amorphous solid was isolated in 67% yield. **^{1}H NMR** (600 MHz, DMSO-d_6): δ (ppm) 11.08 (s, br, 1H), 7.72 (s, 1H), 7.58 (d, J = 8.2 Hz, 1H), 7.21 (d, J = 8.2 Hz, 1H), 7.02 (s, br, 2H), 4.29 (q, J = 6.9 Hz, 2H), 1.32 (t, J = 6.9 Hz, 3H). **^{13}C NMR** (150 MHz, DMSO-d_6): δ (ppm) 166.4, 154.8, 135.5, 128.2, 122.2, 121.4, 117.2, 116.1, 109.9, 61.9, 60.2, 14.3. **HRMS (EI):** calc. for $C_{12}H_{11}N_3O_2$ $[M]^+$ 229.0851; found: 229.0860

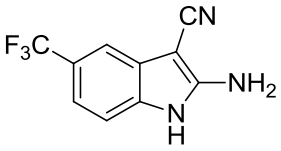

Synthesis of 2-4f: The indole was synthesized in the same manner as **2-4a** starting from **2-2f**. Purification by flash chromatography using EtOAc/Hexanes (1/1) as eluent was carried out and a beige, crystalline solid was isolated in 55% yield. **m.p.:** 212 - 214 °C. **^{1}H NMR** (600 MHz, DMSO-d_6): δ (ppm) 11.11 (s, br, 1H), 7.36 (s, 1H), 7.29 (d, J = 8.2 Hz, 1H), 7.22 (d, J = 8.2 Hz, 1H), 7.09 (s, br, 2H). **^{13}C NMR** (150 MHz, DMSO-d_6): δ (ppm) 155.0, 134.4, 128.4, 125.3 (q, J = 271.3 Hz), 121.4 (q, J = 31.3 Hz), 116.9, 116.4 (q, J = 4.3 Hz), 111.5 (q, J = 3.2 Hz), 110.4, 62.1. **HRMS (EI):** calc. for $C_{10}H_6F_3N_3$ $[M]^+$ 225.0514; found: 225.0510.

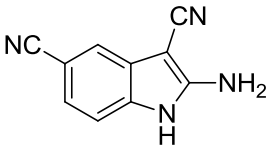

Synthesis of 2-4g: The indole was synthesized in the same manner as **2-4a** starting from **2-2g**. Purification by flash chromatography using EtOAc/Hexanes (7/3) as eluent was carried out and a beige, amorphous solid was isolated in 62% yield. **^{1}H NMR** (400 MHz, DMSO-d_6): δ (ppm) 11.23 (s, br, 1H), 7.50 (s, 1H), 7.32 - 7.25 (m, 2H), 7.17 (s, br, 2H). **^{13}C NMR** (100 MHz, DMSO-d_6): δ (ppm) 155.2, 135.0, 128.7, 123.6, 120.3, 118.7, 116.7, 111.0, 102.6, 61.9. **HRMS (EI):** calc. for $C_{10}H_6N_4$ $[M]^+$ 182.0592; found: 182.0594.

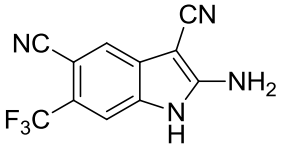

Synthesis of 2-4j: The indole was synthesized in the same manner as **2-3j** starting from **2-2j** and using malonitrile in place of ethyl cyanoacetate. Purification by flash chromatography using EtOAc/Hexanes (3/2) as eluent was carried out and a beige, amorphous solid was isolated in 45% yield. **^{1}H NMR** (400 MHz, DMSO-d_6): δ (ppm) 11.51 (s, br, 1H), 7.80 (s, 1H), 7.63 (s, 1H), 7.58 (s, br, 2H). **^{13}C NMR** (150 MHz, DMSO-d_6): δ (ppm) 156.4, 133.5, 131.2, 123.7 (q, J = 271.3 Hz), 121.5 (q, J = 32.3 Hz), 121.3 116.9, 115.7, 108.7 (q, J = 4.6 Hz), 99.9, 63.1. **HRMS (EI):** calc. for $C_{11}H_5F_3N_4$ $[M]^+$ 250.0466; found: 250.0474.

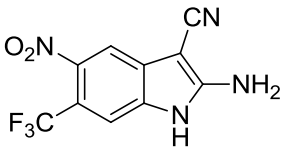

Synthesis of 2-4k: The indole was synthesized in the same manner as **2-4j** starting from **2-3k**. Purification by flash chromatography using EtOAc/Hexanes (5/2) as eluent was

carried out and a beige, amorphous solid was isolated in 57% yield. **^{1}H NMR** (400 MHz, DMSO-d_6): δ (ppm) 11.53 (s, br, 1H), 7.84 (s, 1H), 7.65 (s, 1H), 7.62 (s, br, 2H). **^{13}C NMR** (100 MHz, DMSO-d_6): δ (ppm) 156.9, 141.9, 133.3, 131.1, 123.3 (q, J = 271.8 Hz), 115.6, 112.8 (q, J = 32.3 Hz), 112.1, 108.9 (q, J = 5.3 Hz), 64.0. **^{19}F NMR** (376 MHz, DMSO-d_6): δ (ppm) -56.5. **HRMS (EI):** calc. for $C_{10}H_5F_3N_4O_4$ $[M]^+$ 270.0365; found: 270.0356.

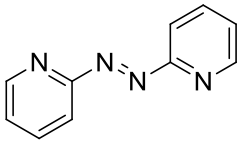

Synthesis of (*E*)-2: Modifying a known procedure,[45] 2-aminopyridine (10 g, 106 mmol) was dissolved in 200 mL of DI water and placed into an ice/water bath. A 5.5 w/v % of aqueous NaOCl (390 mL, 319 mmol) was chilled separately on ice and added dropwise over an hour. The red solution was stirred on ice for an hour and then an hour at room temperature. The solution was extracted 3 times with dichloromethane (200 mL) and the organic layers were combined and washed with water, brine, dried with Na_2SO_4, filtered and solvent removed via rotary evaporation. The red oil was subjected to flash chromatography (100% Et_2O) and recrystallized using hot hexanes to yield pure (*E*)-2 (1.82 g, 19%) as dark red crystals. **m.p.:** 84 - 86 °C. **^{1}H NMR** (600 MHz, $CDCl_3$): δ (ppm) 8.80 (dd, J = 4.7, 1.2 Hz, 2H), 8.02 (d, J = 7.8 Hz, 2H), 7.95 (dt, J = 7.8, 1.9 Hz, 2H), 7.76 – 7.51 (m, 2H). **^{13}C NMR** (150 MHz, $CDCl_3$): δ (ppm) 162.6, 149.6, 138.5, 126.1, 115.4. **HRMS (EI):** calc. for $C_{10}H_8N_4$ $[M]^+$ 186.0749; found 186.0752.

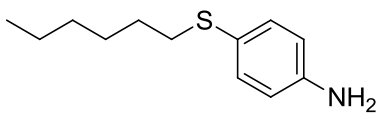

Synthesis of 2-5b: 4-Fluoronitrobenzene (5.00 g, 35.5 mmol) was added to 70 mL dry THF under a dry N_2

atmosphere followed by hexanethiol (6.05 mL, 42.6 mmol) and K_2CO_3 (5.88 g, 42.6 mmol). The contents were stirred and refluxed overnight and then brought to room temperature. The slurry was vacuum filtered and the solids were rinsed with diethyl ether. The filtrate was then dried with $MgSO_4$, filtered and solvent was removed under reduced pressure to obtain a thick oil. This crude oil was diluted with 80 mL mixture of AcOH:H_2O (3:1) and iron metal (7.93 g, 142 mmol) was added and stirred overnight. The following day, AcOH was removed under reduced pressure, 100 mL of H_2O was added and the aqueous layer was extracted 3 times with EtOAc. The organic layers were combined, washed with H_2O, saturated $NaHCO_3$, dried with $MgSO_4$, filtered and the solvent removed under reduced pressure. The remaining crude oil was subjected to flash chromatography using EtOAc/Hexanes (1/4) as eluent. Characterization data matched that of the known compound[46] and a brown oil was isolated in 70% yield (over two steps).

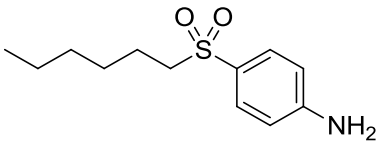

Synthesis of 2-5c: Aniline **2-5b** (1.50 g, 7.12 mmol) was dissolved in 50 mL dry DCM and was cooled to -78 °C. mCPBA (55%, 4.73 g, 15.1 mmol) was dissolved in an additional 50 mL dry DCM and was added dropwise over an hour. The mixture was stirred at -78 °C for an hour and then warmed to room temperature overnight. The solution was neutralized with $NaHCO_{3(sat)}$ and extracted 3 times with DCM. The organic layers were combined, washed with $NaHCO_{3(sat)}$, H_2O and brine. After drying the organic layer with $MgSO_4$, it was filtered and solvent removed under reduced pressure. Purification by flash chromatography using EtOAc/Hexanes (2/3) as eluent was performed and a white, amorphous solid was isolated

in 75% yield. **^{1}H NMR** (400 MHz, $CDCl_3$): δ (ppm) 7.64 (d, *J* = 8.9 Hz, 2H), 6.70 (d, *J* = 8.9 Hz, 2H), 4.21 (s, br, 2H), 3.04 - 3.00 (m, 2H), 1.71 - 1.62 (m, 2H), 1.36 - 1.31 (m, 2H), 1.26 - 1.21 (m, 4H), 0.85 (t, *J* = 6.5 Hz, 3H). **^{13}C NMR** (100 MHz, $CDCl_3$): δ (ppm) 151.8, 130.0, 126.5, 114.0, 56.7, 31.2, 27.9, 22.9, 22.3, 13.9. **HRMS (EI)**: calc. for $C_{12}H_{19}NO_2S$ $[M]^+$ 241.1136; found: 241.1141.

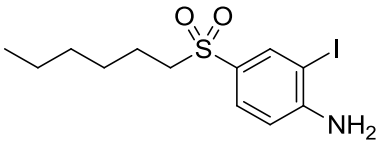

Synthesis of 2-5d: Aniline **2-5c** (1.00 g, 4.15 mmol) was added to 40 mL of MeOH:THF (1:1) along with $TsOH \cdot H_2O$ (5 mol%).[47] The solution was cooled in an ice/water bath and NIS (980 mg, 4.35 mmol) was added in small portions over an hour and stirring on ice continued for an additional 30 minutes then warmed to room temperature and stirred for another 2 hours. The mixture was diluted with H_2O and extracted three times with DCM and the combined organic layers were then washed with H_2O, dried with $MgSO_4$, filtered and solvent was removed under reduced pressure. Purification by flash chromatography using a mixture of EtOAc and Hexanes as eluent was performed and a white, amorphous solid was isolated in 80% yield. **^{1}H NMR** (400 MHz, $CDCl_3$): δ (ppm) 8.13 (d, *J* = 2.1 Hz, 1H), 7.62 (dd, *J* = 8.6, 2.1 Hz, 1H), 6.77 (d, *J* = 8.6 Hz, 1H), 4.67 (s, br, 2H), 3.05 - 3.01 (m, 2H), 1.73 - 1.65 (m, 2H), 1.38 - 1.31 (m, 2H), 1.26 - 1.21 (m, 4H), 0.86 (t, *J* = 6.5 Hz, 3H). **^{13}C NMR** (100 MHz, $CDCl_3$): δ (ppm) 151.6, 138.6, 129.1, 127.1, 113.1, 81.6, 56.4, 30.8, 27.5, 22.5, 22.0, 13.7. **HRMS (EI)**: calc. for $C_{12}H_{18}INO_2S$ $[M]^+$ 367.0103; found: 367.0104.

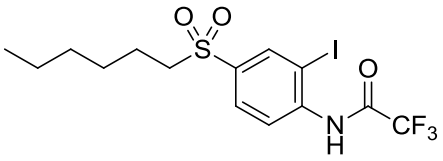

Synthesis of 2-5e: The acetamide was synthesized in the same manner as **2-2a** starting from aniline **2-5d** and purification was not needed to continue to the next step. A white, amorphous solid was isolated in 94% yield. **^{1}H NMR** (400 MHz, $CDCl_3$): δ (ppm) 8.52 (s, br, 1H), 8.50 (d, *J* = 8.6 Hz, 1H), 8.37 (d, *J* = 2.1 Hz, 1H), 7.95 (dd, *J* = 8.6, 2.1 Hz, 1H), 3.11 - 3.07 (m, 2H), 1.75 - 1.67 (m, 2H), 1.41 - 1.34 (m, 2H), 1.34 - 1.25 (m, 4H), 0.87 (t, *J* = 6.8 Hz, 3H). **^{13}C NMR** (100 MHz, $CDCl_3$): δ (ppm) 155.2 (q, *J* = 38.3 Hz), 140.3, 138.8, 137.8, 129.8, 121.6, 115.5 (q, *J* = 289.1 Hz), 89.9, 56.6, 31.3, 28.0, 22.7, 22.4, 14.0. **^{19}F NMR** (376 MHz, $C_7H_5F_3$, $CDCl_3$): δ (ppm) -76.9. **HRMS (EI)**: calc. for $C_{14}H_{17}F_3INO_3S$ $[M]^+$ 462.9926; found: 462.9930.

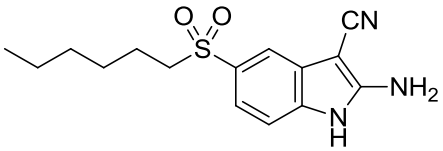

Synthesis of 2-5f: The indole was synthesized in the same manner as **2-4a** starting with **2-5e**. Purification by flash chromatography using EtOAc/Hexanes (3/2) as eluent was carried out and a pale tan, amorphous solid was isolated in 73% yield. **^{1}H NMR** (400 MHz, DMSO-d_6): δ (ppm) 11.26 (s, br, 1H), 7.56 (s, 1H), 7.40 (d, *J* = 8.2 Hz, 1H), 7.31 (d, *J* = 8.2 Hz, 1H), 7.20 (s, br, 2H), 3.23 – 3.19 (m, 2H), 1.53 – 1.45 (m, 2H), 1.31 – 1.24 (m, 2H), 1.22 – 1.16 (m, 6H), 0.80 (t, *J* = 6.8 Hz, 3H). **^{13}C NMR** (150 MHz, DMSO-d_6): δ (ppm) 155.2, 135.3, 131.0, 128.5, 119.3, 117.0, 116.8, 114.4, 110.3, 62.2, 55.3, 30.6, 27.0, 22.5, 21.8, 13.7. **HRMS (EI)**: calc. for $C_{15}H_{19}N_3O_2S$ $[M]^+$ 305.1198; found: 305.1190.

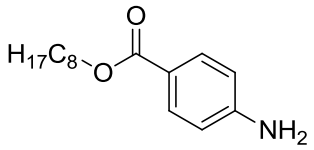

Synthesis of 2-6a: Using a standard coupling procedure,[48] 4-aminobenzoic acid (2.00 g, 14.6 mmol) and n-octanol (2.54 mL, 16.0 mmol) was dissolved in dry dichloromethane (100 mL) under a dry N_2 atmosphere and placed into an ice/water bath. DCC (3.30 g, 16.0 mmol) and DMAP (89.2 mg, 0.73 mmol) was dissolved in additional dry dichloromethane (50 mL) and added dropwise via syringe to the reaction flask over 30 minutes. The contents were allowed to stir for an hour in the ice/water bath then the bath was removed and continued stirring overnight. The resulting white slurry was vacuum filtered through a pad of Celite, rinsed with dichloromethane (50 mL) and washed three times with water. The organic layer was dried with Na_2SO_4, filtered and solvent was removed via rotary evaporation. Purification by flash chromatography using a mixture of EtOAc and Hexanes as eluent was performed and a white, crystalline solid was isolated in 65% yield. **m.p.:** 71 - 73 °C. **^{1}H NMR** (600 MHz, $CDCl_3$): δ (ppm) 7.85 (d, *J* = 8.5 Hz, 2H), 6.64 (d, *J* = 8.5 Hz, 2H), 4.25 (t, *J* = 6.7 Hz, 2H), 4.02 (s, br, 2H), 1.76 – 1.71 (m, 2H), 1.45 – 1.40 (m, 2H), 1.36 – 1.27 (m, 8H), 0.88 (t, *J* = 6.7 Hz, 3H). **^{13}C NMR** (150 MHz, $CDCl_3$): δ (ppm) 166.9, 150.8, 131.7, 120.3, 113.9, 64.7, 31.9, 29.4, 29.3, 29.0, 26.2, 22.8, 14.2. **HRMS (EI):** calc. for $C_{15}H_{23}NO_2$ $[M]^+$ 249.1729; found 249.1730.

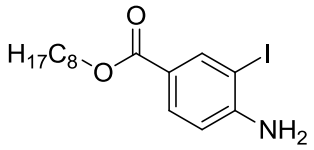

Synthesis of 2-6b: The aniline was synthesized in the same manner as **2-5d** starting from aniline **2-6a**. A white, crystalline solid was isolated in 87% yield. **m.p.:** 44 - 46 °C. **^{1}H NMR** (600 MHz, $CDCl_3$): δ (ppm) 8.33 (d, *J* = 1.3 Hz, 1H), 7.82 (dd, *J* = 8.5, 1.3 Hz, 1H), 6.07

(d, *J* = 8.5 Hz, 1H), 4.50 (s, br, 2H), 4.25 (t, *J* = 6.9 Hz, 2H), 1.76 – 1.71 (m, 2H), 1.44 – 1.39 (m, 2H), 1.36 – 1.28 (m, 8H), 0.89 (t, *J* = 6.8 Hz, 3H). **^{13}C NMR** (150 MHz, $CDCl_3$): δ (ppm) 165.5, 150.7, 141.1, 131.3, 121.7, 113.2, 82.3, 65.0, 31.9, 29.4, 29.3, 28.9, 26.2, 22.8, 14.2. **HRMS (EI)**: calc. for $C_{15}H_{22}INO_2$ $[M]^+$ 375.0695; found: 375.0699.

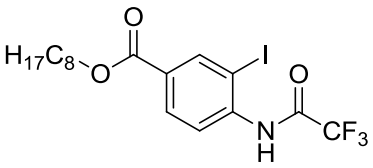

Synthesis of 2-6c: The acetamide was synthesized in the same manner as **2-2a** starting from aniline **2-6b** and purification was not needed to continue to the next step. A white, crystalline solid was isolated in 91% yield. **m.p.:** 62 - 63 °C. **^{1}H NMR** (600 MHz, $CDCl_3$): δ (ppm) 8.50 (d, *J* = 1.5 Hz, 1H), 8.46 (s, br, 1H), 8.36 (d, *J* = 8.5 Hz, 1H), 8.08 (dd, *J* = 8.5, 1.5 Hz, 1H), 4.32 (t, *J* = 6.8 Hz, 2H), 1.79 – 1.74 (m, 2H), 1.45 – 1.40 (m, 2H), 1.37 – 1.28 (m, 8H), 0.89 (t, *J* = 6.8 Hz, 3H). **^{13}C NMR** (150 MHz, $CDCl_3$): δ (ppm) 164.4, 155.0 (q, *J* = 37.8 Hz), 140.5, 139.4, 131.1, 129.6, 120.9, 115.6 (q, *J* = 288.6 Hz), 89.3, 85.9, 31.9, 29.4, 29.3, 28.8, 26.1, 22.8, 14.2. **^{19}F NMR** (376 MHz, $CDCl_3$): δ (ppm) -75.8. **HRMS (EI)**: calc. for $C_{17}H_{21}F_3INO_3$ $[M]^+$ 471.0518; found: 471.0511.

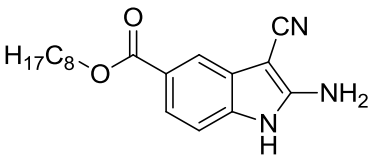

Synthesis of 2-6d: The indole was synthesized in the same manner as **2-4a** starting with **2-6c**. Purification by flash chromatography using EtOAc/Hexanes (3/2) as eluent was carried out and a pale tan, amorphous solid was isolated in 81% yield. **^{1}H NMR** (600 MHz, DMSO-d_6): δ (ppm) 11.08 (s, br, 1H), 7.71 (s, 1H), 7.57 (d, *J* = 8.2 Hz, 1H), 7.21 (d, *J* = 8.2 Hz, 1H), 7.02 (s, br, 2H), 4.23 (t, *J* = 6.6 Hz, 2H), 1.73 – 1.68 (m,

2H), 1.42 – 1.37 (m, 2H), 1.34 – 1.26 (m, 8H), 0.85 (t, J = 6.6 Hz, 3H). **^{13}C NMR** (150 MHz, DMSO-d_6): δ (ppm) 166.4, 154.7, 135.5, 128.2, 122.2, 121.3, 117.1, 116.1, 109.9, 64.1, 61.9, 31.2, 28.6, 28.6, 28.2, 25.5, 22.0, 13.9. **HRMS (EI)**: calc. for $C_{18}H_{23}N_3O_2$ $[M]^+$ 313.1790; found: 313.1794.

2.7 References

1. Lehn, J-M. *Macromol. Chem. Macromol. Symp*., **1993**, *69*, 1.

2. Beijer, F. H.; Sijbesma, R. P., Kooijman, H.; Spek, A. L.; Meijer, E. W. *J. Am. Chem. Soc*., **1998**, *120*, 6761.

3. Folmer, B. J. B.; Sijbesma, R. P.; Meijer, E. W. *J. Am. Chem. Soc*., **2001**, *123*, 2093.

4. Folmer, B. J. B.; Sijbesma, R. P.; Versteegen, R. M.; Van der Rijt, J. A. J.; Meijer, E. W. *Adv. Mater*., **2000**, *12*, 874.

5. Watson, J. D.; Crick, F. H. C. *Nature*, **1953**, *171*, 737.

6. Zimmerman S.C., Corbin P.S. (2000) Heteroaromatic Modules for Self-Assembly Using Multiple Hydrogen Bonds. In: Fuiita M. (eds) Molecular Self-Assembly Organic Versus Inorganic Approaches. Structure and Bonding, vol 96. Springer, Berlin, Heidelberg.

7. Jorgensen, W. L.; Pranata, J. *J. Am. Chem. Soc.*, **1990**, *112*, 2008; Pranata, J.; Wierschke, S. G.; Jorgensen, W.L. *J. Am. Chem. Soc*., **1991**, *113*, 2810.

8. Kyogoku, Y.; Lord, R. C.; Rich, A. *Biochim. Biophys. Acta.*, **1969**, *179*, 10.

9. Kyogoku, Y.; Lord, R. C.; Rich, A. *Proc. Natl. Acad. Sci. U.S.A*., **1967**, *57*, 250.

10. Marangoni, T.; Bonifazi, D. *Nanoscale*, **2013**, *5*, 8837.

11. Berl, V.; Schmutx, M.; Krische, M. J.; Khoury, R .G.; Lehn, J-M. *Chem. Eur. J*., **2002**, *8*, 1227.

12. Djurdjevic, S.; Leigh, D. A.; McNab, H.; Parsons, S.; Teobaldi, G.; Zerbetto, F. *J. Am. Chem. Soc*., **2007**, *129*, 476.

13. Blight, B. A.; Camara-Campos, A.; Djurdjevic, S.; Kaller, M.; Leigh, D. A.; McMillan, F. M.; McNab, H.; Slawin, A. M. Z. *J. Am. Chem. Soc*., **2009**, *131*, 14116.

14. Blight, B. A.; Hunter, C. A.; Leigh, D. A.; McNab, H.; Thompson, P. I. T. *Nat. Chem*., **2011**, *3*, 244.

15. a) Murray, T. J.; Zimmerman, S. C. *J. Am. Chem. Soc*., **1992**, *114*, 4010; b) Meyer, H.; Bossert, F.; Horstmann, H. *Liebigs. Ann. Chem*., **1978**, 1476; c) Zimmerman, S. C.; Murray, T. J. *Tetrahedron Lett*., **1994**, *35*, 4077.

16. Han, Y-F.; Chen, W-C.; Wang, H-B.; Yuan, Y-X.; Wu, N-N.; Song, X-Z.; Yang, L. *Chem. Eur. J*., **2014**, *20*, 16980.

17. Brunsveld, L.; Folmer, B. J. B.; Meijer, E. W. *MRS Bull.*, **2000,** *25*, 49.

18. Mudraboyina, B. P.; Wang, H-B.; Newbury, R.; Wisner, J. A. *Acta Cryst.*, **2011**, *E67*, o1222.

19. a) Hof, K.; Lippert, K. M., Schreiner, P. R. Hydrogen-Bonding Catalysts: (Thio)urea Catalysis. In *Science of Synthesis: Asymmetric Organocatalysis 2*; Maruoka, K.; List, B., Ed; Thieme: New York, 2012; Vol. 2; p 297; b) Shimizu, L. S.; Salpage, S. R.; Korous, A. A. *Acc. Chem. Res*., **2014**, *47*, 2116; c) Takemoto, Y. *Org. Biomol. Chem*., **2005**, *3*, 4299; d) Custelcean, R. *Chem. Commun*., **2008**, 295; e) Bregović, V. B.; Basarić, N.; Mlinarić-Majerski, K. *Coord. Chem. Rev*., **2015**, *295*, 80.

20. a) Xing, R.; Tian, Q.; Liu, Q.; Li, Y. *Chin. J. Chem*., **2013**, *31*, 263; b) Willemann, C.; Grünert, R.; Bednarski, P. J.; Troschütz, R. *Bioorganic Med. Chem*., **2009**, *17*, 4406; c) Landwehr, J.; Troschütz, R. *Synthesis*, **2005**, *14*, 2414.

21. Kobayashi, K.; Komatsu, T.; Yokoi, Y.; Konishi, H. *Synthesis*, **2011**, *5*, 764.

22. Yang, X.; Fu, H.; Qiao, R.; Jiang, Y.; Zhao, Y. *Adv. Synth. Catal*., **2010**, *352*, 1033.

23. Hansch, C.; Leo, A.; Taft, R. W. *Chem. Rev*., **1991**, *91*, 165.

24. Sawyer, J. The Synthesis and Study of a Light-Switchable Hydrogen Bond Motif. Undergraduate Thesis, Western University, London, ON, 2012.

25. a) Khalili, D.; Iranpoor, N.; Firouzabadi, H. *J. Sulfur Chem*., **2015**, *36*, 544; b) Kottelat, E.; Ruggi, A.; Zobi, F. *Dalton Trans*., **2016**, *45*, 6920; c) Fang, W. W.; Liu, X.

Y.; Lu, W.; Tu, T. *Chem. Commun*., **2014**, *50*, 3313; d) Xiong, F.; Qian, C.; Lin, D.; Zeng, W.; Lu, X. *Org. Lett*., **2013**, *15*, 5444; e) Thies, S.; Sell, H.; Schütt, C.; Bornholdt, C.; Näther, C.; Tuczek, F.; Herges, R. *J. Am. Chem. Soc*., **2011**, *133*, 16243; f) Wang, L.; Ishida, A.; Hashidoko, Y.; Hashimoto, M. *Angew. Chem. Int. Ed*., **2017**, *56*, 870; g) Gong, C-B,; He, L-H., Long, J-F., Liue, L-T.; Liu, S.; Tang, Q.; Fu, X-K. *Synth. Met*., **2016**, *220*, 147; h) Bauer, W.; Pfaffeneder, T.; Achterhold, K.; Weber, B. *Eur. J. Inorg. Chem*., **2011**, 3183.

26. Khan, A.; Hecht, S. *Chem. Eur. J*., **2006**, *12*, 4764.

27. Ayyangar, N.R.; Naik, S.N.; Srinivasan, K.V. *Tetrahedron Lett.*, **1989**, *30*, 7253.

28. Tour, J. M.; Shirai, Y.; Yu, B. C. *Tetrahedron*, **2006**, *62*, 10303.

29. Zhang, C.; Jiao, N. *Angew. Chem. Int. Ed*., **2010**, *49*, 6174.

30. Velazquez-Campoy, A.; Freire, E. *Nat. Protocols*, **2006,** *1*, 186.

31. Fielding, L. *Tetrahedron*, **2000**, *56*, 6151.

32. Bisson, A. P.; Carver, F. J.; Eggleston, D. S.; Haltiwanger, R. C.; Hunter, C. A.; Livingstone, D. L.; McCabe, J. F.; Rotger, C.; Rowan, A. E. *J. Am. Chem. Soc.*, **2000,** *122*, 8856.

33. Wang, H-B, Mudraboyina, B. P., Wisner, J. A. *Chem. Eur. J*., **2010**, *18*, 1322.

34. a) Exner, O.; Böhm, S. *J. Org. Chem*., **2002**, *67*, 6320; b) Hammett, L. P. Physical Organic Chemistry, 2nd Ed.; McGraw-Hill: New York, 1970; Chapters 11.9 - 11.16.

35. Lipsitz, R. S.; Tjandra, N. *Annu. Rev. Biomol. Struct*., **2004**, *33*, 387.

36. Housecroft, Catherine E., Sharpe, Alan G. Inorganic Chemistry. Third ed. Pearson / Prentice Hall: Essex, UK. 2008. pp. 31, 1013, 1014

37. Fulmer, G. R.; Miller, A. J. M.; Sherden, N. H.; Gottlieb, H. E.; Nudelman, A.; Stoltz, B. M.; Bercaw, J. E.; Goldberg, K. I. *Organometallics*, **2010**, *29*, 2176.

38. Bhuiyan, M.; Delower, H.; Zhu, K. X.; Jensen, P.; Try, A. C. *Eur. J. Org. Chem.*, **2010**, *24*, 4662.

39. Suh, Y.G. et al. *J. Med. Chem*., **2005**, *48*, 5823.

40. Zhang, M.; Zhang, R-L. *Yingyong Huaxue*, **2010**, *27*, 370.

41. Nery, M. S.; Azevedo, M. S.; Cardoso, J. N.; Slana, G. B. C.; Lopes, R. S. C.; Lopes, C. C. *Synthesis*, **2007**, 1471.

42. Das, B.; Venkateswarlu, K.; Majhi, A.; Siddaiah, V.; Reddy, K.R. *J. Mol. Catal. A-Chem*., **2007**, *267*, 30.

43. Smith, M.B.; Guo, L.; Okeyo, S.; Stenzel, J.; Yanella, J.; LaChappelle, E. *Org. Lett*. **2002**, *4*, 2321.

44. Podgoršek, A.; Stavber, S.; Zupan, M.; Iskra, J. *Tetrahedron* **2009**, *65*, 4429.

45. Campbell, N.; Henderson, A. W.; Taylor, D. *J. Chem. Soc*., **1953**, *APR*, 1281.

46. Wang, X.; Xu, Y.; Mo, F.; Ji, G.; Qiu, D.; Feng, J.; Ye, Y.; Zhang, S.; Zhang, Y.; Wang, J. *J. Am. Chem. Soc*., **2013**, *135*, 10330

47. Lanter, J. C.; Fiordeliso, J. J.; Jiang, W.; Allan, G. F.; Lai, M-T.; Linton, O.; Hahn, D. W.; Lundeen, S. G.; Sui, Z. *Bioorg. Med. Chem. Lett.*, **2007**, *17*, 123.

48. Dabiri, M.; MaGee, D.; Salehi, P.; Torkian, L.; Fakharian, M.; Donahue, J. *Synth. Commun*., **2014**, *44*, 2037.

Chapter 3

3 Synthesis and Characterization of Modified Complementary Hydrogen Bond Arrays

3.1 Solvent Effects

Contiguous hydrogen bond arrays provide stronger complexation when compared to analogous arrays containing adjacent donor and acceptor groups.[1a-e] The hydrogen bonding system introduced in the previous chapter incorporates this principle by employing two arrays which solely contain either donors or acceptors. Experimental association constants thus far have ranged from approximately 10^1 to 10^3 in $CDCl_3$. Chloroform is a common non-competitive solvent for determining complex strength and many strong complexes have been reported in this medium.[1a,c,2a-c] The importance of the solvation environment for hydrogen bond complexation has been demonstrated by Hunter and co-workers in a wide variety of solvents. Utilizing tri-n-butylphosphine oxide as the acceptor and nonafluoro-tert-butyl alcohol as the donor, ^{31}P NMR titrations were performed in a variety of competitive and non-competitive solvents (Figure 3.1). Polar solvents such as DMSO and pyridine disrupt hydrogen bonding to a point where complexation is almost immeasurable. Conversely, chloroform provides an association constant 3 - 4 orders of magnitude greater. Solvents such as benzene and cyclohexane yield even higher values and are considered very non-competitive solvents.

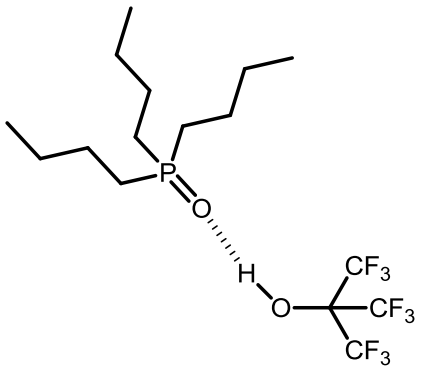

Solvent	K_a (M^{-1})
n-decanol	$1.6 * 10^{-1}$
DMSO	$6.8 * 10^{-1}$
NMF	$8.9 * 10^{-1}$
Pyridine	$6.5 * 10^{0}$
Pyrrole	$1.3 * 10^{1}$
Acetone	$6.5 * 10^{1}$
Acetonitrile	$1.6 * 10^{2}$
THF	$2.4 * 10^{2}$
Nitromethane	$1.5 * 10^{3}$
$CHCl_3$	$2.7 * 10^{3}$
Benzene	$1.9 * 10^{4}$
CCl_4	$7.6 * 10^{4}$
Cyclohexane	$> 10^{5}$

Figure 3.1 Results of ^{31}P NMR titrations showing association constants for a 1:1 complex at 295 K as a function of solvent properties. Experiments were repeated thrice and average values reported. Errors in K_a are ± 20% except for NMF, DMSO, and n-decanol where only 30-40% of the binding isotherm was accessible. Values are accurate to within an order of magnitude.[3]

The above example refers to a single hydrogen bonding interaction but the importance of non-polar solvents is a similar concern when assessing arrays with multiple binding pairs. Recently, our research group designed and studied self-complementary arrays containing an azo moiety similar to this present work. 1,3,5-Triazine cores were substituted with a variety of electron withdrawing groups to assist in polarizing a preinstalled amino donor component. The last substitution was reserved for an azopyridyl acceptor moiety and dimerization experiments were performed in $CDCl_3$ and toluene-d_8 (Figure 3.2).[4a,b] The dilutions performed in $CDCl_3$ resulted in lower dimerization

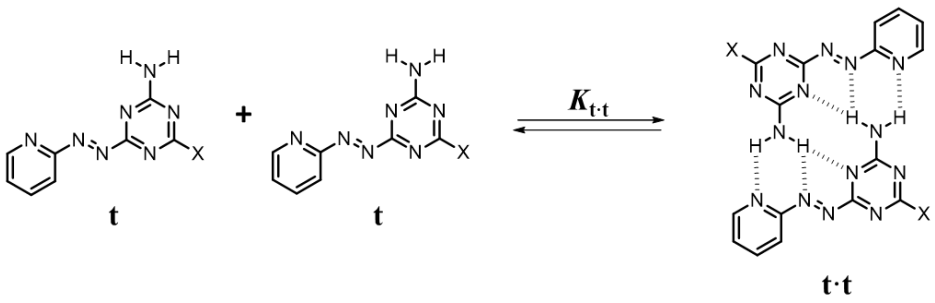

X	$K_{t\cdot t}$ in $CDCl_3$ (M^{-1})	$K_{t\cdot t}$ in Toluene-d_8 (M^{-1})
$O(n\text{-}C_4H_9)$	32 ± 7	900 ± 70
$S(n\text{-}C_6H_{13})$	32 ± 3	590 ± 90
OC_6F_5	180 ± 14	3700 ± 280

Figure 3.2 Dimerization equilibria of self-complementary photoswitchable azo containing arrays. $K_{t\cdot t}$ for three derivatives are given in $CDCl_3$ and toluene-d_8 at 298 K. Experiments were performed in triplicate, average $K_{t\cdot t}$ values reported and errors are stated as twice the standard deviation to give a 95% confidence interval.

constants with the perfluoro-phenoxy analogue being the most stable at 180 M^{-1}. Toluene is a less competitive solvent compared to chloroform so the dimerization constants were determined to be an order of magnitude greater in each case with perfluoro-phenoxy remaining the most stable at 3700 M^{-1}. Several related derivatives were insoluble in toluene so complex strength could not be determined due to the high polarity of these molecules. For example, a methoxy derivative (X = OCH_3) was synthesized and proved insoluble in toluene but altering the methyl to a n-butyl chain was enough to bring the array into solution. Additionally, the phenoxy (X = OC_6H_5) analogue was insoluble in toluene but the perfluorinated version has a more hydrophobic composition which increased solubility. The examination of our complementary system in non-polar solvents will be explored in this chapter with the aforementioned solubilizing modifications taken into consideration.

3.2 Effects of Additional Preorganized Donors or Acceptors

Maximum complexation strength between bonding pairs occurs when alignment of these pairs are as close to 180^{o} as structurally possible. Free rotation about sigma bonds is a common cause of misalignment between these pairings and energy must be sacrificed to align the arrays in the proper manner for binding. Preorganizing the array in a rigid structure removes rotational freedom and "freezes" the array in the ideal bonding conformation. Our group has studied this preorganization technique with double helical AAA-DDD arrays. Figure 3.3 depicts two double helical complexes with bis-indolyl-thiazine dioxide donors and a bis-pyridyl-3,5-lutidine acceptor.[5] ^{1}H NMR titrations were performed with both donors and complexes **A·1** and **B·1** resulted in

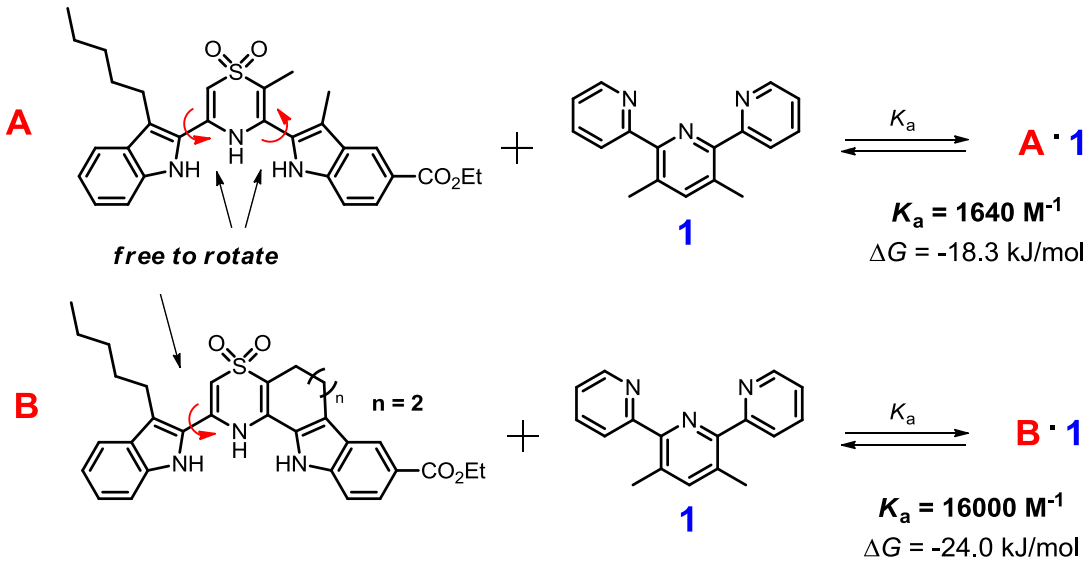

Figure 3.3 Preorganization effects of double helical bis-indolyl-thiazine dioxide · bis-pyridyl-3,5-lutidine complexes in $CDCl_3$.

association constants of 1640 M^{-1} and 16000 M^{-1} , respectively. This gain of 5.7 kJ/mol is attributed to the propylene tether in array **B** which locks the thiazine dioxide and one of the indole units together preventing rotation. Both indole units in array **A** are free to rotate and it takes additional energy upon the addition of acceptor **1** to align them in proper conformation for binding. Array **B** only contains one freely rotating bond between donors and therefore less energy is required for alignment which results in a stronger complex.

Complex stability can also be improved by the addition of extra preorganized donor or acceptor groups. This approach is demonstrated in Figure 3.4 with contiguous fused pyridine arrays as acceptors and 1,4-dihydropyridine analogues as donors. Complex **3A** resulted in a value of 260 M^{-1} with two binding pairs and with the addition of another amino group in complex **3B**, the association constant is raised by an order of magnitude. Greater still, when the naphthyridine is expanded with an additional fused ring in complex **3C**, the resulting association constant is increased by an additional four orders of magnitude. The addition of the preorganized binding pair in **3C** compared to **3A** added a primary bonding site along with two attractive secondary interactions which greatly increased the stability of these complexes by an overall five orders of magnitude,

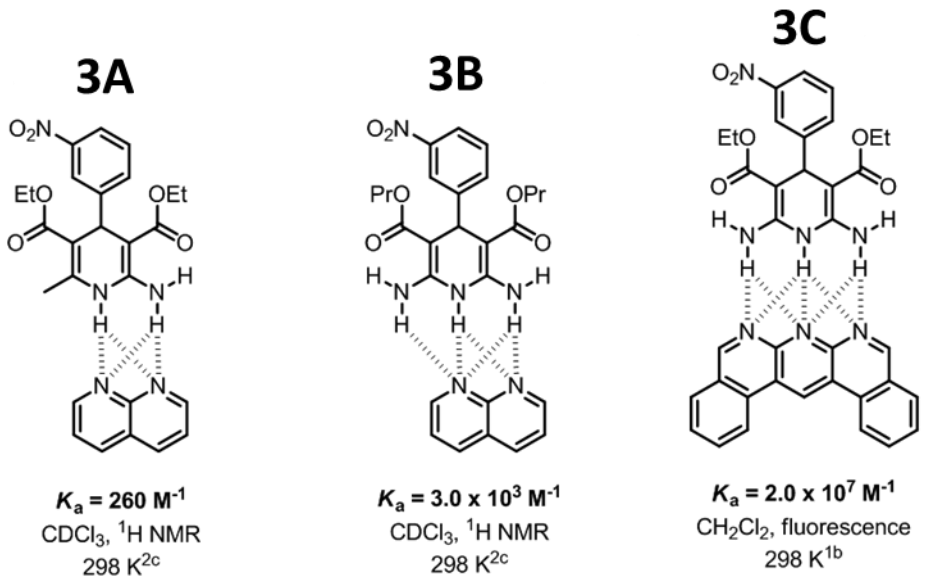

Figure 3.4 1,4-dihydropyridine analogues and fused pyridyl acceptors demonstrating the importance of preorganization in conjunction with the number of contiguous binding pairs.

or 28 kJ/mol. Given the positive results discussed above, expanding our acceptor array with additional acceptor sites will be a topic of exploration in this chapter.

3.3 Design of Improved Donor and Acceptor Arrays

In the previous chapter, each indole product began as its respective aniline incorporating preinstalled substituents followed by acetylation and cyclization. This synthetic strategy works well for a limited series of products but from a diversity standpoint, creating a precursor in bulk and performing subsequent modifications to create a library of compounds is less time consuming and more cost efficient. We set out to develop a divergent synthetic method where an intermediate indole precursor can be synthesized and through a variety of reactions with differing substrates, a grouping of

new 2-aminoindoles can be fashioned. We have examined the importance of incorporating electron withdrawing groups into our donor arrays through modifying mainly the benzenoid region. To further investigate our donor array capabilities, the pyrrole component will be modified from a common intermediate with a vacant 3-position. We wished to create solely the 3-*H*-2-aminoindole but the free amine in the 2-position opens a nucleophilic site for unwanted reactions to occur with added electrophiles. A protecting group was therefore installed which could be removed after a substitution reaction at the 3-position (Figure 3.5).

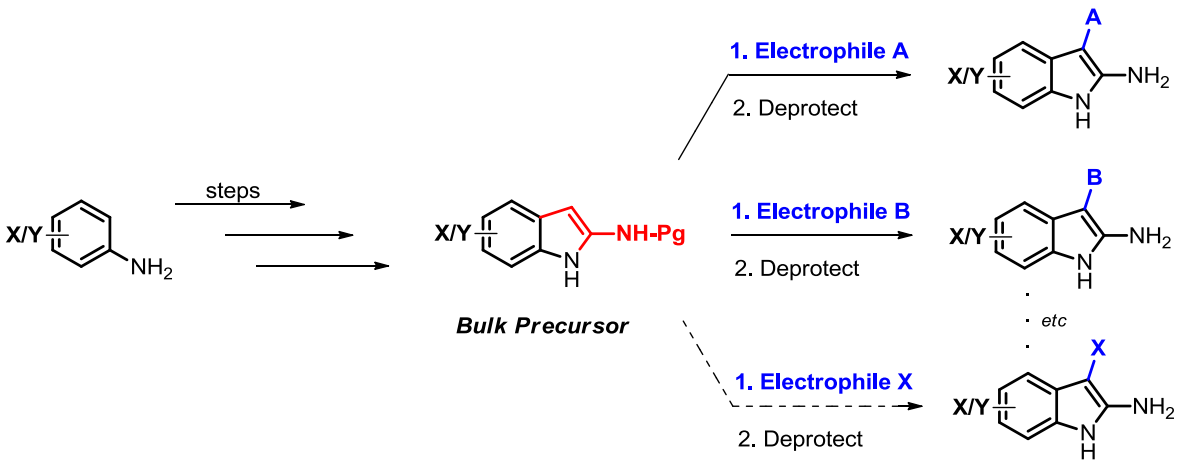

Figure 3.5 Illustration showing the proposed divergent synthesis to create a library of 3-substituted 2-aminoindoles from a common precursor.

2,2'-Azopyridine utilizes 3 acceptor sites when binding to our donor arrays, as one of the amino protons does not participate. An additional acceptor site will therefore be installed in an attempt to interact with that amino proton and increase complex strength. Expanding the heterocyclic system from pyridine to naphthyridine will include an additional preorganized nitrogen acceptor. In a similar manner, an oxygen acceptor can be added such as an alkoxide (Figure 3.6). Consequently, these acceptors are

unsymmetrical and therefore the NaOCl-based synthetic approach would yield poor results. Alternative synthetic strategies were thus explored.

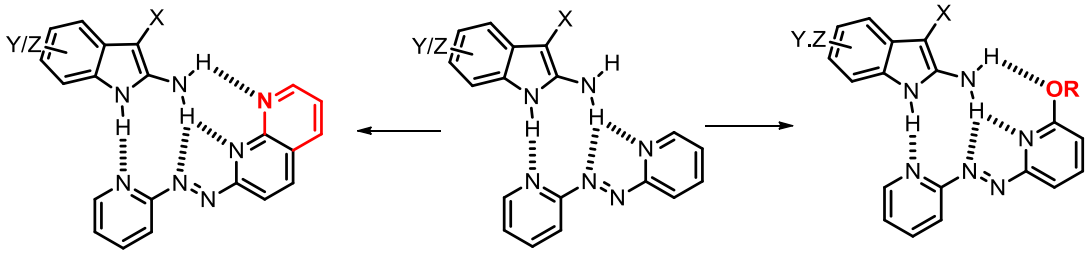

Figure 3.6 Diagram showing the proposed modifications of the 2,2-azopyridine core to add an additional acceptor via a naphthyridine (left) or alkoxide (right).

3.4 Results and Discussion

3.4.1 Synthesis of 3-Substituted-1*H*-2-Aminoindoles

The above elaborations began with choosing the substituents for the 5- (and 6-) positions in the final indoles (Scheme 3.1). Two aniline derivatives were chosen, 4-trifluoromethyl for solubility purposes and 3-nitro-4-trifluoromethyl for stronger complexation.

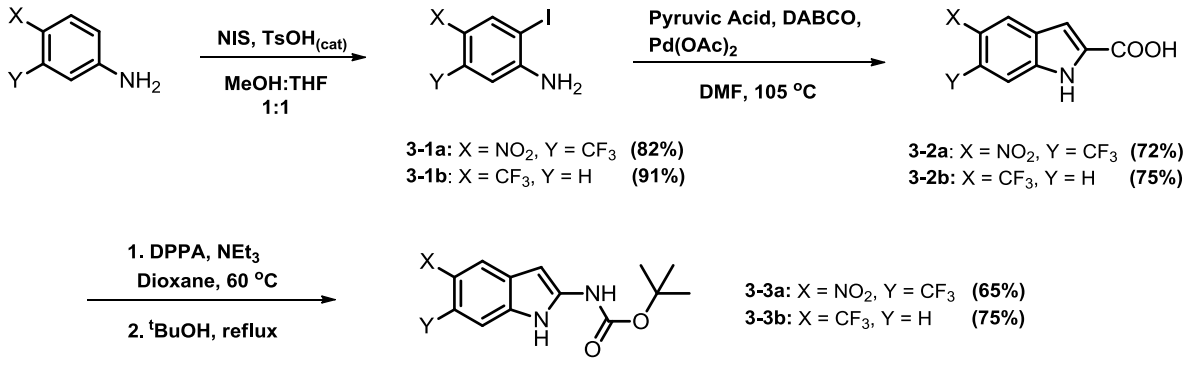

Scheme 3.1 Synthesis of *ortho*-iodinated anilines (**3-1a,b**), 1*H*-2-carboxylic acid indoles (**3-2a,b**), and tert-butyl (1*H*-indol-2-yl)carbamate indoles (**3-3a,b**).

Beginning from the respective anilines, an *ortho*-iodo substituent was installed using NIS and TsOH[6] as outlined in Chapter 2. The di-substituted aniline (**3-1a**) was easily iodinated at room temperature in good yields with no extra purification required. *para*-Trifluoromethyl-aniline (**3-1b**) had to be iodinated using these conditions at 0 °C to avoid complex mixtures of products. Creation of the indole core was then executed using pyruvic acid, DABCO and $Pd(OAc)_2$ catalysis.[7a,b] Imine formation between **3-1a**,**b** and pyruvic acid and subsequent isomerization provides the alkene for an intramolecular Heck coupling to occur creating the indole-2-carboxylate. After heating overnight in DMF, the reaction was poured into cold dilute HCl (pH ~ 3) where the indole precipitates as the acid and can be isolated via vacuum filtration (**3-2a,b**).

The final step to create the precursor was to convert the acid to an amino group in the 2-position. A Curtius rearrangement was performed by deprotonation of the carboxylic acid in dioxane with NEt_3 followed by the addition of DPPA and heating at 60 °C for a minimum of an hour.[8] The resulting crude acyl azide was generated quantitatively as confirmed via ^1H NMR and mass spectrometry. The first attempt to

create the Boc protected precursor was performed solely by removing the dioxane and refluxing the crude mixture in ^{t}BuOH. Conversion was successful but the resulting yield was low and purification was difficult. A cleaner conversion was attempted by stirring the acyl azide reaction vigorously in water to solubilize the diphenyl phosphate by-product and isolating the acyl azide precipitate by vacuum filtration. This method removed approximately 90% of the phosphates and the rearrangement was executed in ^{t}BuOH which increased both Boc-protected indole (**3-3a,b**) yields and purity.

With the intermediate Boc-protected indoles in hand, modifications of the 3-position were then examined. Nitration of indole **3-3a** was performed by adding $HNO_{3(conc.)}$ to cold acetic anhydride[9] creating a strong electrophile for nitration. **3-3a** was added at once as a solid and after an hour of stirring on ice, the solution was poured into water to precipitate the product. Analysis of the solids by ^{1}H NMR showed the disappearance of the signal corresponding to the 3-position and the nitration was successful in high yield (Scheme 3.2).

Installation of a trifluoroacyl substituent was acheived in high yield by the dropwise addition of TFAA into a cold solution of **3-3a** in THF and warming to room temperature overnight (Scheme 3.2).

Aromatic aldehydes are commonly formed by the Vilsmeier-Haack[10a-c] reaction using $POCl_3$ and DMF. These conditions were attempted on **3-3a** but the reaction was unsuccessful and led to alternative products and degradation of the substrate. A modified version with milder conditions was performed using benzoyl chloride in DMF to create the formylating agent.[11] The iminium cation was hydrolyzed with water and heat the following day to create the aldehyde in good yield (Scheme 3.2).

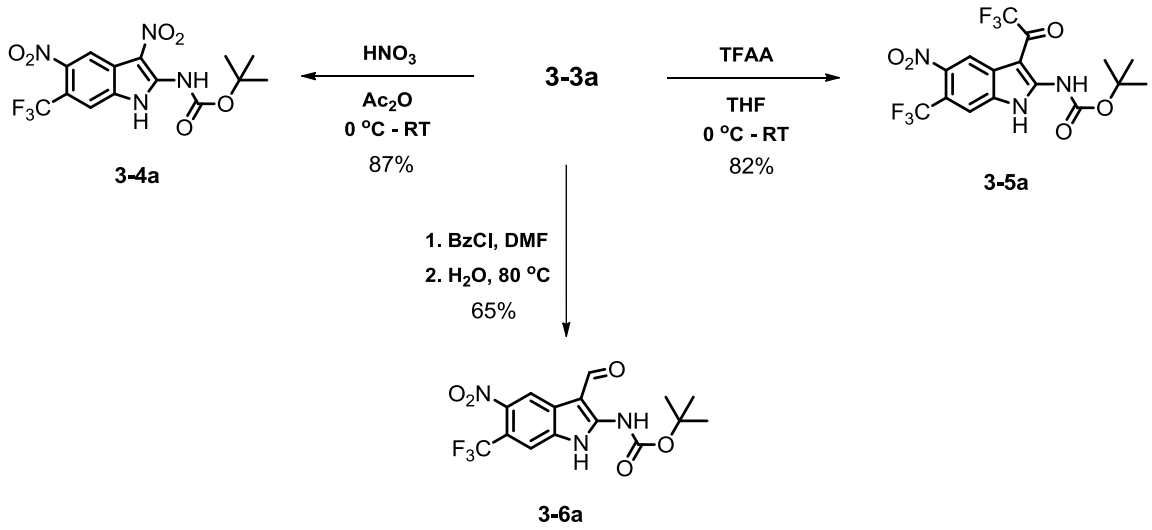

Scheme 3.2 Synthesis of the 3-NO_2 (**3-4a**), 3-$COCF_3$ (**3-5a**), and 3-CHO (**3-6a**) derivatives of tert-butyl (5-nitro-6-(trifluoromethyl)-1*H*-indol-2-yl)carbamate.

The removal of the Boc group was completed in high yields for all indoles with HBF_4 diethyl etherate in diethyl ether (Scheme 3.3). We found that using 100 µL of acid to every 100 mg of solid was an adequate amount to complete the reaction in a few hours the produce clean indole products. Other methods using reagents, such as TFA/DCM were also attempted but yields were lower with longer reaction times and removal of the TFA was difficult.

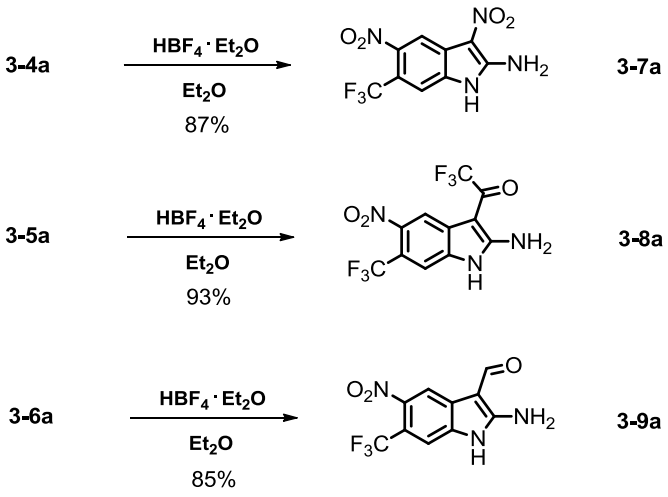

Scheme 3.3 Synthesis of the 3-NO_2 (**3-7a**), 3-$COCF_3$ (**3-8a**), and 3-CHO (**3-9a**) derivatives of 5-nitro-6-(trifluoromethyl)-1*H*-indol-2-amine.

Our knowledge of 2-aminoindoles from the previous chapter showed that highly polar, di-substituted derivatives can be insoluble in non-polar solvents. The solubility of **3-7a, 3-8a and 3-9a** were tested before any other substituted derivatives were attempted. Unfortunately, none of the above examples were soluble in $CDCl_3$ so our attention moved to **3-3b**.

The reactions in Scheme 3.2 were replicated for derivative **3-3b** obtaining similar yields with the nitration being an exception (Scheme 3.4). Adding **3-3b** directly to the HNO_3/Ac_2O reactants resulted in nitrations at both the 3- and 7- positions and chromatographic separation of the products was tedious. Therefore, **3-3b** was cooled in THF and the nitrating agent was added dropwise which increased the yield of the desired 3-substituted product. The deprotection step with HBF_4 was also replicated with the same high yielding results for all derivatives (Scheme 3.5).

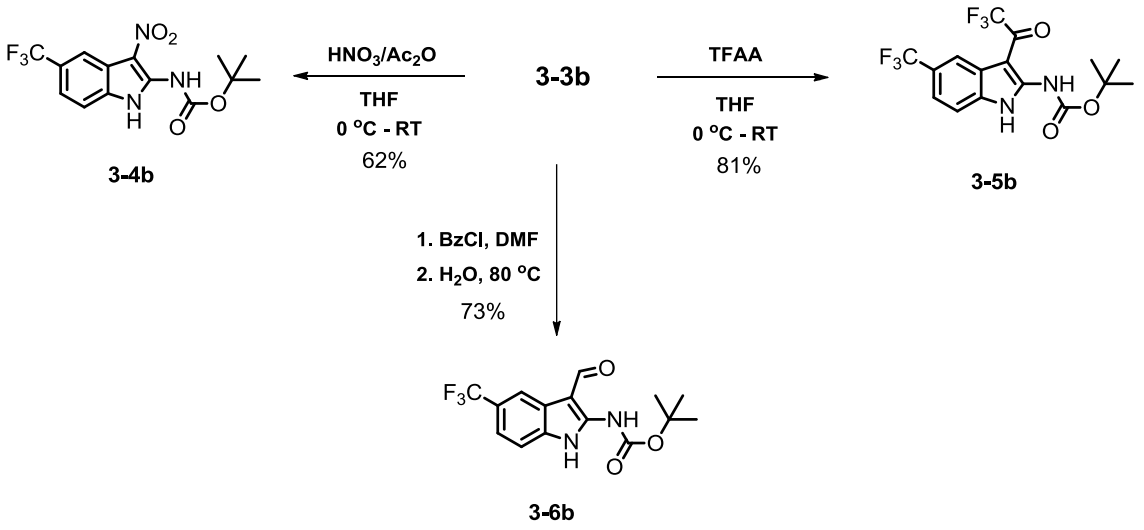

Scheme 3.4 Synthesis of the 3-NO_2 (**3-4b**), 3-$COCF_3$ (**3-5b**), and 3-CHO (**3-6b**) derivatives of tert-butyl (5-(trifluoromethyl)-1*H*-indol-2-yl)carbamate.

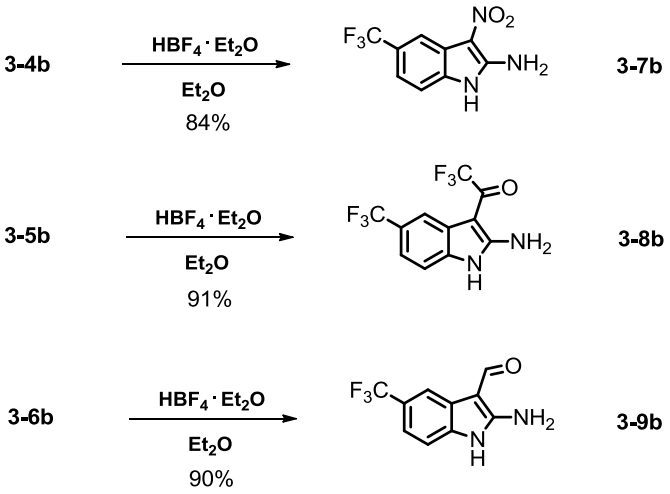

Scheme 3.5 Synthesis of the 3-NO_2 (**3-7b**), 3-$COCF_3$ (**3-8b**), and 3-CHO (**3-9b**) derivatives of 5-(trifluoromethyl)-1*H*-indol-2-amine.

The solubility of these three indoles were examined and **3-8b and 3-9b** proved soluble in $CDCl_3$. **3-7b** was insoluble but with the success of the other two examples, more derivatives were examined. Halogens were installed in the 3 position by cooling **3-**

3b in THF in an ice bath and adding the corresponding *N*-halosuccinimide as a solid in portionwise additions.[12] As the reaction slowly warmed to room temperature, the process was monitored by TLC and halted once all of **3-3b** had been converted. Each of the iodo, bromo and chloro derivatives were isolated in good yields but the deprotections were unsuccessful as side reactions occurred and no starting material or desired product was observed (Scheme 3.6).

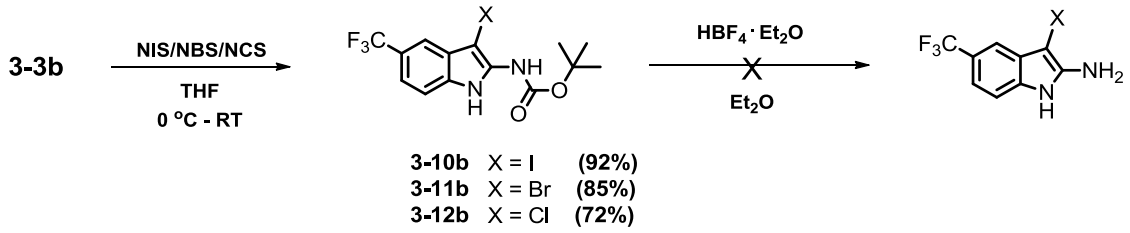

Scheme 3.6 Synthesis of the 3-iodo (**3-10b**), 3-bromo (**3-11b**), and 3-chloro (**3-12b**) derivatives of tert-butyl (5-(trifluoromethyl)-1*H*-indol-2-yl)carbamate and unsuccessful attempt at deprotection.

The installation of a keto substituent on **3-3b** proved to be problematic. Following similar reaction conditions (adding the electrophile at low temperature and subsequent warming), neither hexanoyl chloride nor acetic anhydride reacted and only **3-3b** was recovered (Scheme 3.7). The reactions were repeated at room temperature and the same result was observed. When the temperature was raised to 50 °C, hexanoyl chloride provided ~ 5% yield of the desired product with the remainder being degraded indole by-products while acetic anhydride resulted in degraded starting material. Altering the conditions where an equivalent of base was added proved unsuccessful in obtaining any desired product at low temperature and degraded products at higher temperatures (Scheme 3.7). Reactions with acid were not attempted at the risk of

removing the Boc-group. This led to the conclusion that if an electrophile is to be successfully installed, the reactivity must be high enough so that the reaction occurs at ambient temperature or lower. Additionally, the addition of base can be disregarded since no change in results was observed.

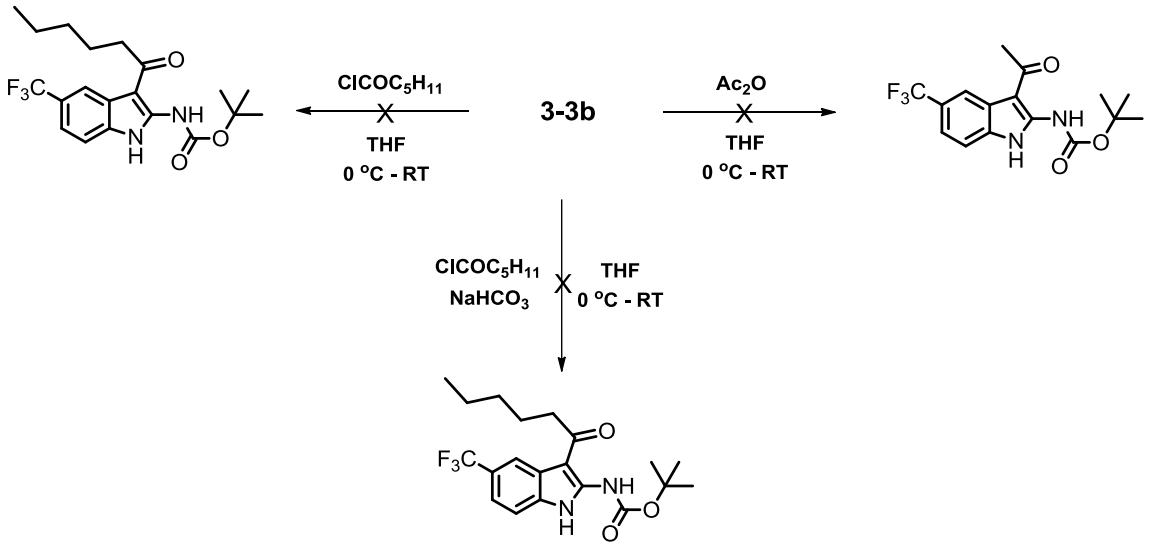

Scheme 3.7 Attempted synthetic strategies to install an alkyl keto-substituent onto tert-butyl (5-(trifluoromethyl)-1*H*-indol-2-yl)carbamate.

4-Nitrobenzoyl chloride was added to a cold solution of **3-3b** in THF and proved to be electrophilic enough to participate under these reaction conditions. The phenacyl component was installed on **3-3b** in good yield and the deprotection with HBF_4 diethyl etherate was completed successfully (Scheme 3.8).

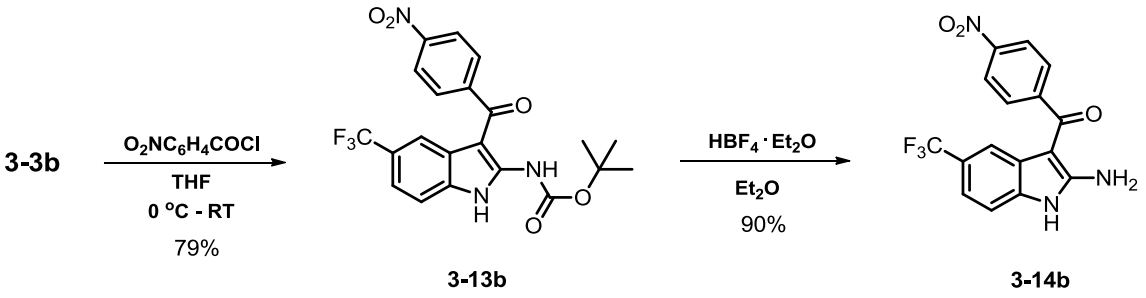

Scheme 3.8 Synthesis of a 3-phen-acyl derivative of tert-butyl (5-(trifluoromethyl)-1*H*-indol-2-yl)carbamate (**3-13b**) and 3-*p*-NO_2-phenacyl-5-(trifluoromethyl)-1*H*-indol-2-amine (**3-14b**).

Synthetic difficulties arose when attempting to install a sulfone substituent. Tosyl chloride yielded no reaction and triflic anhydride in DCM at low temperature resulted in a 50:50 mixture of starting material and the *N*-sulfonylated product. Replicating a literature procedure[13] where tosyl chloride was used in conjunction with catalytic copper in warm MeCN led to degraded starting material and no desired product (Scheme 3.9).

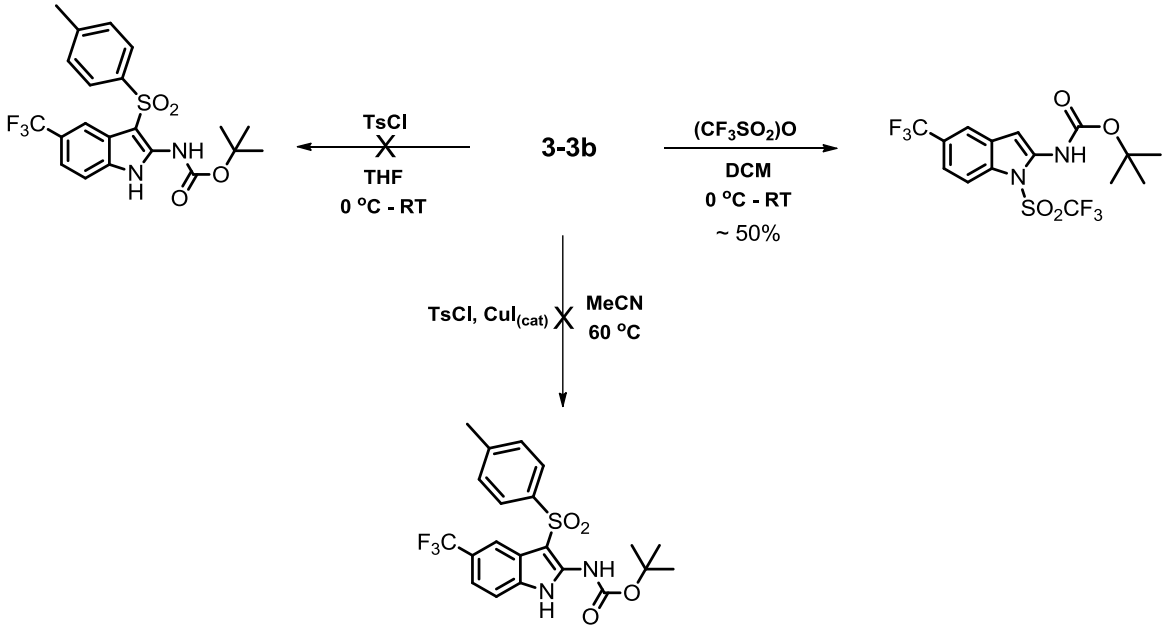

Scheme 3.9 Attempted synthetic strategies to install a sulfone-substituent onto tert-butyl (5-(trifluoromethyl)-1*H*-indol-2-yl)carbamate.

Since the above reactions were unsuccessful, it was decided to explore the original synthetic scheme using copper and active methylene substrates. 1-Hexanethiol was stirred with base and bromoacetonitrile to obtain a thioether in good yields. A combination of UHP/TFAA in acetonitrile oxidized the sulfur in high yield to obtain the appropriate active methylene compound. With **3-1b** already in hand, it was acetylated using TFAA and NEt_3 as discussed in the previous chapter. The 2,2,2-trifluoroacetamide and the sulfonyl-cyano active methylene compound (**3-16b**) were subjected to copper catalysis and 5-trifluoro-3-hexylsulfonyl-1*H*-2-aminoindole was isolated in good yield. To our knowledge, this is the first example of these reaction conditions being used to synthesize this type of indole (Scheme 3.10).

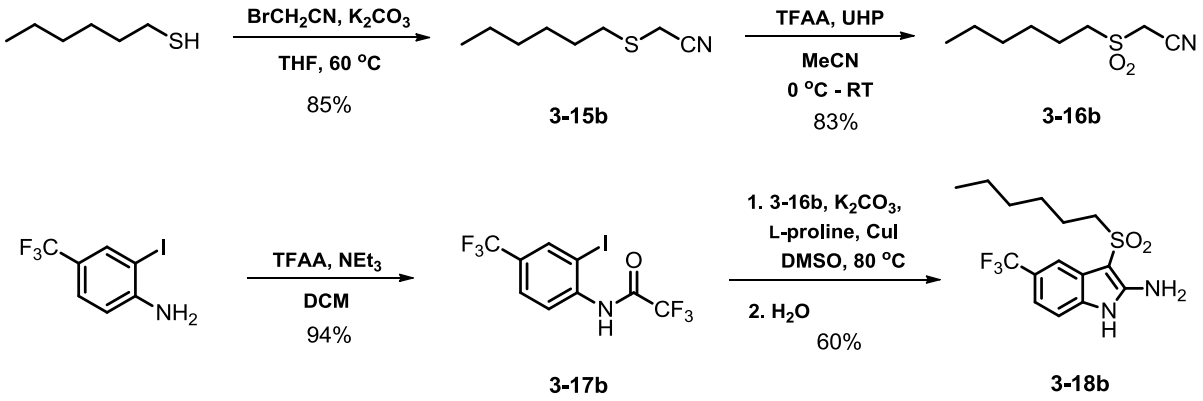

Scheme 3.10 Synthesis of the sulfonyl-cyano active methylene compound (**3-16b**) and the 3-hexyl-sulphonyl derivative of 5-(trifluoromethyl)-1*H*-indol-2-amine (**3-18b**) using the Cu(I) catalysis procedure.

Along with the above examples, the study of a strong donor (e.g. di-substituted derivative) in alternative non-polar solvents was still desired. Given that the ethyl ester version of the di-substituted indole was soluble in $CDCl_3$, extending the carbon chain should enhance the solubility in a less-competitive solvent. Testing this theory, an active methylene compound with an octyl chain was synthesized via DCC coupling with cyanoacetic acid and catalytic DMAP in good yield (**3-19b**, Scheme 3.11). The 2,2,2-trifluoroacetamide of **3-3a** was synthesized with TFAA and NEt_3 in high yield (**3-20b**).

Scheme 3.11 Synthesis of octyl cyanoacetate.

This substrate along with octyl cyanoacetate were reacted via the copper catalysis reaction conditions successfully in moderate yield (Scheme 3.12). This octyl-ester indole

(**3-21b**) proved more soluble in $CDCl_3$ than the ethyl-ester counterpart and also soluble in toluene-d_8. Therefore, solvent comparisons were completed with this indole and the results will be discussed in the following section.

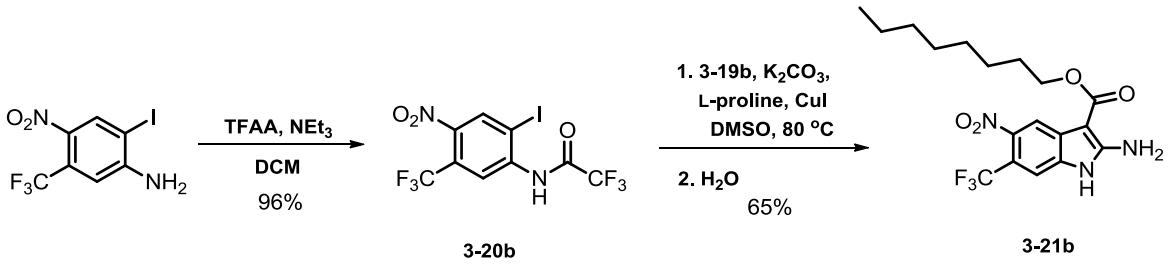

Scheme 3.12 Synthesis of octyl 2-amino-5-nitro-6-(trifluoromethyl)-1*H*-indole-3-carboxylate (**3-21b**).

3.4.2 Synthesis of Extended Acceptor Arrays

The synthesis of our extended acceptor arrays began with the consideration that an additional acceptor site had to be available to extend the binding to both amino hydrogens. Expanding 2,2'-azopyridine's ring system is not possible directly from the compound itself using known methods so an alternative synthetic approach had to be taken. A naphthyridine moiety was fashioned in quantitative yields by heating acetylacetone and 2,6-diaminopyridine in phosphoric acid.[14] This 2-amino-5,7-dimethyl-1,8-naphthyridine (**3-1c**) was diazotized in sulfuric acid at low temperature and heated to create the hydroxyl derivative (**3-2c**) in good yield with no purification needed. Phosphorus oxychloride was employed to convert the hydroxyl group to a chloride substituent (**3-3c**) in high yield to give one half of the new acceptor (Scheme 3.13).[15]

Synthesis of the pyridyl unit was performed cleanly by refluxing 2-fluoropyridine in hydrazine monohydrate.[16] Refluxing chloronaphthyridine (**3-3c**) and 2-hydrazinopyridine (**3-4c**) in *n*-PrOH[17] linked the two components via the hydrazine group (**3-5c**) in good yields with no tedious purification steps required. (Diacetoxyiodo)benzene[18] was employed as a mild oxidant in a mixture of warm DCM and DMSO to give our final pyridyl-azo-naphthyridine acceptor array **(*E*)-3** in high yield (Scheme 3.13).

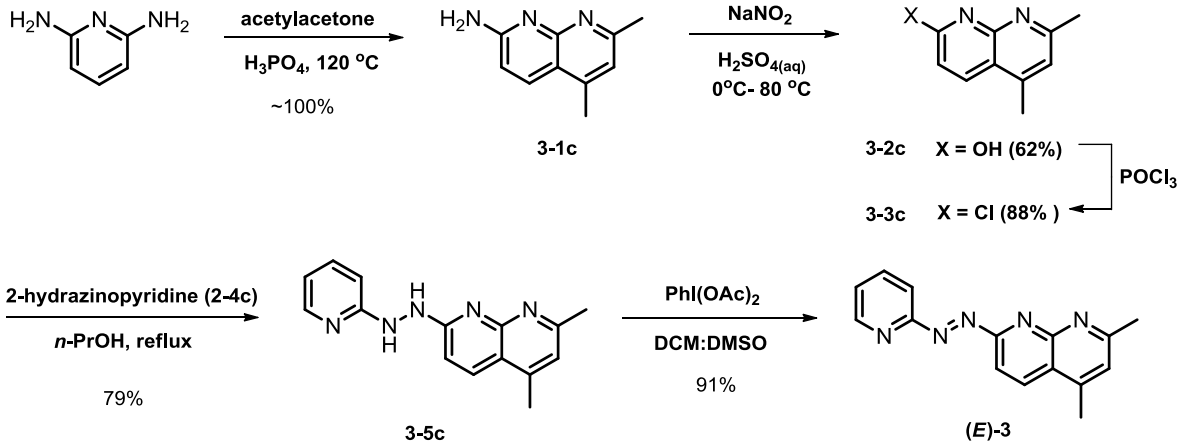

Scheme 3.13 Synthesis of (*E*)-2,4-dimethyl-7-(pyridin-2-yl-diazenyl)-1,8-naphthyridine, **(*E*)-3**.

Synthesis of an acceptor with an oxygen donor group began with cyanuric chloride. Cyanuric chloride is a very useful substrate in that different substitutions can be controlled solely by altering the reaction temperature.[4a,b] Additionally, this compound can act as a scaffold when it comes to connection points for synthesis of supramolecular polymers.[19] The first substitution was performed to increase electron density on the triazine ring to improve hydrogen bond acceptor strength. Piperidine mixed with NEt_3 in

THF was added dropwise to a solution of cyanuric chloride in THF at -78 °C. The di-chloro product (**3-6c**) precipitated in water and was filtered off with no further purification necessary before the next step. Methanol was deprotonated by NaH and added dropwise to **3-6c** at 0 °C to install the oxygen donor in good yield (**3-7c**). The last substitution was performed the same way as in the production of **3-5c** using 2-hydrazinopyridine. The precipitated crude product was difficult to purify so the solids were taken as a whole and subjected to oxidation with (diacetoxyiodo)benzene. Flash chromatography yielded the final pyridyl-azo-triazine array, **(*E*)-4,** in moderate yield (Scheme 3.14).

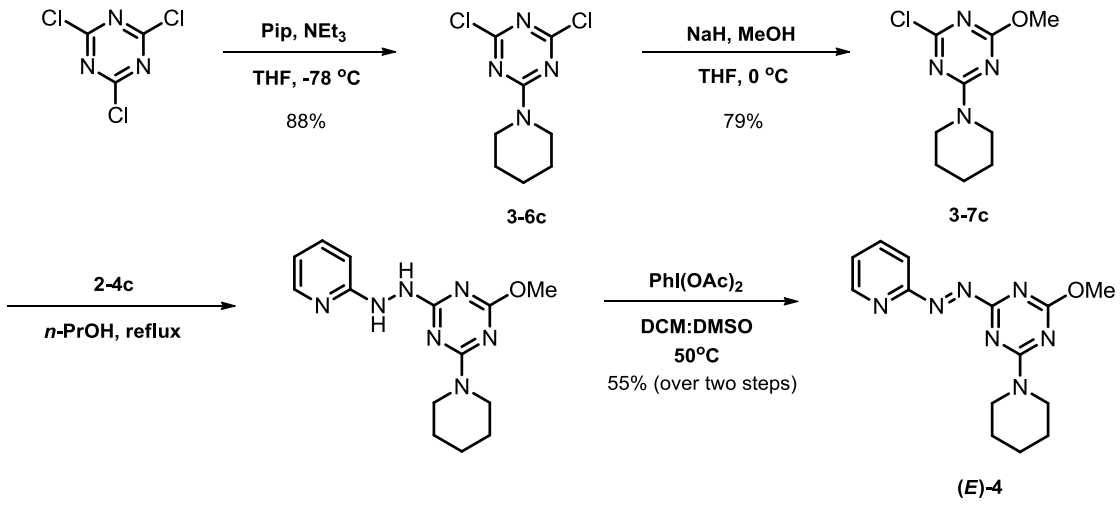

Scheme 3.14 Synthesis of (*E*)-2-methoxy-4-(piperidin-1-yl)-6-(pyridin-2-yl-diazenyl)-1,3,5-triazine, **(*E*)-4**.

3.4.3 Solution State Studies: Complexation of 3-Substituted-1*H*-2-Aminoindoles with (*E*)-2

The association constants of our four new 3-substituted indole derivatives were determined via ^{1}H NMR titrations in $CDCl_3$ (Figure 3.7). 2,2'-Azopyridine **(*E*)-2**, was

chosen as the acceptor because direct comparisons can be made with data collected from the previous chapter. Each of **3-8b**, **3-9b**, **3-14b**, and **3-18b** were titrated with **(*E*)-2** and the data was analyzed using Origin® software. The results are depicted below in Figure 3.8 and summarized in Table 3.1.

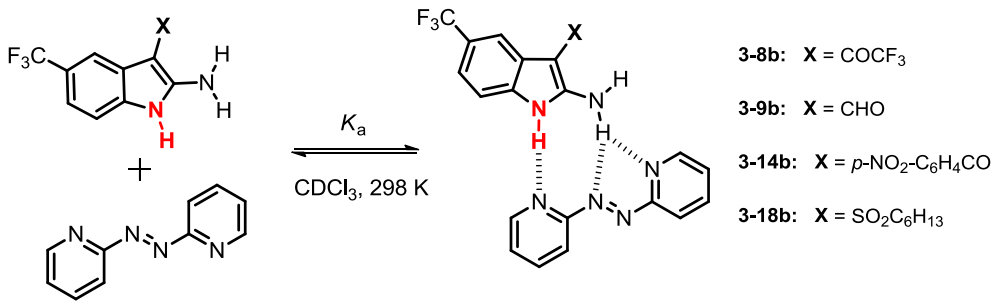

Figure 3.7 Complexation equilibria between indoles **3-8b**, **3-9b**, **3-14b**, and **3-18b** and **(*E*)-2**.

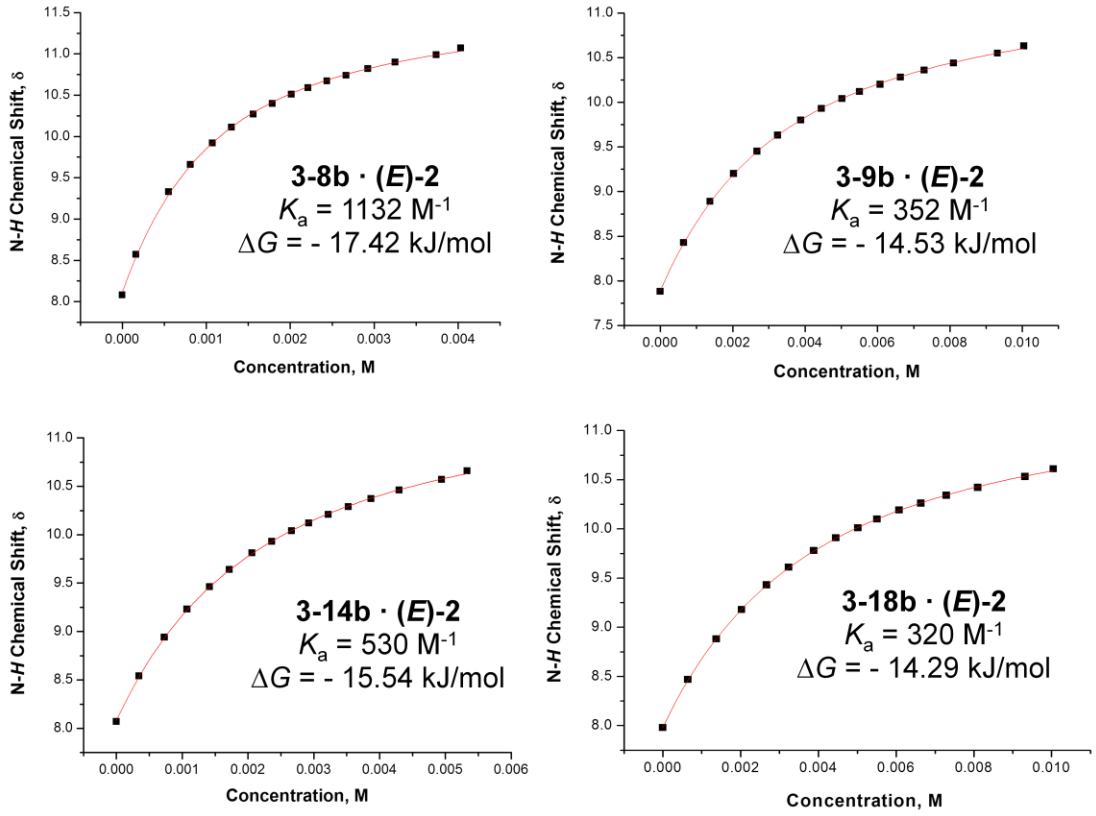

Figure 3.8 Indole N-*H* ^{1}H NMR titration data and calculated binding isotherms for complex formation between **3-8b**, **3-9b**, **3-14b**, and **3-28b** with **(*E*)-2**. K_a and calculated free energy of complexation for each complex are noted beneath their respective binding curves. All titrations were performed in $CDCl_3$ at 298 K.

Table 3.1 Association constants (K_a) of each indole species **3-8b**, **3-9b**, **3-14b**, and **3-18b** with **(*E*)-2**, free energies of complexation (ΔG), calculated chemical shifts of free indole, fully complexed indole and total change in chemical shift (δ_{free}, δ_{bound}, and $\Delta\delta_{max}$ respectively) in $CDCl_3$ at 298 K.

Indole	**Substituent**	**σ_p**	**K_a (M^{-1})[a]**	**ΔG (kJ mol^{-1})[a]**	**δ_{free} (ppm)** N*H*[a] NH_2[b]	**δ_{bound} (ppm)** N*H*[a] NH_2[b]	**$\Delta\delta_{max}$ (ppm)** N*H* NH_2
3-8b	$COCF_3$	0.80	1132 ± 38	-17.42 ± 0.08	8.10 6.99	11.74 8.40	3.64 1.41
3-9b	CHO	0.42	352 ± 8	-14.53 ± 0.06	7.89 6.43	11.43 7.73	3.54 1.30
3-14b	*p*-NO_2-C_6H_4CO	NA	530 ± 5	-15.54 ± 0.02	8.06 6.86	11.61 8.18	3.55 1.32
3-18b	$SO_2C_6H_{13}$	0.72 - 0.77	320 ± 24	-14.29 ± 0.19	7.99 5.42	11.47 6.65	3.48 1.23

[a] Average values calculated from Eq. 6 from the previous chapter using the 1:1 regression software. K_a and ΔG values are calculated from the N*H* data. All titrations were performed in triplicate and errors are reported as twice the standard deviation to provide a 95% confidence level. [b]Same procedure using NH_2 data.

The association constants ranged from 350 to 1132 M^{-1} with **3-8b** being the strongest complex and **(*E*)-2** and **3-18b** being the weakest. The same trend from the previous chapter can be seen where stronger complexes have larger $\Delta\delta_{max}$ values and stronger donor groups generally resonate at higher chemical shifts.

There are unexpected results that deviate from theoretical electron withdrawing trends. If the 3-cyano and 3-ethyl ester derivatives (**2-4f** and **2-3f** from Chapter 2) are also considered, the order of expected complex strength would be CHO, ethyl ester (σ_p = 0.45; K_a = 274 M^{-1}), *p*-NO_2-C_6H_4-CO, CN (σ_p = 0.66; K_a = 735 M^{-1}), $SO_2C_6H_{13}$ and $COCF_3$.[20] This order is based on their corresponding σ_p values because the substituents are in direct conjugation with both the pyrrolo and amino protons. **3-9b** resulted in a

higher value than should be expected even though an aldehyde is the weakest electron withdrawing group studied. We hypothesize that even though an aldehyde (σ_p = 0.42) has a lower electron withdrawing effect when compared to an ester (σ_p = 0.45), the carbonyl is less electron rich and therefore intramolecular hydrogen bonding to the amino proton is weaker. The ester carbonyl donates a greater amount of electron density onto the amino group resulting in weaker complexation. This also explains why **3-18b** resulted in a much lower value than expected even though an alkyl sulfone group (σ_p = 0.72 - 0.77) has an electron withdrawing capability comparable to trifluoroacyl (σ_p = 0.80) substituents. The sulfone oxygen atoms likely donate electron density onto the amino group to a degree where the resulting association constant is the lowest of the indoles studied in this chapter. Indole **3-8b** does contain a carbonyl group but the trifluoro group creates an electron poor oxygen through strong induction effects. In doing so, the donors remain highly polarized and the resulting association constant is the greatest value observed in this comparison. This result is also supported by Hunter's hydrogen bond acceptor numbers where greater β values resulted in lower association constants (CHO: β = 4.7, CO_2Et: β = 5.3, RSO_2R: β = 6.3; *Angew. Chem. Int. Ed*., **2004**, 5310). These results indicate that the substituent in the 3-position cannot contain electron rich oxygen acceptors capable of deactivating the donor groups, regardless of theoretical electron withdrawing strength.

3.4.4 Solution State Studies: Comparison of Complexation Strength and Solvents Effects of 3-21b with Acceptor Arrays (*E*)-2, (*E*)-3, and (*E*)-4

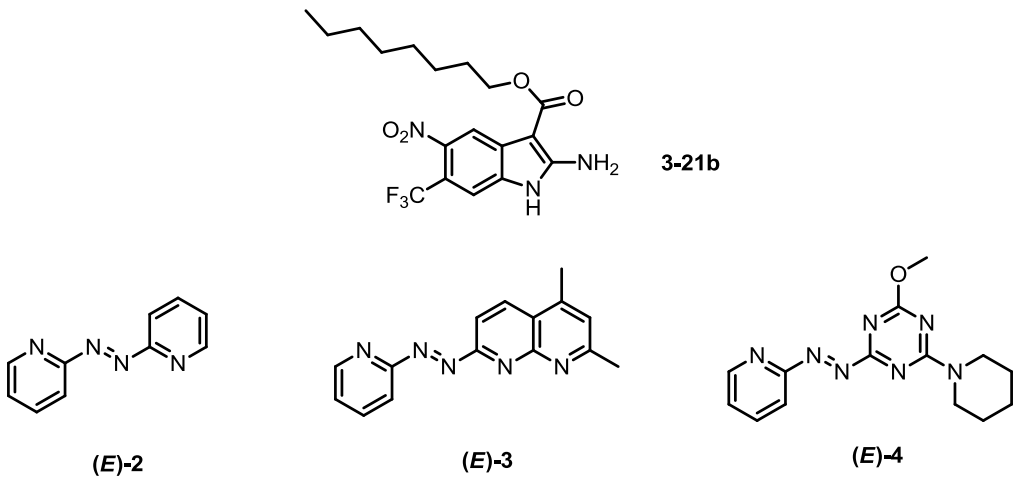

Figure 3.9 Indole **3-21b** and acceptors **(*E*)-2**, **(*E*)-3**, and **(*E*)-4** used for complexation studies in $CDCl_3$ and toluene-d_8.

Indole **3-21b** was synthesized so that strong complexation could be studied in a more non-competitive solvent, as all studies thus far have been performed in $CDCl_3$. The octyl-ester group in position 3 modified the solubility so that analysis could be performed in toluene-d_8 which should lead to stronger complexation. Also, arrays **(*E*)-3** and **(*E*)-4** contain an extra acceptor which should provide stronger complexation when compared to **(*E*)-2**. **3-21b** was titrated with each acceptor array in both $CDCl_3$ and toluene-d_8 to provide insight into how our hydrogen bonded system improves when operating in a more non-polar environment. The Origin® fitting and titration data are displayed in Figures 3.10 - 3.12 and summarized in Table 3.2.

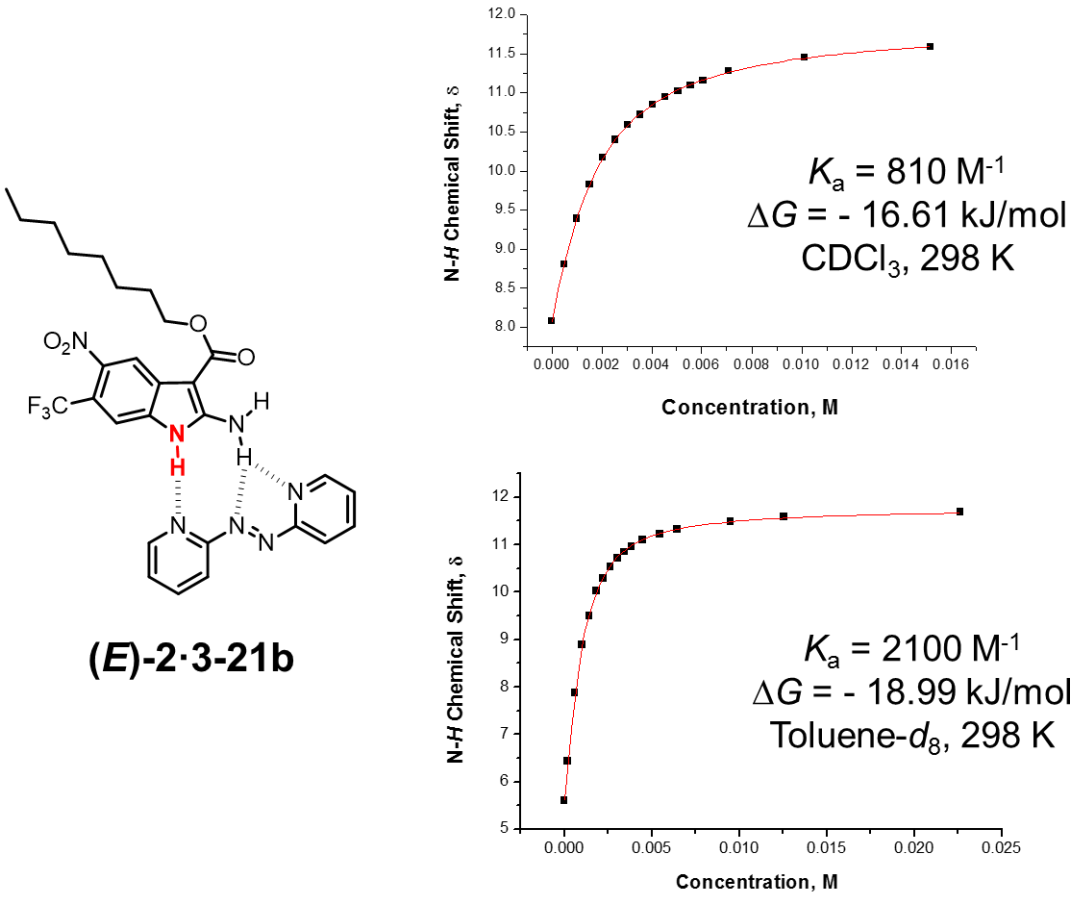

Figure 3.10 Indole N-*H* ^{1}H NMR titration data and calculated binding isotherms for complex formation between **3-21b** and **(*E*)-2**. K_a, calculated free energy of complexation, and titration conditions are noted below their respected curves. Schematic of complex is depicted at left.

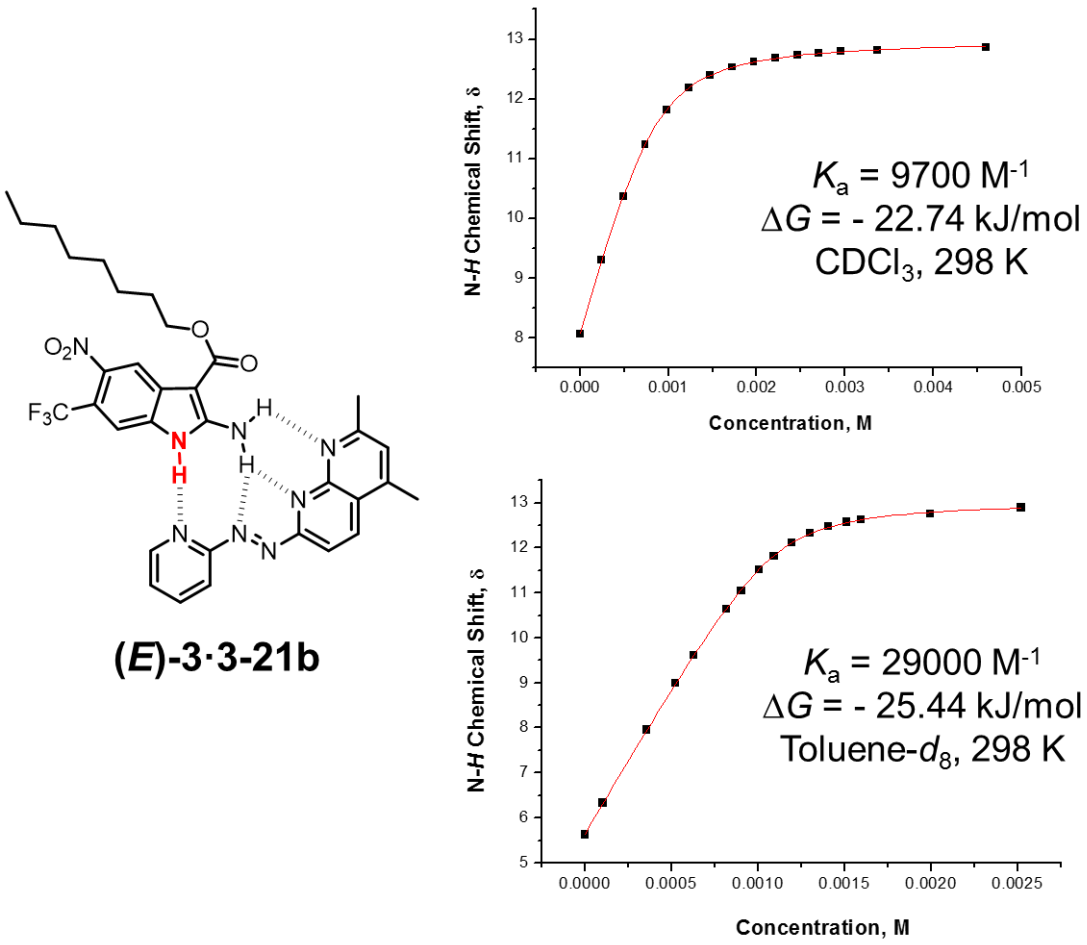

Figure 3.11 Indole N-*H* ^{1}H NMR titration data and calculated binding isotherms for complex formation between **3-21b** and **(*E*)-3**. K_a, calculated free energy of complexation, and titration conditions are noted below their respected curves. Schematic of the predicted complex is depicted at left.

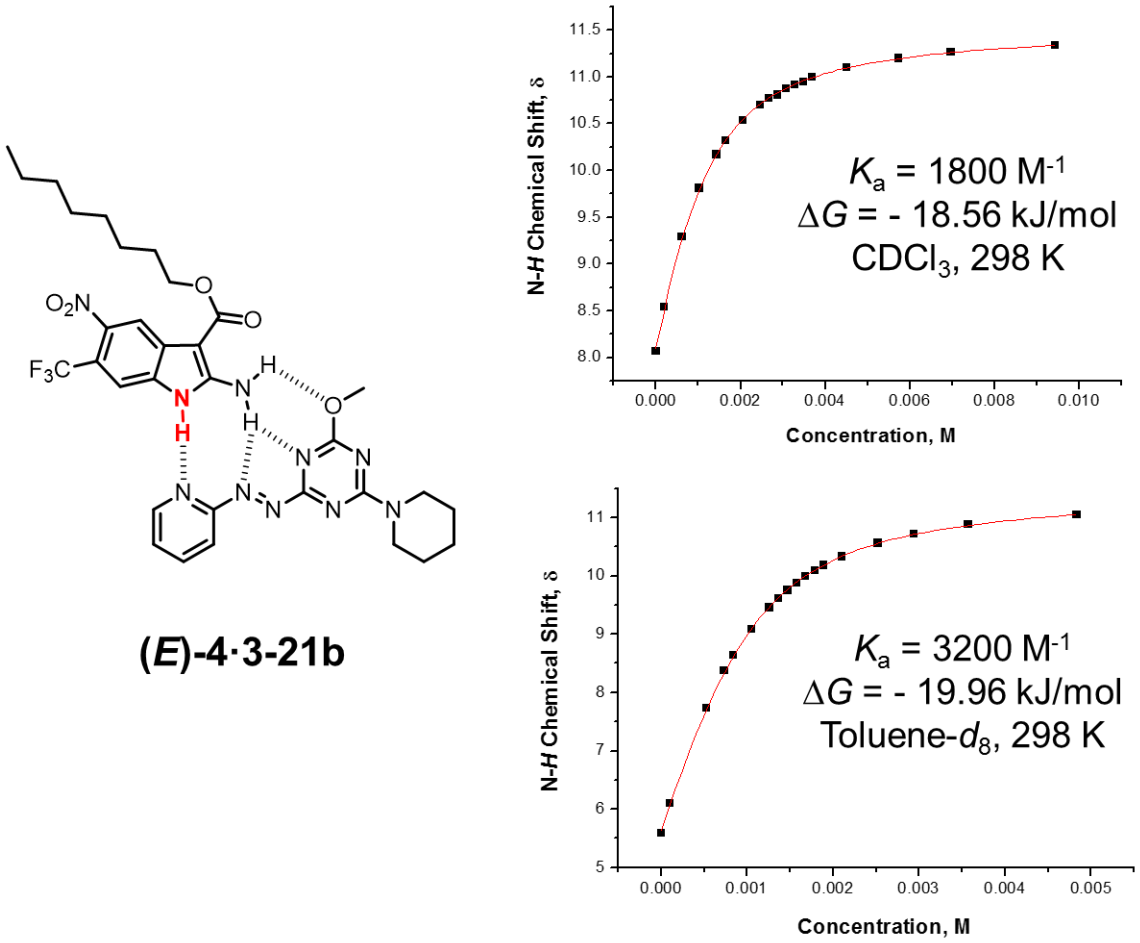

Figure 3.12 Indole N-*H* ^{1}H NMR titration data and calculated binding isotherms for complex formation between **3-21b** and **(*E*)-4**. K_a, calculated free energy of complexation, and titration conditions are noted below their respected curves. Schematic of the predicted complex is depicted at left.

Table 3.2 Association constants (K_a) of indole **3-21b** with **(*E*)-2**, **(*E*)-3**, and **(*E*)-4**, free energies of complexation (ΔG), calculated chemical shifts of free indole, fully complexed indole and total change in chemical shift (δ_{free}, δ_{bound}, and $\Delta\delta_{max}$ respectively) in $CDCl_3$ and Toluene-d_8 at 298 K.

Solvent	Acceptor	K_a (M^{-1})[a]	ΔG (kJ mol^{-1})[a]	δ_{free} (ppm) N*H*[a] NH_2[b]	δ_{bound} (ppm) N*H*[a] NH_2[b]	$\Delta\delta_{max}$ (ppm) N*H* NH_2
$CDCl_3$	**(*E*)-2**	810 ± 22	-16.61 ± 0.07	8.07 6.01	11.89 7.42	3.82 1.41
	(*E*)-3	9700 ± 190	-22.74 ± 0.05	8.09 6.01	13.02 7.91	4.93 1.90
	(*E*)-4	1800 ± 75	-18.56 ± 0.10	8.10 6.01	11.56 7.12	3.46 1.11
Toluene-d_8	**(*E*)-2**	2100 ± 282	-18.99 ± 0.34	5.62 5.01	11.81 7.84	6.19 2.83
	(*E*)-3	29000 ± 2600	-25.44 ± 0.23	5.65 5.03	13.05 8.33	7.40 3.30
	(*E*)-4	3200 ± 44	-19.96 ± 0.04	5.63 5.03	11.49 7.56	5.86 2.53

[a] Average values calculated from Eq. 6 (chapter 2) using a 1:1 regression model and the indole N*H* data. All titrations were performed in triplicate and errors are reported as twice the standard deviation to provide a 95% confidence level. [b]Same procedure using NH_2 data.

The titration of **3-21b** with **(*E*)-2** in $CDCl_3$ resulted in a K_a value of 810 M^{-1} and a value of 2100 M^{-1} in toluene-d_8. This is half an order of magnitude increase in association constant which correlates to a 2.4 kJ/mol increase in free energy of

complexation. A similar result is seen when comparing the two solvents with array **(*E*)-3**. Titration results in $CDCl_3$ yielded a K_a value of 9700 M^{-1} and 29000 M^{-1} in toluene-d_8 which is an increase of 2.7 kJ/mol in free energy.

The largest increase in complexation strength can be seen when comparing **(*E*)-2** and **(*E*)-3** in the same titration solvents. The difference in complexation free energy of these two acceptors with **3-21b** in $CDCl_3$ is 6.1 kJ/mol which is an order of magnitude greater in association constant. Complex formation in toluene-d_8 yielded a similar increase in free energy of 6.4 kJ/mol which again approximates to an order of magnitude increase in the association constant. Literature estimates that on average a primary hydrogen bonding interaction contributes approximately 7.9 kJ/mol in free energy while a secondary interaction is 2.9 kJ/mol.[21] These values can be combined as additional binding pair should stabilize a complex by 13.7 kJ/mol (2.9 x 2 + 7.9). Given our experimental free energy average of ~ 6.2 - 6.3 kJ/mol, it can be concluded that the additional acceptor on **(*E*)-3** does not stabilize the complex to a degree which would be expected for a strong binding pair. This result will be examined further in 2D ^1H experiments. However, these results do reveal that adding an extra contiguous acceptor group has a greater effect on increasing complexation strength than varying $CDCl_3$ to toluene-d_8.

Complexation results with **(*E*)-4** yielded approximately 1 kJ/mol increase in energy when compared to **(*E*)-2** in both $CDCl_3$ and toluene-d_8. Additionally, 1.4 kJ/mol increase in free energy is observed altering $CDCl_3$ to toluene-d_8. We hypothesize that these smaller differences in free energy values arise from two major factors which stem from differences in the structure of **(*E*)-4** when compared to **(*E*)-2** and **(*E*)-3**. Triazine

nitrogen atoms are poorer acceptors when compared to pyridines as each nitrogen draws electron density away from the other nitrogens within the ring. However, likely the main drawback to the structure of **(*E*)-4** is the inclusion of the methoxide substituent. The oxygen atom acts as an effective acceptor but the methyl group is free to rotate and can cause repulsive steric interactions with **3-21b**. This effect has been demonstrated in a similar example using a DAA-ADD complementary complex first examined by Hamilton.[22] An amido-naphthyridine containing an ethoxy group was titrated with a guanosine derivative and an association constant of 126 M^{-1} was obtained which is low for these types of complementary complexes.[23] A similar complex studied by Zimmerman and Murray replaces the ethyl group with a cyclic ester component which preorganizes the oxygen acceptor of the array into a rigid structure.[24] Titration with guanosine resulted in an association constant greater than 10^4 M^{-1}. They attribute this increase in complex stability to the lack of rotational freedom seen in the earlier example which resulted in steric clash between the ethyl group with the guanosine amino group.

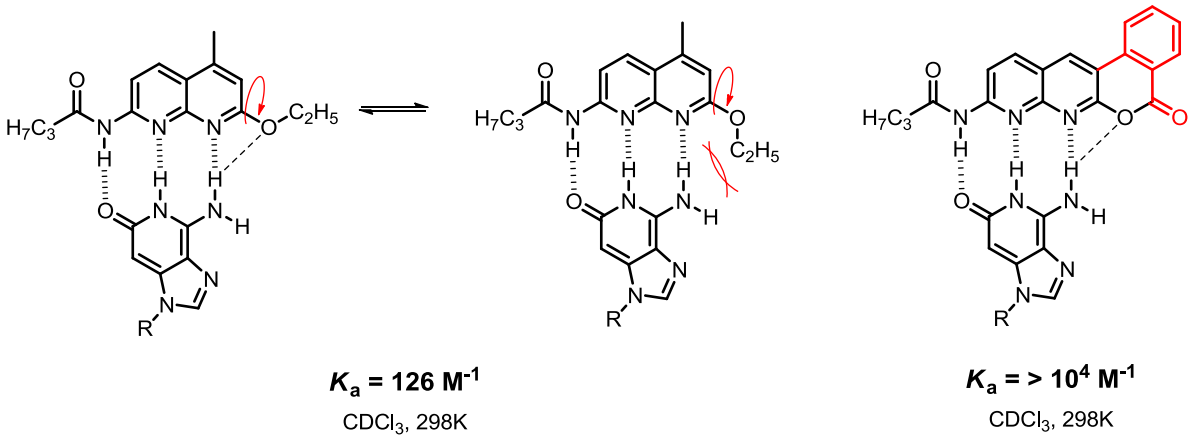

Figure 3.13 Amido-naphthyridine DAA array and a guanosine ADD array studied by Hamilton (shown left) and a similar preorganized complex studied by Zimmerman and Murray (shown right).

The use of toluene-d_8 as a non-competitive solvent resulted in larger association constants for all three complexes. Qualitatively, the initial ^{1}H NMR resonances for the donor groups begin more upfield in toluene-d_8 which resulted in larger $\Delta\delta_{max}$ values. Figure 3.14 shows how the signals for the donor groups in **3-21b** begin at 5.00 (NH_2) and 5.65 (NH) ppm in toluene-d_8 where in $CDCl_3$ they resonate at approximately 6 and 8 ppm, respectively. The δ_{bound} value in both solvents for **(*E*)-3** for the NH shift is approximately 13 ppm so the beginning resonance at 5.65 in toluene-d_8 provided a $\Delta\delta_{max}$ of 7.40 ppm when $CDCl_3$ resulted in a $\Delta\delta_{max}$ of 4.93 ppm. Unchanging in the **3-21b** and **(*E*)-2** titration, here the C7 proton shifts from 6.80 ppm to 7.80 ppm. This large shift in the aryl proton leads to the possibility of multiple binding modes which were examined via 2D ^{1}H NMR experiments.

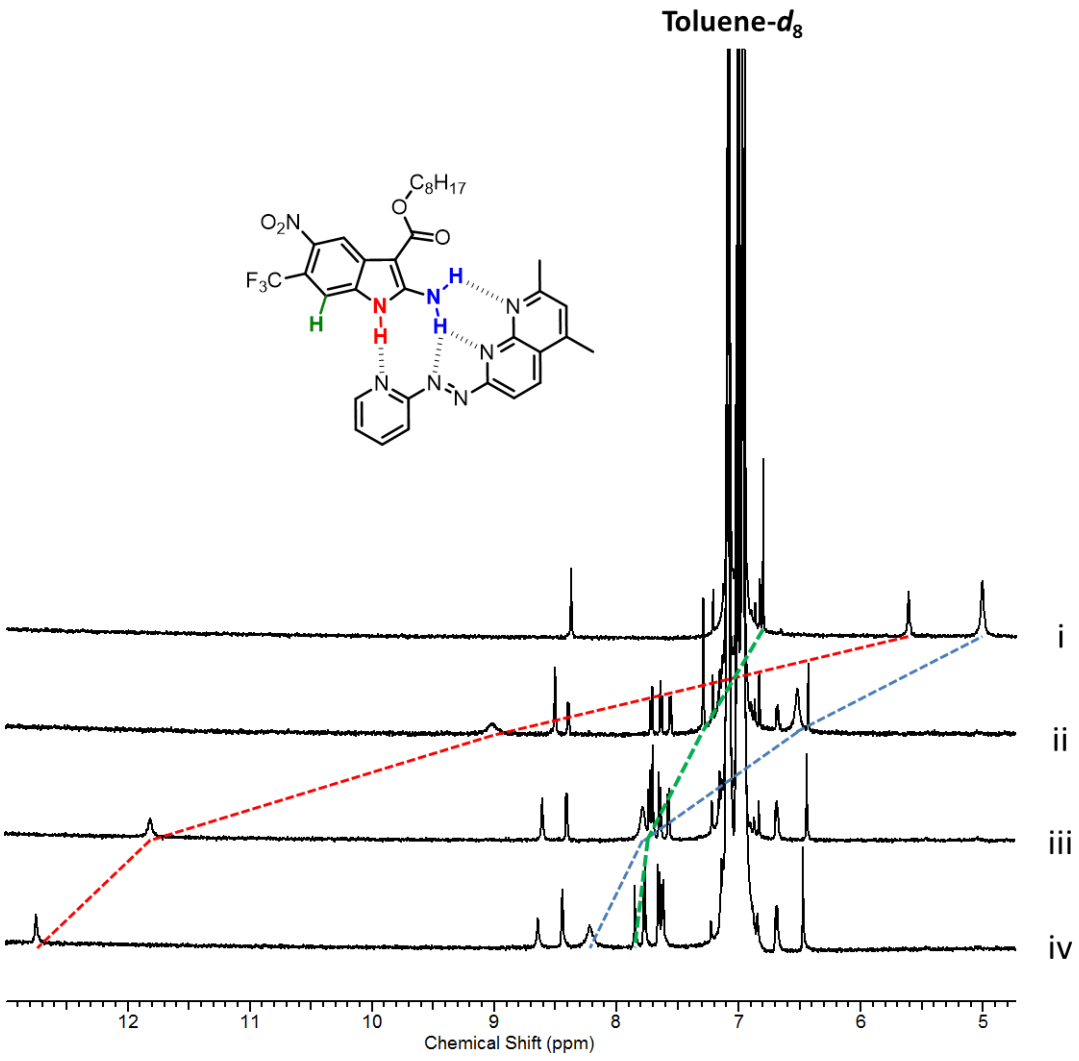

Figure 3.14 Stacked plot of complex **2-21b·(*E*)-3** titration in toluene-d_8 at 298 K; red lines corresponds to the N-*H*, blue lines to NH_2, and green lines to the C7-*H*. i) [**(*E*)-3**]: 0 M, ii) [**(*E*)-3**]: 5.25 x 10^{-4} M, iii) [**(*E*)-3**]: 1.09 x 10^{-3} M, iv) [**(*E*)-3**]: 2.00 x 10^{-3} M. Schematic of the predicted binding complex is depicted above the spectra.

Interestingly, the δ_{bound} value for the NH group is calculated to be approximately the same chemical shift for all acceptors in both solvents. On the other hand, the amino δ_{bound} shifts all increase by approximately 0.44 ppm in toluene-d_8. Therefore, toluene-d_8 has a stronger effect on the amino protons when compared to the pyrrolo proton.

Complexes of **(*E*)-2**, **3** and **4** with **3-21b** were subjected to 2D ^{1}H NOESY experiments with **3-21b** in an attempt to further establish the complexation structure in solution. **(*E*)-2·3-21b** displayed the same $H^{e/e'}$ correlation with H^{c} as previously observed in all 2,2'-azopyridine 2D experiments thus far. Additionally, the $H^{e/e'}$ and amino proton $H^{b/b'}$ correlation which was not observed in the 2D spectrum of the ethyl ester in $CDCl_3$ (Figure 2.19, Chapter 2) is present in this spectrum performed in toluene-d_8 (Figure 3.15).

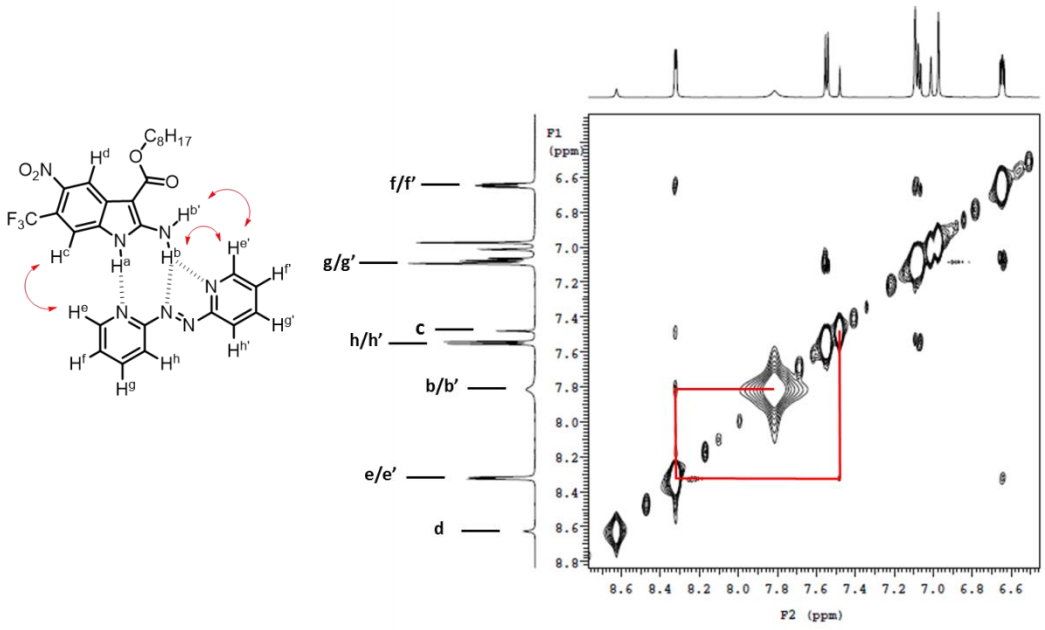

Figure 3.15 2D ^{1}H NOESY spectrum of **(*E*)-2·3-21b** in toluene-d_8 at 298 K. Correlations of interest are indicated by red arrows in structure (shown left) and red lines on spectrum.

The 2D ^{1}H NOESY spectrum of **(*E*)-3·3-21b** resulted in two nOe signals from correlations with the *ortho* methyl peak of the naphthyridine rings and no correlations observed with the *ortho* pyridyl proton. The amino correlation (Figure 3.16, **i**) matches our predicted binding mode for **(*E*)-3**. However, there is also a correlation with the C7-H proton (Figure 3.16, **ii**) where **(*E*)-3** has flipped over and the napthyridine is binding to

the pyrrole NH. This second structure contains a rigid AAA motif which can bind to the DDD array if the C7-H is taken as a potential donor. Also, this possible C7-H hydrogen bond explains the large shift noticed in the titration performed with **2-21b.** These two geometries explain why the complexation energy gained from adding the napthyridine ring did not reach a strong binding pair level. If the first geometry is examined (**i**), the angle between the amino proton and the napthyridine nitrogen is rather acute to attribute strong hydrogen bonding. The second geometry (**ii**) contains an aryl C-H···N hydrogen bond which would not contribute a large amount to the free energy of complexation.

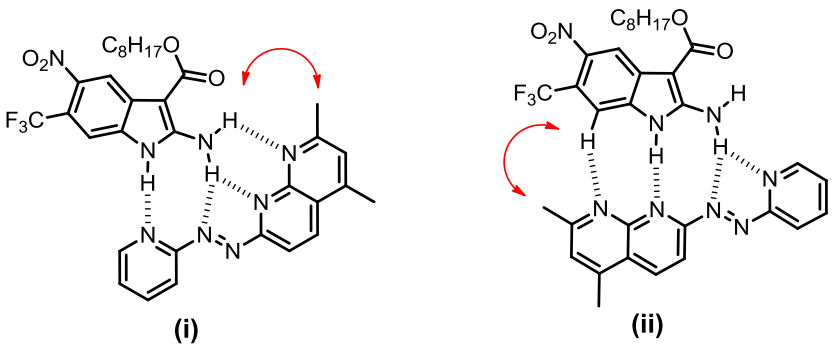

Figure 3.16 Structures of 2 possible complex geometries of **(*E*)-3·3-21b** in solution. Red arrows depict the NOESY correlations detected in the 2D ^{1}H NMR spectrum.

(*E*)-4·3-21b also exhibited two complex geometries in solution. The mode which was predicted correlates to the H^{e}/H^{c} signal (shown in green, Figure 3.17). The methyl H^{i} peak should also correlate with the amino $H^{b/b'}$ signals but was not detected. This could be a result of the methyl group being too far away to obtain an nOe signal or that the second binding mode is preferred. The methyl H^{i} signals in the other binding mode (shown in red, Figure 3.17) displays a correlation with the H^{c} proton on **3-21b**. Additionally, the $H^{e}/H^{b/b'}$ correlation is detected which is analogous to **(*E*)-2** binding.

This mode also matches the **(*E*)-3** binding mode where a hydrogen bond is created between the C7-H (H^c) and the oxygen acceptor creating a AAA-DDD binding complex. The methyl peak is still free to rotate in both of these arrangements which explains why the association constant is lower than expected.

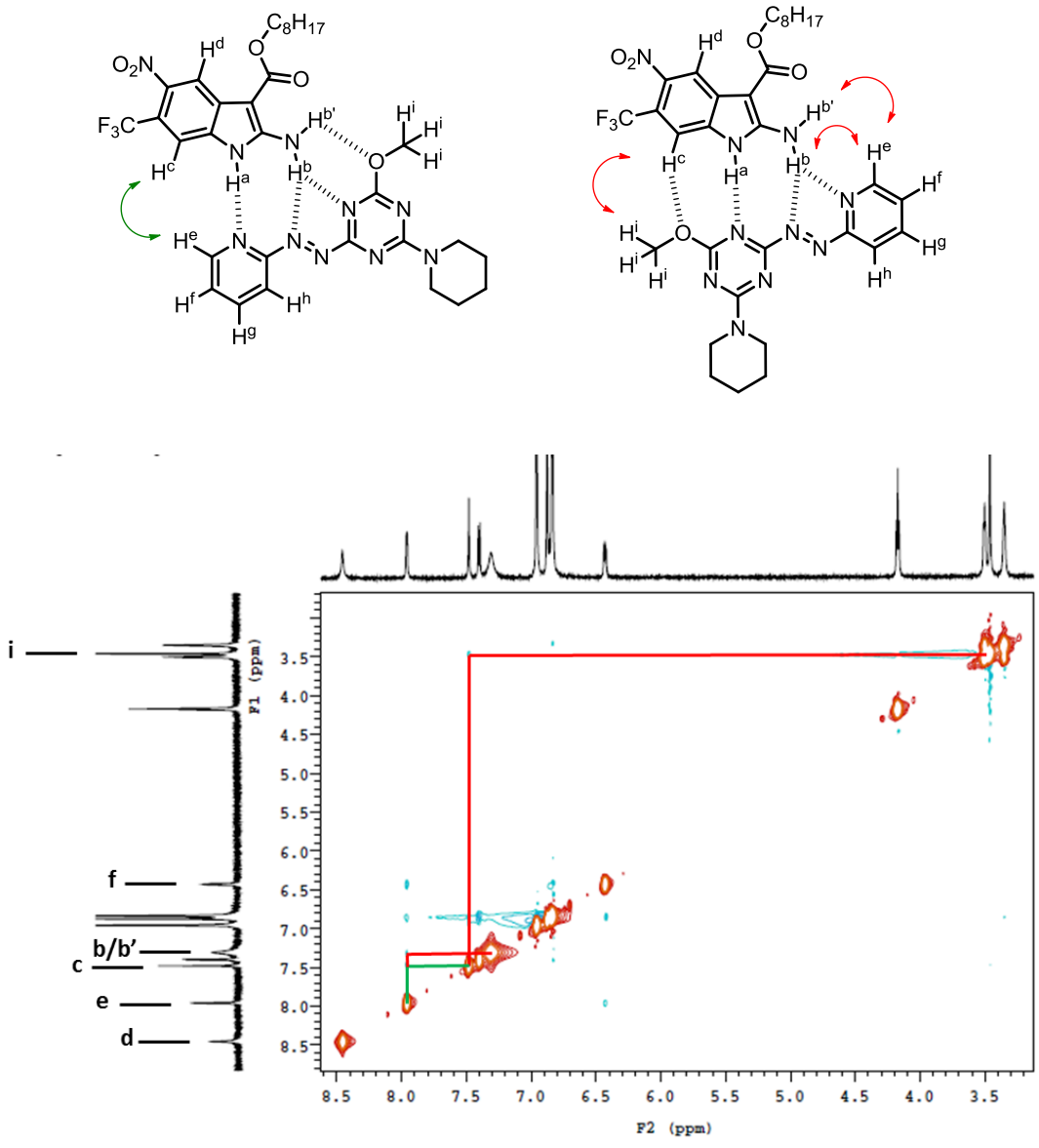

Figure 3.17 2D ^{1}H NOESY spectrum of **(*E*)-4·3-21b·**in toluene-d_8 at 298 K. Correlations of interest are indicated by green and red arrows in the above structures and their corresponding green and red lines on spectrum.

3.4.5 Synthesis and Study of 3-Perfluoroacyl-1*H*-2-Aminoindole Derivatives with (*E*)-2 and (*E*)-3 Acceptor Arrays

Using our results obtained from this work thus far and the work previously discussed from the self-complementary system, one final indole was targeted as an improvement. Increasing the alkyl chain from ethyl to octyl on the ester derivative was effective in making the indole soluble in toluene-d_8. Modifying the phenoxy substituent to pentafluorophenoxy was able to accomplish the same result in the self-complementary examples.[4a,b] Combining these ideas into a perfluorinated acyl group in the 3 position should therefore result in a strong yet soluble derivative (Figure 3.18) as the carbonyl has proven to be a poor hydrogen bond acceptor.

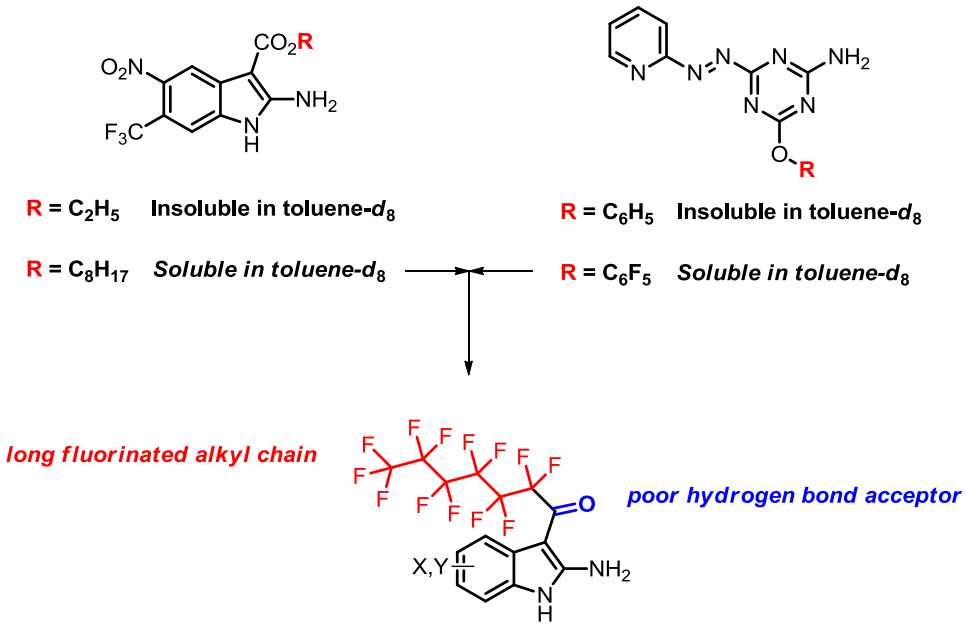

Figure 3.18 Premise for synthesizing strong and soluble 2-aminoindole donors for studies in toluene-d_8.

Perfluoroheptanoic acid was refluxed in dry DCM for 2 hours with oxalyl chloride and 5 drops of DMF to create the perfluoroacyl chloride.[25] The flask contents

was then cooled in an ice bath and diluted with dry THF. Either **3-3a** or **3-3b** were then added and the reaction was left to stir overnight. Both of the Boc-protected perfluoroacyl indoles (**3-1d, 3-1e**) were synthesized in good yields and deprotected with HBF_4 diethyl etherate in high yields (**3-2d, 3-2e**; Scheme 3.15).

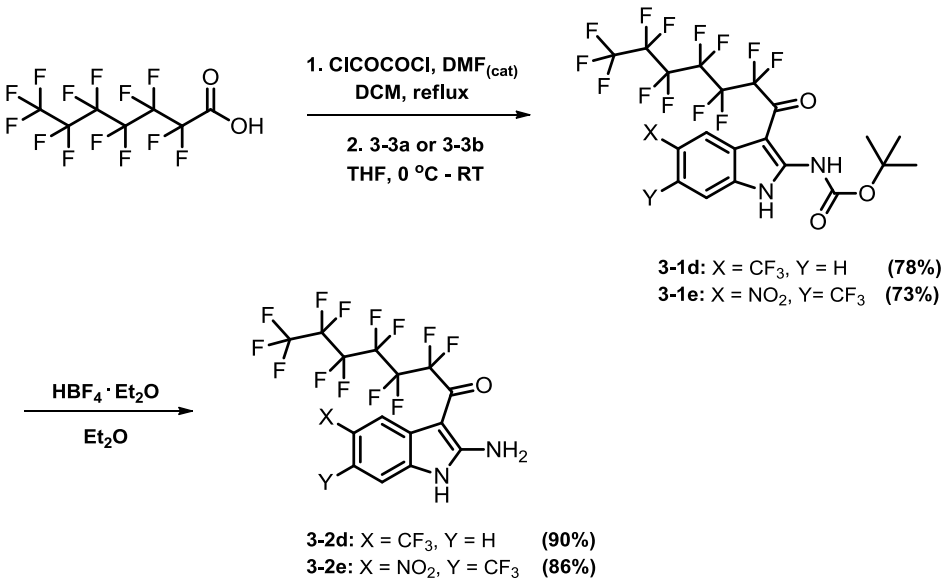

Scheme 3.15 Total synthesis of 5-trifluoromethyl and 5-nitro-6-trifluoromethyl-3-perfluoroacyl-1*H*-2-aminoindoles.

Indole **3-2d** was soluble in both $CDCl_3$ and toluene-d_8 so both solvents were used as titration media. Acceptors **(*E*)-2** and **(*E*)-3** were chosen for comparison to obtain an upper and lower limit for complex stability. The titration data for **(*E*)-2·3-2d** and **(*E*)-3 ·3-2d** are displayed in Figures 3.19 and 3.20 respectively. A more detailed examination of these results are listed in Table 3.3.

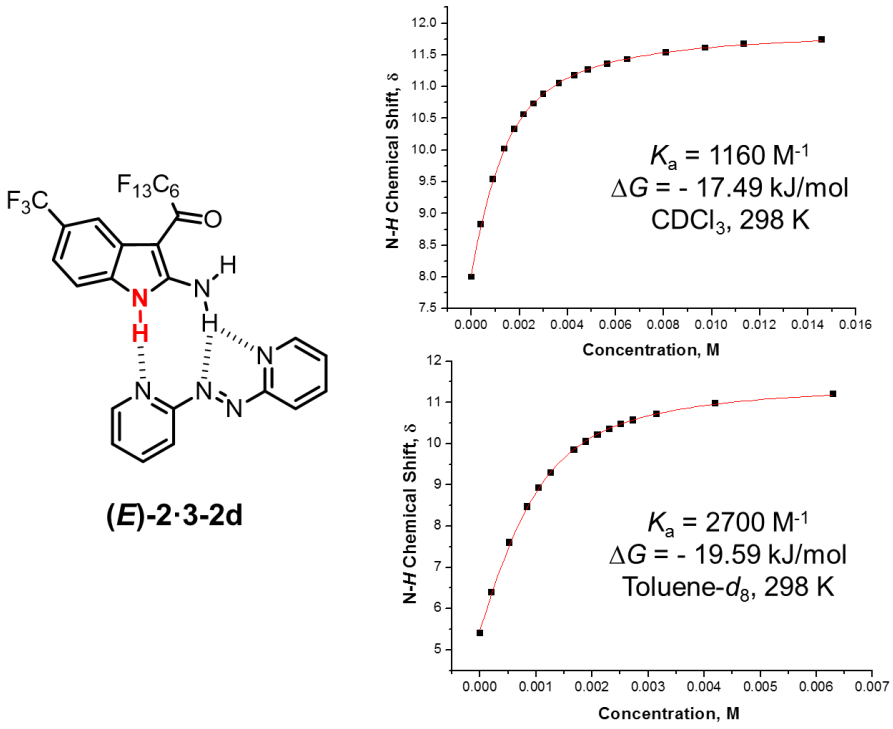

Figure 3.19 Indole N-*H* ^{1}H NMR titration data and calculated binding isotherms for complex formation between **3-2d** and **(*E*)-2**. K_a, calculated free energy of complexation, and titration conditions are noted below their respected curves. Schematic of complex is depicted at left.

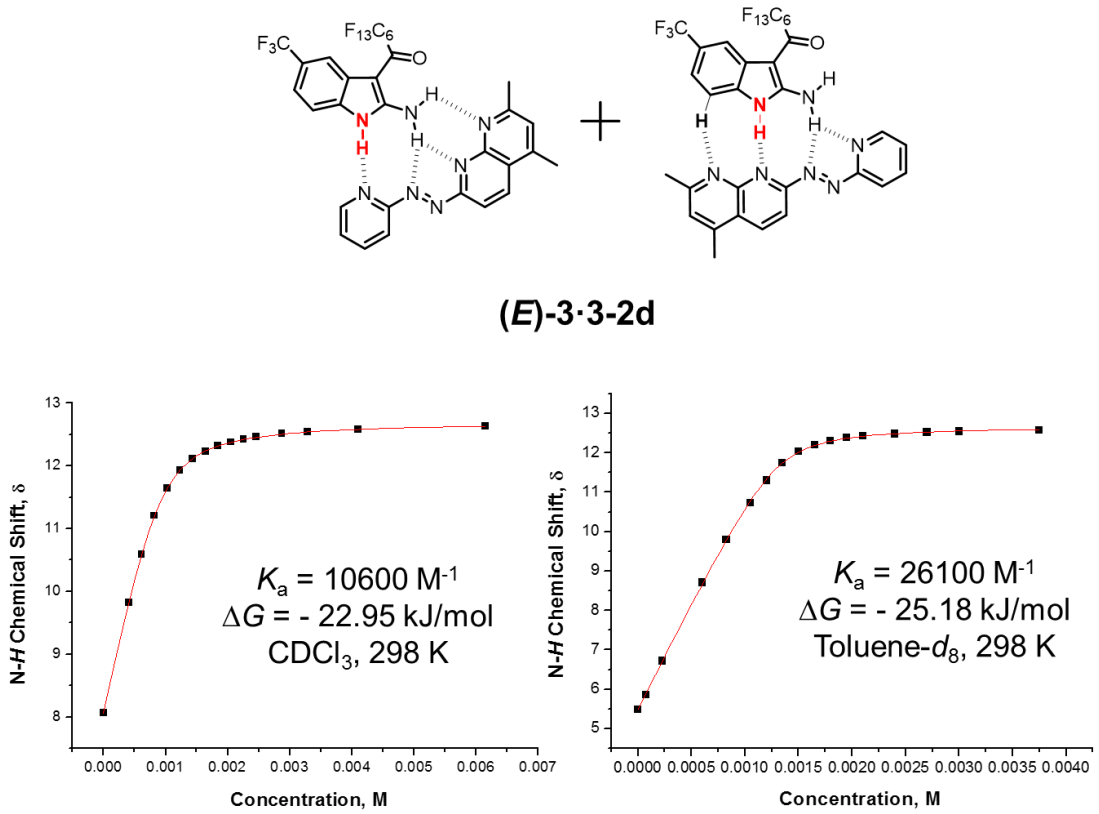

Figure 3.20 Indole N-*H* ^{1}H NMR titration data and calculated binding isotherms for complex formation between **2-2d** and **(*E*)-3**. K_a, calculated free energy of complexation, and titration conditions are noted below their respected curves. Schematic of possible complex geometries is depicted above titration curves.

Table 3.3 Association constants (K_a) of indole **3-2d** with **(*E*)-2** and **(*E*)-3**, free energies of complexation (ΔG), calculated chemical shifts of free indole, fully complexed indole and total change in chemical shift (δ_{free}, δ_{bound}, and $\Delta\delta_{max}$ respectively) in $CDCl_3$ and toluene-d_8 at 298 K.

Solvent	Acceptor	K_a (M^{-1})[a]	ΔG (kJ mol^{-1})[a]	δ_{free} (ppm) N***H***[a] NH_2[b]	δ_{bound} (ppm) N***H***[a] NH_2[b]	$\Delta\delta_{max}$ (ppm) N***H*** NH_2
$CDCl_3$	**(*E*)-2**	1160 ± 31	-17.49 ± 0.07	8.03 7.12	11.96 8.64	3.93 1.52
	(*E*)-3	10600 ± 1000	-22.95 ± 0.24	8.06 7.12	12.72 9.18	4.66 2.06
Toluene-d_8	**(*E*)-2**	2700 ± 129	-19.59 ± 0.12	5.47 5.87	11.59 8.72	6.12 2.85
	(*E*)-3	26100 ± 7900	-25.18 ± 0.72	5.50 5.87	12.71 9.45	7.21 3.58

[a] Average values calculated from Eq. 6 (chapter 2) using a 1:1 regression model and the indole N*H* data. All titrations were performed in triplicate and errors are reported as twice the standard deviation to provide a 95% confidence level. [b]Same procedure using NH_2 data.

The titration of **3-2d** with **(*E*)-2** in $CDCl_3$ resulted in the same association constant as **3-8b** (~ 1100 M^{-1}). Although **3-8b** was not soluble in toluene-d_8, **3-2d** with the longer fluorinated chain was able to be measured in toluene-d_8. A gain of 2.1 kJ/mol is observed comparing $CDCl_3$ to toluene-d_8 which is similar to the results with **3-21b** in section 3.4.4, Table 3.2. The same gain in free energy is demonstrated in complexation with **(*E*)-3** (-22.95 kJ/mol in $CDCl_3$, -25.18 kJ/mol in toluene-d_8). **3-2d** in toluene-d_8 is the first case where the amino protons in the free donor initially resonate downfield from the pyrrole proton. This observation may be attributed to the intramolecular hydrogen bonding interaction between the perfluoroacyl carbonyl and the amino proton. Since toluene-d_8 is

a less competitive solvent, this intramolecular hydrogen bonding pair is stronger and more pronounced than in $CDCl_3$. Nonetheless, the highest association constant for an indole incorporating only two electron withdrawing groups (3- and 5- positions) was achieved in this study in toluene-d_8 with the **(*E*)-3** acceptor array.

Titrations for **3-2e** were performed in CD_2Cl_2 as solubility in $CDCl_3$ was minimal. **3-2e** was also soluble in toluene-d_8 so titrations with **(*E*)-2** and **(*E*)-3** were performed in these two solvents. The titration data for **(*E*)-2·3-2e** and **(*E*)-3·3-2e** are displayed in Figures 3.21 and 3.22, respectively. A more detailed examination of these results are listed in Table 3.4.

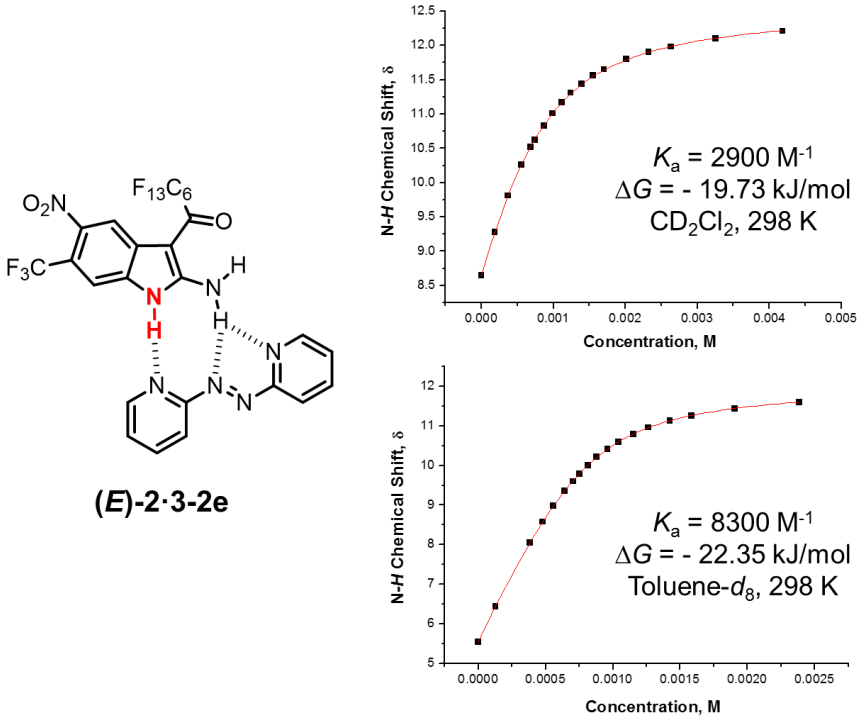

Figure 3.21 Indole N-*H* ^{1}H NMR titration data and calculated binding isotherms for complex formation between **3-2e** and **(*E*)-2**. K_a, calculated free energy of complexation, and titration conditions are noted below their respected curves. Schematic of complex is depicted at left.

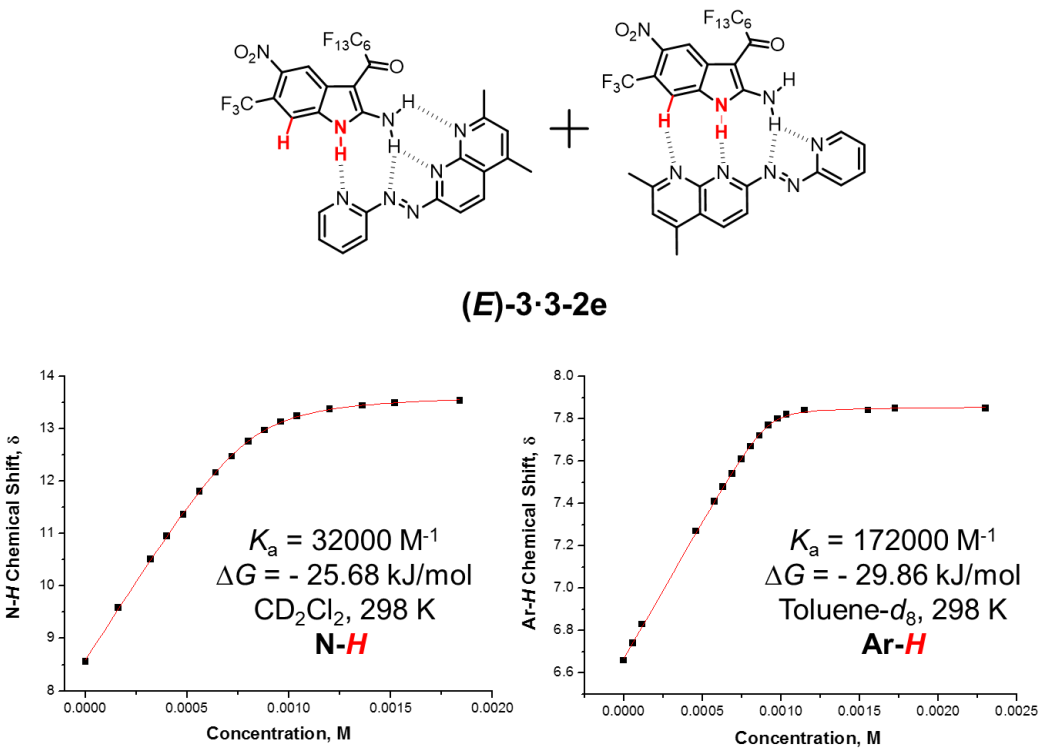

Figure 3.22 Left: Indole N-*H* ^{1}H NMR titration data and calculated binding isotherm for complex formation between **2-2e** and **(*E*)-3**. Right: Indole Ar-*H* ^{1}H NMR titration data and calculated binding isotherm for complex formation between **2-2e** and **(*E*)-3.** K_a, calculated free energy of complexation, and titration conditions are noted below their respected curves. Schematic of possible complex geometries are depicted above titration curves.

Table 3.4 Association constants (K_a) of indole **2-2e** with **(*E*)-2** and **(*E*)-3**, free energies of complexation (ΔG), calculated chemical shifts of free indole, fully complexed indole and total change in chemical shift (δ_{free}, δ_{bound}, and $\Delta\delta_{max}$ respectively) in CD_2Cl_2 and toluene-d_8 at 298 K.

Solvent	Acceptor	K_a (M^{-1})[a]	ΔG (kJ mol^{-1})[a]	δ_{free} (ppm) N*H*[a] NH_2[b]	δ_{bound} (ppm) N*H*[a] NH_2[b]	$\Delta\delta_{max}$ (ppm) N*H* NH_2
CD_2Cl_2	**(*E*)-2**	2900 ± 189	-19.73 ± 0.16	8.67 7.28	12.57 8.98	3.90 1.70
	(*E*)-3	32000 ± 2000	-25.68 ± 0.16	8.60 7.28	13.70 9.40	5.10 2.12
Toluene-d_8	**(*E*)-2**	8300 ± 425	-22.35 ± 0.13	5.52 5.81	12.06 8.94	6.54 3.13
	(*E*)-3	172000 ± 22800	-29.86 ± 0.32	5.51* 5.79*	13.09* 9.20*	7.58 3.71

[a]Average values calculated from Eq. 6 (chapter 2) using a 1:1 regression model and the indole N*H* data. All titrations were performed in triplicate and errors are reported as twice the standard deviation to provide a 95% confidence level. [b]Same procedure using NH_2 data. * Taken directly from the ^{1}H NMR spectra as data could not be plotted using Origin® software.

The titration results demonstrate that indole **2-2e** has the strongest binding observed yet to our acceptor arrays. Titrations of **2-2e** with **(*E*)-2** yielded a value of 2900 M^{-1} and 8300 M^{-1} in CD_2Cl_2 and toluene-d_8, respectively. This gain of 2.60 kJ/mol in free energy is comparable to similar comparisons performed in $CDCl_3$. The **(*E*)-3** titration in CD_2Cl_2 resulted in a value of 32000 M^{-1} which is 2.7 kJ/mol greater than **3-2d** in $CDCl_3$. The highest association constant arose from **3-2e** with **(*E*)-3** in toluene-d_8. This value of 1.7 x 10^5 M^{-1} equates to -29.86 kJ/mol in complexation free energy which is a gain of 7.5 kJ/mol when compared to **(*E*)-2**. The NH and NH_2 shifts were unable to be

used for data calculations because during the titration, both resonances broaden out into the baseline at various titrant concentrations (Figure 3.23). As previously observed in the **3-21b** titration, the C7-H proton also shifts downfield with the addition of **(*E*)-3**. Therefore, C7-H was monitored during this titration and used to calculate the K_a value.

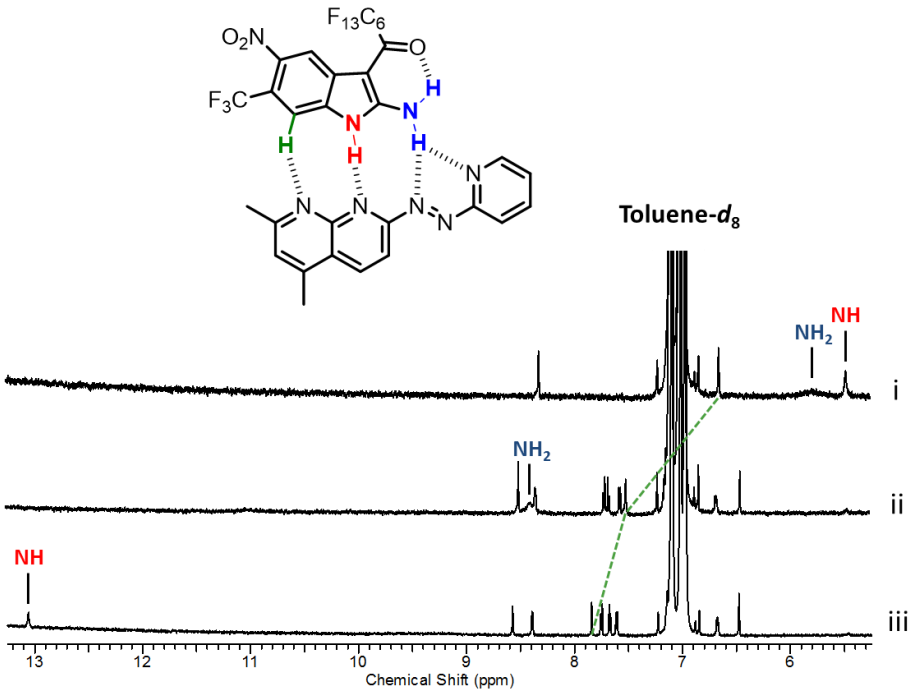

Figure 3.23 Stacked plot of complex **3-23·(*E*)-3** titration in toluene-d_8 at 298K. NH resonances are labeled in red, NH_2 resonances are labeled in blue, green lines correspond to the Ar-*H* shifts. i) [**(*E*)-3**]: 0 M, ii) [**(*E*)-3**]: 7.50 x 10^{-4} M, iii) [**(*E*)-3**]: 1.50 x 10^{-3} M.

3.4.6 Solid State Studies

Indoles **3-8b**, **3-9b**, **3-14b**, and **3-18b** were set up to co-crystallize with **(*E*)-2**. Evaporation of solutions with **3-8b** ($CHCl_3$) and **3-14b** (CH_2Cl_2) resulted in dark red to violet crystals suitable for x-ray analysis. **(*E*)-2·3-8b** consists of 8 molecules per unit cell

arranged as 4 pairs of complexes in a monoclinic space group $P2_1/c$. **(*E*)-2·3-14b** formed a triclinic unit cell in space group P-1. This cell contains a center of inversion consisting of two hydrogen bonded complexes and two DCM molecules within the crystal lattice.

The same hydrogen bonding motif is observed in both crystal systems as discussed in the previous chapter (Figure 3.24). **(*E*)-2·3-8b** and **(*E*)-2·3-14b** contain the shortest N-H···N3 distances of all structures characterized thus far (N1-H1···N3 = 2.88 Å, N1-H1···N3 = 2.00 Å, N1-H1···N3 = 2.88 Å, N1-H1···N3 = 2.03 Å, respectively). Additionally, the angles of these binding pairs are the closest value to the optimum 180° of all **(*E*)-2** complex structures obtained ((**(*E*)-2·3-8b**: N1-H1···N3 = 176°, **(*E*)-2·3-14b**: N1-H1···N3 = 172°). The amino proton forms two hydrogen bonds with the azo and pyridyl nitrogen atoms with bond lengths and angles comparable to previous structures (**(*E*)-2·3-8b**: N2-H2A···N4 = 3.16 Å, N2-H2A···N4 = 2.33 Å, N2-H2A···N4 = 163°, N2-H2A···N6 = 2.94 Å, N2-H2A···N6 = 2.33 Å, N2-H2A···N6 = 128°, **(*E*)-2·3-14b**: N2-H2A···N4 = 3.27 Å, N2-H2A···N4 = 2.46 Å, N2-H2A···N4 = 157°, N2-H2A···N6 = 2.98 Å, N2-H2A···N6 = 2.31 Å, N2-H2A···N6 = 135°). Since both **3-8b** and **3-14b** contain carbonyl groups at the 3-position, the

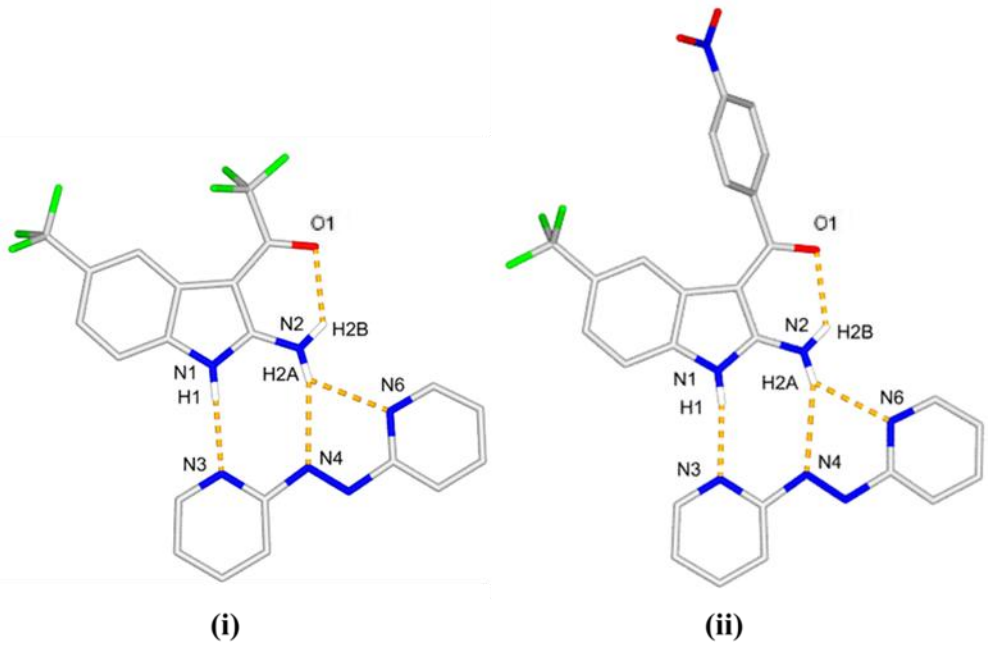

Figure 3.24 Stick representations of complexes **3-8b·(*E*)-2** (i) and **3-14b·(*E*)-2** (ii). All hydrogen bonds of interest are shown as dashed orange lines. C-H protons have been removed for clarity.

non-complexed amino hydrogen atom hydrogen bonds to that carbonyl oxygen atom analogously to the ethyl ester derivatives (**(*E*)-2·3-8b**: N2-H2B···O1 = 2.73 Å, N2-H2B···O1 = 2.06 Å, N2-H2B···O1 = 130°, **(*E*)-2·3-14b**: N2-H2B···O1 = 2.72 Å, N2-H2B···O1 = 2.08 Å, N2-H2B···O1 = 129°).

Both complexes resulted in the same co-planar arrangement as expected. The pyridyl rings least squares planes in the s-*cis*, s-*trans* conformation of **(*E*)-2** take up angles in relation to each other of 3.7° and 7.2° for **(*E*)-2·3-8b** and **(*E*)-2·3-14b**, respectively. The least squares planes of **(*E*)-2** (no atom > ± 0.066 Å from plane) and **3-8b** (excluding 3- and 5- substituents, no atom > ± 0.022 Å from plane) form an angle of 5.0° with each other. Complex **(*E*)-2·3-16b** resulted in a smaller angle between these

least squares planes of 3.7^{o} (**3-14b**: excluding 3- and 5- substituents, no atom > ± 0.062 Å from plane, **(*E*)-2**: no atom > 0.20 Å from plane).

Table 3.5 Crystallographic Data of crystals **(*E*)-2·3-8b** and **(*E*)-2·3-14b**.

Crystal Parameters	**(*E*)-2·3-8b**	**(*E*)-2·3-14b**
Chemical Formula	$C_{21}H_{14}F_6N_6O$	$C_{27}H_{20}Cl_2F_3N_7O3$
Formula Weight	480.38	618.40
Crystal System	Monoclinic	Triclinic
Space Group	P-2_1/c	P-1
***a* (Å)**	7.4759(11)	9.0811(15)
***b* (Å)**	13.268(3)	12.042(2)
***c* (Å)**	20.343(3)	13.866(2)
***α, β, γ* (°)**	90, 95.841(7), 90	68.187(6), 85.137(5), 73.185(5)
***V* (Å)^3**	2007.7(6)	1347.1(4)
***T* (K)**	110	110
Z	4	2
λ (Cu Kα) (Å)	1.54178	1.54178
D_{calc} (mg/cm^3)	1.590	1.525
μ (mm^{-1})	1.241	2.752
***F* (000)**	976	632
Total Reflections	20524	24249
Unique Reflections	3520	4553
Absorption	Multi-scan	Multi-scan
refinement on	F^2	F^2
$R(F_0)$(I>2σ (I))	0.0333	0.0389
$Rw(F_0^2)$(I>2σ (I))	0.0835	0.0954
$R(F_0)$ (all data)	0.0393	0.0517
$Rw(F_0^2)$ (all data)	0.0865	0.1022
GOF on F^2	1.039	1.040

Table 3.6 Crystallographic data of crystals **(*E*)-2·3.21b**, **(*E*)-3·2-5f**, and **(*E*)-4·2-3b**.

Crystal Parameters	**(*E*)-2·3.21b**	**(*E*)-3·2-5f**	**(*E*)-4·2-3b**
Chemical Formula	$C_{28}H_{30}F_3N_7O_{24}$	$C_{30}H_{32}N_8O_2S$	$C_{25}H_{28}FN_9O_3$
Formula Weight	585.59	568.69	521.56
Crystal System	Triclinic	Triclinic	Triclinic
Space Group	P-1	P-1	P-1
***a* (Å)**	5.448(2)	7.2867(11)	10.687(3)
***b* (Å)**	11.020(3)	9.8060(16)	10.810(3)
***c* (Å)**	24.109(6)	19.745(3)	12.253(4)
***α, β, γ* (°)**	92.282(10), 90.238(11), 99.051(9)	88.190(5), 87.984(5), 84.259(7)	66.478(8), 72.71(3), 83.826(13)
***V* (Å)^3**	1428.1(7)	1402.4(4)	1239.1(7)
***T* (K)**	243	173	110
Z	2	2	2
***λ* (Mo K*α*) (Å)**	0.71073	1.54178 (Cu Kα)	0.71073
***D*$_{calc}$ (mg/cm^3)**	1.362	1.347	1.398
***μ* (mm^{-1})**	0.107	1.381	0.102
***F* (000)**	612	600	548
Total Reflections	26446	16424	19648
Unique Reflections	5902	4825	5908
Absorption	Multi-scan	Multi-scan	Multi-scan
refinement on	F^2	F^2	F^2
***R*(F_0)(*I*>2σ (*I*))**	0.0524	0.0434	0.0471
***R*w(F_0^2)(*I*>2σ (*I*))**	0.1295	0.0556	0.0947
***R*(F_0) (all data)**	0.0899	0.1134	0.0938
***R*w(F_0^2) (all data)**	0.1532	0.1281	0.1136
GOF on F^2	1.024	1.053	1.002

Acceptors **(*E*)-2**, **-3**, and **-4** were each set up to co-crystallize with **3-21b**. Only **(*E*)-2·3-21b** provided dark red crystals suitable for X-ray analysis which developed from slow diffusion of DIPE into a 1:1 solution in $CHCl_3$. These crystals formed a triclinic lattice in space group P-1 containing 4 molecules. The same hydrogen bonding motif is observed between the donor and acceptor (Figure 3.25) and bond lengths and angles of interest are listed in Table 3.7.

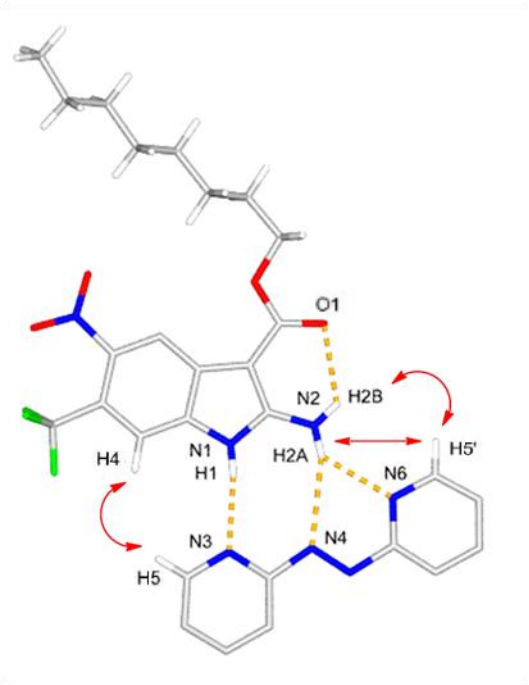

Figure 3.25 Stick representation of complex **(*E*)-2·3-21b**. All hydrogen bonds of interest as shown as dashed orange lines. NOESY interactions are shown as red arrows; aryl protons without NOESY interactions have been omitted for clarity.

Table 3.7 Bond length and bond angles of hydrogen bonds of interest from crystal **(*E*)-2·3.21b**.

Bond Lengths (Å)				Bond Angles (°)	
N1-H1···N3	3.00	N2-H2A···N6	2.96	N1-H1···N3	171
N1-H1···N3	2.14	N2-H2A···N6	2.29	N2-H2A···N4	160
N2-H2A···N4	3.40	N2-H2B···O1	2.84	N2-H2A···N6	134
N2-H2A···N4	2.56	N2-H2B···O1	2.26	N2-H2B···O1	124
H4···H5	2.59	H2A···H5'	3.17		
		H2B···H5'	2.92		

All hydrogen bond lengths and angles listed are similar to structures already analyzed. The distance between the pyridyl *ortho* proton H5 and the aryl hydrogen H4 of **3-21b** is 2.59 Å. The *ortho* proton H5' and amino hydrogens measure 3.17 Å (H2A) and 2.92 Å (H2B). These short distances in the solid state support the presence of correlations observed in the 2D ^{1}H spectrum collected in toluene-d_8 (Section 3.4.4, Figure 3.15). Once again, these NOESY interactions are made possible by the co-planar hydrogen bonding motif. **(*E*)-2** in the s-*cis*, s-*trans* conformation has the pyridyl rings least squares planes at an angle of 4.3° with no **(*E*)-2** atom being > ± 0.073 Å from the plane. The two arrays are angled by their least squares planes at 6.4° (no atom in **3-21b** > ± 0.075 Å from plane; excluding 3-, 5-, and 6- substituents) which is similar for all complexes thus far in the solid state.

Similar to **(*E*)-2**, array **(*E*)-3** had a high affinity for self-crystallization when subjected to co-crystallization techniques with 2-aminoindoles. Luckily, **(*E*)-3** was successfully co-crystallized with 5-hexylsulphonyl-1*H*-2-aminoindole-3-carbonitrile (**2-5f** from Chapter 2) by slow evaporation of a DCM solution containing a 1:1 mixture of arrays. These violet crystals formed a triclinic unit cell in space group P-1. Each unit

cell contains a center of inversion with 2 hydrogen bonded complexes. The complex geometry observed here is not our initially predicted structure but a geometry implied by the collected 2D ^{1}H NOESY spectra of **(*E*)-3·3-21b** (Figure 3.26). Hydrogen bond lengths are analogous to **(*E*)-2** complexes (N1-H1···N4 = 3.01 Å, N1-H1···N4 = 2.16 Å, N2-H2A···N5 = 3.21 Å, N2-H2A···N5 = 2.37 Å, N2-H2A···N7 = 2.96 Å, N2-H2A···N7 = 2.41 Å). Additionally, similar bond angles are present which show no deviation from previous

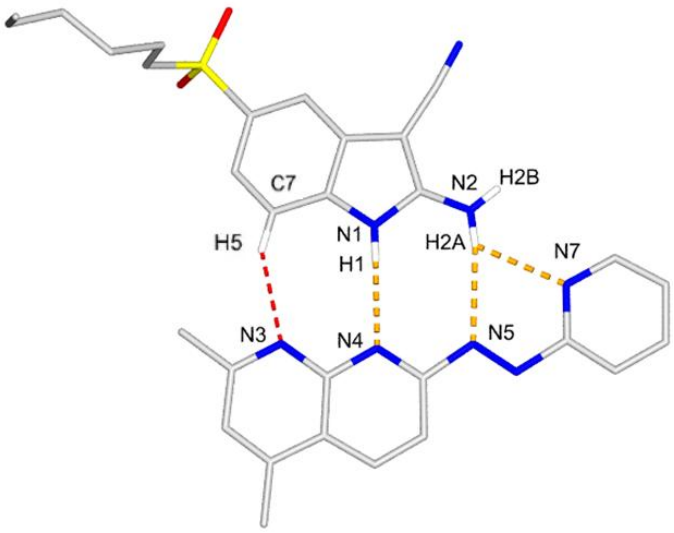

Figure 3.26 Stick representations of complex **(*E*)-3·2-5f**. All N-H···N hydrogen bonds of are shown as dashed orange lines, 7C-H5···N3 shown in red. All protons not participating in hydrogen bonding have been removed for clarity.

structures (N1-H1···N4 = 179^{o}, N2-H2A···N5 = 171^{o}, N1-H2A···N7 = 123^{o}). Unforeseen in all previous structures, the aryl proton on **2-5f** forms a hydrogen bond with one of the naphthyridine rings (shown in red). The C7···N3 distance was measured to be 3.33 Å (C7-H5···N3 = 147^{o}) which is close to the sum of the VDW radii for a C-H···N hydrogen bond (3.25 Å).[26]

The s-*cis*, s-*trans* conformations of the naphthyridine and pyridine rings are at an angle of 1.5^{o} using their least squares planes with the least squares plane of **(*E*)-3** being ± 0.065 Å. This AAA array allows for the additional C-N hydrogen bond to occur with the angle of their least squares planes of the two arrays being 7.5^{o}. The same N-H···NC hydrogen bonded indole dimers are observed in this structure (Figure 3.27) as discussed in Chapter 2. The dimerization may influence the selection of this complex geometry with **(*E*)-3** in the solid state due to potential steric interactions between the napthyridyl methyl group and opposing indole CN group in the competing complex geometry (see Figure 3.16 (i)).

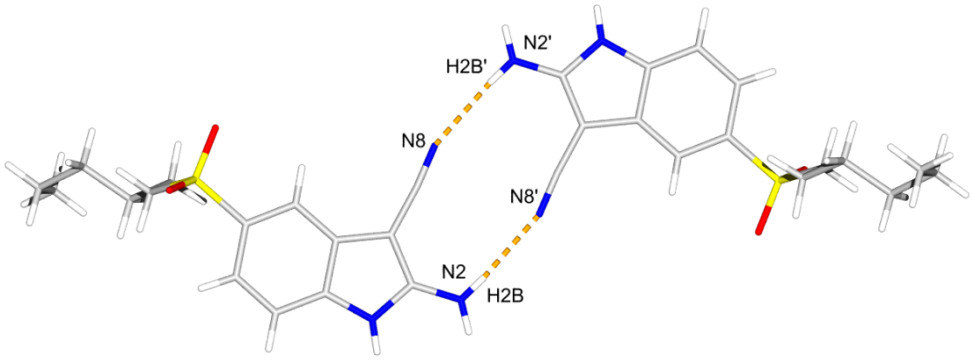

Figure 3.27 Stick representation of the **1-5f·1-5f** hydrogen bonded dimer in complex **(*E*)-3·1-5f**. N2-H2B···N8' = N2'-H2B'···N8 = 3.03 Å, N2-H2B···N8' = N2'-H2B'···N8 = 171^{o}.

(*E*)-4 was successfully co-crystallized with ethyl-5-fluoro-1*H*-2-aminoindole-3-carboxylate (**2-3b** from Chapter 2) by slow evaporation of a DCM solution containing a 1:1 mixture of the arrays. The resulting triclinic unit cell has a center of inversion containing two indole and **(*E*)-4** arrays in space group P-1. The arrays crystallized in the complex geometry we initially predicted where the alkoxide is binding to the second

amino proton (Figure 3.28). All hydrogen bonds and angles analogous to similar **(*E*)-2** structures are listed in Table 3.8.

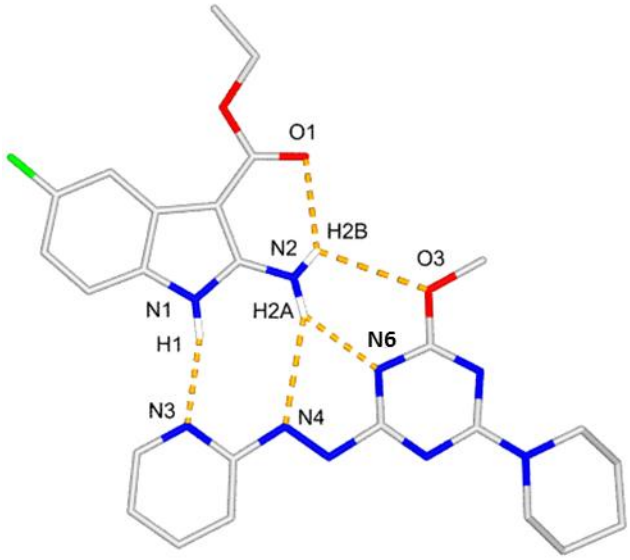

Figure 3.28 Stick representations of complex **(*E*)-4·2-3b**. All hydrogen bonds are shown as dashed orange lines. All protons not participating in hydrogen bonding have been removed for clarity.

Table 3.8 Bond length and bond angles of hydrogen bonds of interest from crystal **(*E*)-4·2-3b**.

Bond Lengths (Å)				Bond Angles (°)	
N1-H1···N3	2.97	N2-H2A···N6	2.94	N1-H1···N3	164
N1-H1···N3	2.11	N2-H2A···N6	2.16	N2-H2A···N4	152
N2-H2A···N4	3.49	N2-H2B···O1	2.85	N2-H2A···N6	141
N2-H2A···N4	2.65	N2-H2B···O1	2.24	N2-H2B···O1	130

The bond lengths and angles listed above are comparable to analogous **(*E*)-2** complexes with the exception of the additional hydrogen bond formed with the alkoxide. This N2-H2B···O3 bond length measures 3.23 Å (N2-H2B···O3 = 2.82 Å) which is within range of the combined VDW radii definition for a N···O hydrogen bond (2.95

Å).[26] The angle of N2-H2B···O3 measures 112° which is acute for being a strong hydrogen bonding interaction. This bond therefore by definition would be considered weak and this **(*E*)-4** conformation in the solid state may be preferred for packing purposes.

The structure contains the greatest deviation from planarity from all complexes collected. The s-*trans*, s-*cis* least squares planes of the pyridine and triazine core are at an angle of 18.2°. **(*E*)-4**'s least squares plane being is ± 0.384 Å which excludes the piperidine and methoxide substituents. The indoles least squares plane is ± 0.049 Å which excludes the 3- and 5- substituents. The two arrays form an angle of 13.6°.

3.5 Summary and Conclusions

This chapter explored effective modifications to our initial contiguous arrays which were successful at increasing hydrogen bonding strength. A series of new 3-substituted-2-aminoindoles were synthesized with only four being soluble in $CDCl_3$. Their association constants were determined with 2,2'-azopyridine with unexpected results. Having an electron rich carbonyl substituent in the 3-position resulted in a depressed association constant, regardless of theoretical withdrawing effect of the group. Two crystal structures were obtained with **(*E*)-2** which formed solid state structures analogous to complexes from the previous chapter.

Octyl 5-nitro, 6-trifluoromethyl-1*H*-2-aminoindole-3-carboxylate (**3-21b**) was synthesized for complexation in toluene-d_8. Two new azo-containing acceptor arrays were also synthesized with an additional nitrogen (**(*E*)-3**) or oxygen (**(*E*)-4**) acceptor

capable of forming an additional binding pair. **3-21b** was titrated with all three acceptor arrays in both $CDCl_3$ and toluene-d_8. For both **(*E*)-2** and **(*E*)-3**, a change from $CDCl_3$ to toluene-d_8 resulted in an increase of 2.4 - 2.7 kJ/mol in the free energy of complexation. In the same titration solvent, an increase of 6.1 and 6.4 kJ/mol in free energy was determined when comparing **(*E*)-2** to **(*E*)-3**, in $CDCl_3$ and toluene-d_8 respectively. **(*E*)-4** resulted in lower association constants than expected. We attribute this to the fact that the methyl group is undertaking free rotation and therefore causes repulsive steric interactions with **3-21b**. The crystal structure obtained of **(*E*)-3** displayed a complex geometry in the solid state where the extra fused pyridine ring forms a C-H hydrogen bond with the indole array. This matches the ^{1}H NMR titration data where ~ 1 ppm shift was seen for that aryl proton in the bound form. The crystal structure obtained of **(*E*)-4** exhibited our predicted complex geometry where the oxygen is creating a weak hydrogen bond with the second amino proton. Lengths and angles of the primary hydrogen bonds matched with similar **(*E*)-2** structures.

Lastly, two indoles with a perfluoroacyl group in the 3-position were synthesized and titrations were performed in $CDCl_3/CD_2Cl_2$ and toluene-d_8. 5-Nitro-6-trifluoromethyl-3-perfluoroacyl-1*H*-2-aminoindole (**3-2e**) provided the strongest complexes. The strongest association constant measured was **(*E*)-3·3-2e** in toluene-d_8 which was 1.7 x 10^5 M^{-1}, or nearly 30 kJ/mol in complexation free energy.

The next chapter will examine the photoswitchability of our hydrogen bonding system. Association constants will be determined for the (*Z*)-isomers of our arrays and compared to the known association constants of the (*E*)-isomers. The reversibility of our system will also be examined with solution state fatigue resistance experiments.

3.6 Experimental Methodology

3.6.1 General Information

Chemicals were purchased from Sigma Aldrich, Alfa Aesar or Oakwood Products Inc. and used as received. All non-deuterated solvents for reaction purposes were dried (if needed) using an Innovative Technology Inc. Solvent Purification System SPS-400-5. $CDCl_3$, DMSO-d_6, and Toluene-d_8 were purchased from Cambridge Isotope Laboratories or Sigma Aldrich and dried (chloroform and toluene) over 4Å molecular sieves before use. α,α,α-Trifluorotoluene (^{19}F NMR standard, $C_7H_5F_3$) was purchased from Sigma and used as received as an internal standard if mentioned in the molecular characterization data. ^{1}H ,^{13}C and ^{19}F NMR spectra were collected @ 298 K on a Varian Mercury 400 MHz or a Bruker AvanceIII HD 400 MHz spectrometer (operating at 400.08, 100.61 and 376.42 MHz respectively) and the Inova 600 MHz spectrometer (599.37 and 150.72 MHz respectively). ^{1}H NMR titrations were performed on a Varian Inova 600 MHz spectrometer. Spectra are reported with residual solvent peak as reference from TMS.[27] Chromatography was performed using Silicycle 40-63 μm silica gel-60 (R10030B). EI mass spectra were obtained on a Finnigan MAT 8400 mass spectrometer. X-Ray diffraction data were collected on Bruker Apex II and Nonius Kappa CCD X-Ray diffractometers using graphite monochromatic Mo-Kα radiation (γ = 0.71073 Å) and Cu-Kα radiation (γ = 1.54178 Å), respectively.

3.6.2 Titration Procedure

A stock solution of Indole was prepared in dry $CHCl_3$ (CH_2Cl_2 was used for **3-2d**) to the desired concentration (from 1.0 x 10^{-3} M to 0.25 x 10^{-4} M) and 0.5 mL was

transferred into an NMR tube and 4 mL in a small vial and placed under vacuum in a dessicator to remove solvents. $CDCl_3$, CD_2Cl_2, or toluene-d_8 (0.5 mL) was added to the NMR tube and a ^{1}H NMR spectrum was recorded. An accurately weighed amount of guest array was added to the vial prepared along with 4 mL of $CDCl_3$, CD_2Cl_2, or toluene-d_8 to produce a guest solution of 30 – 50 times the host concentration (10 times for **(*E*)-3** in toluene-d_8). As a precaution, the vial was wrapped with black tape to exclude light. Aliquots of guest solution were added successively to the NMR tube containing the host solution, the tube was shaken after each addition and the ^{1}H spectrum was recorded. The chemical shifts of the NH and NH_2 protons (or C7-H if needed) from the hydrogen bond donors in each sample were recorded and fit satisfactorily to a 1:1 binding model (J.A.C.S., **2000**, *122*, 8856) using Origin® data analysis software.

3.6.3 Synthetic Methods

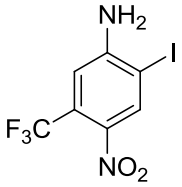

Synthesis of 3-1a: 4-Nitro-5-(trifluoromethyl)aniline (5.00 g, 24.3 mmol) was dissolved in a 1:1 mixture of THF:MeOH (80 mL). p-TsOH·H_2O (23.1 mg, 1.22 mmol) was added followed by *N*-iodosuccinimide (6.00 g, 26.7 mmol) in portionwise additions over a period of 30 minutes. The mixture was allowed to stir overnight at room temperature and then poured into 10% $Na_2S_2O_{5(aq)}$ (200 mL). The solid was vacuum filtered and rinsed with water. A yellow powder was isolated in 82% yield and was pure enough to continue to the next step. 100 mg were purified by flash chromatography using Hexanes/EtOAc (3/2) as eluent for analytical characterization. **^{1}H NMR** (400 MHz, $CDCl_3$): δ (ppm) 8.44 (s, 1H), 7.01, (s, 1H), 4.93 (s, br, 2H). **^{13}C NMR** (100 MHz, DMSO-d_6): δ (ppm) 154.3, 138.1, 134.3, 124.3 (q, *J* =

32.5 Hz), 122.4 (q, *J* = 272.7 Hz), 110.8 (q, *J* = 6.5 Hz). **^{19}F NMR** (376 MHz, DMSO-d_6, $C_7H_5F_3$): δ (ppm) - 61.6. **HRMS (EI):** calc. for $C_7H_4F_3IN_2O_2$ $[M]^+$ 331.9270; found 331.9260.

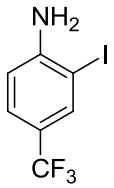

Synthesis of 3-1b: 4-(Trifluoromethyl)aniline (5.00 g, 17.4 mmol) and $TsOH{\cdot}H_2O$ (5 mol% , 165 mg, 0.87 mmol) were dissolved in MeOH:THF (100 mL, 1:1) and placed in an ice/water bath. With stirring, *N*-iodosuccinimide (4.12 g, 18.3 mmol) was added portionwise as a solid over 30 minutes. The mixture was left to stir overnight and saturated $Na_2S_2O_{3aq}$ (10 mL) was added to decolorize excess iodine. The flask contents were transferred to a separatory funnel, extra water was added and extracted twice with DCM. The organic layers were combined, washed three times with water, once with brine and dried with Na_2SO_4 and filtered. The solvent was removed under reduced pressure and the crude oil was purified using flash chromatography using DCM/Hexanes (1/4) as eluent. A colorless oil was isolated in 91 % yield which crystallized upon cooling. **m.p.** 51-52 °C. **^{1}H NMR** (400 MHz, $CDCl_3$): δ (ppm) 7.87 (d, *J* = 1.2 Hz, 1H), 7.38 (dd, *J* = 8.4 Hz, 1.6 Hz, 1H), 6.74 (dd, *J* = 8.4 Hz, 0.5 Hz, 1H), 4.41 (s, br, 2H). **^{13}C NMR** (100 MHz, $CDCl_3$): δ (ppm) 149.7, 136.3 (q, *J* = 4.0 Hz), 126.7 (q, *J* = 3.5 Hz), 123.7 (q, *J* = 271.0 Hz), 121.6 (q, *J* = 33.1 Hz), 113.6, 82.3. **^{19}F NMR** (376 MHz, $CDCl_3$): δ (ppm) -61.3. **HRMS (EI):** calc. for $C_7H_5F_3IN$ $[M]^+$ 286.9419; found 286.9425.

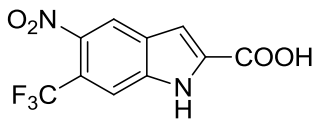

Synthesis of 3-2a: The indole was synthesized in the same manner as indole **3-2b** starting from aniline **3-1a**. Purification

was carried out with flash chromatography using EtOAc/Hexanes (2/3) with 3% AcOH as eluent and a pale yellow, amorphous solid was isolated in 72% yield. **^{1}H NMR** (600 MHz, DMSO-d_6): δ (ppm) 13.73 (s, br, 1H), 12.87 (s, br, 1H), 8.65 (s, 1H), 7.94 (s, 1H), 7.41 (s, 1H). **^{13}C NMR** (100 MHz, DMSO-d_6): δ (ppm) 161.8, 140.6, 136.6, 134.4, 127.6, 123.1 (q, J = 272.2 Hz), 121.6, 117.4 (q, J = 33.0 Hz), 112.8 (q, J = 6.1 Hz), 109.1. **^{19}F NMR** (376 MHz, DMSO-d_6): δ (ppm) -57.1. **HRMS (EI):** calc. $C_{10}H_5F_3N_2O_4$ $[M]^+$ 274.0201; found: 274.0209.

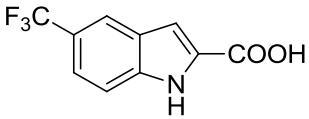

Synthesis of 3-2b: Following a literature procedure,[7a,b] aniline **3-1b** (3.00 g, 10.5 mmol), DABCO (3.52 g, 31.4 mmol), pyruvic Acid (2.22 mL, 31.4 mmol) and $Pd(OAc)_2$ (11.8 mg, 0.53 mmol) were loaded into a round bottom flask containing dry DMF (30 mL) under a dry N_2 atmosphere. An air condenser was attached and the contents were heated to 105 °C and stirred overnight. The flask was cooled to room temperature and poured into ice cold 0.5 M HCl and the solids were filtered off using vacuum and rinsed with water. The solids were adsorbed onto silica gel and purified using flash chromatography using EtOAc/Hexanes (3/7) with 3% AcOH as eluent. A white, amorphous solid was isolated in 75% yield. **^{1}H NMR** (600 MHz, DMSO-d_6): δ (ppm) 13.21 (s, br, 1H), 12.20 (s, br, 1H), 8.09 (s, 1H), 7.61 (d, J = 8.8 Hz, 1H), 7.52 (d, J = 8.8 Hz, 1H), 7.25 (s, 1H). **^{13}C NMR** (150 MHz, DMSO-d_6): δ (ppm) 162.5, 138.5, 130.7, 126.2, 125.3 (q, J = 271.8 Hz), 120.9 (q, J = 31.1 Hz), 120.4, 120.0, 113.5, 108.3. **^{19}F NMR** (376 MHz, DMSO-d_6): δ (ppm) -58.4. **HRMS (EI):** calc. $C_{10}H_6F_3NO_2$ $[M]^+$ 229.0351; found: 229.0355.

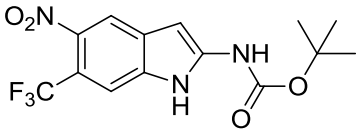

Synthesis of 3-3a: The indole was synthesized in the same manner as indole **3-3b** starting from indole **3-2a**. A pale yellow, amorphous solid was isolated in 65% yield. **^{1}H NMR** (600 MHz, DMSO-d_6): δ (ppm) 11.81 (s, br, 1H), 10.68 (s, br, 1H), 8.19 (s, 1H), 7.96 (s, 1H), 6.21 (s, 1H), 1.53 (s, 9H). **^{13}C NMR** (100 MHz, DMSO-d_6): δ (ppm) 152.2, 141.3, 140.8, 132.9, 129.1, 123.7 (q, J = 271.5 Hz), 116.2, 112.0 (q, J = 33.0 Hz), 110.7 (q, J = 6.1 Hz), 87.2, 80.8, 27.9. **^{19}F NMR** (376 MHz, $CDCl_3$): δ (ppm) -57.4. **HRMS (EI):** calc. $C_{14}H_{14}F_3N_3O_4$ $[M]^+$ 345.0936; found: 345.0924.

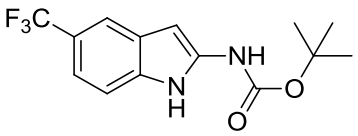

Synthesis of 3-3b: Indole **3-2b** (3.00 g, 13.1 mmol) was dissolved in dry dioxane (50 mL) under a dry N_2 atmosphere. Triethylamine (2.01 mL, 14.1 mmol) was then added and stirred for 15 minutes followed by DPPA (3.04 mL, 13.8 mmol). The flask was heated to 60 °C and stirred for 2 hours then allowed to cool to room temperature. The flask contents were poured into cold water and solids were vacuum filtered, rinsed with water and left on vacuum overnight. The next day, the white solids were transferred to a flask of ^{t}BuOH (50 mL) and refluxed with stirring for 6 hours. After cooling to room temperature, silica gel was added and ^{t}BuOH was removed under reduced pressure and subjected to flash chromatography using EtOAc/Hexanes (1/9) as eluent where a white, amorphous solid was isolated in 75% yield. **^{1}H NMR** (400 MHz, DMSO-d_6): δ (ppm) 11.17 (s, br, 1H), 10.26 (s, br, 1H), 7.68 (s, 1H), 7.53 (d, J = 8.6 Hz, 1H), 7.20 (dd, J = 8.6, 1.7 Hz, 1H), 6.03 (d, J = 1.7 Hz, 1H), 1.51 (s, 9H). **^{13}C NMR** (150 MHz, DMSO-d_6): δ (ppm) 152.4, 137.5, 134.6, 127.1, 125.8 (q, J = 271.8 Hz), 120.0 (q, J = 31.1 Hz), 115.3, 115.3, 111.5,

86.0, 80.1, 28.0. **^{19}F NMR** (376 MHz, $CDCl_3$): δ (ppm) -60.4. **HRMS (EI):** calc. $C_{14}H_{15}F_3N_2O_2$ $[M]^+$ 300.1086; found: 300.1078.

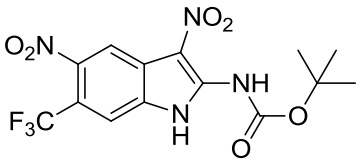

Synthesis of 3-4a: Acetic anhydride (15 mL) was added to a small RBF and placed in an ice/water bath. With stirring, 0.50 mL of conc. HNO_3 was added very slowly dropwise and stirring continued for an additional 10 minutes. Indole **3-3a** (1.00 g, 2.90 mmol) was added all at once as a solid and stirred for an hour in the ice/bath. The contents were poured into room temperature water with vigorous stirring and then vacuum filtered. The solids were purified via flash chromatography using a mixture of EtOAc and Hexanes as eluent and a pale yellow solid was isolated in 87% yield. **^{1}H NMR** (600 MHz, DMSO-d_6): δ (ppm) 13.15 (s, br, 1H), 10.18 (s, 1H), 8.57 (s, 1H), 8.14 (s, 1H), 1.59 (s, 9H). **^{13}C NMR** (150 MHz, DMSO-d_6): δ (ppm) 150.7, 143.3, 142.9, 131.6, 122.5 (q, J = 271.8 Hz), 121.3, 116.7 (q, J = 33.4 Hz), 115.9, 113.4, 112.5, 84.2, 27.6. **^{19}F NMR** (376 MHz, DMSO-d_6, $C_7H_5F_3$): δ (ppm) – 60.0. **HRMS (EI):** calc. $C_{14}H_{13}F_3N_4O_6$ $[M]^+$ 390.0787; found 390.0788.

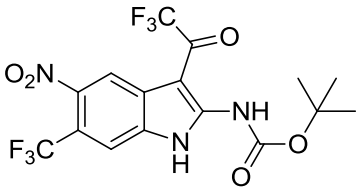

Synthesis of 3-5a: Indole **3-3a** (1.00 g, 2.90 mmol) was dissolved in dry THF (20 mL) under inert atmosphere and placed in an ice/water bath. With stirring, TFAA (0.44 mL, 3.19 mmol) was added dropwise and stirred overnight while cooling to room temperature. The solution was transferred to a separatory funnel containing water and extracted twice with EtOAc. The combined organic layers were washed twice with water

followed by brine, dried with Na_2SO_4 and filtered. The solvent was removed under reduced pressure and the crude solid was adsorbed onto silica gel and purified using flash column chromatography using a mixture of EtOAc and Hexanes where a white solid was isolated in 82% yield. **^{1}H NMR** (600 MHz, DMSO-d_6): δ (ppm) 13.32 (s, br, 1H), 10.49 (s, br, 1H), 8.23 (s, 1H), 8.20 (s, 1H), 1.58 (s, 9H). **^{13}C NMR** (150 MHz, CD_2Cl_2): δ (ppm) 175.1 (q, *J* = 38.4 Hz), 153.1, 152.9, 144.8, 133.7, 125.1 123.2 (q, *J* = 272.6 Hz), 119.0 (q, *J* = 34.6 Hz), 117.9 (q, *J* = 6.0 Hz), 117.4 (q, *J* = 287.6 Hz), 111.9 (q, *J* = 6.0 Hz), 95.8, 86.2, 28.3. **^{19}F NMR** (376 MHz, CD_2Cl_2): δ (ppm) -59.1, -75.8. **HRMS (EI):** calc. $C_{16}H_{13}F_6N_3O_5$ $[M]^+$ 441.0759; found: 441.0757.

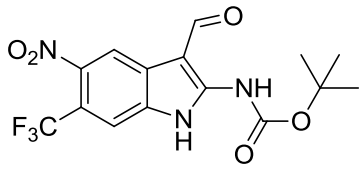

Synthesis of 3-6a: From a modified literature procedure,[11] dry DMF (15 mL) was cooled on an ice/water bath under inert atmosphere and benzoyl chloride (677 µL, 5.83 mmol) was added dropwise. The flask was allowed to stir for 15 minutes then the ice/water bath was removed and stirred for an additional 4 hours. Indole **3-3a** (1.45 g, 3.89 mmol) was added and contents were stirred overnight. Water (2 mL) was added and the flask was heated with a heat gun for 5 minutes or until dimethylamine fumes ceased. Once the flask reached room temperature, the contents were diluted with dichloromethane (100 mL) and transferred to a separatory funnel and washed twice with dilute $Na_2CO_{3(aq)}$, followed by water and brine. The organic layer was dried with Na_2SO_4, filtered and the solvent was removed under reduced pressure. The crude solid was adsorbed onto silica gel and purified using flash chromatography using a mixture of EtOAc and Hexanes and a yellow, amorphous solid was isolated in 65% yield. **^{1}H NMR**

(400 MHz, DMSO-d_6): δ (ppm) 12.68 (s, br, 1H), 11.34 (s, br, 1H), 10.16 (s, 1H), 8.64 (s, 1H), 8.09 (s, 1H), 1.58 (s, 9H). **^{13}C NMR** (150 MHz, DMSO-d_6): δ (ppm) 184.0, 151.9, 147.2, 142.5, 133.8, 126.1, 123.0 (q, J = 271.8 Hz), 116.4, 115.1 (q, J = 33.4 Hz), 111.7, 102.0, 82.7, 27.8. **^{19}F NMR** (376 MHz, DMSO-d_6, $C_7H_5F_3$): δ (ppm) -59.7. **HRMS (EI):** calc. $C_{15}H_{14}F_3N_3O_5$ $[M]^+$ 373.0886; found: 373.0880.

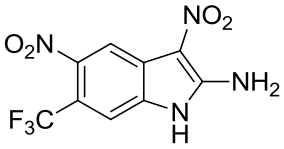

Synthesis of 3-7a: The indole was synthesized in the same manner as indole **3-8a** starting from indole **3-4a**. An orange, amorphous solid was isolated in 87% yield. **^{1}H NMR** (600 MHz, DMSO-d_6): δ (ppm) 11.77 (s, br, 1H), 8.63 (s, br, 2H), 8.38 (s, 1H), 7.71 (s, 1H). **^{13}C NMR** (100 MHz, DMSO-d_6): δ (ppm) 151.9, 142.5, 133.0, 123.6, 122.9 (q, J = 271.8 Hz), 115.9 (q, J = 33.1 Hz), 114.5, 110.5, 109.6 (q, J = 6.0 Hz). **^{19}F NMR** (376 MHz, DMSO-d_6): δ (ppm) -57.3. **HRMS (EI):** calc. $C_9H_5F_3N_4O_4$ $[M]^+$ 290.0263; found 290.0271.

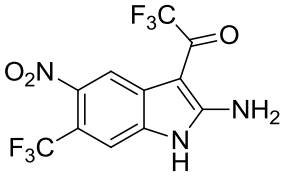

Synthesis of 3-8a: Indole **3-5a** (0.50 g, 1.47 mmol) was dissolved in dry Et_2O (10 mL) and $HBF_4{\cdot}Et_2O$ (0.50 mL, 50-55% w/w HBF_4) was added dropwise slowly. The deprotection was monitored by TLC and when the reaction was complete, the solvents were removed with a stream of air until dry. The solids were taken up in EtOAc (50 mL), washed three times with water then brine. The organic layer was dried with Na_2SO_4, filtered and the solvent removed under reduced pressure. The crude indole was purified by flash

chromatography using a mixture of EtOAc and Hexanes and an amorphous, tan solid was isolated in 93% yield. **^{1}H NMR** (600 MHz, DMSO-d_6): δ (ppm) 11.83 (s, br, 1H), 8.52 (s, br, 2H), 8.04 (s, 1H), 7.75 (s, 1H). **^{13}C NMR** (100 MHz, DMSO-d_6): δ (ppm) 171.2 (q, J = 35.4 Hz), 159.7, 142.0, 136.0, 125.9, 122.9 (q, J = 271.8 Hz), 117.3 (q, J = 288.4 Hz), 115.5 (q, J = 33.1 Hz), 114.8 (q, J = 6.0 Hz), 109.7 (q, J = 6.8 Hz), 92.1. **^{19}F NMR** (376 MHz, DMSO-d_6): δ (ppm) -57.5, -74.5. **HRMS (EI):** calc. for $C_{11}H_5F_6N_3O_3$ $[M]^+$ 341.0235; found 341.0229.

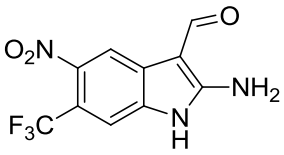

Synthesis of 3-9a: The indole was synthesized in the same manner as indole **3-8a** starting from indole **3-6a**. A yellow, amorphous solid was isolated in 85% yield. **^{1}H NMR** (600 MHz, DMSO-d_6): δ (ppm) 11.40 (s, br, 1H), 9.93 (s, br, 1H), 8.37 (s, 1H), 7.85 (s, br, 2H), 7.63 (s, 1H). **HRMS (EI):** calc. for $C_{10}H_6F_3N_3O_3$ $[M]^+$ 273.0361; found 273.0370.

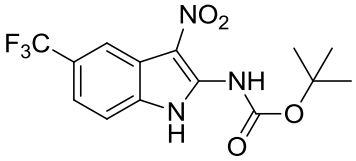

Synthesis of 3-4b: Indole **3-3b** (500 mg, 1.67 mmol) was dissolved dry THF (20 mL) and placed in an ice/water bath with stirring. Acetic anhydride (8 mL) was placed in an ice/water bath and with stirring then $HNO_{3(conc)}$ (0.5 mL) was added slowly dropwise and stirring continued for 10 minutes. The acetic anhydride mixture was added very slowly dropwise to the indole flask where the solution slowly turned purple and stirred for an additional 30 minutes. Following stirring, the solution was poured into cold water (100 mL) and stirred for 10 minutes and transferred to a separatory funnel. The aqueous layer was extracted twice with EtOAc and the organic layers were combined, rinsed with water and brine and dried with Na_2SO_4. The solution was filtered and EtOAc was removed

under reduced pressure. The crude indole was subjected to flash chromatography using a mixture of EtOAc and Hexanes and a yellow, crystalline solid was isolated in 62% yield. **m.p.** > 250 °C. **^{1}H NMR** (400 MHz, DMSO-d_6): δ (ppm) 12.84 (s, br, 1H), 10.09 (s, br, 1H), 8.21 (s, 1H), 7.79 (d, J = 8.6 Hz, 1H), 7.61 (d, J = 8.6 Hz, 1H), 1.58 (s, 9H). **^{13}C NMR** (100 MHz, DMSO-d_6): δ (ppm) 150.7, 141.6, 133.3, 124.8 (q, J = 271.5 Hz), 124.1 (q, J = 31.4 Hz), 120.6 (q, J = 3.1 Hz), 119.0, 115.4 (q, J = 4.6 Hz), 113.8, 113.1, 83.7, 27.6. **^{19}F NMR** (376 MHz, DMSO-d_6, $C_7H_5F_3$): δ (ppm) -62.3. **HRMS (EI):** calc. $C_{14}H_{14}F_3N_3O_4$ $[M]^+$ 345.0936; found: 345.0932.

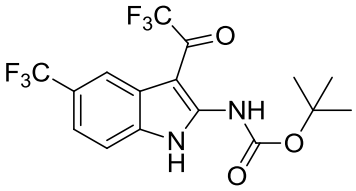

Synthesis of 3-5b: The indole was synthesized in the same manner as indole **3-5a** starting from indole **3-3b**. A white amorphous solid was isolated in 81% yield. **^{1}H NMR** (400 MHz, DMSO-d_6): δ (ppm) 12.97 (s, br, 1H), 10.60 (s, 1H), 7.84 – 7.82 (m, 2H), 7.59 (dd, J = 8.6, 1.0 Hz, 1H), 1.57 (s, 9H). **^{13}C NMR** (400 MHz, CD_2Cl_2): δ (ppm) 174.8 (q, J = 36.9 Hz), 153.4, 151.5, 135.0, 126.0 (q, J = 32.4 Hz), 125.5 (q, J = 271.8 Hz), 122.5, 120.8 (q, J = 3.8 Hz), 117.8 (q, J = 287.6 Hz), 117.6 - 117.5 (m), 112.5, 95.7, 85.3, 28.3. **^{19}F NMR** (376 MHz, CD_2Cl_2): δ (ppm) -61.4, -75.9. **HRMS (EI):** calc. $C_{16}H_{14}F_6N_2O_3$ $[M]^+$ 396.0909; found: 396.0894.

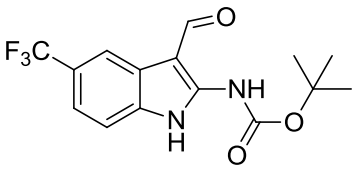

Synthesis of 3-6b: The indole was synthesized in the same manner as indole **3-6a** starting from indole **3-3b**. A white, amorphous solid was isolated in 73% yield. **^{1}H NMR** (400

MHz, DMSO-d_6): δ (ppm) 12.25 (s, br, 1H), 11.01 (s, br, 1H), 10.11 (s, 1H), 8.28 (s, 1H), 7.79 (d, J = 8.5 Hz, 1H), 7.43 (d, J = 8.5 Hz, 1H), 1.57 (s, 9H). **^{13}C NMR** (100 MHz, DMSO-d_6): δ (ppm) 183.8, 152.0, 145.4, 135.2, 125.3 (q, J = 271.5 Hz), 123.9, 122.8 (q, J = 30.7 Hz), 118.6 (q, J = 3.1 Hz), 115.8, 112.8, 101.7, 82.2, 27.8. **^{19}F NMR** (376 MHz, DMSO-d_6, $C_7H_5F_3$): δ (ppm) -61.7. **HRMS (EI):** calc. $C_{15}H_{15}F_3N_2O_3$ $[M]^+$ 328.1035; found: 328.1027.

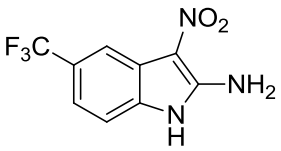

Synthesis of 3-7b: The indole was synthesized in the same manner as indole **3-8a** starting from indole **3-4b**. A yellow, amorphous solid was isolated in 84% yield. **^{1}H NMR** (400 MHz, DMSO-d_6): δ (ppm) 11.52 (s, br, 1H), 8.40 (s, br, 2H), 8.07 (d, J = 1.7 Hz, 1H), 7.44 (dd, J = 8.2 Hz, 1.7 Hz, 1H), 7.37 (d, J = 8.2 Hz, 1H). **^{13}C NMR** (150 MHz, DMSO-d_6): δ (ppm) 151.2, 134.2, 125.1 (q, J = 270.6 Hz), 122.7 (q, J = 31.1 Hz), 121.2, 119.8, 114.6, 111.0, 110.4. **^{19}F NMR** (376 MHz, DMSO-d_6, $C_7H_5F_3$): δ (ppm): -62.0. **HRMS (EI):** calc. for $C_9H_6F_3N_3O_2$ $[M]^+$ 245.0412; found 245.0419.

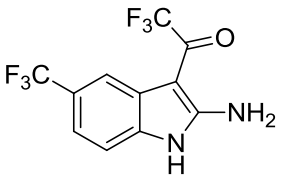

Synthesis of 3-8b: The indole was synthesized in the same manner as indole **3-8a** starting from indole **3-5b**. A white, amorphous solid was isolated in 91% yield. **^{1}H NMR** (600 MHz, DMSO-d_6): δ (ppm) 11.56 (s, br, 1H), 8.30 (s, br, 2H), 7.67 (s, 1H), 7.39 (s, 2H). **^{13}C NMR** (150 MHz, DMSO-d_6): δ (ppm) 169.3 (q, J = 34.9 Hz), 159.0, 136.7, 125.1 (q, J = 270.7 Hz), 123.1, 122.1 (q, J = 30.3 Hz), 118.9, 117.8 (q, J = 289.7 Hz), 114.1, 111.1,

92.0. **^{19}F NMR** (376 MHz, DMSO-d_6): δ (ppm) -59.4, -74.3. **HRMS (EI):** calc. for $C_{11}H_6F_6N_2O$ $[M]^+$ 296.0384; found 296.0390.

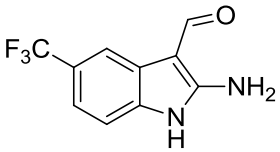

Synthesis of **3-9b**: The indole was synthesized in the same manner as indole **3-8a** starting from indole **3-6b**. A beige, amorphous solid was isolated in 90% yield. **^{1}H NMR** (400 MHz, $CDCl_3$): δ (ppm) 10.02 (s, 1H), 7.90 (m, N-*H*, Ar-H), 7.34 (d, *J* = 8.3 Hz, 1H), 7.20 (d, *J* = 8.3 Hz, 1H). **^{19}F NMR** (376 MHz, $CDCl_3$): δ (ppm) -60.1 ppm. **HRMS (EI):** calc. for $C_{10}H_7F_3N_2O$ $[M]^+$ 228.0510; found: 228.0502.

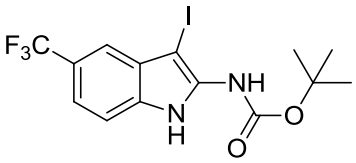

Synthesis of 3-10b: Indole **3-3b** (1.30 g, 4.33 mmol) was dissolved in THF (25 mL) and placed in an ice/water bath. With stirring, NIS (1.02 g, 4.55 mmol) was added portionwise over 30 minutes and the reaction flask was stirred for an additional 30 minutes on the ice/water bath and an hour warming to room temperature. Once the starting material was consumed, determined by TLC monitoring, the contents were poured into water (100 mL) and extracted twice with EtOAc. The organic layers were combined, washed twice with water, once with brine and dried with Na_2SO_4 and filtered. The solvent was removed under reduced pressure where the crude solids were subjected to flash chromatography using a mixture of EtOAc and Hexanes. A yellow, amorphous solid was isolated in 92% yield. **^{1}H NMR** (400 MHz, DMSO-d_6): δ (ppm) 11.99 (s, br, 1H), 9.52 (s, br, 1H), 7.54 (d, *J* = 8.5 Hz, 1H), 7.46 (s, 1H), 7.39 (dd, *J* = 8.5, 1.0 Hz,

1H), 1.50 (s, 9H). **^{13}C NMR** (100 MHz, DMSO-d_6): δ (ppm) 153.1, 137.4, 135.7, 128.7, 125.4 (q, J = 271.5 Hz), 120.9, (q, J = 30.7 Hz), 117.8, 116.2, 112.4, 80.2, 28.0. **^{19}F NMR** (376 MHz, DMSO-d_6, $C_7H_5F_3$): δ (ppm) -61.3. **HRMS (EI):** calc. $C_{14}H_{14}F_3IN_2O_2$ $[M]^+$ 426.0052; found: 426.0043.

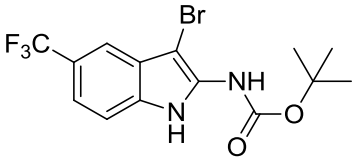

Synthesis of 3-11b: The indole was prepared in the same manner as **3-10b** using NBS in place of NIS. A beige, amorphous solid was isolated in 85% yield. **^{1}H NMR** (600 MHz, DMSO-d_6): δ (ppm) 11.94 (s, br, 1H), 9.75 (s, br, 1H), 7.58 – 7.57 (m, 2H), 7.40 (dd, J = 8.8, 1.8 Hz, 1H), 1.50 (s, 9H). **^{13}C NMR** (100 MHz, DMSO-d_6): δ (ppm) 153.0, 134.1, 133.9, 125.4, 125.4 (q, J = 271.5 Hz), 120.9 (q, J = 31.4 Hz), 117.6, 114.1, 112.5, 80.3, 78.3 (br), 27.9. **^{19}F NMR** (376 MHz, DMSO-d_6, $C_7H_5F_3$): δ (ppm) -61.5. **HRMS (EI):** calc. $C_{14}H_{14}BrF_3N_2O_2$ $[M]^+$ 378.0191; found: 378.0194.

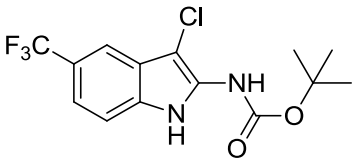

Synthesis of 3-12b: The indole was prepared in the same manner as **3-10b** using NCS in place of NIS. A white, amorphous solid was isolated in 72% yield. **^{1}H NMR** (400 MHz, DMSO-d_6): δ (ppm) 11.85 (s, br, 1H), 9.89 (s, br, 1H), 7.63 (s, br, 1H), 7.58 (d, J = 8.5 Hz, 1H), 7.39 (dd, J = 8.5, 1.4 Hz, 1H), 1.51 (s, 9H). **^{13}C NMR** (100 MHz, DMSO-d_6): δ (ppm) 152.9, 133.1, 132.3, 125.4 (q, J = 271.5 Hz), 123.8, 120.9 (q, J = 31.4 Hz), 117.5, 113.2, 112.5, 91.6 (br), 80.4, 28.0. **^{19}F NMR** (376 MHz, DMSO-d_6, $C_7H_5F_3$): δ (ppm) -61.3. **HRMS (EI):** calc. $C_{14}H_{14}ClF_3N_2O_2$ $[M]^+$ 334.0696; found: 334.0682.

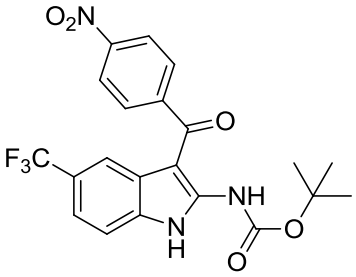

Synthesis of 3-13b: Indole **3-3b** (1.00 g, 3.33 mmol) was dissolved in dry THF (20 mL) under a dry N_2 atmosphere and placed in an ice/water bath. With stirring, 4-nitrobenzoyl chloride (649 mg, 3.50 mmol) was added all at once as a solid and stirred overnight while cooling to room temperature. The solution was transferred to a separatory funnel containing water and extracted twice with EtOAc. The organic layer was washed twice with water followed by brine, dried with Na_2SO_4 and filtered. Solvent was removed under reduced pressure and the crude solid was adsorbed onto silica gel and purified using flash column chromatography using a mixture of EtOAc and Hexanes where a pale orange, amorphous solid was isolated in 79 % yield. **^{1}H NMR** (400 MHz, DMSO-d_6): δ (ppm) 12.69 (s, br, 1H), 10.72 (s, br, 1H), 8.41 (d, J = 8.6 Hz, 2H), 7.87 (d, J = 8.6 Hz, 2H), 7.74 (d, J = 8.6 Hz, 1H), 7.43 (dd, J = 8.6, 1.0 Hz, 1H), 6.90 (s, 1H), 1.55 (s, 9H). **^{13}C NMR** (100 MHz, DMSO-d_6): δ (ppm) 189.1, 151.3, 148.7, 146.3, 146.2, 135.5, 128.7, 124.8 (q, J = 271.5 Hz), 123.8, 123.6, 122.5 (q, J = 30.7 Hz), 118.6, 115.0, 113.4, 98.8, 82.8, 27.7. **^{19}F NMR** (376 MHz, DMSO-d_6, $C_7H_5F_3$): δ (ppm) -62.2. **HRMS (EI):** calc. $C_{21}H_{18}F_3N_3O_5$ $[M]^+$ 449.1199; found: 449.1190.

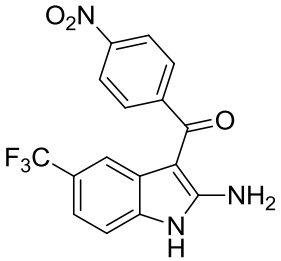

Synthesis of 3-14b: The indole was synthesized in the same manner as indole **3-8a** starting from indole **3-13b**. An orange, amorphous solid was isolated in 90% yield. **^{1}H NMR** (400 MHz, DMSO-d_6): δ (ppm) 11.37 (s, br 1H), 8.38 (d, J = 8.8 Hz, 2H), 7.95 (s, br, 2H), 7.78 (d, J = 8.8 Hz, 2H), 7.32 (d, J = 8.3 Hz, 1H), 7.21 (d, J = 8.3 Hz,

1H), 6.53 (s, 1H). **^{13}C NMR** (150 MHz, DMSO-d_6): δ (ppm) 186.0, 156.6, 148.1, 148.0, 135.9, 128.3 (q, J = 6.9 Hz), 125.7, 125.1 (q, J = 270.6 Hz), 123.9, 121.2 (q, J = 31.1 Hz), 117.3, 113.3, 110.6, 95.3. **^{19}F NMR** (376 MHz, DMSO-d_6, $C_7H_5F_3$): δ (ppm): -62.2. **HRMS (EI):** calc. for $C_{16}H_{10}F_3N_3O_3$ $[M]^+$ 349.0674; found 349.0671.

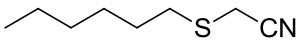

Synthesis of 3-15b: 1-Hexanethiol (5.00 mL, 35.2 mmol), bromoacetonitrile (2.70 mL, 38.7 mmol) and K_2CO_3 (5.35 g, 38.7 mmol) were added into dry THF (100 mL) under a dry N_2 atmosphere. The reaction was stirred and heated to 60 °C overnight and brought to room temperature the following day and vacuum filtered to remove salts. The mother liquor was added into a separatory funnel along with 200 mL of water and was extracted three times with Et_2O. The organic layers were combined, rinsed with water, brine and dried with $MgSO_4$. The drying agent was filtered and the solvent was removed under reduced pressure. The crude oil was flash chromatographed using EtOAc/Hexanes (1/9) as eluent and a clear, colourless oil was obtained in 85% yield. **^{1}H NMR** (600 MHz, $CDCl_3$): δ (ppm) 3.29 (s, 2H), 2.75 - 2.73 (m, 2H), 1.67 - 1.62 (m, 2H), 1.43 - 1.41 (m, 2H), 1.31 (s, br, 4H), 0.91 - 0.89 (m, 3H). **^{13}C NMR** (150 MHz, $CDCl_3$): δ (ppm) 32.7, 31.3, 28.6, 28.4, 22.6, 17.1, 14.1.

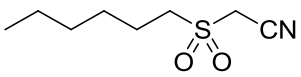

Synthesis of 3-16b: TFAA (7.95 mL, 57.3 mmol) was added into dry acetonitrile (50 mL) and vigorously stirred while adding UHP (7.19 g, 76.4 mmol) for 5 minutes then immediately put into an ice/water bath. Thioether **3-15b** (3.00 g, 19.1 mmol) was dissolved in an additional 20 mL acetonitrile and placed into a

separate ice/water bath. The TFAA/UHP solution was pipetted slowly into the thioether flask and stirred for an hour on ice and left to stir overnight warming to room temperature. The next day, the acetonitrile solution was poured into water (200 mL) and vigorously stirred for 30 minutes and vacuum filtered. The solids were subjected to flash chromatography using Et_2O as eluent and a white, crystalline solid was isolated in 83% yield. **m.p.:** 47 - 49 °C. **^{1}H NMR** (600 MHz, $CDCl_3$): δ (ppm) 3.94 (s, 2H), 3.29 - 3.26 (m, 2H), 1.95 - 1.89 (m, 2H), 1.51 - 1.49 (m, 2H), 1.35 - 1.34 (m, 4H), 0.92 - 0.90 (m, 3H). **^{13}C NMR** (150 MHz, $CDCl_3$): δ (ppm) 53.6, 42.3, 31.2, 28.0, 22.3, 22.0, 14.0.

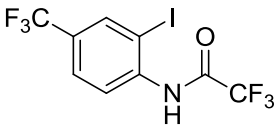

Synthesis of 3-17b: The same procedure was adapted from the previous chapter using TFAA and NEt_3 in DCM as solvent with aniline **3-1b**. The white, crystalline product was isolated in 94% yield and was pure enough to continue to the next step without purification. **m.p.:** 83 - 84 °C. **^{1}H NMR** (400 MHz, $CDCl_3$): δ (ppm) 8.42 - 8.39 (m, N-*H*, Ar-*H*), 8.09 (d, *J* = 1.2 Hz, 1H), 7.00 (dd, *J* = 8.6 Hz, 1.2 Hz). **^{13}C NMR** (100 MHz, $CDCl_3$): δ (ppm) 155.1 (q, *J* = 38.4 Hz), 138.9, 136.3 (q, *J* = 3.8 Hz), 129.6 (q, *J* = 33.9 Hz), 127.0 (q, *J* = 3.0 Hz), 122.7 (q, *J* = 272.6 Hz), 121.5, 115.6 (q, *J* = 288.4 Hz), 89.5. **^{19}F NMR** (376 MHz, $CDCl_3$): δ (ppm) -62.6, -75.8.

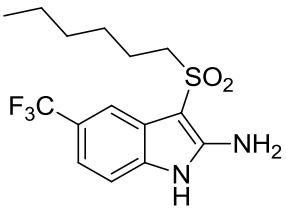

Synthesis of 3-18b: Indole forming procedure was replicated from the previous chapter using **3-16b** as the active methylene substrate. Purification by flash chromatography using

EtOAc/Hexanes (2/3) as eluent was performed and a beige, amorphous solid was isolated in 60% yield. **^{1}H NMR** (600 MHz, DMSO-d_6): δ (ppm) 11.18 (s, br, 1H), 7.60 (s, 1H), 7.34 (d, J = 8.2 Hz, 1H), 7.25 (d, J = 8.2 Hz, 1H), 6.60 (s, br, 2H), 3.12 – 3.10 (m, 2H), 1.60 – 1.55 (m, 2H), 1.31 – 1.26 (m, 2H), 1.18 – 1.14 (m, 4H), 0.78 (t, J = 6.7 Hz, 3H). **^{13}C NMR** (100 MHz, DMSO-d_6): δ (ppm) 151.5, 134.4, 126.1, 125.4 (q, J = 271.5 Hz), 121.4 (q, J = 30.7 Hz), 116.4, 112.1, 110.4, 86.4, 55.9, 30.7, 27.1, 22.6, 21.7, 13.7. **^{19}F NMR** (376 MHz, DMSO-d_6, $C_7H_5F_3$): δ (ppm): -61.6. **HRMS (EI):** calc. for $C_{15}H_{19}F_3N_2O_2S$ $[M]^+$ 348.1119; found 348.1124.

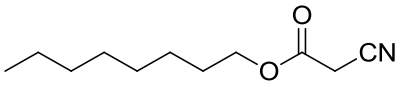

Synthesis of 3-19b: Cyanoacetic acid (2.00 g, 23.5 mmol) and n-octanol (3.72 mL, 23.5 mmol) was dissolved in dry dichloromethane (100 mL) under a dry N_2 atmosphere and placed into an ice/water bath. DCC (4.85 g, 23.5 mmol) and DMAP (290 mg, 2.35 mmol) were dissolved in an additional 50 mL dichloromethane and added dropwise via syringe to the reaction flask over 30 minutes. The contents were allowed to stir for an hour in the ice/water bath then the bath was removed and stirring continued overnight. The resulting white slurry was vacuum filtered through a pad of Celite, rinsed with dichloromethane (50 mL) and washed three with water in a separatory funnel. The organic layer was dried with Na_2SO_4, filtered and the solvent was removed under reduced pressure. The resulting yellow oil was purified by flash chromatography using EtOAc/Hexanes (1/6) as eluent which resulted in a clear, colourless liquid in 85% yield. **^{1}H NMR** (600 MHz, $CDCl_3$): δ (ppm) 4.20 (t, J = 6.7 Hz, 2H), 3.45 (s, 2H), 1.69 - 1.66 (m, 2H), 1.36 - 1.27 (m, 10H), 0.88 (t, J = 7.2 Hz, 3H). **^{13}C NMR** (100 MHz, $CDCl_3$): δ (ppm) 163.1, 113.2, 67.1, 31.8,

29.1, 29.1, 28.4, 25.7, 24.8, 22.7, 14.1. **HRMS (EI):** calc. for $C_{11}H_{19}NO_2$ $[M+H]^+$ 198.1494; found 198.1475.

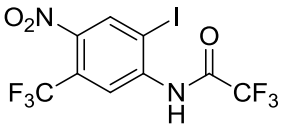

Synthesis of 3-20b: The acetamide was synthesized in the same manner as **3-17b** starting with aniline **3-1a**. The fluffy, pale yellow solid was isolated in 96% yield and was pure enough to continue to the next step. **^{1}H NMR** (400 MHz, $CDCl_3$): δ (ppm) 8.83 (s, 1H), 8.53 (s, br, 1H), 8.43 (s, 1H). **^{13}C NMR** (100 MHz, $CDCl_3$): δ (ppm) 155.4 (q, *J* = 39.3 Hz), 144.5, 140.3, 136.0, 125.7 (q, *J* = 35.6 Hz), 121.2 (q, *J* = 274.2 Hz), 119.5, 115.3 (q, *J* = 288.6 Hz). **^{19}F NMR** (376 MHz, $CDCl_3$, $C_7H_5F_3$): δ (ppm) -76.9, -61.5. **HRMS (EI):** calc. for $C_9H_3F_3IN_2O_3$ $[M]^+$ 427.9093; found 427.9101.

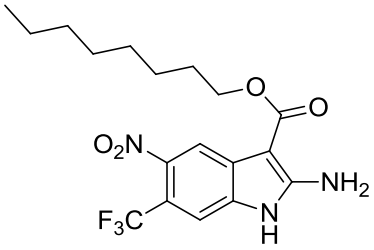

Synthesis of 3-21b: The indole was synthesized in the same manner as indole **3-18b** using acetamide **3-20b** and ester **3-19b** as the active methylene compound. Purification by flash chromatography using EtOAc/Hexanes (2/3) as eluent was performed and a bright yellow, amorphous solid was isolated in 65% yield. **^{1}H NMR** (400 MHz, DMSO-d_6): δ (ppm) 11.39 (s, br, 1H), 8.12 (s, 1H), 7.65 (s, 1H), 7.36 (s, br, 2H), 4.23 (t, *J* = 6.4 Hz, 2H), 1.75 - 1.68 (m, 2H), 1.45 - 1.39 (m, 2H), 1.37 - 1.25 (m, 8H), 0.83 (t, *J* = 7.0 Hz, 3H). **^{13}C NMR** (100 MHz, DMSO-d_6): δ (ppm) 164.7, 156.1, 141.7, 133.8, 129.3, 124.4 (q, *J* = 271.3 Hz), 114.3, 112.5 (q, *J* = 33.2 Hz), 108.6 (q, *J* = 5.8 Hz), 85.0, 62.8, 31.2, 28.7, 28.7, 28.5, 22.1, 13.8.

^{19}F NMR (376 MHz, DMSO-d_6, $C_7H_5F_3$): δ (ppm) -59.2. **HRMS (EI):** calc. for $C_{18}H_{22}F_3N_3O_4$ $[M]^+$ 401.1562; found 401.1569.

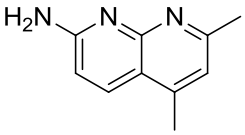

Synthesis of 3-1c: Synthesis was replicated from a literature method and characterization data matched that of the known compound.[14]

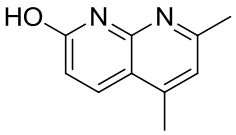

Synthesis of 3-2c: Synthesis was replicated from a literature method and characterization data matched that of the known compound.[15]

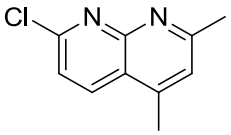

Synthesis of 3-3c: Synthesis was replicated from a literature method and characterization data matched that of the known compound.[15]

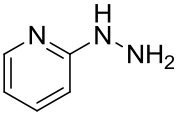

Synthesis of 3-4c: Synthesis was replicated from a literature method and characterization data matched that of the known compound.[16]

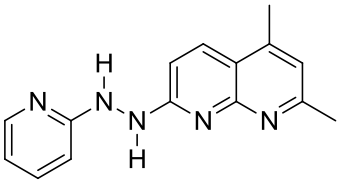

Synthesis of 3-5c: **3-3c** and **3-4c** were dissolved in *n*-PrOH (50 mL) and refluxed overnight. The following day, the mixture was poured into water (200 mL) and vacuum filtered. The filter cake was stirred in cold DCM (50 mL) and solids were vacuum filtered and the filter cake was washed twice with cold DCM (10 mL). No further purification was needed and a light pink, amorphous solid was isolated in 79% yield. **^{1}H NMR** (400 MHz, $CDCl_3$): δ (ppm) 8.19 (d, J = 4.4 Hz, 1H), 8.11 (d, J = 8.1 Hz, 1H),

7.52 - 7.48 (m, 1H), 7.21 (s, br, 1H), 7.12 (d, *J* = 8.7 Hz, 1H), 6.97 (s, 1H), 6.84 (s, br, 1H), 6.80 - 6.77 (m, 2H), 2.65 (s, 3H), 2.57 (s, 3H). **HRMS (EI):** calc. for $C_{15}H_{15}N_5$ $[M]^+$ 265.1327; found: 265.1323.

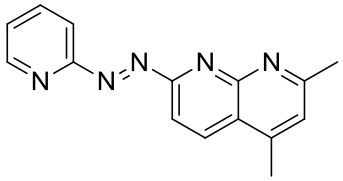

Synthesis of (*E*)-3: Hydrazine **3-5c** (1.23 g, 4.64 mmol) was added into a flask containing a 1:1 mixture of DCM and DMSO (50 mL). (Diacetoxyiodo)benzene (1.64 g, 5.10 mmol) was added as a solid portionwise over a period of 20 minutes and stirring continued for an additional 3 hours at 50 °C. The solution was diluted with DCM (100 mL) and washed twice with water, followed by brine and the organic layer was dried with Na_2SO_4. The drying agent was filtered and the solvent was removed under reduced pressure. The crude product was purified by flash chromatography using acetone as eluent and a red, amorphous solid was isolated in 91% yield. **^{1}H NMR** (400 MHz, $CDCl_3$): δ (ppm) 8.83 (m, 1H), 8.53 (d, *J* = 8.5 ppm, 1H), 8.12 (d, *J* = 8.5 Hz, 1H), 8.05 (d, *J* = 8.1 Hz, 1H), 7.96 (m, 1H), 7.50 (m, 1H), 7.30 (s, 1H), 2.81 (s, 3H), 2.74 (s, 3H). **^{13}C NMR** (100 MHz, $CDCl_3$): δ (ppm) 164.1, 163.3, 162.9, 155.4, 149.7, 145.4, 138.8, 136.0, 126.6, 124.7, 122.5, 144.1, 111.4, 25.7, 18.3. **HRMS (ESI):** calc. for $C_{15}H_{13}N_5$ $[M]^+$ 263.1171; found: 263.1161.

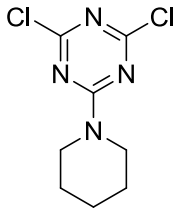

Synthesis of 3-6c: Cyanuric chloride (3.00 g, 16.3 mmol) was dissolved in dry THF (75 mL) and cooled to -78 °C in a dry ice/acetone bath. Piperidine (1.61 mL, 16.3 mmol) and NEt_3 (2.40 mL, 17.1 mmol) were dissolved in an additional 30 mL dry THF. With stirring, the bases in THF were added

via dropping funnel over an hour and left to stir for an hour then slowly warmed to room temperature. The reaction contents were poured into cold water (200 mL) and solids were vaccuum filtered and rinsed wth water. The dichloro product was pure enough to continue to the next step and characterization data matched that of the known compound.[28]

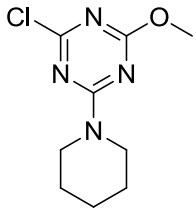

Synthesis of 2-7c: Triazine **2-6c** (1.50 g, 6.44 mmol) was dissolved in dry THF (50 mL) and placed into a brine/ice bath. Methanol (290 µL, 7.08 mmol) was added into an additional 30 mL dry THF under N_2 atmosphere and placed into an ice bath. NaH (60% dispersion, 290 mg, 7.08 mmol) was added to the MeOH/THF flask and left to stir for an hour. The methoxide solution was transferred into a dropping funnel under N_2 atmosphere and added to the **2-6c** solution with stirring over 30 mins. The reaction was allowed to stir at low temperature for an hour and was allowed to warm to room temperature. The contents were poured into water and vacuum filtered and rinsed with water. The solids were subjected to flash chromatography and triazine **2-7c** was isolated in 79% yield. Characterzation data matches that of the known compound.[29]

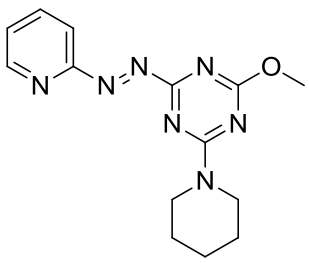

Synthesis of (*E*)-4: **3-7c** (1.80 g, 7.87 mmol) and **3-4c** (860 mg, 7.87 mmol) were refluxed in *n*-PrOH (50 mL) overnight. The flask contents were poured into water and vaccum filtered. The collected solids were dissolved in 40 mL of a 1:1 mixture of DCM:DMSO and (diacetoxyiodo)benzene (2.03 g, 6.30 mmol) was added portionwise

over 20 minutes. The reaction was heated for 30 hours at 50 °C and extracted 3 times with DCM. The organic layers were combined, dried with Na_2SO_4 and filtered. Solvent was removed under reduced pressure and crude solids subjected to flash chromatography. **(*E*)-4** was isolated as an amorphous, red solid in 55% yield. **^{1}H NMR** (600 MHz, $CDCl_3$): δ (ppm) 8.78 - 8.77 (m, 1H), 7.96 - 7.90 (m, 2H), 7.49 - 7.47 (m, 1H), 4.03 (s, 3H), 3.92 - 3.87 (m, 4H), 1.72 - 1.69 (m, 2H), 1.67 - 1.60 (m, 4H). **^{13}C NMR** (150 MHz, $CDCl_3$): δ (ppm) 175.7, 172.2, 166.1, 162.3, 149.7, 138.4, 126.6, 117.1, 54.8, 45.0, 44.8, 25.7, 25.6, 24.5. **HRMS (EI):** calc. for $C_{14}H_{17}N_7O$ $[M]^+$ 299.1495; found: 299.1500.

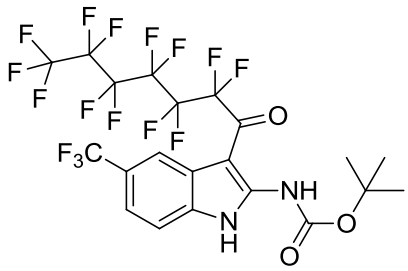

Synthesis of 3-1d: Perfluoroheptanoic acid (1.00 g, 2.75 mmol) was added into dry DCM (5 mL) under a dry N_2 atmosphere. Oxalyl chloride (260 µL, 3.02 mmol) was added along with 3 drops of dry DMF and the reaction was refluxed and stirred for 2 hours to form the acid chloride. The mixture was then cooled on an ice/water bath and dry THF (20 mL) was added followed by indole **3-3b** (783 mg, 2.61 mmol). The contents were stirred on ice for an hour and then stirred at room temperature for 6 hours. The contents were then diluted with DCM (100 mL) and washed two times with water, once with brine and the organic layer was dried with $MgSO_4$ and filtered. After removal of the solvent under reduced pressure, the crude oil was subjected to flash chromatography using EtOAc/Hexanes (1/9) as eluent. Solvent was once again removed and the oil was dissolved in hexanes and precipitated using a dry ice/acetone bath at -78 °C and after vacuum filtration, a pale yellow, amorphous solid was isolated in 78% yield. **^{1}H NMR** (400 MHz, DMSO-d_6): δ (ppm) 12.99 (s, br, 1H),

10.81 (s, br, 1H), 7.85 (s, 1H), 7.82 (d, *J* = 8.6 Hz, 1H), 7.58 (d, *J* = 8.6 Hz, 1H), 1.57 (s, 9H). **^{13}C NMR** (150 MHz, $CDCl_3$): δ (ppm) 177.5 (t, *J* = 28.5 Hz), 153.1, 151.4, 134.4, 126.1 (q, *J* = 32.2 Hz), 124.8 (q, *J* = 271.6 Hz), 122.0, 120.6, 118.4, 117.4 (qt, *J* = 288.2, 33.1 Hz), 111.8, 111.6*, 111.1*, 110.7*, 110.4*, 108.5*, 97.6, 85.0, 28.1. **^{19}F NMR** (376 MHz, DMSO-d_6, $C_7H_5F_3$): δ (ppm) -62.7, -83.1 (t, *J* = 9.3 Hz), -119.0 (t, *J* = 11.9 Hz), -123.4, -123.7, -125.4, -128.5. **HRMS (EI):** calc. $C_{21}H_{14}F_{16}N_2O_3$ $[M]^+$ 646.0749; found: 646.0756.

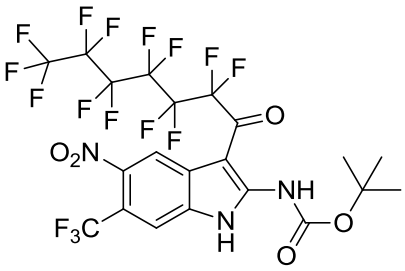

Synthesis of 3-1e: The indole was synthesized in the same manner as Indole **3-1d** using Indole **3-3a**. Purification of the crude material was performed with flash chromatography using EtOAc/Hexanes (1/9) as eluent and a white solid was isolated in 73% yield. **^{1}H NMR** (400 MHz, DMSO-d_6): δ (ppm) 13.35 (s, br, 1H), 10.69 (s, br, 1H), 8.27 (s, 1H), 8.22 (s, 1H), 1.58 (s, 9H). **^{13}C NMR** (150 MHz, $CDCl_3$): δ (ppm) 177.8 (q, *J* = 28.9 Hz), 152.8, 152.8, 144.4, 133.3, 124.5, 122.5 (q, *J* = 272.9 Hz), 119.2 (q, *J* = 33.8 Hz), 118.6, 117.4 (qt, *J* = 287.4, 32.8 Hz), 111.4, 111.4*, 111.0*, 110.4*, 110.3*, 108.5*, 97.5, 85.9, 28.0. (* indictates determination of chemical shift via gHSQCAD). **^{19}F NMR** (376 MHz, DMSO-d_6, $C_7H_5F_3$): δ (ppm) -60.0, -82.0 (t, *J* = 9.3 Hz), -117.8 (t, *J* = 11.9 Hz), -121.9, -122.3, -123.8, -127.1. **HRMS (EI):** calc. $C_{21}H_{13}F_{16}N_3O_5$ $[M]^+$ 691.0600; found: 691.0605.

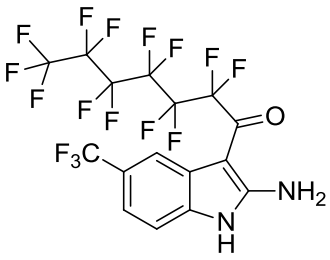

Synthesis of 3-2d: Indole **3-1d** was deprotected in the same manner as compound **3-8a**. The crude solid was subjected to

flash chromatography using EtOAc/Hexanes (3/2) as eluent and a white amorphous solid was isolated in 90% yield. **^{1}H NMR** (400 MHz, DMSO-d_6): δ (ppm) 11.60 (s, br, 1H), 8.46 (s, br, 2H), 7.69 (s, 1H), 7.41 – 7.36 (m, 2H). **^{13}C NMR** (150 MHz, DMSO-d_6): δ (ppm) 171.7 (t, *J* = 26.7 Hz), 159.4, 136.8, 125.1 (q, *J* = 270.7 Hz), 123.0, 122.4 (q, *J* = 31.3 Hz), 118.9, 116.8 (qt, *J* = 288.2, 33.1 Hz), 115.4, 111.9*, 111.3*, 111.1*, 111.0, 110.3*, 108.5*, 94.5 (* dictates determination of chemical shift via gHSQCAD). **^{19}F NMR** (376 MHz, DMSO-d_6, $C_7H_5F_3$): δ (ppm) -62.4, -83.1 (t, *J* = 9.3 Hz), -118.8 (t, *J* = 11.3 Hz), -123.3, -123.7, -125.4, -128.4. **HRMS (EI):** calc. $C_{16}H_6F_{16}N_2O$ $[M]^+$ 546.0225; found: 546.0229.

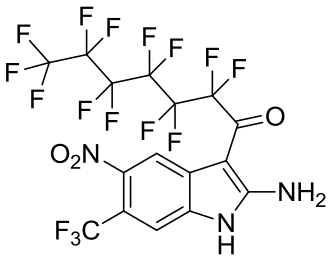

Synthesis of 3-2e: Indole **2-1e** was deprotected in the same manner as compound **3-8a**. The crude solid was subjected to flash chromatography using EtOAc/Hexanes (3/2) as eluent and a pale yellow, amorphous solid was isolated in 86% yield. **^{1}H NMR** (400 MHz, DMSO-d_6): δ (ppm) 11.86 (s, br, 1H), 8.68 (s, br, 2H), 8.08 (s, 1H), 7.75 (s, 1H). **^{13}C NMR** (150 MHz, DMSO-d_6): δ (ppm) 172.6 (t, *J* = 27.6 Hz), 160.1, 141.9, 136.2, 125.7, 122.9 (q, *J* = 271.6 Hz), 116.8 (qt, *J* = 288.2, 33.1 Hz), 115.9 (q, *J* = 34.1 Hz), 115.8, 109.7, 94.3. (* indictates determination of chemical shift via gHSQCAD). **^{19}F NMR** (376 MHz, DMSO-d_6, $C_7H_5F_3$): δ (ppm) -59.8, -83.0, -118.2, 122.6, 123.2, -124.8, -128.0. **HRMS (EI):** calc. $C_{16}H_5F_{16}N_3O_3$ $[M]^+$ 591.0075; found: 591.0068.

3.7 References

1. a) Bell, D. A.; Anslyn, E. V. *Tetrahedron*, **1995**, *51*, 7161; b) Djurdjevic, S.; Leigh, D. A.; McNab, H.; Parsons, S.; Teobaldi, G.; Zerbetto, F. *J. Am. Chem. Soc*., **2006**, *129*, 476; c) Blight, B.A.; Camara-Campos, A.; Djurdjevic, S.; Kaller, M.; Leigh, D. A.; McMillan, F. M.; McNab, H.; Slawin, A.M.Z. *J. Am. Chem. Soc*., **2009**, *131*, 14116; d) Blight, B. A.; Hunter, C. A.; Leigh, D. A.; McNab, H.; Thomson, P. I. T. *Nat. Chem*., **2011**, *3*, 244; e) Leigh, D. A.; Roberston, C. C.; Slawin, A. M. Z.; Thomson, P. I. T. *J. Am. Chem. Soc*., **2013**, *135*, 9939.

2. a) Murray, T. J.; Zimmerman, S. C. *J. Am. Chem. Soc*., **1992**, *114*, 4010; b) Han, Y-F.; Chen, W-Q.; Wang, H-B.; Yuan, Y-X.; Wu, N-N.; Song, X-Z,; Yang, L. *Chem. Eur. J*., **2014**, *20*, 16980; c) Zimmerman, S. C.; Murray, T. J. *Tetrahedron Lett*., **1994**, *35*, 4077.

3. Cook, J. L.; Hunter, C. A.; Low, C. M. R.; Perez-Velasco, A.; Vinter, J. G. *Angew. Chem. Int. Ed*., **2007**, *46*, 3706.

4. a) Mendez, I. J. M.; Pleizier, J. S.; Wang, H-B.; Wisner, J. A. *J. Phys. Org. Chem*., **2018**, *31*, e3805; b) Mendez, I. J. M. Photo-Isomerizable Self-Complementary Hydrogen Bond Arrays. Ph.D. Dissertation, Western University, London, ON, 2016.

5. Mudraboyina, B. P. Complementary and Self-Complementary Hydrogen Bond Double Helical Complexes. Ph.D. Dissertation, Western University, London, ON, 2012.

6. Lanter, J. C.; Fiordeliso, J. L.; Jiang, W.; Allan, G. F.; Lai, M-T.; Linton, O.; Hahn, D. W.; Lundeen, S. G.; Sui, Z. *Bioorg. Med. Chem. Lett*., **2007**, *17*, 123.

7. a) Chen, C.; Lieberman, D. R.; Larsen, R. D.; Verhoeven, T. R.; Reider, P. J. *J. Org. Chem*., **1997**, *62*, 2676; b) Robertson, W. M.; Kastrinsky, D. B.; Hwang, I.; Boger, D. L. *Bioorg. Med. Chem. Lett*., **2010**, *20*, 2722.

8. Xu, G.; Zheng, L.; Dang, Q.; Bai, X. *Synthesis*, **2013**, *45*, 743.

9. Urwyler, S.; Floersheim, P.; Roy, B. L.; Koller, M. *J. Med. Chem*., **2009**, *52*, 5093.

10. a) Seshadri, S. *J. Sci. Ind. Res. India*, **1973**, *32*, 128; b) Beniwal, M.; Jain, N. *European J. Biomed. Pharm. Sci*., **2015**, *2*, 1340; c) Rajput, A. P.; Girase, P. D. *Int. J. Pharm. Biol Sci*., **2013**, *3*, 25.

11. Ranise, A.; Lucchesini, F.; Caviglia, M.; Alfei, S.; Spallarossa, A.; Caneva, C. *Tetrahedron*, **2013**, *69*, 10858.

12. Wen, W.; Young, S. E.; Duvernay, M. T.; Schulte, M. L.; Nance, K. D.; Melancon, B. J.; Engers, J.; Locuson II, C. W.; Wood, M. R.; Daniels, J. S.; Wu, W.; Lindsley, C. W.; Hamm, H. E., Stauffer, S. R. *Bioorg. Med. Chem. Lett*., **2014**, *24*, 4708.

13. Rahman, M.; Ghosh, M.; Hajra, A.; Majee, A. *J. Sulfur Chem*., **2013**, *34*, 342.

14. Bernstein, J.; Stearns, B.; Shaw, E.; Lott, W. A. *J. Am. Chem. Soc*., **1947**, *69*, 1151.

15. Gan, X.; Chi, S-M.; Mu, W-H.; Yao, J-C.; Quan, L.; Bian, Z-Y.; Chen, Y.; Fu, W-F. *Dalton Trans*., **2011**, *40*, 7365.

16. Padalkar, V. S.; Patil, V. S.; Phatangare, K. R.; Umape, P. G.; Sekar, N. *Synth. Commun*., **2011**, *41*, 925.

17. Kucharska, E.; Hanuza, J.; Lorenc, J. *Spectrochim. Acta A*., **2014**, *127*, 370.

18. Iranpoor, N.; Firouzabadi, H.; Khalili, D. *Bull. Chem. Soc. Jpn*., **2010**, *83*, 923.

19. Wang, H-B. *Mini-Rev. Org. Chem*., **2013**, *10*, 171.

20. Hansch, C.; Leo, A.; Taft, R. W. *Chem. Rev*., **1991**, *91*, 165.

21. Sartorius, J.; Schneider, H. J. *Chem. Eur. J*., **1996**, *2*, 1446.

22. Hamilton, A. D.; Pant, N. *J. Chem. Soc., Chem. Commun*., **1988**, 765.

23. Zimmerman S.C., Corbin P.S. (2000) Heteroaromatic Modules for Self-Assembly Using Multiple Hydrogen Bonds. In: Fuiita M. (eds) *Molecular Self-Assembly Organic Versus Inorganic Approaches. Structure and Bonding*, vol 96. Springer, Berlin, Heidelberg.

24. Murray, T. J.; Zimmerman, S. C. *Tett. Lett*., **1995**, *36*, 7627.

25. Ambler, B. R.; Peddi, S.; Altman, R. A. *Org. Lett*., **2015**, *17*, 2506.

26. Housecroft, Catherine E., Sharpe, Alan G. *Inorganic Chemistry*. Third ed. Pearson / Prentice Hall: Essex, UK. 2008. pp. 31, 1013, 1014

27. Fulmer, G. R.; Miller, A. J. M.; Sherden, N. H.; Gottlieb, H. E.; Nudelman, A.; Stoltz, B. M.; Bercaw, J. E.; Goldberg, K. I. *Organometallics*, **2010**, *29*, 2176.

28. Sunduru, N.; Gupta, L.; Chaturvedi, V.; Dwivedi, R.; Sinha, S.; Chauhan, P. M. S. *Eur. J. Med. Chem*., **2010**, *45*, 3335.

29. El-Faham, A.; Soliman, S. M.; Ghabbour, H. A.; Elnakady, Y. A.; Mohaya, T. A.; Siddiqui, M. R. H.; Albericio, F. *J. Mol. Struct*., **2016**, *1125*, 121.

Chapter 4

4 Photochemistry of Photoswitchable Complementary Hydrogen Bond Arrays

4.1 Photoisomerizable Hydrogen Bonded Complexes

Hydrogen bonding is one of the most widely explored non-covalent interactions to assemble and control supramolecular frameworks. The directionality and resultant specificity of these interactions creates the possibility for applications in tunable polymers with desirable behaviors. The addition of a photochromic subunit into these assemblies creates an additional possibility for manipulation of the hydrogen bonding interactions. This method is advantageous as no additional chemical species are added to the system as stimuli. Utilizing light as an external stimulus therefore allows for a non-invasive technique to modify the efficacy of a hydrogen bonded complex or polymer. These "smart materials" use a photochromic group to control "on" and "off" states which ideally gives two different physical responses. There are two common uses for this type of technique. Generally, hydrogen bonded groups are attached to the periphery of the photochromic moiety which when "switched" changes the orientation or strength of the interacting units. The result creates higher or lower ordered hydrogen bonded aggregates.[1] Another common use for a photoswitch is as a steric block to alter physical attributes of a complex.[2] Diaryl azo derivatives are often used for these types of applications as the *trans* to *cis* isomerization provides a large amplitude spatial rearrangement which can result in a large response.

A typical example of photoswitching of ordered hydrogen bonded aggregates uses azodicarboxylic acids. Sleiman and co-workers demonstrated how linear oligomers, or tapes formed from *trans*-*p*-azodibenzoic acid hydrogen bonded end groups.[3] Isomerization to *cis*-*p*-azodibenzoic acid repositions the acid end groups resulting in a cyclic tetramer (Figure 4.1). Furthermore, the tetramers participate in π-stacking interactions creating an elongated rod-like aggregate. This example demonstrates how microscopic structural changes can be achieved simply by modifying the spatial arrangement of hydrogen bonded end groups with respect to a central photochromic unit.

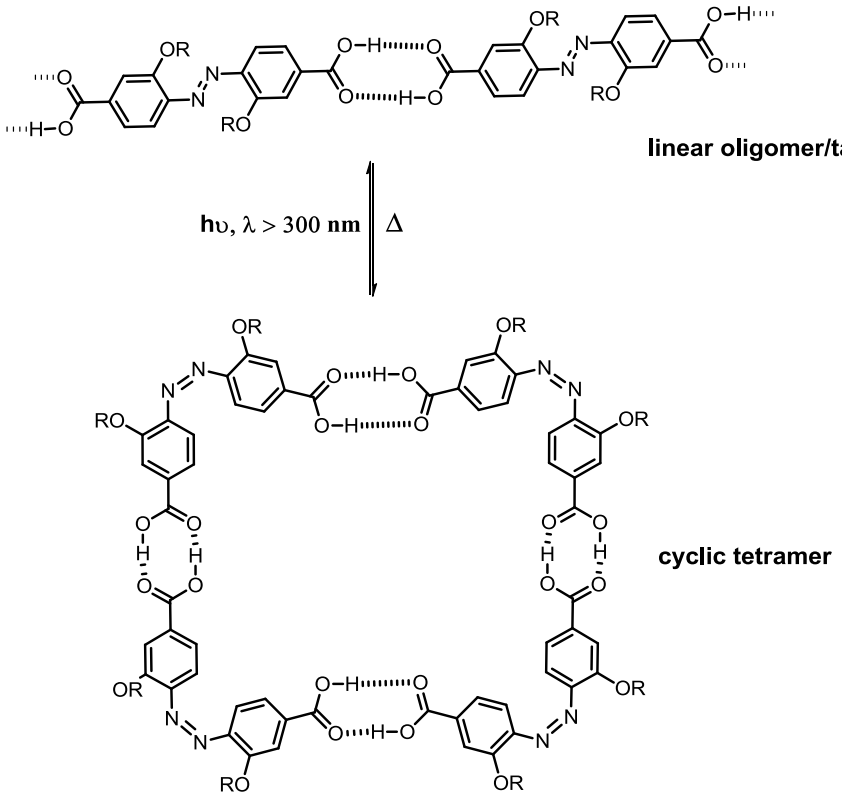

Figure 4.1 Alternate forms of hydrogen bonded aggregates of *trans*- and *cis*-*p*-azodibenzoic acids studied by Sleiman and co-workers.

In terms of modifying the hydrogen bond complexation interaction using irradiation, there are few examples available that show large deviations in the "on" and

"off" states of these complexes. Hecht and co-workers utilized the popular diarylethene photoswitch in conjunction with DAD-ADA complementary arrays. The open form of a diarylethene maleimide hydrogen bonds with a diaminotriazine producing association constants of 132 M^{-1} (X = O-*n*-C_6H_{13}) and 142 M^{-1} (X = CO_2-*n*-C_6H_{13}) in $CDCl_3$ (Left complex; Figure 4.2)[4] Photocyclization to the closed form raises the respective association constants to 231 M^{-1} (X = O-*n*-C_6H_{13}) and 318 M^{-1} (X = CO_2-*n*-$C_6H_{13,}$ Right complex; Figure 4.2). The result is only a small increase in complexation free energy of 1.4 kJ/mol and 2.0 kJ/mol, respectively. The small difference can be attributed to the fact that the arrays themselves are unchanged and only the conjugation in the backbone of the maleimide was altered. Modifying the array from the open to closed form alters the resonance pathways to the peripheral aryl groups which do not have a large total effect on complex stability.

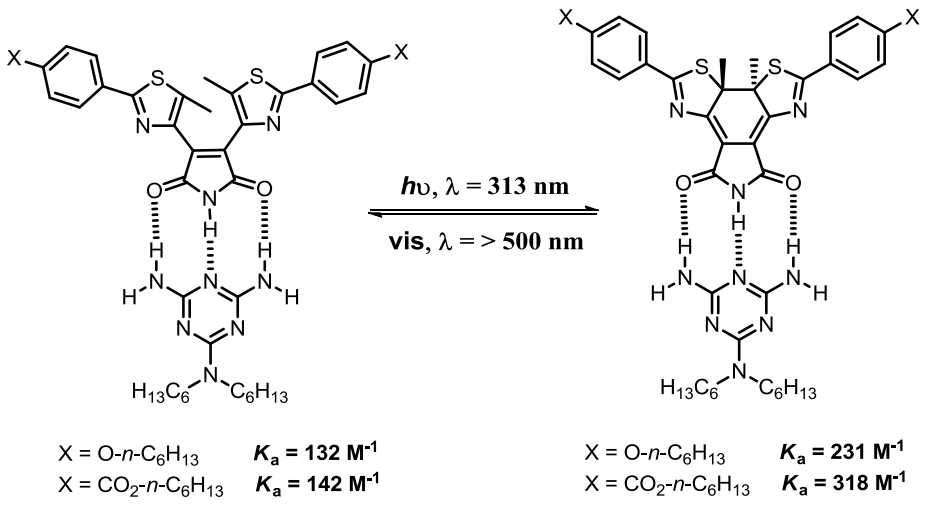

Figure 4.2 Diarylethene maleimide and diaminotriazine hydrogen bonded complexes studied by Hecht and co-workers. K_a values were determined via ^{1}H NMR in $CDCl_3$ at 298 K.

Yokoyama and co-workers accomplished a similar result using fulgimides. The same DAD motif was incorporated in an indolyfulgimide photoswitch and was paired with 2,6-bis(octanoylamino)pyridine as its ADA complement (Figure 4.3). The open form of the indolyfulgimide in this case was the stronger complex which was determined to have a K_a of 885 M^{-1} in toluene.[5] Irradiation with UV light (λ = 366 nm) produced the closed isomer which formed a weaker complex with a lower K_a of 156 M^{-1}. This difference of 4.3 kJ/mol from the closed to open complex is larger than Hecht's diarylethene example. The open form of the indolylfulgimide is a non-planar molecule where the indole nitrogen is in conjugation with a carbonyl group which increases the acceptor strength. The closed form is now planar and conjugation with the indole has been removed, in turn reducing the acceptor strength of the carbonyl.

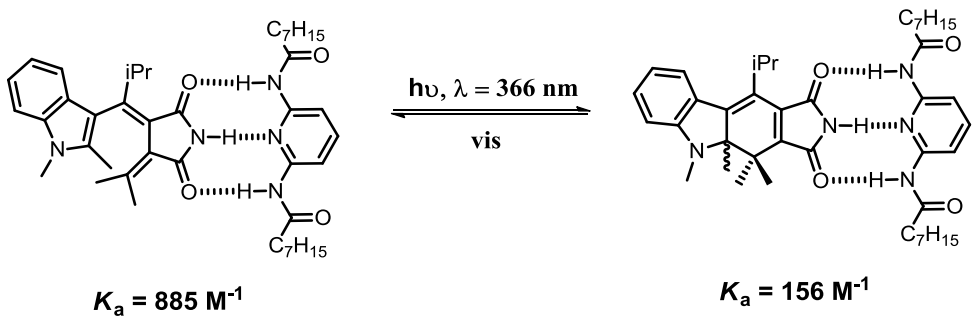

Figure 4.3 Photoswitchable indolylfulgimide and 2,6-bis(octanoylamino)pyridine hydrogen bonded complexes studied by Yokoyama and co-workers. K_a values were determined via UV-Vis methods in toluene at 294 K.

An example of host-guest molecular recognition using the azobenzene photoswitch was studied by Hunter. Two azobenzene units with *p*-carboxylate groups were attached to a central 1,3-diamidobenzene linker (Figure 4.4). The 100% pure *trans* isomer when titrated with guanidinium hydrochloride in DMSO resulted in an association constant of 2200 M^{-1}.[6] Irradiation using UV light (λ = 345 nm) resulted in a 1:1:1 mixture of *trans-trans*, *cis-trans*, and *cis-cis* isomers. Separation of the isomers was not achievable so the next titration was carried out with the mixture as each isomer had different resolved signals in the spectrum. Using the proton signals of the *cis-cis* isomer, the association constant with guanidinium hydrochloride was calculated to be 2.0 x 10^4 M^{-1}. The authors note that each association constant determined should be taken as an estimate as the complexation has large errors due to the complexity of the system. For example, both the azobenzene arrays and guanidinium have multiple binding sites and the second titration was carried out on a mixture and not pure *cis-cis* isomer. Nonetheless, the *cis-cis* isomer resulted in an order of magnitude increase in association constant which was possible due to a successful manipulation of the photoswitchable array.

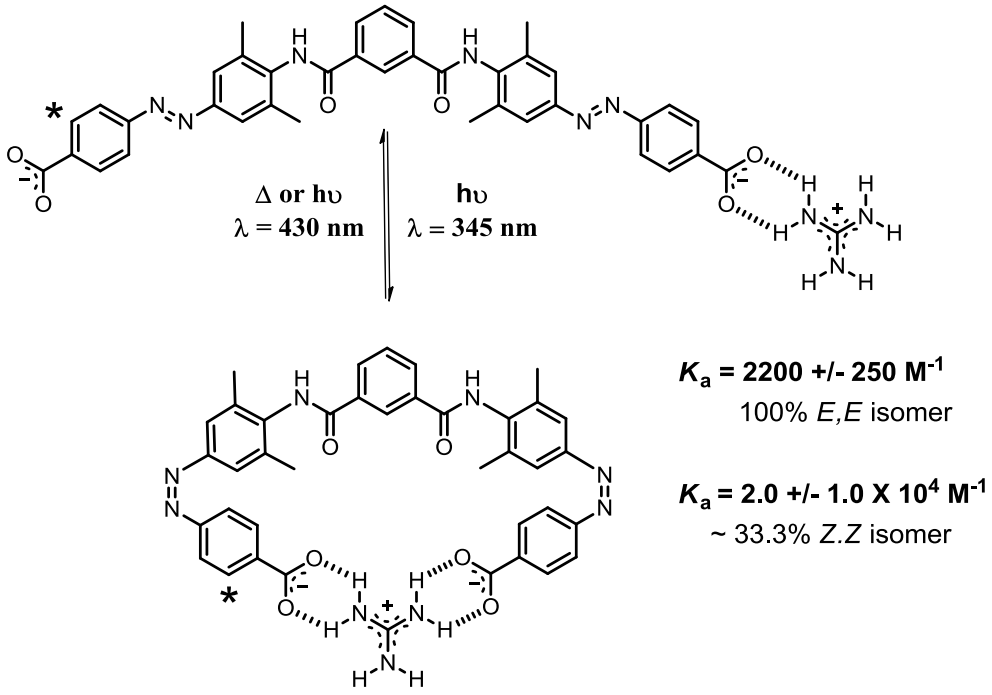

Figure 4.4 Complexation of guanidinium to a *trans, trans* di-azo isomer and a 33.3% mixture of a *cis, cis* di-azo isomer studied by Hunter and co-workers. The star indicates the signals monitored via ^{1}H NMR to determine K_a values in DMSO-d_6 at 298 K.

The above examples were all successful in utilizing a photoswitching moiety to achieve modulated binding results for different isomers. In all of these cases, the photoswitch was not incorporated into the binding array itself. Alternatively, the photoswitch either altered the spatial arrangement of the interacting groups which surrounded the switch, or modified the electronic backbone of the array while the array itself remained unaltered. The acceptor arrays which were studied in Chapters 2 and 3 differ from these examples in that the photoswitching unit is directly incorporated into the array itself. This inclusion of the diaryl azo (Ar-N=N-Ar) photoswitch will allow for a spatial rearrangement of acceptors when light is used as a stimulus. The *trans* isomer has been shown to provide an optimal arrangement for binding with the 2-aminoindole donor arrays. Isomerization to the *cis* isomer creates a non-planar array which differs

greatly in the arrangement of the nitrogen donor atoms (Figure 4.5). The concept has been introduced and studied in our group with DDAAA self-complementary photoswitching arrays.[7,8] The study was more complicated than the present work as multiple binding modes were possible between multiple arrays. Nonetheless, lower association constants were determined for *cis-cis* isomer complexation when compared to *trans-trans* binding. Herein, this chapter will focus on a comparative study between *trans* and *cis* isomers of our photoswitching arrays. Arrays **(*E*)-2** and **(*E*)-3** were chosen for analysis to achieve upper and lower limits for our binding arrays. Triazine containing azo-compounds have been found to isomerize poorly in non-polar solvents[7,8] so **(*E*)-4** has been omitted. Utilizing light as the external stimulus, the photochemical properties will be assessed and complexation with 2-aminoindole donor arrays will be determined.

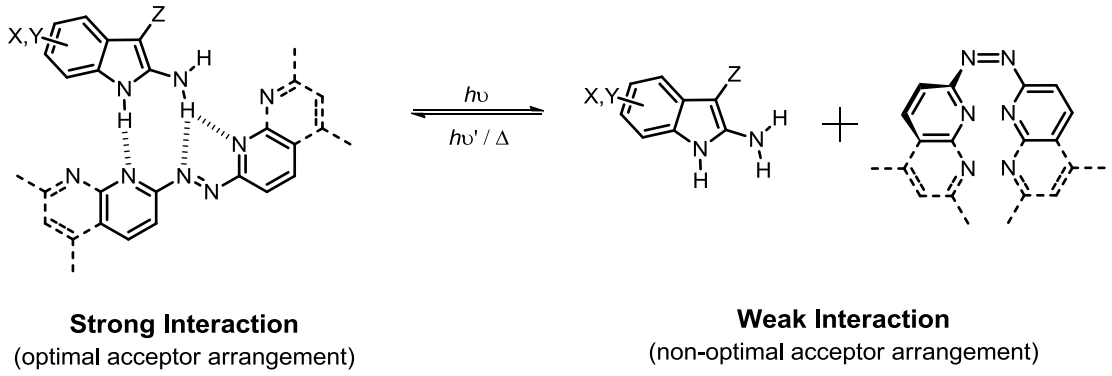

Figure 4.5 Isomerization of our hydrogen bonded complexes depicting strong and weak interactions as a result of the Z isomers. The dashed lines of the acceptor array indicates possible binding geometries.

4.2 Results and Discussion

4.2.1 Isomerization behavior of (*E*)-2 and (*E*)-3 and isolation of (*Z*)-2 and (*Z*)-3

The UV-Vis spectrum of arrays **(*E*)-2** and **(*E*)-3** were obtained in $CHCl_3$ at 10^{-4} M (Figure 4.6). 2,2'-Azopyridine has been studied previously[9] and our results duplicated what has been previously reported. Analogous to **(*E*)-2**, **(*E*)-3** displayed two absorption bands. The large absorption at 342 nm correlates to the $\pi \rightarrow \pi^*$ transition while the weak $n \rightarrow \pi^*$ transition is located at 462 nm. These λ_{max} absorption bands correlate to the approximate wavelengths used for the isomerization of both **(*E*)-2** and **(*E*)-3**.

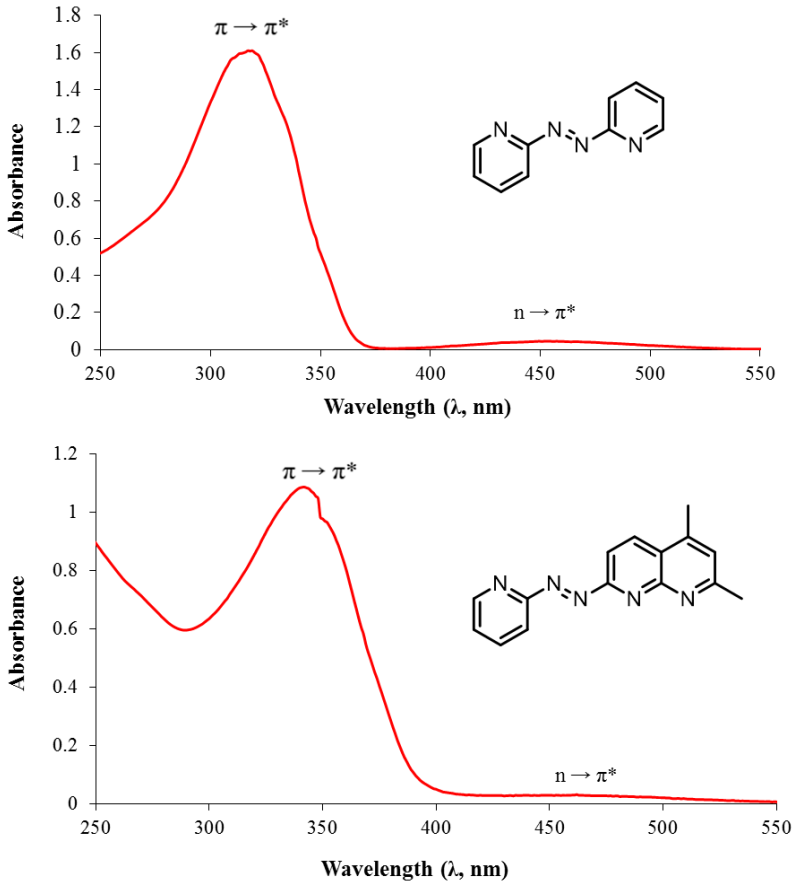

Figure 4.6 UV-Vis absorption spectra of **(*E*)-2** (top) and **(*E*)-3** (bottom). Spectra were recorded in $CHCl_3$ at 1.0 x 10^{-4} M^{-1}.

The *trans* to *cis* isomerizations of **(*E*)-2** and **(*E*)-3** were tested in toluene-d_8 at 1.0 mM concentrations. UV light centered at 360 nm (UVA) was chosen and the isomerization was monitored via ^{1}H NMR. A spectrum was taken at intervals of 10 minutes and the photostationary state was achieved at approximately 30 minutes in both cases. **(*E*)-2** reached approximately 70% conversion to the *cis* isomer, **(*Z*)-2**, which was determined through integration of the *ortho*-hydrogen (Ha) signals of both isomers (Figure 4.7). **(*E*)-3** achieved approximately 35% conversion to **(*Z*)-3** determined by integration of the singlet of proton Hg (Figure 4.8). The smaller conversion of **(*Z*)-3** may

be caused by the bathocromic shift of the π→π* absorption band of **(*E*)-3** when compared to **(*E*)-2**. This red shifting likely results in more energy being absorbed by the aryl groups (eg: naphthyridine) which in turn results in less isomerization.

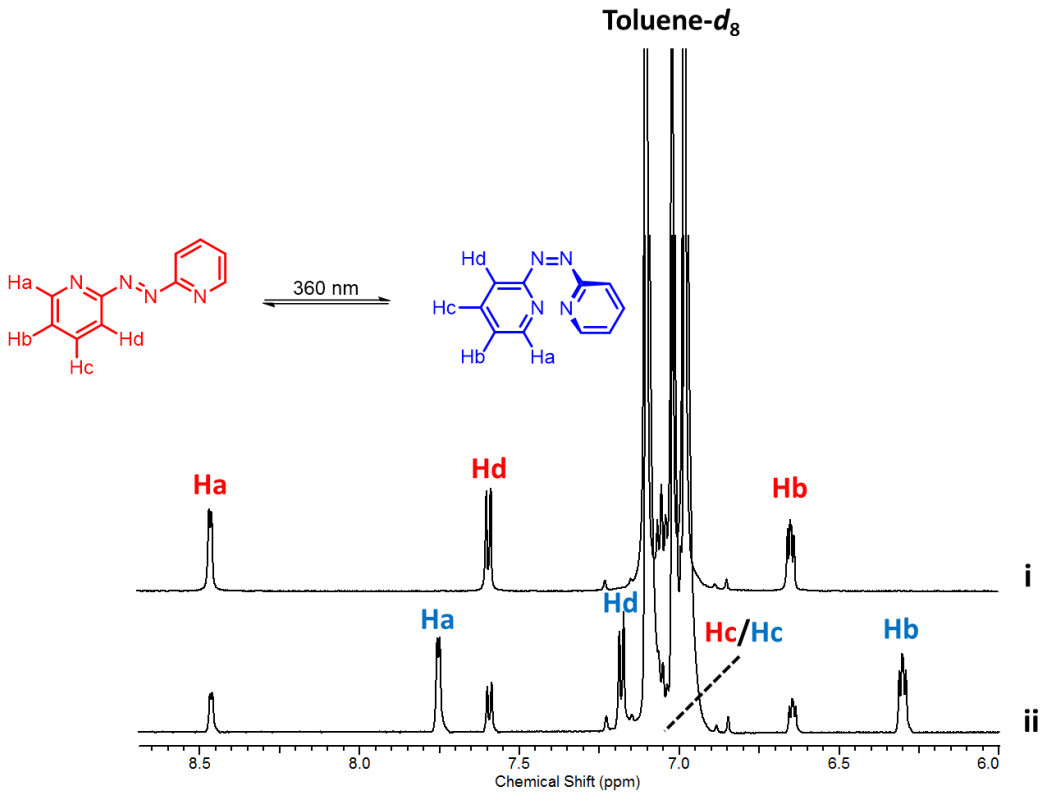

Figure 4.7 ^{1}H NMR spectra of **(*E*)-2** recorded at 1 mM in toluene-d_8 at 298 K (**i**) and the photostationary state after 30 minutes of irradiation @ 360 nm (**ii**). Approximately 70% **(*Z*)-2** was formed at the steady state.

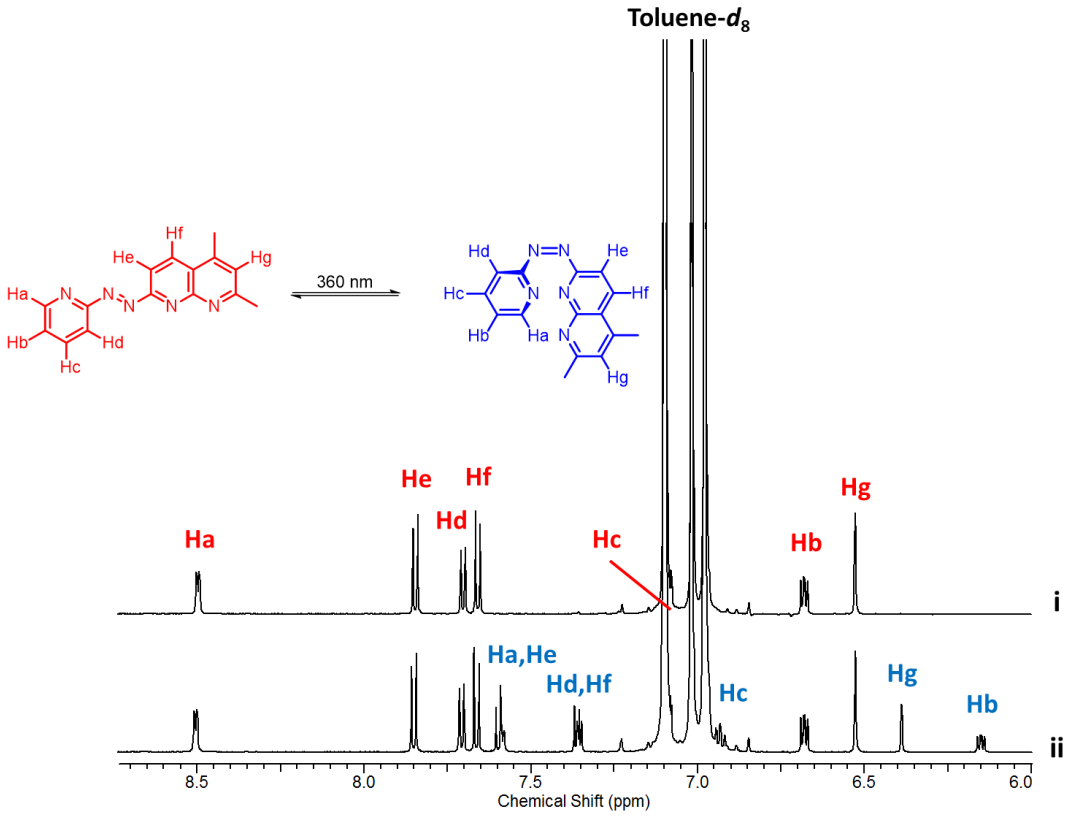

Figure 4.8 ^{1}H NMR spectra of **(*E*)-3** recorded at 1 mM in toluene-d_8 at 298 K (**i**) and the photostationary state after 30 minutes of irradiation @ 360 nm (**ii**). Approximately 35% **(*Z*)-3** was formed at the steady state.

Given the conditions for successful *trans* to *cis* isomerizations, the isolation of the *Z* isomers was then attempted. A known amount of **(*E*)-2** was dissolved in toluene and irradiated at 360 nm for 4 hours to ensure the photostationary state was reached. TLC analysis was performed using diethyl ether as eluent and two spots were visible, one which matched **(*E*)-2** and another with a greater R_f value which was presumed as **(*Z*)-2**. Removal of the toluene under reduced pressure and performing flash chromatography yielded no **(*Z*)-2** isomer. During the heating and removal of the toluene, all of the *cis* isomer which formed converted back to the *trans* isomer. Understanding that any heat applied to the crude isomer mixture would lead to isomerization back to *trans*, a new

method without that influence was attempted. The irradiation of **(*E*)-2** was repeated using acetone in place of toluene as solvent. After the allotted time, the acetone was removed by a stream of dry air while keeping the sample wrapped in foil to exclude light. This method was also advantageous as during the acetone evaporation, the flask remained cold which slows down the thermal reversion. Once a red oil remained, flash chromatography using diethyl ether was repeated which resulted in **(*Z*)-2** eluting first as an orange band. The fraction was collected and the ether was removed with a stream of dry air which resulted in **(*Z*)-2** as a solid in 45% yield (Figure 4.9). The same process was repeated for **(*E*)-3** using acetone as the chromatographic eluent and **(*Z*)-3** was isolated in 35% yield (Figure 4.10). Both *Z* isomers can be stored in a dark freezer indefinitely and used when required.

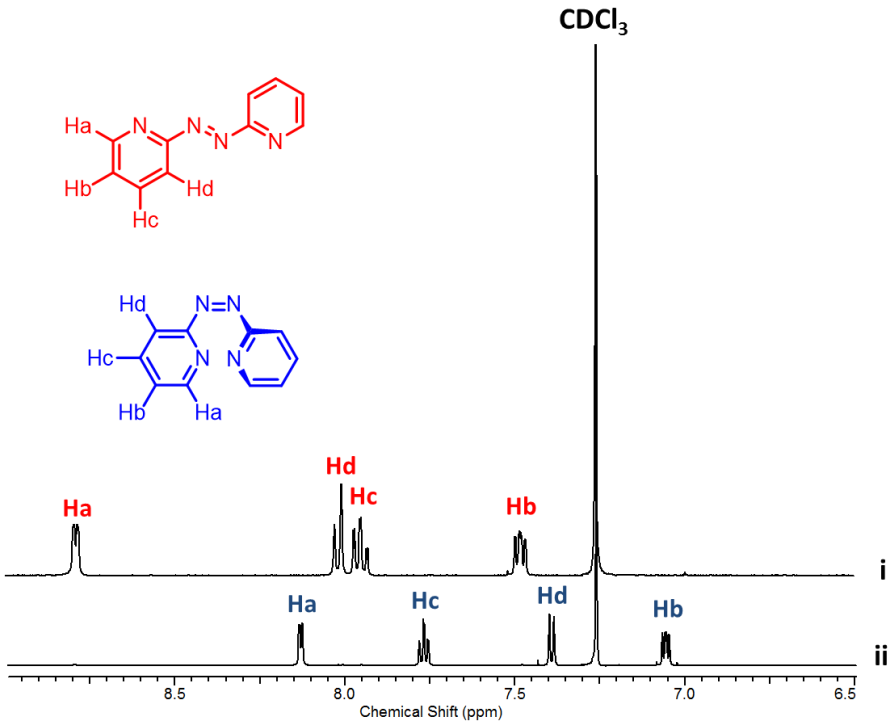

Figure 4.9 ^{1}H NMR spectra of pure **(*E*)-2** isomer (**i**) and **(*Z*)-2** isomer (**ii**) in $CDCl_3$ at 298 K.

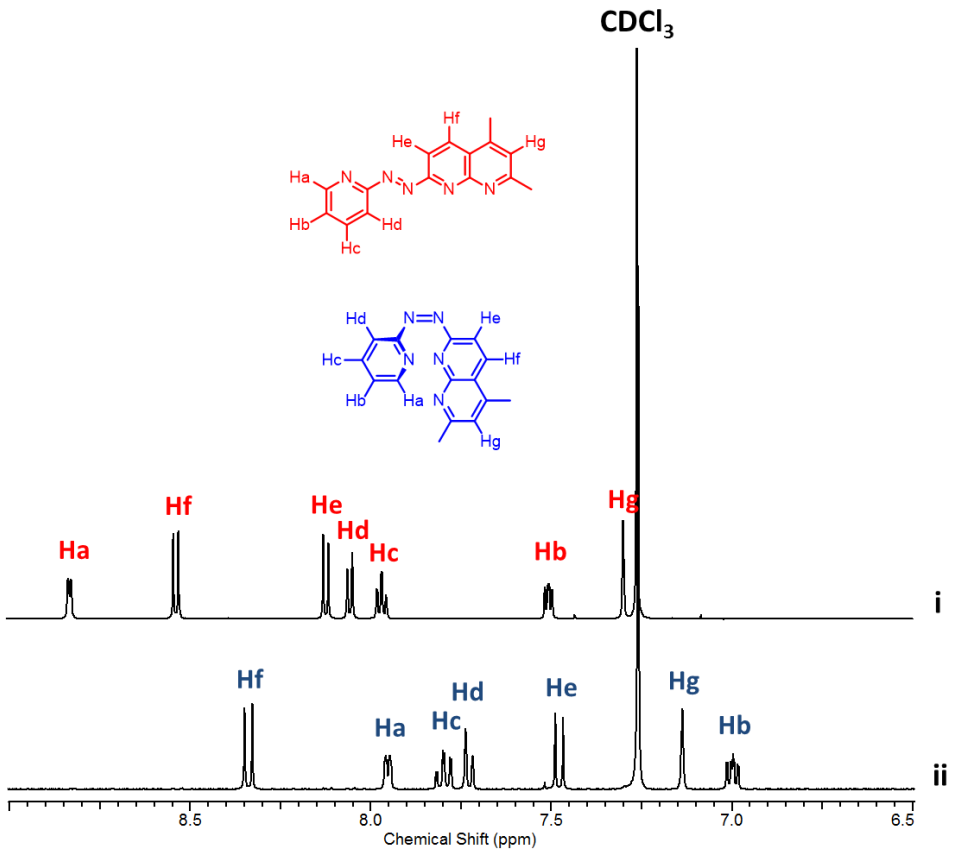

Figure 4.10 ^{1}H NMR spectra of pure **(*E*)-3** isomer (**i**) and **(*Z*)-3** isomer (**ii**) in $CDCl_3$ at 298 K.

UV-Vis absorption spectra were taken of **(*Z*)-2** in toluene which provided a much different spectrum than of pure **(*E*)-2**. Figure 4.11 displays a series of absorption spectra of the thermal reversion of **(*Z*)-2** to **(*E*)-2**. The π→π* transition at 330 nm begins to increase with the subsequent decrease of the n→π* transition at 450 nm. The isosbestic point at 380 nm reveals no other species in solution and the reversion of **(*Z*)-2** to **(*E*)-2** involves no intermediate moieties. The photostationary state was almost completely reached after an hour under ambient conditions.

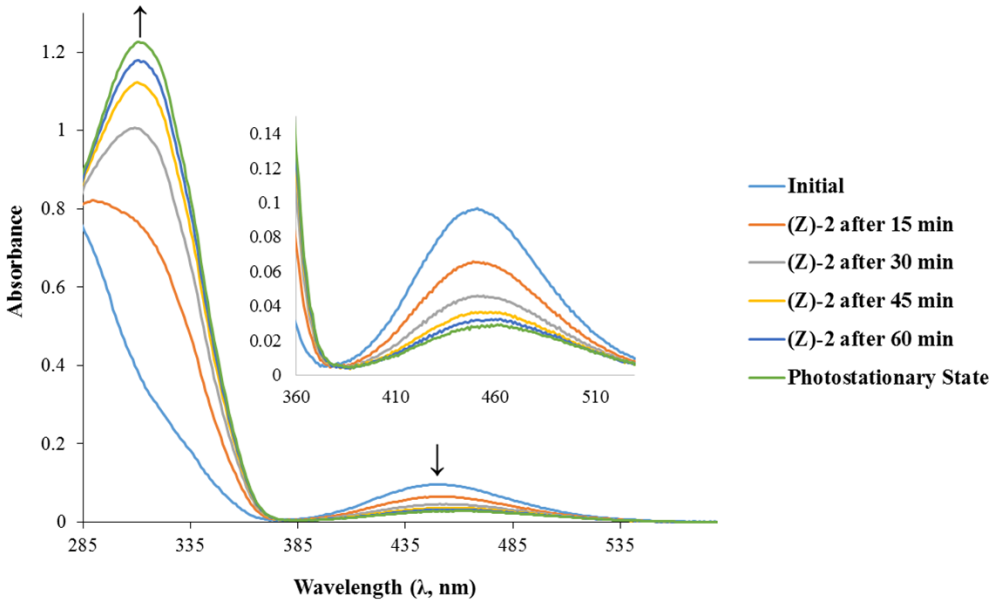

Figure 4.11 UV-Vis absorption spectra of **(*Z*)-2** and its thermal reversion to **(*E*)-2** in toluene at 298 K. [**(*Z*)-2**] = 1.0 x 10^{-4} M^{-1}. Isosbestic point at 380 nm.

An absorption spectrum was also taken of **(*Z*)-3** in $CDCl_3$ as the UV cut-off is at a shorter wavelength. Oddly, there is not much difference in the **(*Z*)-3** spectrum when compared to **(*E*)-3** (Figure 4.12). The photostationary state was reached after approximately 30 minutes as each spectrum recorded after that point did not display any noticeable changes. From visual inspection, it appears that there are two or three isosbestic points. Upon closer inspection of the enhanced areas, the absorption spectra do not overlap at a single point. It is unclear at this time why no pure isosbestic points were observed, as the **(*Z*)-2** spectra contained one. To ensure no other species

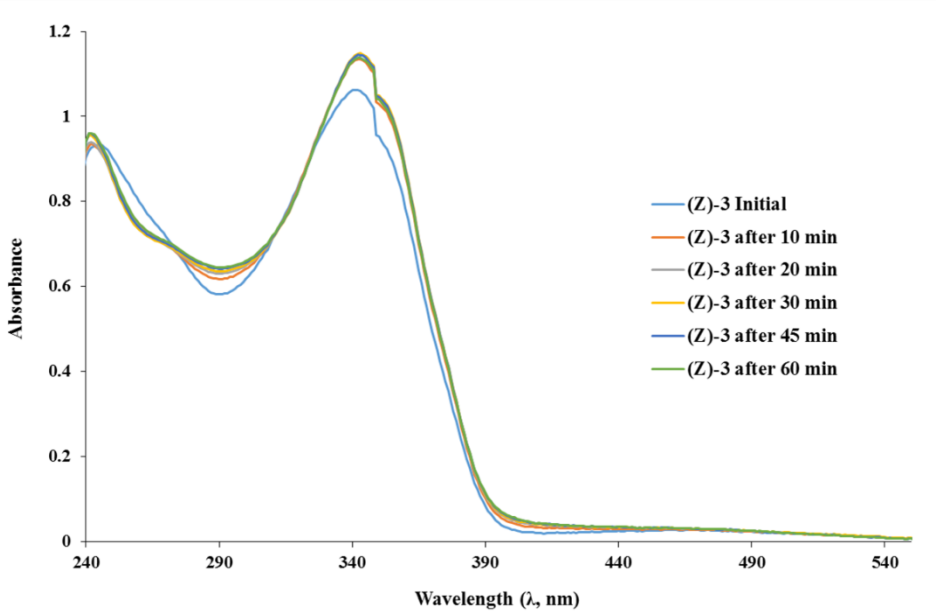

Figure 4.12 UV-Vis absorption spectra **(*Z*)-3** and its thermal reversion to **(*E*)-3** in $CHCl_3$ at 298K. [**(*Z*)-3**] = 1.0 x 10^{-4} M^{-1}.

are existing in solution, the thermal reversion was monitored via ^{1}H NMR. A spectrum was taken of **(*Z*)-3** after 30 minutes of thermal reversion and only **(*Z*)-3** and **(*E*)-3** were observed (Figure 4.13). **(*Z*)-2** was also tested via ^{1}H NMR and the same result was observed.

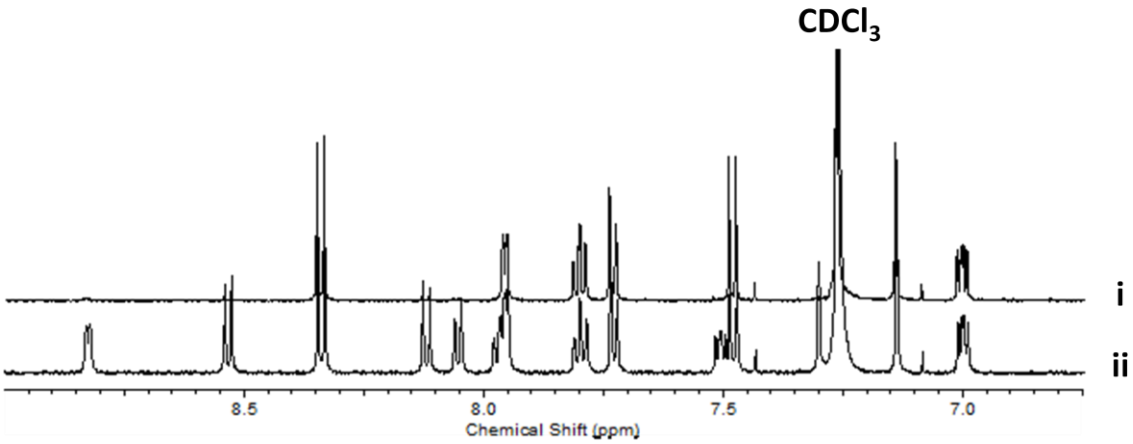

Figure 4.13 Initial ^{1}H NMR spectrum in $CDCl_3$ at 298 K of **(*Z*)-3** (**i**) and after 30 minutes of thermal reversion to **(*E*)-3** (**ii**) proving no other species in solution.

4.2.2 Determination of Complex Stability of (*Z*)-2 in $CDCl_3$

The first titration attempt to measure an association constant for **(*Z*)-2** was performed in $CDCl_3$ with ethyl 2-amino-6-nitro-5-(trifluoromethyl)-1*H*-indole-3-carboxylate (**2-3k**; Chapter 2). The same titration method was used from previous chapters and the NH chemical shift data was input in the Origin® software. The association constant for this particular indole and **(*Z*)-2** was calculated to be 265 M^{-1}. A value of 960 M^{-1} was calculated from pure **(*E*)-2** which is a decrease of 695 M^{-1}. This lower value is indicative that **(*Z*)-2** binds less strongly than **(*E*)-2** to the 2-aminoindole donors as predicted. Although a lower K_a value was determined, the thermal reversion to the *trans* isomer creates some uncertainty within the calculated value. Shown in Figure 4.14 is the spectrum taken at 7 molar equivalents of acceptor which shows approximately 25% **(*E*)-2** isomer. The sample not containing 100% **(*Z*)-2** makes it difficult to deduce

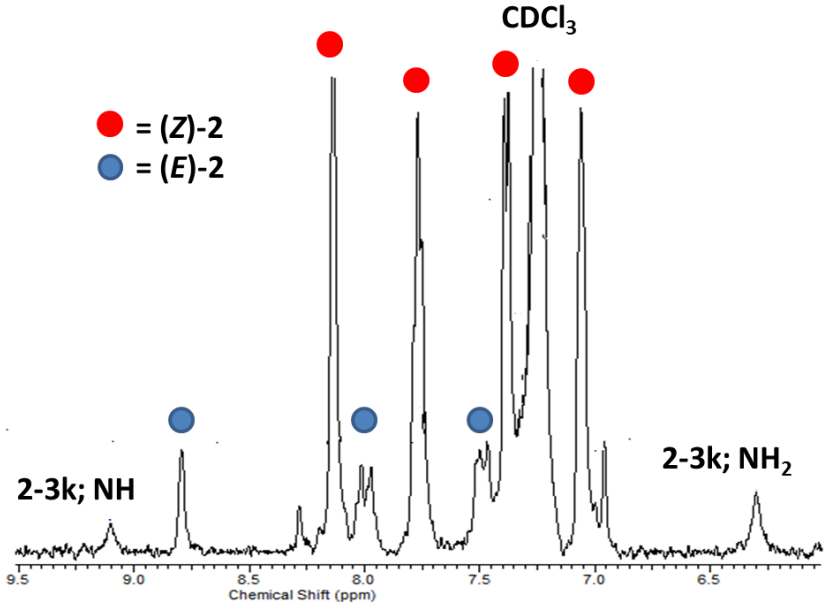

Figure 4.14 ^1H NMR spectrum taken at 7 molar equivalents of acceptor during the titration with **2-3k** showing approximately 25% **(*E*)-2**. Red dots are **(*Z*)-2** and blue dots are **(*E*)-2**. Titration was performed in $CDCl_3$ at 298 K.

how much of the calculated association constant is attributed to the *trans* or *cis* complexation. This problem can be overcome by utilizing the thermal *cis* to *trans* reversion in solution to our advantage. A measured equivalent of **(*Z*)-2** was added to the donor and allowed to thermally isomerize to **(*E*)-2** whilst monitoring the donor groups via ^{1}H NMR. Figure 4.15 is the reversion experiment performed with 1 molar equivalent of **(*Z*)-2**. The percentage of **(*Z*)-2** is pictured to the right of each spectrum which was determined by integrations of the *ortho*-protons. The initial spectrum is labeled in quotations because, as the spectrum appears to have no *E* isomer, there is no way to be certain that none exists in solution. If small amounts of *E* isomer have indeed formed, the concentration may be out of the spectrometer sensitivity range. As **(*E*)-2** starts to form more noticeably in solution, the chemical shift of the NH group starts to resonate more downfield since **(*E*)-2** complexation is more stable than **(*Z*)-2**. The amino group participates in the same downfield shift behaviour but has been omitted for clarity. Once a photostationary state has been reached (or a maximum of 5 hours), the calculated amount of **(*E*)-2** in

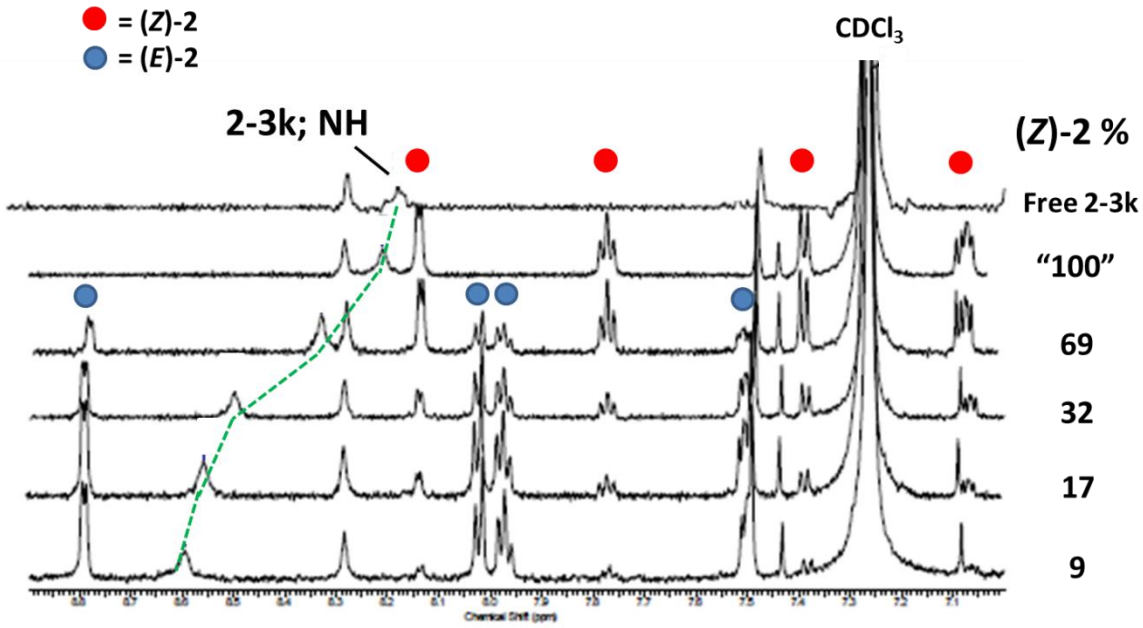

Figure 4.15 ^{1}H NMR stacked plot of the **(*Z*)-2·2-3k** reversion experiment performed in $CDCl_3$ at 298 K for 1 molar equivalent of **(*Z*)-2**. Red dots are **(*Z*)-2** and blue dots are **(*E*)**-2. The percentage of **(*Z*)-2** for the correlating spectra is depicted at the right. The shifting of the NH peak is illustrated by green dashed lines.

solution is plotted against the chemical shift. This collection of data points can then be extrapolated back to where theoretically there is 0 % **(*E*)-2**, or in other words 100% **(*Z*)-2** (Figure 4.16). This reversion process was repeated for a number of different equivalents of **(*Z*)-2** and the results are compiled in Table 4.1. These values were input in Origin® software and fit to the 1:1 binding model. As displayed in Figure 4.17, the curve for the extrapolated

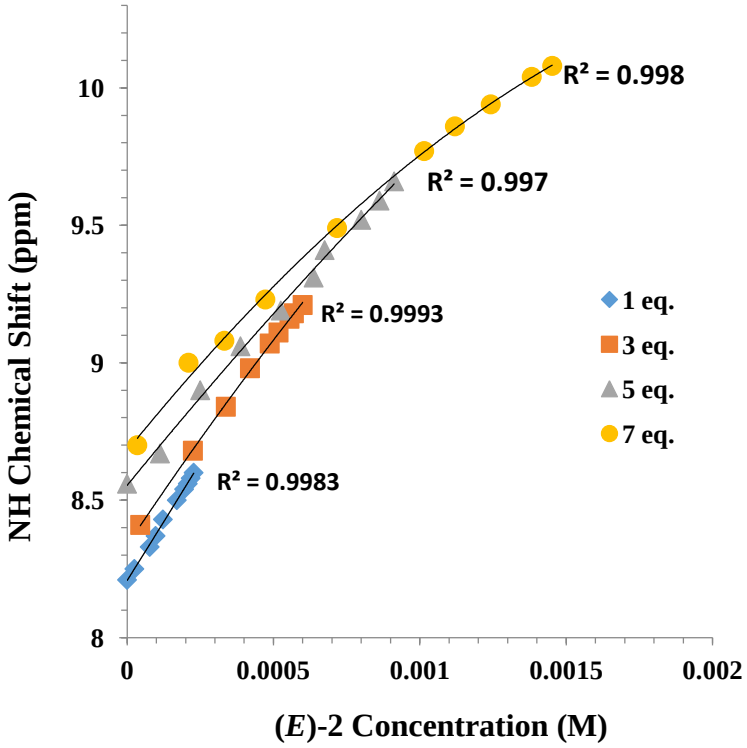

Figure 4.16 Plot of **(*E*)-2** concentration and the NH chemical shift for 1, 3, 5, and 7 molar equivalents of **(*Z*)-2** with respect to **2-3k**. Regression fits are shown at the end of the corresponding curves.

Table 4.1 The extrapolated NH chemical shifts of each **(*Z*)-2** reversion experiment.

Molar Equivalents of (*Z*)-2	**Extrapolated NH Chemical Shift; 0% (*E*)-2 (ppm)**
1	8.21
1.5	8.23
2	8.30
2.5	8.34
3	8.38
4	8.45
5	8.55
7	8.68

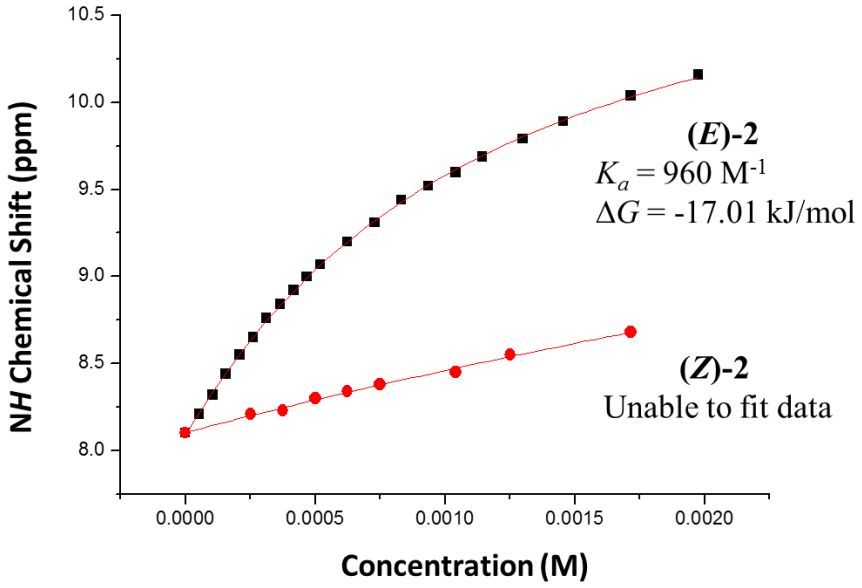

Figure 4.17 The NH chemical shift data of **(*E*)-2** titration (black squares) and calculated 1:1 binding isotherm (red curve) and **(*Z*)-2** extrapolated values (red dots) with a line of best fit to guide the eye (red line).

(*Z*)-2 values varies greatly from the curve for the **(*E*)-2** titration. Unfortunately, the non-linear regression could not calculate an association constant as the data points form a straight line. We can estimate that the value would be considerably lower than 265 M^{-1} but more data points to delineate the isotherm would be needed to confirm that opinion. Nonetheless, this method of reversion proved effective at estimating chemical shifts at theoretical concentrations of 100% **(*Z*)-2**.

4.2.3 Determination of Complex Strength of (*Z*)-2 and (*Z*)-3 with 3-21b in Toluene-d_8

Examination of our extrapolation method continued using toluene-d_8 in place of $CDCl_3$. This decision was made because the measured association constants were higher

in this solvent and thermal reversion back to the *trans* isomer occurs at a slower rate. Octyl 2-amino-6-nitro-5-(trifluoromethyl)-1*H*-indole-3-carboxylate (**3-21b**; Chapter 3) was chosen as it is soluble in toluene-d_8 and the association constants have already been determined with **(*E*)-2** and **(*E*)-3** (Chapter 3). The same ^{1}H NMR based extrapolation method was performed with a wide range of equivalents (1.0 - 30.0 mmol) of **(*Z*)-2** to ensure delineation of the binding isotherm. The same downfield chemical shift of the donor groups can be observed during the thermal reversion to the *trans* isomer (Figure 4.18). Figures 4.19, 4.20, and 4.21 depict the results of the extrapolation trials where the extrapolated values are compiled in Table 4.2.

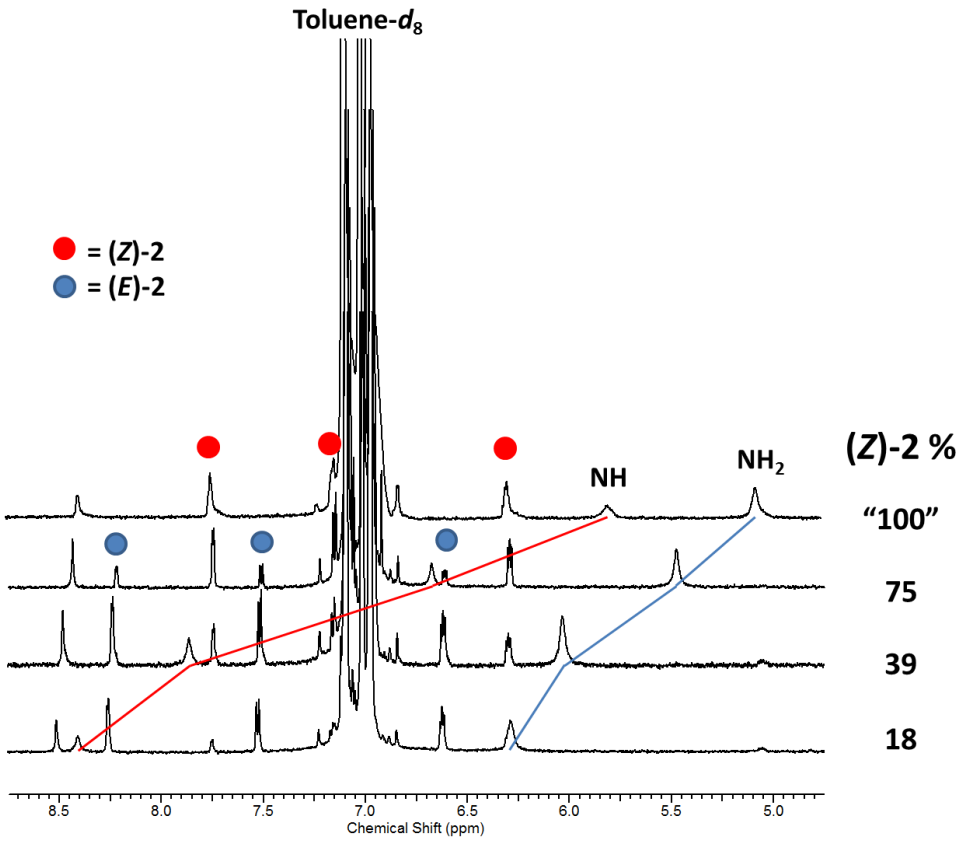

Figure 4.18 ^{1}H NMR stacked plot of the **(*Z*)-2·3-21b** reversion experiment performed in toluene-d_8 at 298 K for 1 molar equivalent of **(*Z*)-2**. Red dots are **(*Z*)-2** and blue dots are **(*E*)-2**. The percentage of **(*Z*)-2** for the spectra is depicted at the right. The shifting of the NH peak is identified using red lines and NH_2 peak is identified using blue lines.

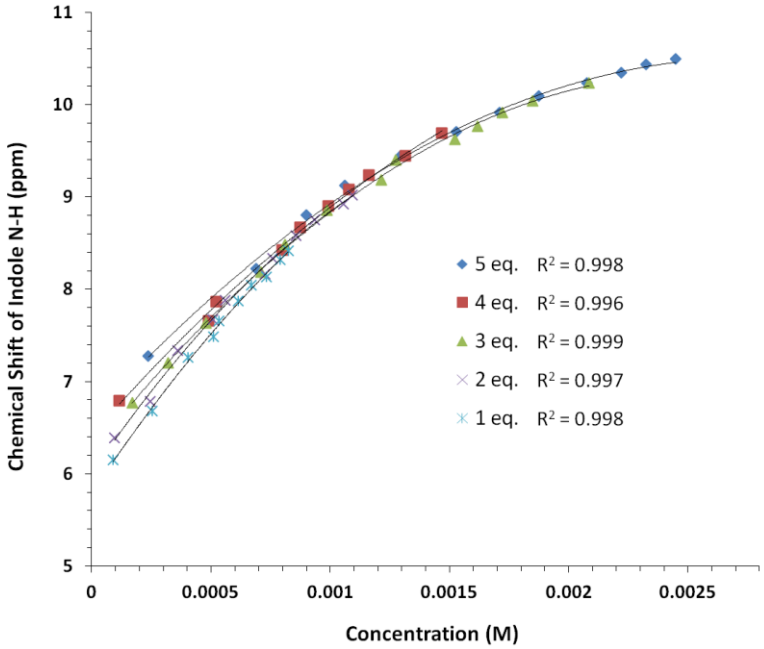

Figure 4.19 Plot of **(*E*)-2** concentration and the NH chemical shift for 1, 2, 3, 4, and 5 molar equivalents of **(*Z*)-2** with respect to **3-21b**. Regression R^2 values are noted beside the legend.

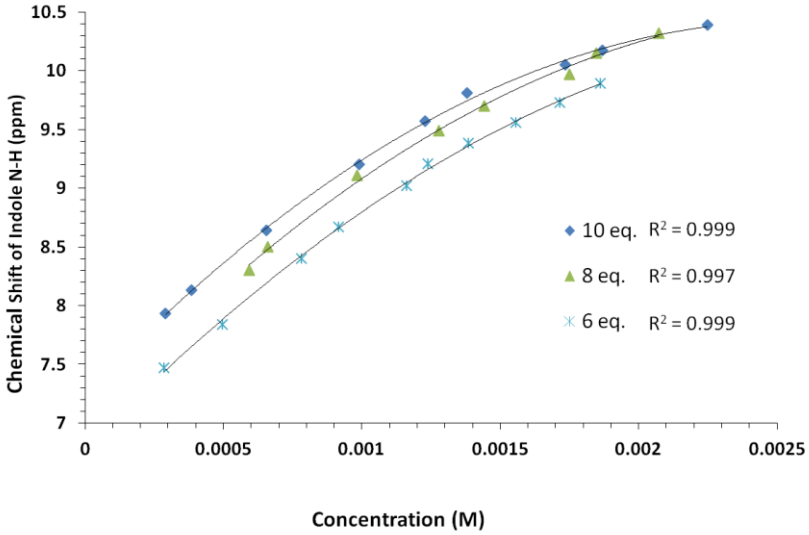

Figure 4.20 Plot of **(*E*)-2** concentration and the NH chemical shift for 6, 8, and 10 molar equivalents of **(*Z*)-2** with respect to **3-21b**. Regression R^2 values are noted beside the legend.

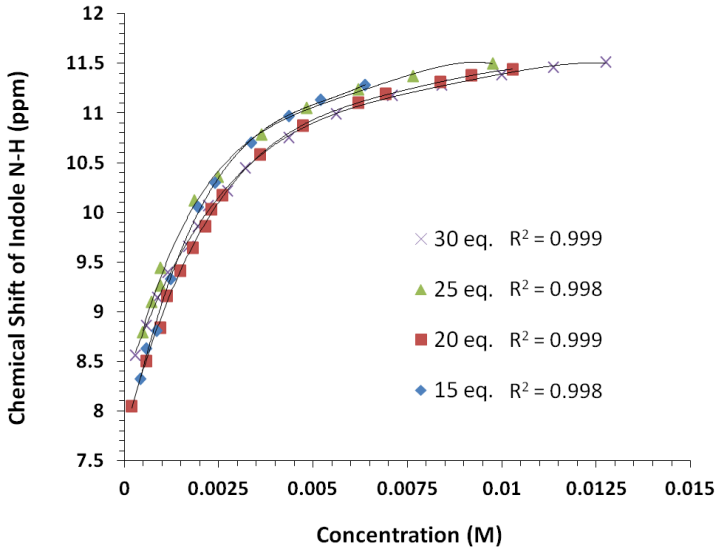

Figure 4.21 Plot of **(*E*)-2** concentration and the NH chemical shift for 15, 20, 25, and 30 molar equivalents of **(*Z*)-2** with respect to **3-21b**. Regression R^2 values are noted beside the legend.

Table 4.2 The extrapolated NH chemical shifts of each **(*Z*)-2** reversion experiment with **3-21b**.

Equivalents of (*Z*)-2	N*H* δ[a]	Equivalents Of (*Z*)-2	N*H* δ[a]	Equivalents Of (*Z*)-2	N*H* δ[a]
1	5.79	**5**	6.63	**15**	7.63
2	6.01	**6**	6.78	**20**	7.76
3	6.24	**8**	7.00	**25**	8.13
4	6.42	**10**	7.24	**30**	8.28

[a]Calculated from the regression fit of the individual reversion experiments; [(*E*)-2] % = 0

12 different reversions were performed with each extrapolation regression fitting very well ($R^2 \geq 0.996$) to the collected data. 30 molar equivalents of **(*Z*)-2** were needed to achieve delineation of the binding isotherm. Plotting these values using the 1:1 non-linear regression resulted in an excellent fit ($R^2 = 0.997$) and an association constant of 75

M^{-1} (ΔG = -10.70 kJ/mol; Figure 4.22) was calculated. A titration with pyridine was also performed to compare the binding with a single similar acceptor site (Figure 4.23). All titration data is summarized in Table 4.3 and Figure 4.24 depicts the three combined isotherms.

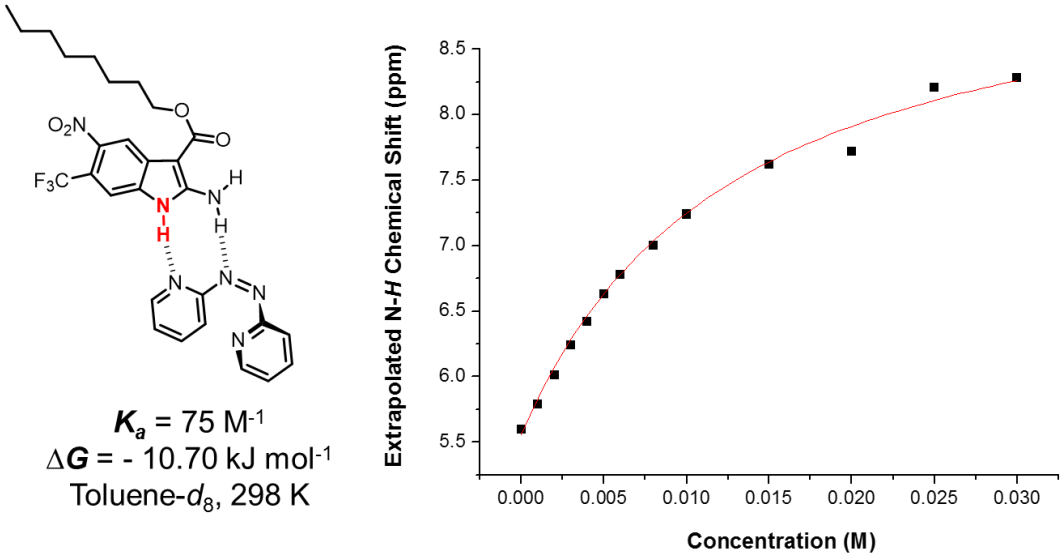

Figure 4.22 Calculated indole N-*H* binding isotherm and the extrapolated data points of the **(*Z*)-2·3-21b** reversions. K_a, calculated free energy of complexation, and experimental conditions are noted below the schematic of the possible complex.

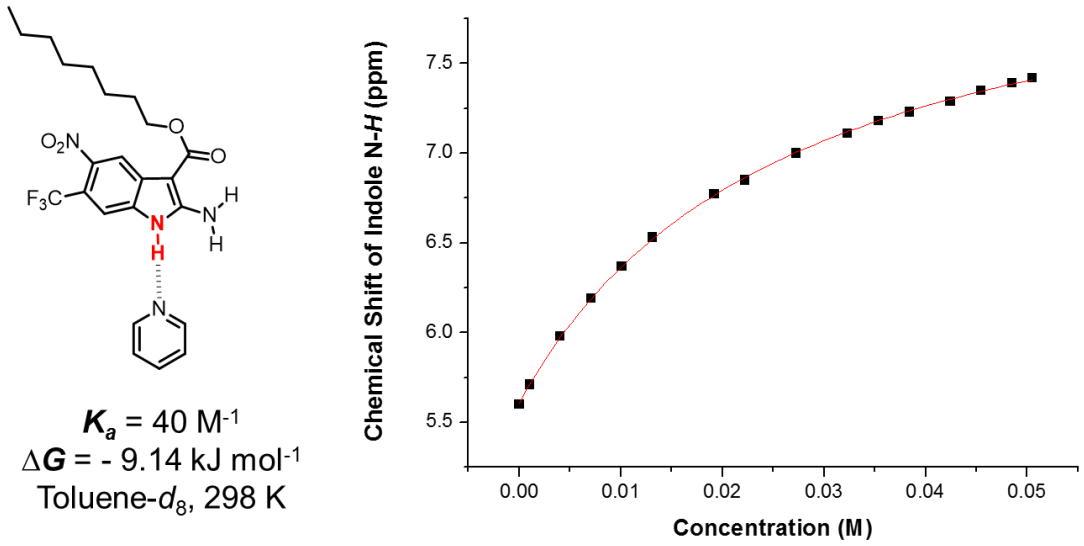

Figure 4.23 Calculated indole N-*H* binding isotherm and ^{1}H NMR titration data for complex formation between Pyridine and **3-21b**. K_a, calculated free energy of complexation, and titration conditions are noted below the schematic of the complex.

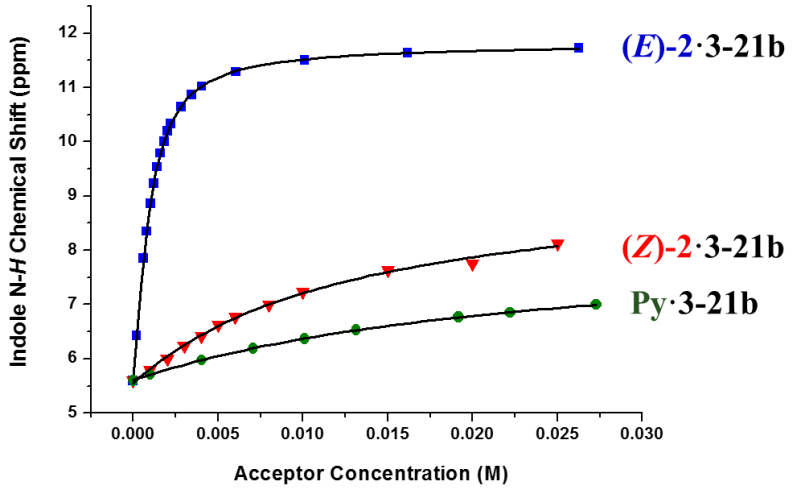

Figure 4.24 A comparison of all data points and calculated N-*H* binding isotherms for **(*E*)-2**, **(*Z*)-2**, and Py with **3-21b**.

Table 4.3 Association constants (K_a), free energies of complexation (ΔG), calculated chemical shifts of free indole, fully complexed indole, and total change in chemical shift (δ_{free}, δ_{bound}, and $\Delta\delta_{max}$ respectively) of **(*E*)-2**, **(*Z*)-2**, and Py with **3-21b**. All experiments were performed in toluene-d_8 at 298 K.

Acceptor	K_a (M^{-1})[a]	ΔG (kJ mol^{-1})[a]	δ_{free} (ppm) N*H*[a] NH_2[b]	δ_{bound} (ppm) N*H*[a] NH_2[b]	$\Delta\delta_{max}$ (ppm) N*H* NH_2
(*E*)-2*	2100 ± 282	-18.99 ± 0.34	5.62 5.01	11.81 7.84	6.19 2.83
(*Z*)-2	75	-10.70	5.56 4.99	9.44 7.01	3.88 2.02
Py	40	-9.1	5.61 5.02	8.32 5.41	2.71 0.39

[a] Values calculated from Eq. 6 (chapter 2) using a 1:1 regression model and the indole N*H* data. . [b]Same procedure using NH_2 data. * Data taken from chapter 3.

The value of 75 M^{-1} for the **(*Z*)-2** trials correlates to a drop of 8.3 kJ/mol in free energy of complexation when compared to the titration of **3-21b** with **(*E*)-2**. This result is to be expected due the certain misalignment of the acceptor atoms when compared to the optimal binding geometry of **(*E*)-2**. Also, the magnitude of the chemical shifts of the donor groups are mirrored by their complex stabilities. The shifts for both donor groups in the **(*E*)-2** titration are greater than **(*Z*)-2** and pyridine as the association constant was larger. The slightly higher value of **(*Z*)-2** compared to pyridine is most likely attributed to the potential of an azo nitrogen to participate in weak complexation. The small $\Delta\delta_{max}$ for the amino group in the pyridine titration (0.39) is smaller than would be expected. We attribute this small number to the pyridine binding largely or solely with the indole NH and having limited interaction with the neighboring amino proton.

The same extrapolation procedure was repeated for **(*Z*)-3** and indole **3-21b**. A titration of 2,4-dimethyl-1,8-naphthyridine (Nap) was performed initially to get an estimate of the potential complex strength of **(*E*)-3** (Figure 4.25). The heterocycle was synthesized by hydrogenation of the chloride derivative (**3-3c**; chapter 3). The titration results yielded an association constant of 9100 M^{-1} which is 2.84 kJ/mol lower than the titration with **(*E*)-3**. These results are indicative that **(*Z*)-3** should bind just slightly

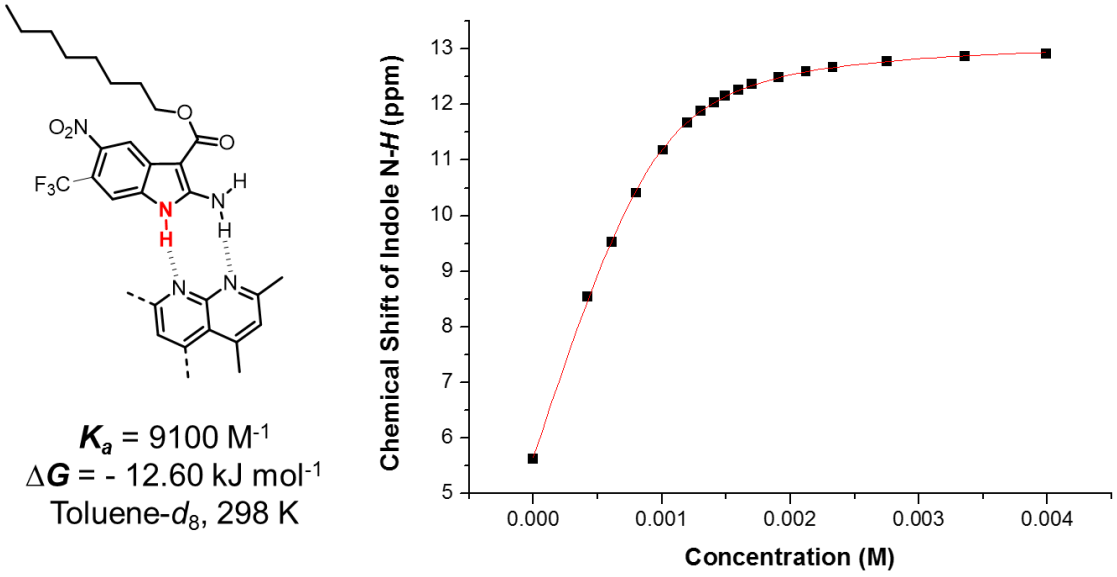

Figure 4.25 Calculated indole N-*H* binding isotherm and ^{1}H NMR titration data for complex formation between Nap and **3-21b**. K_a, calculated free energy of complexation, and titration conditions are noted below the schematic of the complex.. Dashed methyl groups indicate that they could be on either side during complexation.

more strongly than Nap due to the additional azonitrogen acceptor, assuming the analogous trend is followed compared to the pyridine and **(*Z*)-2** results. A series of five extrapolations were performed with **(*Z*)-3** and the plotted results are shown in Figure 4.26 with the extrapolated values being compiled in Table 4.4.

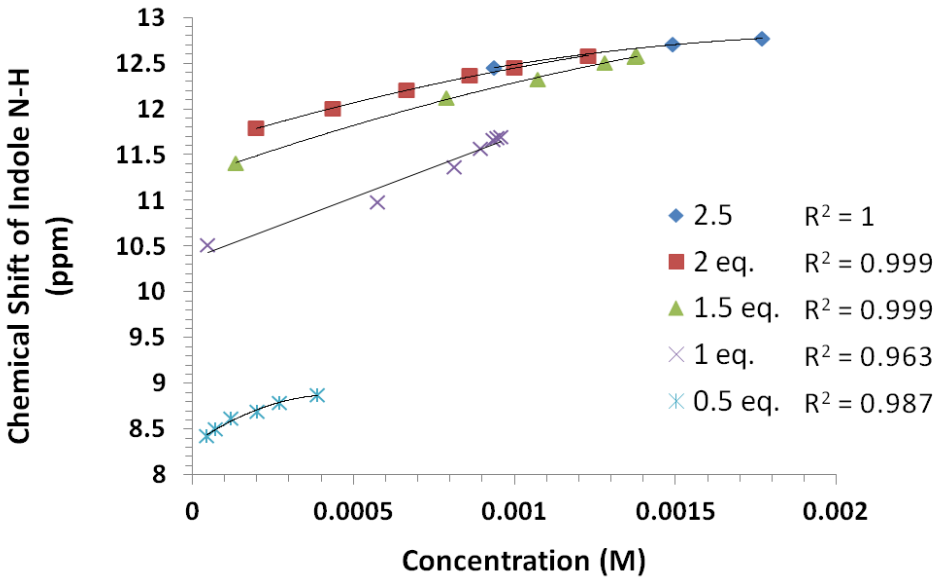

Figure 4.26 Plot of **(*E*)-3** concentration and the NH chemical shift for 0.5, 1, 1.5, 2, and 2.5 molar equivalents of **(*Z*)-3** with respect to **3-21b**. Regression R^2 values are noted beside the legend.

Table 4.4 The extrapolated NH chemical shifts of each **(*Z*)-3** reversion experiment with **3-21b**.

Molar Equivalents of (*Z*)-3	**Extrapolated NH Chemical Shift; 0% (*E*)-3 (ppm)**
0.5	8.33
1	10.37
1.5	11.25
2	11.58
2.5	11.69

The interpretation of the ^{1}H NMR data from these reversions was more complex than the **(*Z*)-2** trials. There are a total of 14 proton chemical shifts in the spectrum of a mixture of **(*E*)-3** and **(*Z*)-3**. During the course of the reversion, both the indole proton and especially the amino protons overlapped with these signals which meant no chemical

shift could be recorded. Also, the thermal reversion from **(*Z*)-3** to **(*E*)-3** was much faster than the **(*E*)-2** reversions. These two factors led to a shortage of data points in the reversion data (i.e. 2.5 eq. has three points) to a point where not enough data could be collected to determine the amino results. Nonetheless, these five points were fit to the 1:1 non-linear regression ($R^2 = 0.999$) and resulted in a K_a value of 13000 M^{-1}. This large value is indicative of strong binding which is likely a result of multiple complex geometries in solution similar to **(*E*)-3** if a C-H hydrogen bond is considered (Figure 4.27). Figure 4.28 depicts all the binding isotherms which illustrates what little difference there exists in the association constants with the three acceptor arrays. Table 4.5 lists the binding data collected from this study.

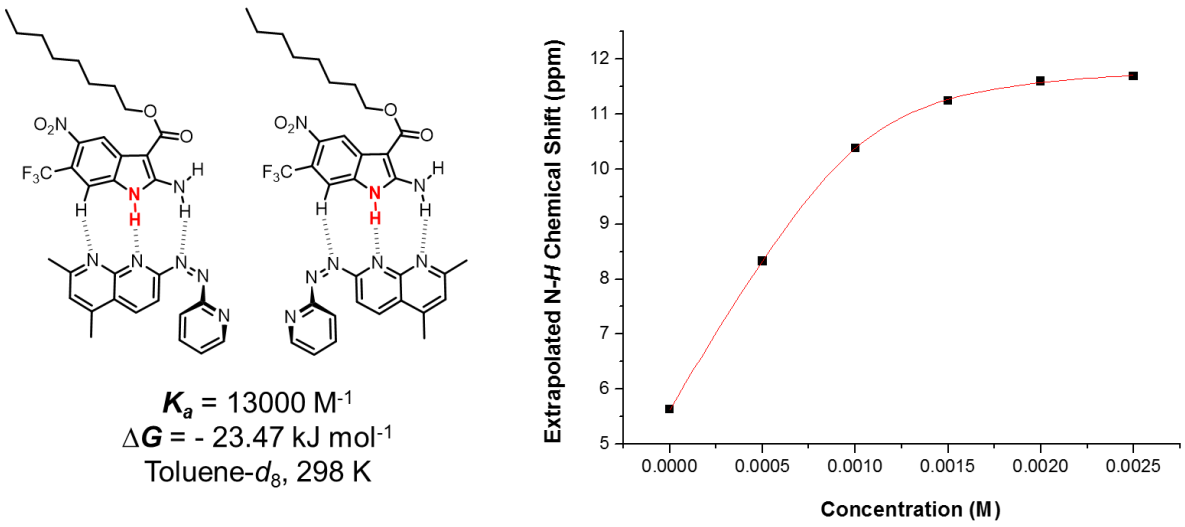

Figure 4.27 Calculated indole N-*H* binding isotherm and the extrapolated data points of the **(*Z*)-3·3-21b** reversions. K_a, calculated free energy of complexation, and experimental conditions are noted below the schematic of two possible complex geometries.

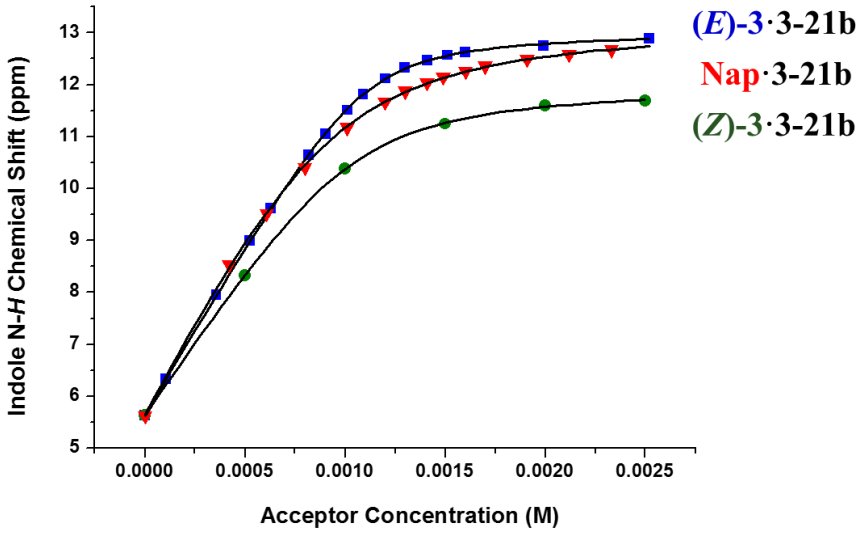

Figure 4.28 A comparison of all calculated N-*H* binding isotherms for **(*E*)-3**, **(*Z*)-3**, and Nap with **3-21b**.

Table 4.5 Association constants (K_a), free energies of complexation (ΔG), calculated chemical shifts of free indole, fully complexed indole, and total change in chemical shift (δ_{free}, δ_{bound}, and $\Delta\delta_{max}$ respectively) of **(*E*)-3**, **(*Z*)-3**, and Nap with **3-21b**. All experiments were performed in toluene-d_8 at 298 K.

Acceptor	K_a (M^{-1})[a]	ΔG (kJ mol^{-1})[a]	δ_{free} (ppm) N*H* [a] NH_2 [b]	δ_{bound} (ppm) N*H* [a] NH_2 [b]	$\Delta\delta_{max}$ (ppm) N*H* NH_2
(*E*)-3*	29000 ± 2600	-25.44 ± 0.23	5.65 5.03	13.05 8.33	7.40 3.30
(*Z*)-3	13000	-23.47	5.63 NA	12.01 NA	6.38 NA
Nap	9100	-22.60	5.65 5.04	13.19 7.95	7.54 2.91

[a] Values calculated from Eq. 6 (chapter 2) using a 1:1 regression model and the indole N*H* data. . [b]Same procedure using NH_2 data. * Data taken from chapter 3.

The calculated K_a value for the **(*Z*)-3** extrapolations is less than half the value of the titration results with **(*E*)-3**. However, this is only a 1.97 kJ/mol drop in the free energy of complexation. The naphthyridine ring proved to be effective at keeping the complexation strength elevated with the pyridine not being a larger contributor to the overall stability of the complex. The $\Delta\delta_{max}$ value of the NH group for the Nap titration remained relatively unchanged. The amino $\Delta\delta_{max}$ for the Nap result is slightly lower which is likely due to the lack of azo nitrogen and pyridine which are the main bonding components to that donor group. As mentioned above, no amino results were able to be collected from the **(*Z*)-3** extrapolations.

A recent study by Bonifazi and co-workers can provide some potential rationale for some of the results which has been observed in this study thus far. Observed in the **(*Z*)-3** extrapolation results, the δ_{bound} value for the NH shift has dropped by approximately 1 ppm when compared to both the **(*E*)-3** and Nap titration results. This decrease in the δ_{bound} value seems unusual considering Nap which has one less acceptor nitrogen remained the same δ_{bound} value as the **(*E*)-3** titration. The same result was observed by Bonifizi and co-workers with their own complementary array. An ADA uracil-azobenzene derivative was titrated with its complementary DAD diaminopyridine array.[10] A value of 6170 M^{-1} was determined in toluene-d_8 when the azobenzene tail was in the *trans* form. Once the *cis* form was isolated and the same titration performed, a lower association constant of 4040 M^{-1} was calculated. Considering the binding complex geometry of both arrays remains unchanged, the *cis* conformer must be participating in a repulsive steric clash with the incoming DAP which resulted in weaker complexation (Figure 4.29). Additionally, the δ_{bound} and $\Delta\delta_{max}$ of the imide proton of the *cis*-uracil

component was lower than the *trans* imide isomer results. These two results are analogous to the lower association constant determined for the **(*Z*)-3** extrapolations and smaller δ_{bound} and/or $\Delta\delta_{max}$ for the NH group.

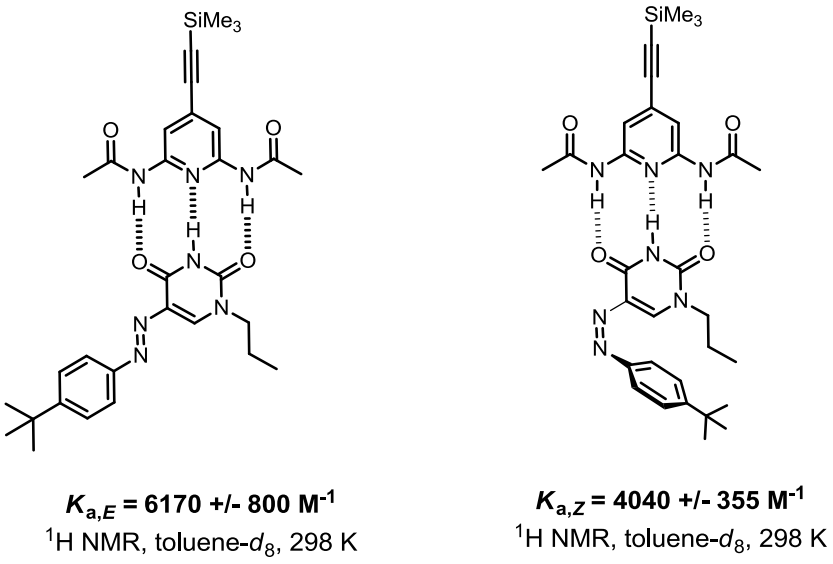

Figure 4.29 The diaminopyridine and uracil-*E*- and *Z*-azobenzene hydrogen bonded DAD-ADA complexes studied by Bonifizi and co-workers.

The rate of thermal reversion was also studied with the ADA-DAD complex just discussed. A four-fold increase of thermal reversion was calculated when the DAD component was binding to the *cis* isomer when compared solely to the *cis* isomer (Figure 4.30). They attribute this phenomenon to the redistribution of electron density of the azo double

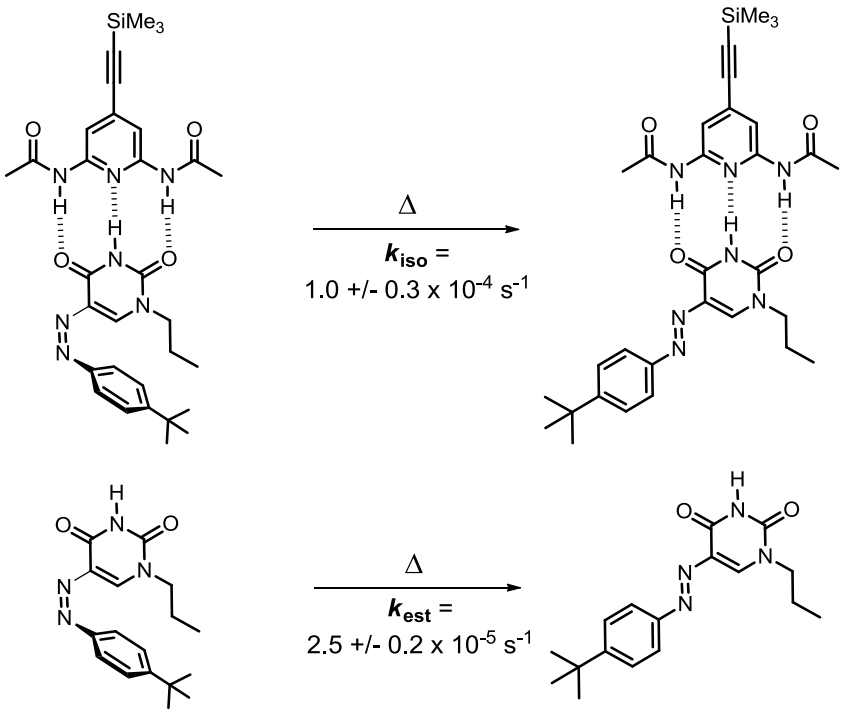

Figure 4.30 The rate of thermal reversion of the *Z*-DAD-ADA complex (above) and the uracil-*Z*-azobenzene separately (below).

bond. Utilizing DTF methods, they determined that this redistribution of electron density of the C-N=N-C moiety when the ADA component is binding is expected to lower the torsional energy barrier. This lowering of energy therefore results in faster thermal reversion to the *trans* isomer. If this concept is applied to this work, the conclusion could be made that this discovery can explain why the thermal reversion of **(*Z*)-2** and **(*Z*)-3** is accelerated when in solution with **3-21b**. Determination of these rate constants could be a topic of future examinations for this work.

Photochromic reversibility of these complexes is an important characteristic which needed to be accessed for possible applications as photoisomerizable supramolecular polymers. An NMR tube was injected with 0.5 mL of a 1.0 mM solution of both **3-21b** and **(*E*)-2** in a 1:1 ratio dissolved in toluene-d_8. The tube was irradiated for

one hour using a mercury lamp equipped with a 350 nm bandpass filter. A spectrum was taken after the allotted time for which the tube was then irradiated for one minute using 4 LED lights centered at ~ 530 nm and a spectrum was recollected. Figure 4.31 depicts the ^{1}H NMR spectra of this photoirradiation evaluation.

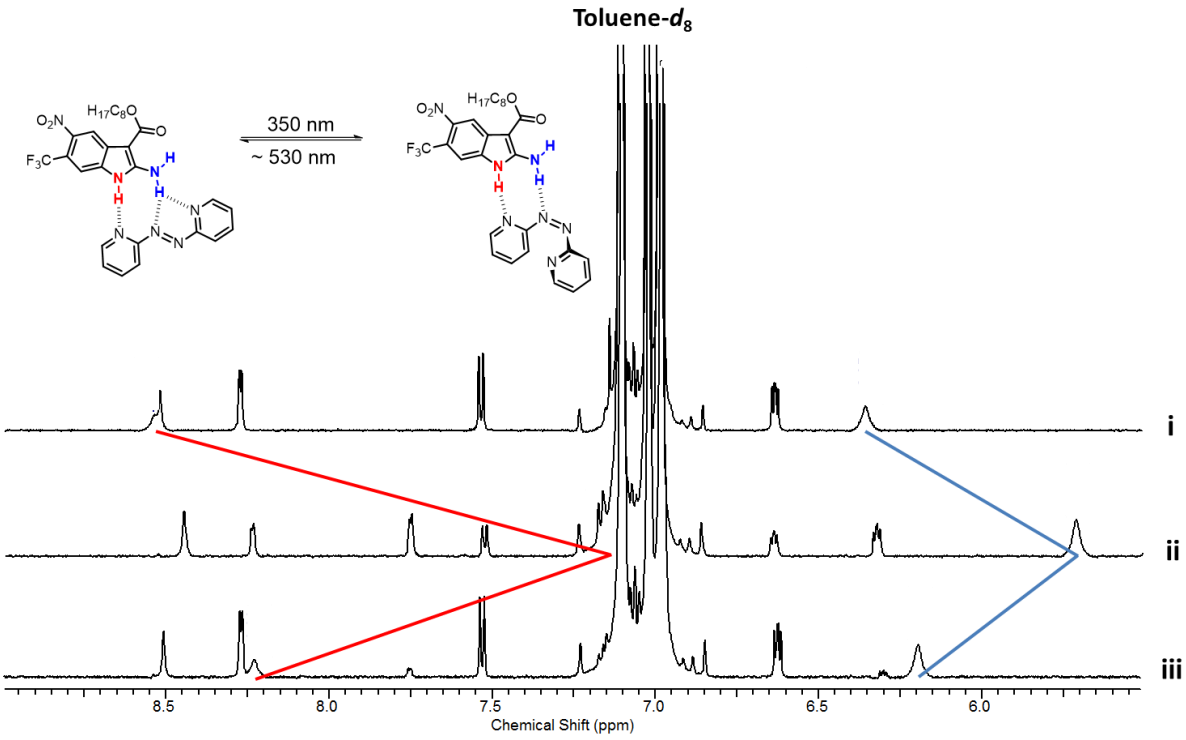

Figure 4.31 ^{1}H NMR spectra of a 1:1 solution of **(*E*)-2·3-21b** (**i**), the same solution after 350 nm irradiation (**ii**), the same solution after 530 nm irradiation (**iii**). The shifting of the NH peaks are identified by red lines and the NH_2 peaks by blue lines. Spectra were collected in toluene-d_8 at 298 K.

After the 350 nm irradiation, both the NH and NH_2 shifts resonate upfield due to formation of **(*Z*)-2**. Approximately 60% of **(*E*)-2** was converted into **(*Z*)-2** which is slightly less than results performed previously on solely **(*E*)-2** in toluene-d_8 using centered UVA bulbs. Increasing the irradiation time past one hour did not increase the yield of **(*Z*)-2** and attempting the UVA bulbs resulted in a lower amount of **(*Z*)-2** being

formed in the 1:1 mixture. Isomerization back to **(*E*)-2** using 530 nm light resulted in almost complete conversion to the original state. Longer irradiation time did not yield further conversion back to **(*E*)-2** and leaving the sample under ambient light also did not achieve 100% conversion. This process was repeated four more times with no large deviation in results (Figure 4.32). The conversion of **(*Z*)-2** remained constant

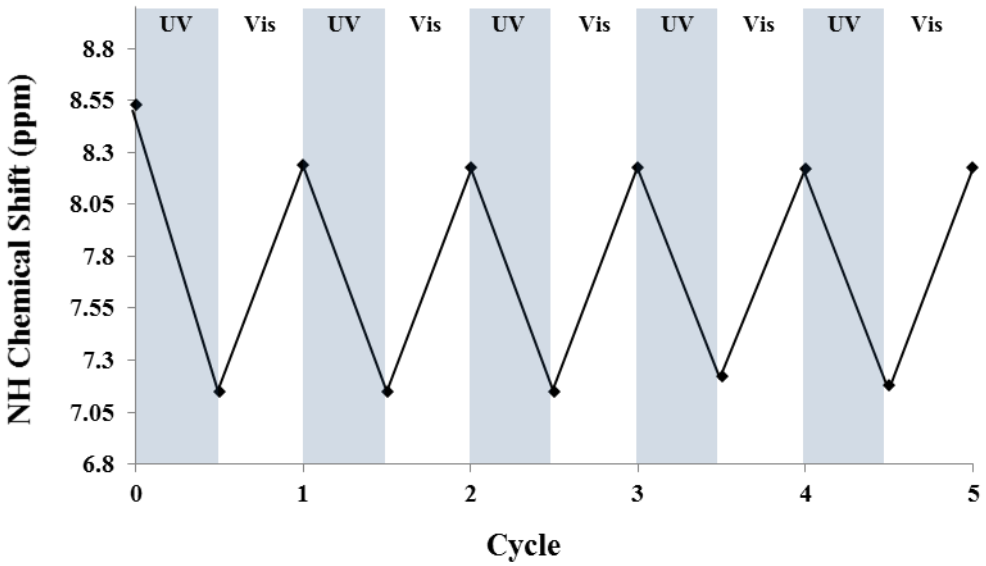

Figure 4.32 Cyclization isomerization plot of a 1:1 solution of **(*E*)-2·3-21b** in toluene-d_8 at 298 K. Blue areas indicate UV irradiation (350 nm) and white areas visible light irradiation (~530 nm).

at 60% (± 3%) and chemical shifts of both the NH and NH_2 shifts remained the same with no large deviation greater than 0.10 ppm. Most importantly, after five cycles there was no apparent loss of either array resulting from side reactions due to photodegradation.

The same isomerization experiment was performed with a 1:1 solution of **3-21b** and **(*E*)-3** in tolune-d_8. Unfortunately, no visible **(*Z*)-3** formed using any of the

conditions discussed above. A 2:1 ratio was tested (**(*E*)-3:3-21b**) and approximately 10% **(*Z*)-3** was produced (Figure 4.33). There was no change in the NH and NH_2 chemical shifts greater than 0.05 ppm. We attribute the lack of **(*Z*)-3** forming is due to the strong complexation between the two arrays. Also, the reversion back to the **(*E*)-3** was accelerated with **3-21b** in solution so between the time the irradiation was halted and the spectrum was taken, most of **(*Z*)-3** isomer may have converted back to **(*E*)-3**. Studies are currently underway to rationalize these results.

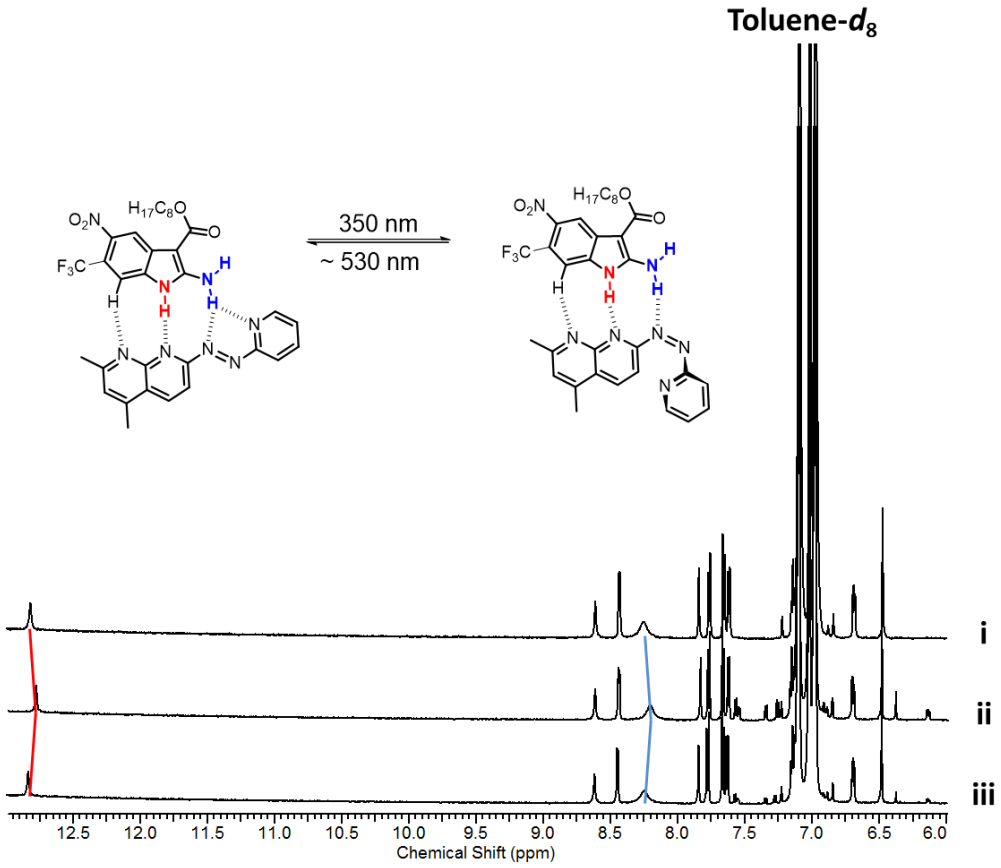

Figure 4.33 ^{1}H NMR spectra of a 2:1 solution of **(*E*)-3·3-21b** (**i**), the same solution after 350 nm irradiation (**ii**), the same solution after 530 nm irradiation (**iii**). The shifts of the NH peaks are identified by red lines and the NH_2 peaks by blue lines. Spectra were collected in toluene-d_8 at 298 K.

4.2.4 Determination of Complex Strength of (*Z*)-2 and (*Z*)-3 with 3-2e in Toluene-d_8

Following the success of the extrapolations with **3-21b**, the process was replicated with an alternate donor array. 5-Nitro-6-trifluoromethyl-3-perfluoroacyl-1*H*-2-aminoindole (**3-2e** from Chapter 3) was chosen as it produced the strongest complexes with our arrays. The studies were performed in toluene-d_8 as it is soluble in that solvent. A series of 7 reversion experiments with **(*Z*)-2** were performed analogous to the procedure with **3-21b**. Trials were performed on two different days to obtain more data points by analyzing less samples at one time. The extrapolated values are compiled in Table 4.6.

Table 4.6 The extrapolated NH chemical shifts of each **(*Z*)-2** reversion experiment with **3-2e**.

Molar Equivalents of (*Z*)-2	Extrapolated NH Chemical Shift; 0% (*E*)-2 (ppm)
1	5.92
1.5	6.02
2	6.18
2.5	6.31
3	6.53
4	6.59
5	6.62

Each of the regression fits (R^2) was equal to or greater than 0.994. These points were then plotted and fit to the 1:1 binding model. Figure 4.34 depicts this resulting curve along with the original curve of the **3-2e** titration with **(*E*)-2**.

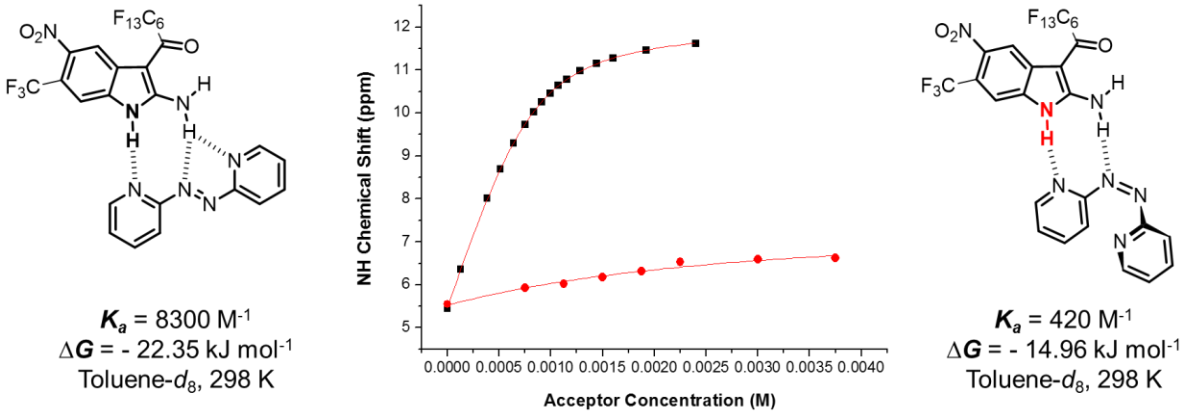

Figure 4.34 The NH binding data and calculated isotherms of **(*E*)-2** titration (black squares) and **(*Z*)-2** extrapolated values (red dots) with **3-2e**. Association constants, free energies of complexation, and experimental conditions are listed below the respective complexes.

There is a large difference in the respective curves just by visual inspection. The calculated association constant of 420 M^{-1} is a 7.39 kJ/mol drop in the free energy of complexation. This value looked promising but the chemical shift data calculated from the 1:1 binding model questioned the validity of this result (Table 4.7). The δ_{bound} value for the NH group was calculated to be 7.50 ppm with the $\Delta\delta_{max}$ being 1.97 ppm. These values are low considering the **(*Z*)-2·3-21b** extrapolation resulted in values of 9.44 ppm and 3.88 ppm, for δ_{bound} and $\Delta\delta_{max}$ respectively.

Table 4.7 Association constants (K_a), free energies of complexation (ΔG), calculated chemical shifts of free indole, fully complexed indole, and total change in chemical shift (δ_{free}, δ_{bound}, and $\Delta\delta_{max}$ respectively) of **(*E*)-2** and **(*Z*)-2** with **3-2e**. All experiments were performed in toluene-d_8 at 298 K.

Acceptor	K_a **(M^{-1})[a]**	ΔG **(kJ mol^{-1})[a]**	δ_{free} **[a] (ppm)** N*H* NH_2	δ_{bound} **[a] (ppm)** N*H* NH_2	$\Delta\delta_{max}$ **(ppm)** N*H* NH_2
(*E*)-2*	8300 ± 425	-22.35 ± 0.13	5.52 5.81	12.06 8.94	6.54 3.13
(*Z*)-2; NH	420	-14.96	5.53	7.50	1.97
(*Z*)-2; NH_2	62	-10.22	5.82	7.67	1.85

[a]Values calculated from Eq. 6 (chapter 2) using a 1:1 regression model and chemical shift data from the donor group. * Data taken from chapter 3.

Examination of the NH_2 extrapolations also provided some concerns. The δ_{bound} value calculated surpassed the NH value which has never been the case in any extrapolation or titration performed. The K_a value of 62 M^{-1} is also too low of a result considering a higher value was determined for the **(*Z*)-2·2-21b** trials (75 M^{-1}). We hypothesize these results suffer from a lack of data points in the **(*Z*)-2** binding isotherm. 30 molar equivalents of **(*Z*)-2** was needed to delineate the isotherm for the **2-21b** trials so more extrapolations in the higher molar equivalent region will have to be performed. Also, a titration with pyridine can be conducted as previous to obtain the association constant for which the **(*Z*)-2** result should not greatly exceed it.

Similar to the **(*Z*)-2** examination, reversion extrapolations of **(*Z*)-3** with **3-2e** were performed in two collections to obtain more data points for each respective curve. All donor groups on **3-2e** were able to be tracked during the course of the reversions even

though only the C7-H proton was visible throughout the titration of **(*E*)-3** and **3-2e**. All extrapolated values are compiled in Table 4.8 and the binding isotherms are depicted in Figure 4.35.

Table 4.8 The extrapolated NH, NH_2, and C7-H chemical shifts of each **(*Z*)-3** reversion experiment with **3-2e**.

Molar Equivalent of (*Z*)-3	**Extrapolated NH Chemical Shift (ppm)**	**Extrapolated NH_2 Chemical Shift (ppm)**	**Extrapolated C7-H Chemical Shift (ppm)**
0	5.55	5.80	6.66
1	NA	NA	7.29
1.25	10.84	8.02	7.43
1.5	11.57	8.33	7.54
1.75	11.79	8.39	7.57
2	12.09	8.57	7.63
2.5	12.32	8.69	7.66
3	12.47	8.72	7.66

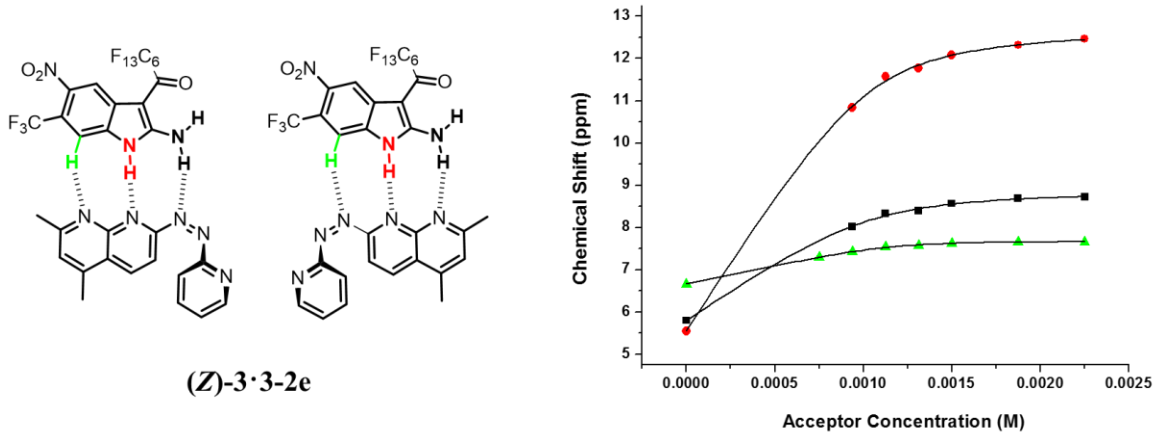

Figure 4.35 The NH (red dots), NH_2 (black squares), and C7-H (green triangles) binding data and calculated binding isotherms of the **(*Z*)-3** extrapolated values with **3-2e**. Possible binding geometries are depicted on the left. All data collected in toluene-d_8 at 298 K.

Each of the respective curves modeled excellently to the regression fits (R^2 = 0.999 for all regressions). The one molar equivalent data point for the NH and NH_2 curves could not be determined due to broadening of the signals into the baseline. Each of the binding isotherms resulted in a lower K_a value compared to the **(*E*)-3** titration which are listed in Table 4.9. An order of magnitude drop in association is seen for all three donor

Table 4.9 Association constants (K_a), free energies of complexation (ΔG), calculated chemical shifts of free indole, fully complexed indole, and total change in chemical shift (δ_{free}, δ_{bound}, and $\Delta\delta_{max}$ respectively) of **(*E*)-3** and **(*Z*)-3** with **3-2e**. All experiments were performed in toluene-d_8 at 298 K.

Acceptor (Donor Group)	K_a **(M^{-1})**[a]	ΔG **(kJ mol^{-1})**[a]	δ_{free}[a] **(ppm)**	δ_{bound}[a] **(ppm)**	$\Delta\delta_{max}$ **(ppm)**
(*E*)-3 (C7-H)*	172000 ± 22800	-29.86 ± 0.32	6.66	7.86	1.20
(*Z*)-3 (NH)	17200	-24.16	5.55	12.77	7.22
(*Z*)-3 (NH_2)	14100	-23.67	5.80	8.90	3.10
(*Z*)-3 (C7-H)	31100	-25.63	6.66	7.69	1.03

[a]Values calculated from Eq. 6 (chapter 2) using a 1:1 regression model and chemical shift data from the donor group dictated in brackets. * Data taken from chapter 3.

groups: 17200, 14100 and 31100 M^{-1} for NH, NH_2 and C7-H, respectively. This correlates to an average free energy of complexation value of -24.49 kJ/mol. Therefore, the average loss of free energy from **(*Z*)-3** complexation is 5.37 kJ/mol which is approximately 2.7 times greater than the **(*Z*)-3** results with **3-21b**.

The same photoswitching procedure was performed analogous to **3-21b**. A l:1 solution of **(*E*)-2** and **3-2e** in toluene-d_8 was irradiated for an hour with the 350 nm bandpass filter. Approximately 25% *trans* to *cis* conversion was achieved which is less than the 60% conversion observed with **3-21b**. The *cis* to *trans* irradiation reached approximately 8 to 10 % which matches the **3-21b** results (Figure 4.36). The similar upfield of the NH and NH_2 donor groups is observed when **(*Z*)-2** formed in

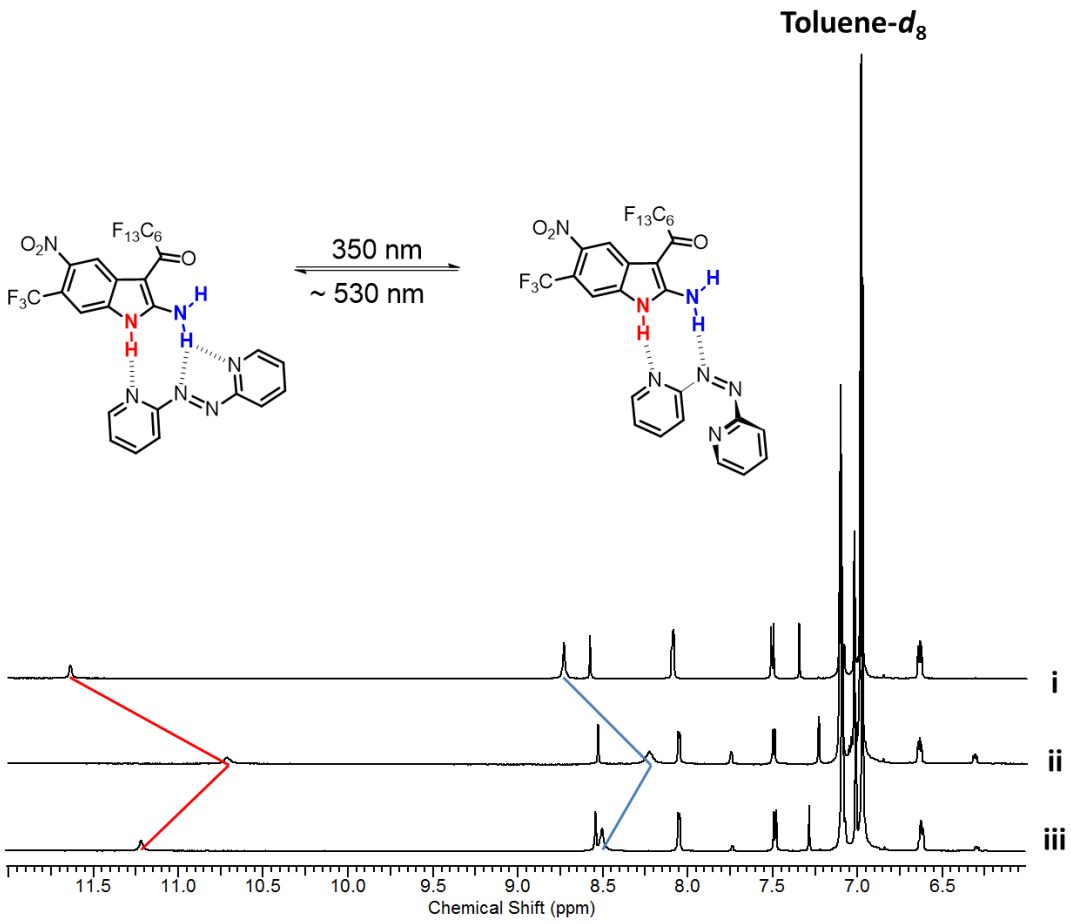

Figure 4.36 ^{1}H NMR spectra of a 1:1 solution of **(*E*)-2·3-2e** (**i**), the same solution after 350 nm irradiation (**ii**), the same solution after 530 nm irradiation (**iii**). The shifts of the NH peaks are identified by red lines and the NH_2 peaks by blue lines. Spectra were collected in toluene-d_8 at 298 K.

solution and resonate back downfield upon the reformation of **(*E*)-2**. It is unsure why only 25% conversion to the *cis* isomer was achieved as opposed to 60% for **3-21b**. One hypothesis for the decrease in conversion could be that **3-2e** provided a stronger complex (8200 M^{-1}) with **(*E*)-2** as opposed to **3-21b** (2100 M^{-1}). Studies are currently underway to rationalize these results and to increase the yield of **(*Z*)-2** isomerization. The switching procedure was only completed once due to time constraints so more trials will be explored in the future to access reversibility and system stability. Additionally, when the

1:1 solution of **(*E*)-3** and **3-2e** was irradiated at 350 nm, no **(*Z*)-3** was detected in the spectrum. Studies of **(*E*)-3** and **3-2e** will be examined at a later date.

4.2.5 Solid State Structure of (*Z*)-2

The spatial rearrangement of **(*E*)-2** to a non-ideal binding arrangement is the main rationale as to why the association constants decrease when studied with the donor arrays. Solid state heterocyclic *cis* azo compounds are extremely rare and only one structure has been documented.[11] During the isolation of **(*Z*)-2**, the solids after column purification and solvent removal resulted in small, red crystals. Recrystalization of these crystals by a slow diffusion of isopropyl ether into a diether ethyl solution containing **(*Z*)-2** excluded from light resulted in high quality crystals suitable for X-ray analysis. A monoclinic system containing 12 molecules per unit cell in space group C 2/c was achieved. There are two molecules, A and B, within the crystal lattice. Molecules A are arranged as dimers with an inversion center with each dimer containing a conformer of *P* (right handed) and *M* (left handed) helicity (Figure 4.37). Molecules B exist as a single *P* or *M* conformer in a column where the conformers alternate when examining the adjacent column.

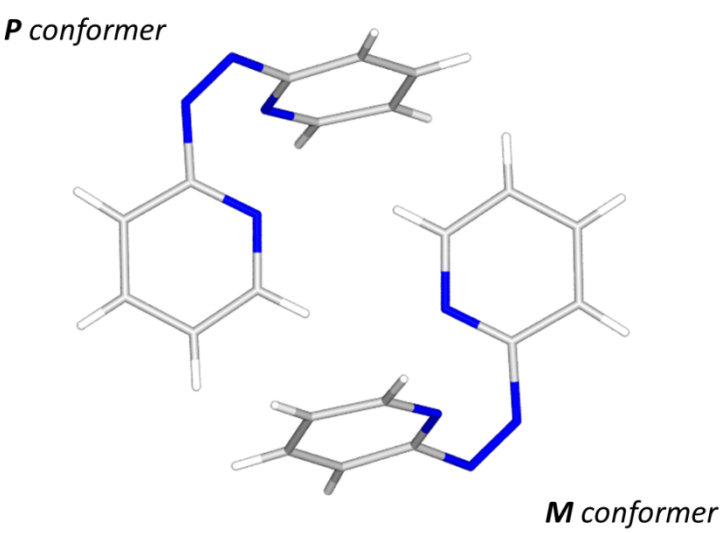

Figure 4.37 Stick representation of the *P* and *M* conformers of molecule A of **(*Z*)-2**.

Most obviously, the organization of the acceptor atoms when compared to **(*E*)-2** has changed dramatically. The C-N=N-C torsion for molecules A and B are 9.8^{o} and 9.1^{o} respectively when **(*E*)-2** comprises a 180^{o} torsion angle.[12] **(*E*)-2** is a planar molecule where the least squares planes of the pyridyl rings are coplanar where molecules A and B take up angles of 64^{o} and 58^{o}, respectively. In both *cis*-conformers, the nitrogen atoms within the pyridine rings are arranged in an endogenous manner (i.e. *syn*-*syn*) which is in accordance to dipole moment studies performed by Vogel and co-workers.[13] Also, the structural parameters for **(*Z*)-2** mimic the *cis*-azobenzene structure reported by Mostad and Rømming.[14] Overall, the structure of **(*Z*)-2** has drastically changed in planarity and acceptor array alignment from **(*E*)-2.** The structural parameters of **(*Z*)-2** crystal are compiled in Table 4.10 and relevant data comparing **(*Z*)-2** and **(*E*)-2** in the solid state is listed in Table 4.11.

Table 4.10 Crystal data and structure refinement for *cis*-2,2'-azopyridine, **(*Z*)-2**.

Structural Parameters	**(*Z*)-2**
Chemical Formula	$C_{10}H_8N_4$
Molecular Weight (g·mol^{-1})	184.20
Crystal System	Monoclinic
Space Group	C2/c
***a* (Å)**	23.485 (4)
***b* (Å)**	5.9241 (12)
***c* (Å)**	21.656 (4)
α (°)	90
β (°)	115.608 (7)
γ (°)	90
***V* (Å^3)**	2717.1 (9)
Z	12
***F* (000)**	1152
***T* (K)**	110
λ (Å)	1.54178
D_{calc} (g·cm^{-3})	1.351
μ (Cu-$K\alpha$) (mm^{-1})	0.705
Total Reflections	13701
Independent Reflections	2302
Absorption Correction	Multi-scan
Refinement on	F^2
Parameters Refined	238
$R(F_0)(I>2\sigma(I))$	0.0352
$R_w(F_0^2)(I>2\sigma(I))$	0.0886
***R*(F_0)(*all data*)**	0.0448
***R*$_w$(F_0^2)(*all data*)**	0.0932
GOF on F^2	1.069

Table 4.11 Selected bond distances and angles of **(*Z*)-2** and *trans*-2,2'-azopyridine in their respected crystal structures.

	(*Z*)-2 Molecule A	**(*Z*)-2 Molecule B**	***Trans*-2,2'-azopyridine (*E*)-2**[12]
C_{ipso}-N Bond Distance (Å)	1.4434 (21) 1.4421 (17)	1.4417 (19)	1.4316 (16)
N=N Bond Distance (Å)	1.2479 (16)	1.2524 (23)	1.2455 (14)
Angle between least square pyridyl planes (º)	64.070 (49)	57.605 (44)	0.000 (52)
C-N=N-C Torsion Angle (º)	9.809 (217)	9.085 (212)	180.000(92)

4.3 Summary and Conclusions

This chapter focused on the isomerization of our two acceptor arrays, **(*E*)-2** and **(*E*)-3**. Irradiation conditions were determined for conversions of the *Z* isomers in the bulk and microscale state. Methods of isolating these isomers were carried out yielding pure **(*Z*)-2** and **(*Z*)-3**. These isomers were characterized via UV-Vis methods and ^{1}H NMR where both methods revealed different spectra between the *trans* and *cis* isomers.

A titration with **(*Z*)-2** and indole **2-3k** was carried out in $CDCl_3$ and a value of 265 M^{-1} was calculated. This was drop in complex strength when compared to **(*E*)-2** titration results but due to thermal reversion, the accuracy of this value was taken into question. Utilizing the thermal reversion of **(*Z*)-2** to our advantage, an extrapolation method was devised and applied to solve the problem. Monitoring the chemical shifts of the donor groups while **(*Z*)-2** isomerized to **(*E*)-2** and plotting those values against the

concentration of **(*E*)-2** in solution provided a trend where the points could be extrapolated back to a point where, theoretically, **(*Z*)-2** concentration is 100%. Not enough extrapolated points were achieved for **2-3k** as there was no curvature in the 1:1 binding isotherm. Although a value could not be determined, it was evident that the binding of **(*Z*)-2** is much lower than **(*E*)-2** as the binding isotherms were very different in appearance.

The extrapolation method was repeated for **(*Z*)-2** and indole **3-21b** in toluene-d_8. Up to 30 molar equivalents of **(*Z*)-3** were required for delineation of the binding isotherm which resulted in an association constant of 75 M^{-1} which correlates to a decrease of 8.29 kJ/mol in free energy of complexation. The K_a value is only slightly larger than the results of the pyridine titration (40 M^{-1}) which we attribute to the weak interaction with an azo-nitrogen acceptor. **(*Z*)-3** was then analyzed with **3-21b** analogously to **(*Z*)-2.** The **(*Z*)-3** extrapolations resulted in an association constant of 1.3 x 10^4 M^{-1} which unfortunately was only a 1.97 kJ/mol decrease in free energy of complexation compared to the titration with **(*E*)-3**. It is apparent that the rigid AAA subunit in this acceptor array is the main contributor to complex strength with the pyridyl acceptor not adding significant stability to the complex.

Indole **3-2e** was then subjected to the same procedures. The results with **(*Z*)-2** thus far are inconclusive as not enough data points for delineation of the binding isotherm have been created. However, by visual inspection the two curves for **(*E*)-2** and **(*Z*)-2** look similar to the previous **3-21b** results so a large drop in free energy of complexation is likely. The **(*Z*)-3** extrapolations resulted in an average decrease of 5.37 kJ/mol in free energy of complexation when compared to the **(*E*)-3** titration results.

The reversibility of the system was tested with a 1:1 solution of **(*E*)-2·3-21b** in toluene-d_8. After irradiation at 350 nm, approximately 60% **(*Z*)-2** formed in solution which caused the donor groups to resonate upfield due to the weaker complexation. Irradiation with visible light (~ 530 nm) returned the system to the original state with approximately 5 to 10 % **(*Z*)-3** remaining. The process was repeated 5 times with no large deviations in steady state percentages of isomers being created and chemical shifts of the donor groups. Most importantly, the system remained stable as no degraded products were visible in the spectra. The process was repeated with a 1:1 solution of **(*E*)-3·3-21b** but no **(*Z*)-3** was detected. A 2:1 **(*E*)-3·3-21b** solution was tested which provided approximately 10% **(*Z*)-3** conversion. When photoswitching was performed with indole **3-2e**, approximately 25% **(*Z*)-2** was created and **(*Z*)-3** was not detected analogous to **3-21b**.

4.4 Experimental Methodology

4.4.1 General Information

$CDCl_3$, DMSO-d_6, and Toluene-d_8 were purchased from Cambridge Isotope Laboratories or Sigma Aldrich and dried (chloroform and toluene) over 4Å molecular sieves before use. Synthesis and chromatography solvents were purchased from Caledon Laboratories and used as received. Pd/C was purchased from Sigma Aldrich and used as received. Pyridine was freshly distilled over CaH_2 before use. ^1H and ^{13}C NMR spectra were collected @ 298 K on a Varian Mercury 400 MHz or a Bruker AvanceIII HD 400 MHz spectrometer (operating at 400.08 and 100.61 MHz respectively) and the Varian Inova 600 MHz spectrometer (599.37 and 150.72 MHz respectively). ^1H NMR titration

and photoswitching spectra were collected on the Inova 600 MHz spectrometer. Reversion experiments were collected on the Inova 600 MHz and the Varian Inova 400 MHz (399.76 MHz) spectrometers. Spectra are reported with residual solvent peak as reference from TMS.[15] Chromatography was performed using Silicycle 40-63 μm silica gel-60 (R10030B). EI mass spectra were obtained on a Finnigan MAT 8400 mass spectrometer.

4.4.2 Titration Procedure

A stock solution of **3-21b** was prepared in dry $CHCl_3$ to a concentration of 1.0 x 10^{-3} M. 3.5 mL was transferred to a clean, dry vial and placed in the dessicator to remove solvents. Once dry, 3.5 mL of toluene-d_8 was added and once **3-21b** dissolved, 0.5 mL was put into an NMR tube. To the remaining 3.0 mL was added a known weight of pyridine to a concentration of 7.0 x 10^{-2} M. An initial spectrum of **3-21b** was taken and aliquots of the guests solution were added in succession with a spectrum taken after each addition. Up to 50 molar equivalents of pyridine needed to be added to achieve delineation of the isotherm. The chemical shifts of the NH and NH_2 protons were recorded from each spectrum and fit satisfactorily to a 1:1 binding model (*J.A.C.S.*, **2000**, *122*, 8856) using Origin® data analysis software. The same process was repeated for Nap and **3-21b**. The Nap concentration in the guest solution was 7.0 x 10^{-3} M.

4.4.3 Extrapolation Procedure for (*Z*)-2 and 2-3k

A stock solution of **2-3k** was prepared in dry $CHCl_3$ to a concentration of 2.5 x 10^{-4} M. Two dry vials were each filled with 4 mL of that solution and placed in a

dessicator to remove the solvents. Once dry, one vial was filled with 4 mL of $CDCl_3$ and which was then transferred equally into 8 NMR tubes (0.5 mL each). The remaining vial was filled with 4 mL of $CDCl_3$ and a known amount of **(*Z*)-2** to a concentration of 5.0 x 10^{-3} M. Each of the NMR tubes was injected with the **(*Z*)-2** solution to a different molar equivalent (1, 1.5, 2, 2.5, 3, 4, 5, 7) with respect to **2-3k** and a spectrum was recorded. Alternating the NMR tubes, spectra were repeatedly taken over time until a photostationary state of isomerization was reached, or a maximum of 5 hours. Analyzing the spectra for each equivalent, the concentration of **(*E*)-2** was determined through integrations of the *ortho* protons of both **(*E*)-2** and **(*Z*)-2** and the NH and NH_2 chemical shifts were recorded. These two variables were plotted and the regression fit was extrapolated to where the concentration of **(*E*)-2** is 0 or (***Z***)**-2** is 100%, theoretically. All extrapolated values were then inputted into the regression software and fit to the 1:1 binding model using the concentrations of **(*Z*)-2** used for each trial.

4.4.4 Extrapolation Procedure for (*Z*)-2 and 3-21b

A stock solution of **3-21b** was prepared in dry $CHCl_3$ to a concentration of 1.0 x 10^{-3} M. Three dry vials were each filled with 3 mL of that solution and placed in a dessicator to remove the solvents. Once dry, two vials were filled each with 3 mL toluene-d_8 and split equally into 12 NMR tubes (0.5 mL each). The remaining vial was filled with 3 mL toluene-d_8 and a known amount of **(*Z*)-2** to a concentration of 4.0 x 10^{-2} M. The remainder of the procedure was performed analogous to **(*Z*)-2** and **2-3k** using **(*Z*)-2** molar equivalents of 1, 2, 3, 4, 5, 6, 8, 10, 15, 20, 25, and 30 with respect to **3-21b**.

4.4.5 Extrapolation Procedure for (*Z*)-3 and 3-21b

Two vials were each filled with 3 mL of the same stock solution of 1.0 x 10^{-3} M **3-21b** already prepared and placed in the dessicator. Once dry, one vial was filled with 3 mL toluene-d_8 and 0.5 mL of this solution was each placed into 5 NMR tubes. The remaining vial was filled with 3 mL toluene-d_8 and a known amount of **(*Z*)-3** to a concentration of 1.0 x 10^{-2} M. The remainder of the procedure was performed analogous to **(*Z*)-2** and **3-21b** using **(*Z*)-3** molar equivalents of 0.5, 1, 1.5, 2, and 2.5 with respect to **3-21b**. The concentration of **(*E*)-3** was determined through integrations of the singlet aryl proton of both **(*E*)-3** and **(*Z*)-3**.

4.4.6 Extrapolation Procedure for (*Z*)-2 and 3-2e

A stock solution of **3-2e** was prepared in dry CH_2Cl_2 to a concentration of 7.5 x 10^{-4} M. Two vials were each filled with 2 mL of this solution and place in the dessicator. Once dry, one vial was filled with 2 mL toluene-d_8 and split into 4 NMR tubes (0.5 mL each). The remaining vial was filled with 2 mL toluene-d_8 and a known amount of **(*Z*)-3** to a concentration of 7.5 x 10^{-3} M. The remainder of the procedure was performed analogous to **(*Z*)-2** and **3-21b** using 1, 2, 3, and 4 molar equivalents of **(*Z*)-2** with respect to **3-2e**. This preparation and method was replicated the following day with 1.5, 2.5, and 5 molar equivalents of **(*Z*)-2**.

4.4.7 Extrapolation Procedure for (*Z*)-3 and 3-2e

Two vials were each filled with 2 mL of the same stock solution of 7.5 x 10^{-4} M **3-2e** already prepared and placed in the dessicator. Once dry, one vial was filled with 2

mL toluene-d_8 and split into 4 NMR tubes (0.5 mL each). The remaining vial was filled with 2 mL toluene-d_8 and a known amount of **(*Z*)-3** to a concentration of 5.25 x 10^{-3} M. The remainder of the procedure was performed analogous to **(*Z*)-2** and **3-2e** using **(*Z*)-3** molar equivalents of 1, 1.5, 2, and 3 with respect to **3-2e.** This preparation and method was replicated the following day with 1.25, 1.75, and 2.5 molar equivalents of **(*Z*)-3**.

4.4.8 Reversible Photoswitching Procedure

A 1:1 solution of **(*E*)-2**:**3-21b** (1.0 x 10^{-3} M, 0.5 mL, toluene-d_8) was placed in an NMR tube and bubbled with N_2 gas for 10 minutes. A ^{1}H NMR spectrum was then taken and NH and NH_2 shifts were recorded. The tube was then irradiated with a mercury lamp (220 watts) equipped with a 350 nanometer bandpass filter (Thorlabs, FB350-10) for an hour. Every ten minutes, the NMR tube was removed and shocked in an ice/water bath for ~ 20 seconds to prevent any thermal isomerization from occurring. After that hour, a ^{1}H NMR spectrum was taken and shifts recorded. The tube was then irradiated by 4 green LED lights (10 watts each, λ_{max} ~ 530 nm) for 60 seconds and another ^{1}H NMR spectrum taken and shifts recorded. This process was repeated another 4 times. This method was repeated for 1:1 **(*E*)-3**:**3-21b** (1.0 x 10^{-3} M, 0.5 mL, Toluene-d_8) but no **(*Z*)-3** was detected in the ^{1}H NMR spectra. The 2:1 **(*E*)-3**:**3-21b** (2.0 x 10^{-3} M:1.0 x 10^{-3} M, 0.5 mL, toluene-d_8) mixture was performed with one cycle. **3-2e** with the two acceptor arrays was performed by the same method.

4.4.9 Synthetic Methods

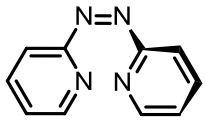

Synthesis of (*Z*)-2: (*E*)-2 (500 mg, 2.72 mmol) was dissolved in 200 mL of acetone and split into small test tubes, capped with a septum and sealed with parafilm. These samples were irradiated for 5 hours in a Luzchem photoreactor (model LZC-4V) equipped with 14 UVA bulbs centered at 360 nm. After irradiation, the samples were combined in a RBF flask wrapped in aluminum foil and the acetone was removed by a stream of dry air until a red oil remained. The oil was subjected to flash chromatography (100% Et_2O) and the first fraction was collected and the ether was removed by a stream of dry air. Once all the ether has been removed, red crystals of pure **(*Z*)-2** was isolated in 45% yield which can be stored in the freezer until needed. **^{1}H NMR** (600 MHz, $CDCl_3$): δ (ppm) 8.14 - 8.12 (m, 2H), 7.76 (dt, *J* = 7.7, 1.5 Hz, 2H), 7.39 (d, *J* = 7.7 Hz, 2H), 7.07 - 7.05 (m, 2H). **^{13}C NMR** (150 MHz, $CDCl_3$): δ (ppm) 164.5, 147.8, 137.8, 122.4, 118.6. **HRMS (EI):** calc. for $C_{10}H_8N_4^+$ $[M]^+$ 186.0749; found 186.0752.

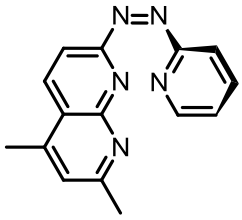

Synthesis of (*Z*)-3: The same procedure to isolate **(*Z*)-3** was performed analogous to **(*Z*)-2** starting from **(*E*)-3** (250 mg, 0.95 mmol). Flash chromatography was performed with 100% acetone and **(*Z*)-3** was isolated in 32% yield. **^{1}H NMR** (400 MHz, $CDCl_3$): δ (ppm) 8.34 (d, *J* = 8.7 Hz, 1H), 7.96 - 7.94 (m, 1H), 7.80 (dt, *J* = 7.7, 1.7 Hz, 1H), 7.74 - 7.72 (m, 1H), 7.48 (d, *J* = 8.7 Hz, 1H), 7.14 (s, 1H), 7.01 - 6.98 (m, 1H), 2.66 (s, 3H), 2.62 (s, 3H). **^{13}C NMR** (150 MHz, $CDCl_3$): δ (ppm) 168.2, 163.2, 162.6, 154.7, 147.3, 145.3, 138.3, 134.3, 123.6, 123.2, 121.4, 119.1, 115.7, 25.5, 18.2.

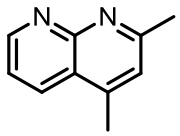

Synthesis of 2,4-dimethyl-1,8-napthyridine: 7-Chloro-2,4-dimethyl-1,8-naphthyridine (500 mg, 2.60 mmol) was dissolved in 10 mL of a 1:1 mixture of THF and methanol. 10% Pd/C (13.8 mg, 0.13 mmol) was added and the flask was purged with a balloon filled with hydrogen gas for 5 minutes. The reaction was left to stir for 4 hours under a hydrogen atmosphere then vacuum filtered through a thin pad of Celite. The solvents were removed under reduced pressure and the crude solids were purified using flash chromatography with EtOAc/Hexanes (1:1) as eluent. Title compound was isolated as a tan, amorphous solid in 50% yield. **^{1}H NMR** (400 MHz, $CDCl_3$): δ (ppm) 9.06 (dd, *J* = 4.4, 2.0 Hz, 1H), 8.33 (dd, *J* = 8.3, 2.0 Hz, 1H), 7.44 (dd, *J* = 8.3, 4.4 Hz, 1H), 7.22 (s, 1H), 2.76 (s, 3H), 2.68 (s, 3H). **^{13}C NMR** (100 MHz, DMSO-d_6): δ (ppm) 161.9, 155.3, 152.8, 145.9, 133.8, 123.3, 121.2, 120.6, 25.0, 17.5. **HRMS (EI):** calc. for $C_{10}H_{10}N_2^+$ $[M]^+$ 158.0844; found 158.0851.

4.5 References

1. a) Nojiri, A.; Kumangai, N.; Shibasaki, M. *Angew. Chem. Int. Ed*., **2012**, *51*, 2137; b) Takeshita, M.; Hayashi, M.; Kadota, S.; Mohammed, K. H.; Yamato, T. *Chem. Commun*., **2005**, 761; c) Natali, M.; Giordani, S. *Chem. Soc. Rev*., **2012**, *41*, 4010; d) Xu, J-F.; Chen, Y-Z.; Wu, D.; Wu, L-Z.; Tung, C-H.; Yang, Q-Z. *Angew. Chem. Int. Ed*., **2013**, *52*, 9738.

2. a) Viehmann, P.; Hecht, S. *Beilstein J. Org. Chem*., **2012**, *8*, 1825; b) Stoll, R. S.; Hecht, S. *Org. Lett*., **2009**, *11*, 4790; c) Dai, Z.; Cui, Y.; Chen, C.; Wu, J. *Chem. Commun*., **2016**, *52*, 9731; d) Peters, M. V.; Stoll, R. S.; Kühn, A.; Hecht, S. *Angew. Chem. Int. Ed*., **2008**, *47*, 5968; e) Banghart, M.; Borges, K.; Isacoff, E.; Trauner, D.; Kramer, R. H. *Nat. Neurosci*., **2004**, *7*, 1381.

3. Rakotondradany, F.; Whitehead, M. A.; Lebuis, A-M.; Sleiman, H. F. *Chem. Eur. J*., **2003**, *9*, 4771.

4. Herder, M.; Pätzel, M.; Grubert, L.; Hecht, S. *Chem. Commun*., **2011**, *47*, 460.

5. Okuyama, T.; Yokoyama, Y.; Yokoyama, Y. *Bull. Chem. Soc. Jpn*., **2001**, *74*, 2181.

6. Hunter, C. A.; Togrul, M.; Tomas, S. *Chem. Commun*., **2004**, 108.

7. Mendez, I. J. M.; Pleizier, J. S.; Wang, H-B.; Wisner, J. A. *J. Phys. Org. Chem*., **2018**, *31*, e3805.

8. Mendez, I. J. M. Photo-Isomerizable Self-Complementary Hydrogen Bond Arrays. Ph.D. Dissertation, Western University, London, ON, 2016.

9. Campbell, N.; Henderson, A.W.; Taylor, D. *J. Chem. Soc.*, **1953**, *APR*, 1281.

10. Vulcano, R.; Pengo, P.; Velari, S.; Wouters, J.; De Vita, A.; Tecilla, P.; Bonifazi, D. *J. Am. Chem. Soc*., **2017**, *139*, 18271.

11. Yuan, J.; Shu-Ming, P.; Ning, L.; Ming-Feng, L.; Cheng, H. *Chinese J. Inorg. Chem*., **2016**, *32*, 1676.

12. Bock, H.; Dienelt, R.; Schödel, H.; Van, T. T. H. *Struct. Chem*., **1998**, *9*, 279.

13. Bullock, D. J. W.; Cumper, C. W. N.; Vogel, A. I. *J. Chem. Soc*., **1965**, 5316.

14. Mostad, A.; Rømming, C. *Acta. Chem. Scand*., **1971**, *25*, 3561.

15. Fulmer, G. R.; Miller, A. J. M.; Sherden, N. H.; Gottlieb, H. E.; Nudelman, A.; Stoltz, B. M.; Bercaw, J. E.; Goldberg, K. I. *Organometallics*, **2010**, *29*, 2176.

Chapter 5

5 Conclusions and Future Work

5.1 Conclusions

The azo photoswitching unit has proven to be useful in a wide variety of photochromic molecules and macromolecules. The *trans* to *cis* isomerization is triggered by UV irradiation and the resulting spatial arrangement of the molecule is altered to elicit a large response. We were able to utilize this quality in hydrogen bonding complexes when the pendant groups of the azo bond (-N=N-) contained hydrogen bonding acceptors. Additionally, one of the azo nitrogen atoms also acted as a acceptor group which resulted in AAA or AAAA hydrogen bond acceptor arrays. Complementary hydrogen bonded complexes were formed with 2-aminoindole donor arrays (DD or DDD) which resulted in stable complexes when the acceptor arrays were in the *trans* form.

These complexes were studied in the solution state via ^{1}H NMR to obtain association constants in conjunction with a wide variety of donor arrays. A library of 2-aminoindoles were synthesized where the substitution pattern of the 5 and 6 positions were modified. Titration results in $CDCl_3$ with the AAA array, **(*E*)-2**, resulted in K_a values ranging from 9.0×10^{1} to 1.3×10^{3} M^{-1}. LFER plots were constructed and revealed strong linear correlations between the withdrawing character of the substituents (Hammett constants, σ) and the observed K_a values. Modifying the substituent in the 3 position of the donor arrays revealed that electron rich carbonyls or sulfonyl groups are

strong intramolecular hydrogen bond acceptors which resulted in weaker complexation with **(*E*)-2**. Solid state studies were conducted on single crystals resulting in X-ray crystal structures of 7 hydrogen bonded complexes that all displayed the predicted binding geometry.

(*E*)-2 was covalently expanded to give AAAA arrays incorporating an additional pyridyl (**(*E*)-3**) or methoxide acceptor (**(*E*)-4**). All three acceptor arrays were studied in $CDCl_3$ and toluene-d_8 with a soluble donor array **3-21b**. The addition of an additional acceptor on **(*E*)-3** and titrations in a non-polar medium proved effective at raising complex stability to a value of 2.9×10^4 M^{-1}. The highest association constant throughout this work was achieved by modifying the octyl ester of indole **3-21b** to a perfluoro acyl group. Titrations with **(*E*)-3** in toluene-d_8 resulted in a K_a value of 1.7×10^5 M^{-1} which is strong for a neutral DDD·AAAA hydrogen bonding complex. The crystal structure obtained with **(*E*)-3** demonstrated that there was a C-H···N hydrogen bond occurring during complexation. The structure was verified using 2D ^{1}H NMR analysis which implied multiple binding geometries in solution.

The complex stability was measured with the *cis* isomers of **(*E*)-2** and **(*E*)-3**. Methods of isolation for **(*Z*)-2** and **(*Z*)-3** were established and the *Z*-isomers proved to be stable in the solid state at low temperature in the absence of light. A titration with **(*Z*)-2** was attempted but the thermal reversion to **(*E*)-2** in solution prevented the achievement of an accurate K_a value. An extrapolation method was then formulated which utilized the thermal reversion to our advantage. The results of these experiments with **(*Z*)-2** and **3-21b** resulted in a K_a value of 75 M^{-1} which was a decrease of 8.3 kJ/mol in free energy compared to the **(*E*)-2** titration results. **3-2e** was subjected to the same procedure and a

rough estimate of 420 M^{-1} was measured for **(*Z*)-2** which correlates to 7.4 kJ/mol decrease in the free energy of complexation. **(*Z*)-3** was analyzed in the same manner which resulted in a decrease in association constant by approximately half for both **3-21b** and **3-2e**. Unfortunately, this only correlates to a decrease of 2.0 (**3-21b**) and 5.4 kJ/mol (**3-2e**) which means **(*Z*)-3** still hydrogen bonds strongly to the donor arrays. **(*Z*)-2** performed better in this study as the spatial arrangement of the acceptor atoms has changed more completely than **(*Z*)-3** which was observed in the crystal structure of **(*Z*)-2**.

Lastly, photoswitchable reversibility was tested with 1:1 mixtures of donor and **(*Z*)-2**. **(*E*)-2** was irradiated at 350 nm with **3-21b** in toluene-d_8 and approximately 60% conversion to **(*Z*)-2** was observed. The chemical shifts of both donor groups resonated at lower chemical shifts as the binding to the *Z* isomer is weaker. Irradiation using 530 nm light returned the system to nearly the original state. The cycling was completed a total of 5 times with replicable results and no apparent photodegradation. When **(*E*)-3** was attempted in a 1:1 solution, no **(*Z*)-3** was observed and studies are underway to determine the cause.

5.2 Scope for Future Work

The donor arrays in this work consisted of a DDD motif of either NH and NH_2 or NH, one amino NH, and a weak C-H interaction. Expanding these array was not examined so adding an additional amino group could be a focus of future complexation studies. Very strong association constants would be expected as these DDD arrays have been shown to exhibit strong complexation in solution (Figure 5.1). The acceptor arrays can also be modified further by

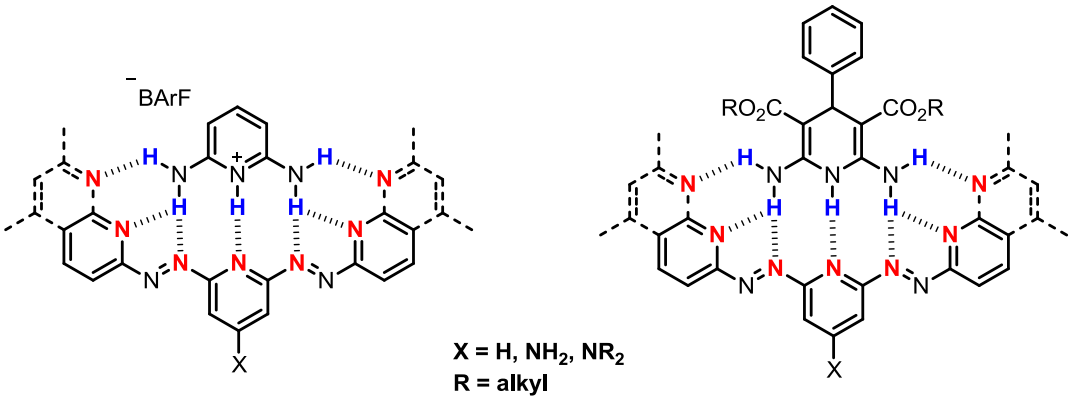

Figure 5.1 Plausible hydrogen bonded complexes which would provide strong association constants.

the inclusion of additional photoswitchable acceptor sites. A central pyridyl acceptor mirrored on both sides by azopyridyl or azonapthyridyl units would provide DDD·AAAAA and DDDDD·AAAAAAA arrays, respectively. Assessing the photoswitchability of these arrays would be of higher complexity due to the possibility of *cis*, *trans*, and *cis*, *cis* isomers but could lead to interesting results.

The efficacy of the *trans* to *cis* isomerization of **(*E*)-3** proved not to be as successful as was initially hypothesized. Modifications could be made to **(*E*)-3** where binding to the *cis* isomer could be stronger than the *trans*. Utilizing the photoswitch as a steric block, the pyridyl unit could be modified into an aryl group with large substituents which would block binding in the trans conformer. Figure 5.2 depicts how using DAP·BArF as an example, the trans isomer would sterically repulse/block the incoming donor (left) but isomerization to the *cis* isomer would open the AAA array for binding (right).

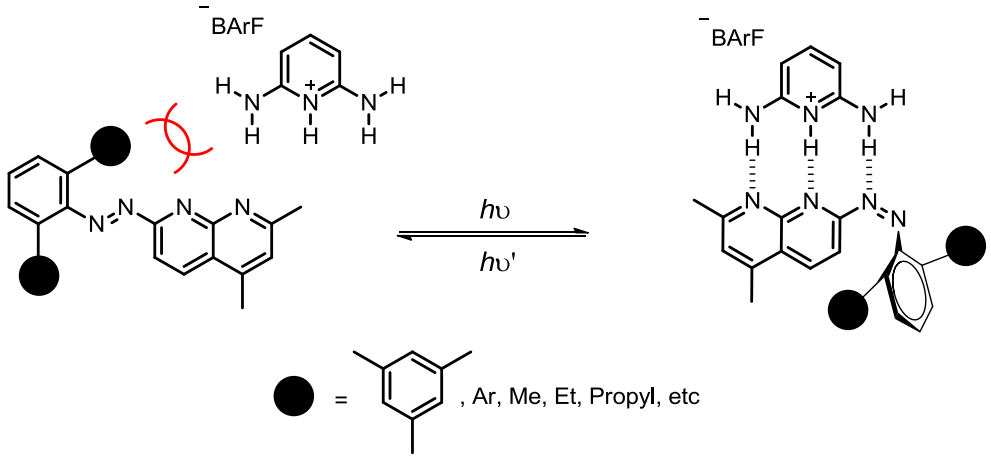

Figure 5.2 Modification of **(*E*)-3** where an aryl group would sterically block hydrogen bonding in the *trans* form and strong binding in the *cis* form.

All strong association constants determined in this work were due to the planarity of both arrays. Each array being planar maximized the binding geometry which was disrupted by the spatial arrangement of the *cis* isomer. This concept can be applied to previous work performed on double helical arrays (discussed in Chapter 3). Utilizing the preorganized DDD double helical array, a non-linear photoswitchable acceptor array can be fashioned to complex in a double helical manor. Isomerization to the *cis* isomer would yield a bulky acceptor array which would not complex to the donor array as the binding pocket cannot encumber such a sterically crowded array (Figure 5.3).

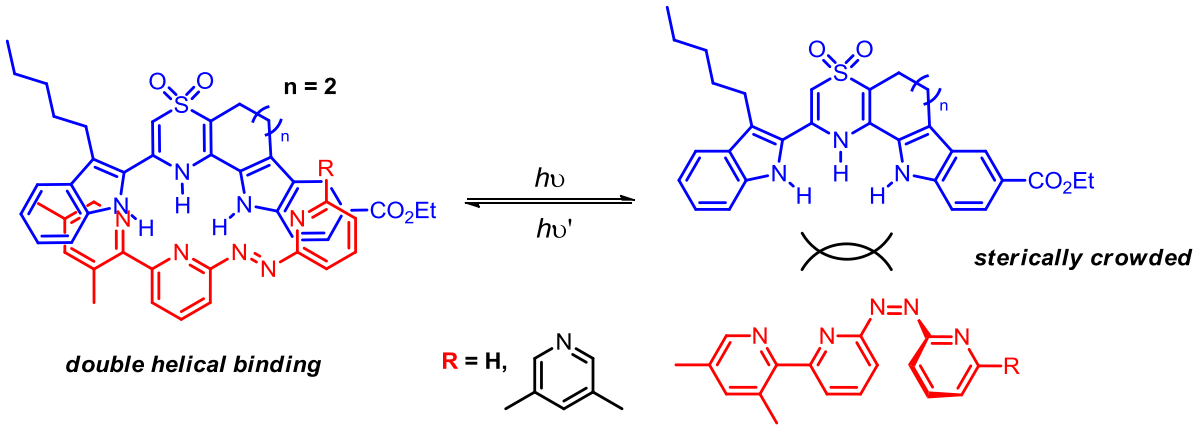

Figure 5.3 A photoswitchable, double helical hydrogen bonded complex.

Lastly, the connection of these arrays onto scaffolds would create complementary photoswitchable supramolecular polymers. The indole arrays in particular provide a wide range of connection points which can lead to a number of possibilities. For example, an alkyne can be included in the indole array which is a versatile functional group for coupling reactions. Tritopic hydrogen bonding donor monomers can be produced via Sonogashira or click-chemistry from 1,3,5 tri-substituted benzene analogues (Figure 5.4). Ditopic monomers can also be synthesized using standard coupling reactions. Also, since the perfluoroacyl chain was the strongest indole synthesized (**3-2e**; Chapter 3), a strong ditopic monomer with a perfluoroacyl connector would be ideal (Figure 5.5).

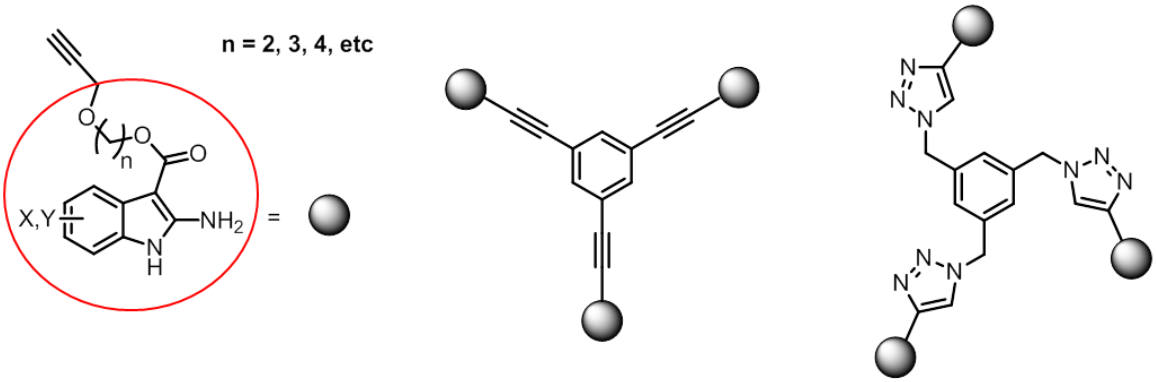

Figure 5.4 Plausible tritopic indole monomers synthesized via Sonogashira and click coupling.

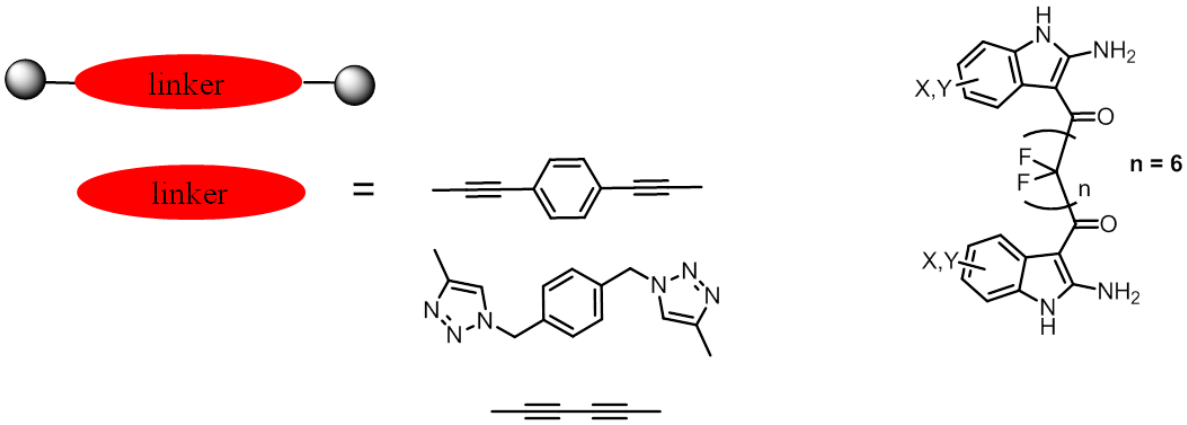

Figure 5.5 Plausible ditopic indole monomers synthesized by coupling reactions **(i)** and a perfluoro-diacyl chloride derivative **(ii)**.

Similar monomers can be synthesized with the acceptor arrays. Coupling reactions (e.g. Sonogashira) have been tested previously in our group with iodinated derivatives of **(*E*)-2** and **(*E*)-2** but have been unsuccessful. Therefore, other synthetic strategies would have to be examined. The same can be said for monomers containing both donor and acceptor arrays.

Curriculum Vitae

Jeffrey Pleizier

EDUCATION

B.Sc. – Honors Specialization in Chemistry – Graduated June 2011
- Minor Advanced Chemistry

Western University, London Ontario

Ph.D. – Organic Chemistry – May 2011 – Decemeber 2018
- Supervisor: Dr. J. Wisner

Western University, London Ontario

RESEARCH EXPERIENCE

Undergraduate Research Thesis – **September 2010 – April 2011**
- Supervised by Dr. J. Wisner
- Title of Thesis: *New Acceptor Arrays for Formation of Hydrogen and Halogen Bonded Double Helices*

Chemistry Department, Western University, London Ontario

RELEVENT WORK EXPERIENCE

Summer Research Student – May 2010 – August 2010
- Engineering project in collaboration with LANXESS
- Minor Experiment: *Mechanism of Arsenic Sequestration using Fe-enriched combustion Ash*
    - Supervised by Dr. B. Hart

Surface Science Western, London Ontario

Teaching Assistant - Sept. 2011 – April 2016
- Chemistry 2213A; **Organic Chemistry for Life Sciences** (Resource Room and Laboratory)
- Chemistry 2223B; **Organic Chemistry of Biological Molecules** (Laboratory)

PRESENTATIONS

Synthesis and Characterization of a Photoisomerizable Hydrogen Bond Array.
(Oral) Pleizier, J.; Mendez, I.; Wisner, J.
96th Canadian Chemistry Conference and Exhibition, May 2013.

Synthesis and Characterization of a Photoisomerizable Hydrogen Bond Interaction.
(Oral) Pleizier, J.; Mendez, I.; Wisner, J.
CAMBR Distinguished Lecturer and Research Day, Nov, 2013.

Studying the Effects of Photoisomerization on a Hydrogen Bonded Complex.
(Poster)
Pleizier, J.; Mendez, I.; Wisner, J.
98th Canadian Chemistry Conference and Exhibition, June 2015.

A Survey of Hydrogen Bond Donor Arrays Paires with Photoswitchable Acceptor Arrays (Poster)
Pleizier, J.; Wisner, J.
100th Canadian Chemistry Conference and Exhibition, May 2017.

PUBLICATIONS

Mendez, I. J. M.; Pleizier, J. S.; Wang, H-B.; Wisner, J. A. *J. Phys. Org. Chem*., **2018**, *31*, e3805.

Mendez, I. J. M.; Pleizier, J. S.; Wang, H-B.; Wisner, J. A. *J. Chem. Crystallogr*., **2018**, *Ahead of Print*, DOI: 10.1007/s10870-018-0737-z.

AWARDS

Lipson-Baines 9658 Award

- Awarded for receiving one of the highest grades in the 9658 Chemistry seminar course

OUTREACH

Chemistry Outreach Activities – March 2013 – Present

- March Break Open House
- Various Outreach Events hosted by the Chemistry department

Chemistry Department, Western University, London Ontario